THE UNIVERSITY OF TASMANIA LIBRARY

THE DISTRIBUTION OF COSMIC RAY NEUTRONS IN THE ATMOSPHERE

BY

J. G. GREENHILL, B.Sc. (Hons.) (Tas.)

Submitted in fulfilment of the requirements for the Degree of

DOCTOR OF PHILOSOPHY

UNIVERSITY OF TASMANIA

HOBART

January, 1966

PREFACE

The Hobart cosmic ray balloon programme was begun in 1959 under the direction of Dr. A.G. Fenton, leader of the Cosmic Ray Group in the University of Tasmania. I participated in the design and construction of the single geiger counter flight units used in the early years of the programme. Details of these instruments and the results of several successful flights are described in my Bachelor of Science (Honours) thesis submitted for examination in April, 1960.

Measurements with these instruments were continued for several years and in the latter part of 1962 I participated in a series of balloon flights from Hobart coincident with the high altitude nuclear detonations over Johnston Island. A radiation enhancement wasobserved on July 9, 1962, a few seconds after the nuclear explosion Starfish Prime over Johnston Island. This event is described by Edwards et al (1962) and has been analysed in detail by Edwards (1964).

During the southern summmer of 1961-1962 an auroral X-ray group, led by Dr. R.R. Brown of the University of California, made a series of balloon flights from Macquarie Island during periods of auroral activity. Members of the Hobart Cosmic Ray Group and of the Antarctic Division, Australian Department of External Affairs, participated in these measurements. Neutron detectors were hitch-hiked on a number of the X-ray flight units following a suggestion by

Dr. K.B. Fenton (Physics Department, University of Tasmania) that protons may sometimes be accelerated in the same process which gives rise to the auroral X-ray bursts. The precipitation of protons with insufficient energy to reach the balloon level could be detected by observation of the neutrons produced in proton-air nuclei interactions.

I undertook the design and construction of the neutron detector units and spent a week on Macquarie Island matching these units to the University of California X-ray rigs. The flights were made jointly by Dr. N.R. Parsons (at that time a member of the Hobart Group) and by the University of California Auroral X-ray Group.

The results of the Macquarie Island flights were ambiguous and it was decided to make further measurments at Wilkes, Antarctica during the 1962-1963 summer season. I designed and supervised the construction of the flight units and ground station for these measurements and spent five months in the Antarctic making the flights.

Much of this thesis is devoted to the analysis of neutron flux measurements made in a series of balloon flights from five stations ranging from Wilkes, Antarctica, to Lae, New Guinea. I supervised the construction of the flight units and assisted in the measurements which involved many members of the Hobart Group.

I was also responbible for the experiment s on the neutron counter response made in flights from Mildura during 1964 and 1965.

The analysis of the data presented in this thesis is entirely my own work and none of the material has been accepted for the award of any other degree or diploma in any University. This thesis contains no paraphrase of material previously wirtten or published by any other person except where due reference is made in the text.

As indicated above, the experimental work described here is the result of the cooperation of many people. I am particularly indebted to Dr. N.R. Parsons (now at the University of Alberta, Calgary, Canada) for his collaboration in the experimental programme and for making the Hobart flight H_2 and the Macquarie Island 1964 data available to me. Mr. John Phillips assisted in making the Macquarie Island 1964 measurements and I am also very grateful to him for his assistance in preparations for the latitude survey measurements and in the conduct of the flights from Brisbane and Lae in conjunction with Dr. A.G. Fenton.

I wish to thank Mr. M. Bowthorpe and Mr. G. Smith of the Antarctic Division for making the Wilkes 1964 flight data available to me. Acknowledgement is also due to Mr. John Boyd of the Antarctic Division for the Wilkes flight DN3 data and to all those members of the Australian National Antarctic Research Expeditions at Wilkes and Macquarie Island whose willing cooperation made the balloon flights possible.

I am indebted to the Department of Supply for permission to fly equipment at Mildura and in aprticular to Mr. E. Curwood, Project Leader at the Mildura Balloon Launching Station. Thanks are also due to Dr. R.R. Brown of the

University of California and to members of his group for allowing cur detectors to be hitch-hiked on their X-ray rigs at Macquarie Island.

Many members of the Physics Department staff assisted in the construction of the equipment and in the read-out of the data. Special acknowledgement is due to Mr. M. Mason who was responsible for the production of the corona regulator tubes and the geiger counters and for the preliminary construction = work on the neutron counters.

I am very grateful to all the members of the Hobart Cosmic Ray Group for their help and advice. Special thanks are due to Dr. A.G. Fenton, leader of the group and to Dr. K.B. Fenton, who supervised this work, for their invaluable assistance in the experimental programme and for encouragement and advice during the course of the work.

Finally my sincere thanks are due to my wife for typing this thesis.

Publications

1. "Radiation Enhancement Following Johnston Island Thermonuclear Explosion", Edwards, P.J., Fenton, A.G., Fenton, K.B., Greenhill, J.G., and Parsons, N.R., Nature, 196(4852), 367(1962)
2. "A Neutron Intensity Increase Observed At High Altitude in Association with an Auroral Zone X-ray Event", Parsons, N.R., Greenhill, J.G., Fenton, K.B., and Fenton, A.G., Proceedings of the Jaipur International

Conference on Cosmic Rays, Volume 2, 38-42 (1963).

3. "The Neutron Flux in the Upper Atmosphere During the 1964 Solar Minimum", Greenhill, J.G., Phillips, J., Fenton, K.B., Fenton, A.G., and Bowthorpe, M., Proceedings of the International Conference on Cosmic Rays, London, September 1965.

4. "Balloon Observations in the Southern Hemisphere by the Hobart Group", Fenton, A.G., Fenton, K.B., Greenhill, J.G., and Parsons, N.R.,, Bulletin of the Solar Particlws and Radiation Monitoring Organisation, in press November 1965.

CONTENTS

SUMMARY

CHAPTER I — An introduction to the demography of cosmic ray neutrons including a detailed description of neutron diffusion theory with special reference to diffusion in the atmosphere.

CHAPTER II — The design and performance of the detectors, flight unit electronics, telemetry system and receiving and recording equipment are described. The theory of frequency division multiplexing methods is described and applied to the optimisation of the telemetry system used in the experiments.

CHAPTER III — The experiments are described and smoothed curve counting rate data for a number of the balloom ascents tabulated.

CHAPTER IV — The energy sensitivity of the neutron detectors is discussed. Experimental data on the background and directional response of the detectors are presented and analysed. The contribution to the counting rate of neutrons produced in the detector materials is estimated for various altitudes and latitudes.

CHAPTER V — An increase in the neutron counting rate at high altitudes over Macquaries Island is described. This event occured at a time of high geophysical activity and was accompanied by intense bursts of auroral X-rays. Possible causes of the increase

are discussed and the neutron flux is estimated on the assumption that the event was genuine. The flux of protons, required to produce the neutrons by interactions with air nuclei, is estimated and shown to be barely compatible with riometer and other observations at the time of the event. Possible sources of such a proton flux increase are discussed.

CHAPTER VI — The results of the latitude survey measurements in August-October 1964 are described and compared with other experimental and theoretical data. Good agreement is obtained with the theoretical results of Newkirk (1963). Time variations in the neutron flux over Wilkes and Mildura are discussed and evidence is presented for a decrease between 1962 and 1964 in the absorption length of the neutron producing radiation over Macquarie Island. Differences between the neutron flux, measured in simultaneous flights from Wilkes and Macquarie Island, are discussed.

CHAPTER VII — The latitude dependence of the neutron leakage flux is estimated from the count rate variation at 15gm cm^{-2} and compared with various experimental and theoretical results.

CHAPTER VIII — It is shown that the latitude distributions of the slow neutron density are essentially the same as the counting rate distributions for our

detectors. These distributions are compared with the results of Lingenfelter (1963) and Soberman (1956) and significant differences are found to exist. The absolute neutron density distributions are evaluated by normalising our data to those of Miles (1964). The results are compared with other experimental and theoretical data and a value for the global average carbon 14 production rate is obtained. An anomaly in the literature on the efficiency of slow neutron detectors is discussed.

I THE PRODUCTION AND DISTRIBUTION OF COSMIC-RAY NEUTRONS IN THE ATMOSPHERE

1. Introduction

Because of their short half life (about 12 minutes) neutrons are not likely to arrive in the cosmic radiation from outside the solar system. It has been suggested (Swetnick et al 1952, Haymes 1959, Simpson 1963, Lingenfelter and Flamm 1964a) that the sun may make a minor contribution to the high altitude atmospheric neutron flux but the majority of cosmic ray neutrons are undoubtedly secondary products of the galactic and solar charged particle radiation. These high energy particles react violently with the air nuclei giving rise to the so-called nuclear stars. Protons and neutrons together with many other nuclear particles are produced in these reactions.

Many of the protons and neutrons have sufficient energy to cause further reactions of the same type and a chain reaction or nucleonic cascade is set up in the atmosphere. This so-called N radiation moves down through the atmosphere gradually being degraded in energy and intensity by nuclear disintegrations, ionisation, nuclear capture and elastic scattering.

1.2 Neutron production reactions.

There are two processes involved in neutron production by nuclear stars - the intra-nuclear cascade and the evaporation reaction. "Knock-on" neutrons having energies from a few Mev to several Bev are produced in an intra-nuclear cascade process. They have an angular distribution sharply peaked in the direction of the

incident particle and many have sufficient energy to initiate further stars. Neutrons with energy less than the lowest excited states of air nuclei (2.3 Mev in N^{14} and 6.05 Mev in O^{16}) cannot initiate further nuclear stars so that at lower energies they lose energy by elastic collisions only. Hess et al (1961) have estimated that 48% of knock-on neutrons either leak out of the atmosphere or are captured in (n,α) or (n,γ) reactions before reaching these energies.

At the conclusion of the intra-nuclear cascade reaction the nucleus is left in an excited state and returns to its ground state by "boiling off" one or more neutrons, protons or α particles together with emission of gamma rays. If the residual energy exceeds about 15 Mev the nucleus may break up completely into α particles, protons and neutrons (Muirhead and Rosser 1955). The neutrons produced in the evaporation process have directions isotropic in the centre of mass systems and a roughly Maxwellian energy distribution peaked at about 1 Mev. This can be represented by the expression

$$N(E)dE \propto E \exp\left(-\frac{E}{\theta}\right) dE \qquad (1.1)$$

where E is the neutron energy in Mev, θ = 1 Mev is the "nuclear temperature" and N(E)dE is the number of neutrons with energies between E and E + dE.

Hess et al (1961) have estimated from measurements of the low altitude neutron energy spectrum that the relative strengths of the knock-on and evaporation sources is about 1 to 4. Experiments (Camerini et al 1950 - see Hess et al 1961) with cosmic rays on nuclear emulsions suggest that the knock-on neutron energy spectrum may be represented by the expression

$$N(E)dE = kE^{-2} \exp(-160E^{-2})dE \qquad (1.2)$$

where E is in Mev. It seems probable however, that both this spectrum and the knock-on to evaporation source ratio will depend on the energy of the initiating particle (Fermi 1950, p.219).

1.3 Neutron demography

Elastic scattering is the main slowing down process for neutrons having energy less than a few Mev. The scattering mean free path is energy dependent but can be approximated by two constant values: 18 $gm.cm^{-2}$ for energies greater than 570 Kev and 2.8 $gm.cm^{-2}$ for lower energies. (Fujimoto and Tamura 1952). Most neutrons are captured in the $N^{14}(n,p)C^{14}$ reaction before reaching thermal energies (0.025 e.v.). This is a $\frac{1}{v}$ type reaction and Fermi (1950, p.184) has estimated that 87% of neutrons passing 100 Kev are captured to produce carbon 14 before being thermalised.

There have been several estimates of the relative importance of the various processes by which neutrons are removed from the atmosphere and these are set out in Table 1.1.

	Newkirk (1963)	Hess et al (1961)
Captured to form C^{14}	56%	64%
" " " H^3	2%	
Captured by (n,) and (n,) reactions	31%	19.4%
Leakage	11%	16.6%
Capture by the earth	-	<0.01%

Table 1.1 Cosmic ray neutron demography

In the lower atmosphere the average lifetime before capture is a fraction of a second so that neutron decay is relatively unimportant. Lingenfelter (1963) has estimated that loss by decay accounts for less than 0.5% of the neutrons produced in the atmosphere but that at very high altitudes (pressures of the order of 10 mb) it becomes a significant loss mechanism since the neutron slowing down time is almost inversely proportional to pressure.

1.4 Application of Diffusion Theory

The neutron sources discussed above, together with leakage from the atmosphere and absorption during thermalisation result in an equilibrium neutron energy spectrum. Given the spatial, energy and angular distribution of these sources together with the scattering and absorption parameters of the atmosphere and its boundaries it is possible in principle to calculate the neutron energy spectrum and spatial distribution by means of the neutron transport equation (Davisson 1957). This is a rigorous fundamental equation expressing the principle of conservation of neutrons but its solution is very difficult for most practical situations. (Hess et al 1961). The diffusion equation is an approximation to transport theory which subject to certain limitations (to be discussed later) can be expected to give accurate results when applied to the problem of neutron diffusion in the atmosphere.

In making a survey of the distribution of neutrons in the atmosphere we first study the distribution of the neutron source. We then discuss some of the methods of solution of the diffusion equation and compare the results of these solutions. Finally we compare these results with recent measurements.

1.5 The spatial distribution of neutron production.

(i) Equilibrium region

At atmospheric depths greater than about 200 gm.cm^{-2} the altitude and latitude distributions of the 10 Mev neutron flux and the parent N radiation are virtually identical (Yuan 1951, Simpson 1951). This is to be expected since the neutron diffusion mean free path is an order of magnitude less than the absorption mean free path of the N radiation. This part of the atmosphere is called the equilibrium region since there is spatial equilibrium between the neutron source, the low energy neutron flux and the capture processes. The energy spectrum depends only on the scattering and absorption parameters of the atmosphere and on the energy spectrum of the neutron source.

The fraction of neutrons produced by knock-on reactions and their energy distribution are functions of the energy of the N radiation and hence of altitude, latitude and solar activity. These effects are presumably not very significant however (due no doubt in part to the relatively small numbers of knock-on neutrons) and it is customary to assume that the neutron energy distribution is constant throughout the equilibrium region. Consequently the spatial distribution observed by neutron detectors is independent of the energy sensitivity of the detector and similar to the distribution of the N radiation.

There have been numerous measurements (Simpson 1951, Simpson and Fagot 1953, Meyer and Simpson 1955, Rose et al 1956, Soberman 1956, Storey 1960, Gauger 1964) of the altitude and latitude distribution of the low energy neutron flux and N radiation in the

equilibrium region although unfortunately only one of these (Meyer and Simpson 1955) gives any detailed information on the distribution at or near solar minimum. This measurement covers the geomagnetic latitude range from 40^{o} to 65^{o}N at an atmospheric depth of 312 $gm.cm^{-2}$. While further information for this period would be desirable the data are sufficiently comprehensive to enable us to obtain a fairly reliable picture of the distribution at most times during the solar cycle.

Broadly speaking, it is found that the flux, at a given atmospheric depth, increases with latitude until a "knee" is reached beyond which the level remains constant. The knee may be produced by either geomagnetic or atmospheric absorption effects and moves towards the poles with increasing altitude and decreasing solar activity. Three of these latitude distribution curves (copied from Lingenfelter 1963) are illustrated in figure 1.1. The shape of the curves is a function of solar activity since the intensity increases towards solar minimum with the increase being most marked at high latitudes.

It is frequently assumed that the intensity decreases exponentially with atmospheric depth and the effective attenuation length latitude dependence is illustrated in figure 1.2 (copied from Lingenfelter 1963). However, Simpson and Fagot (1953) have shown that the attenuation length is a strong function of altitude particularly at low latitudes and significant errors may be introduced by ignoring this factor. The absorption length decreases with increasing atmospheric depth as a result of the degradation in energy of the N radiation.

The energy of this radiation is dependent on the energy distribution of the primary cosmic rays and there-

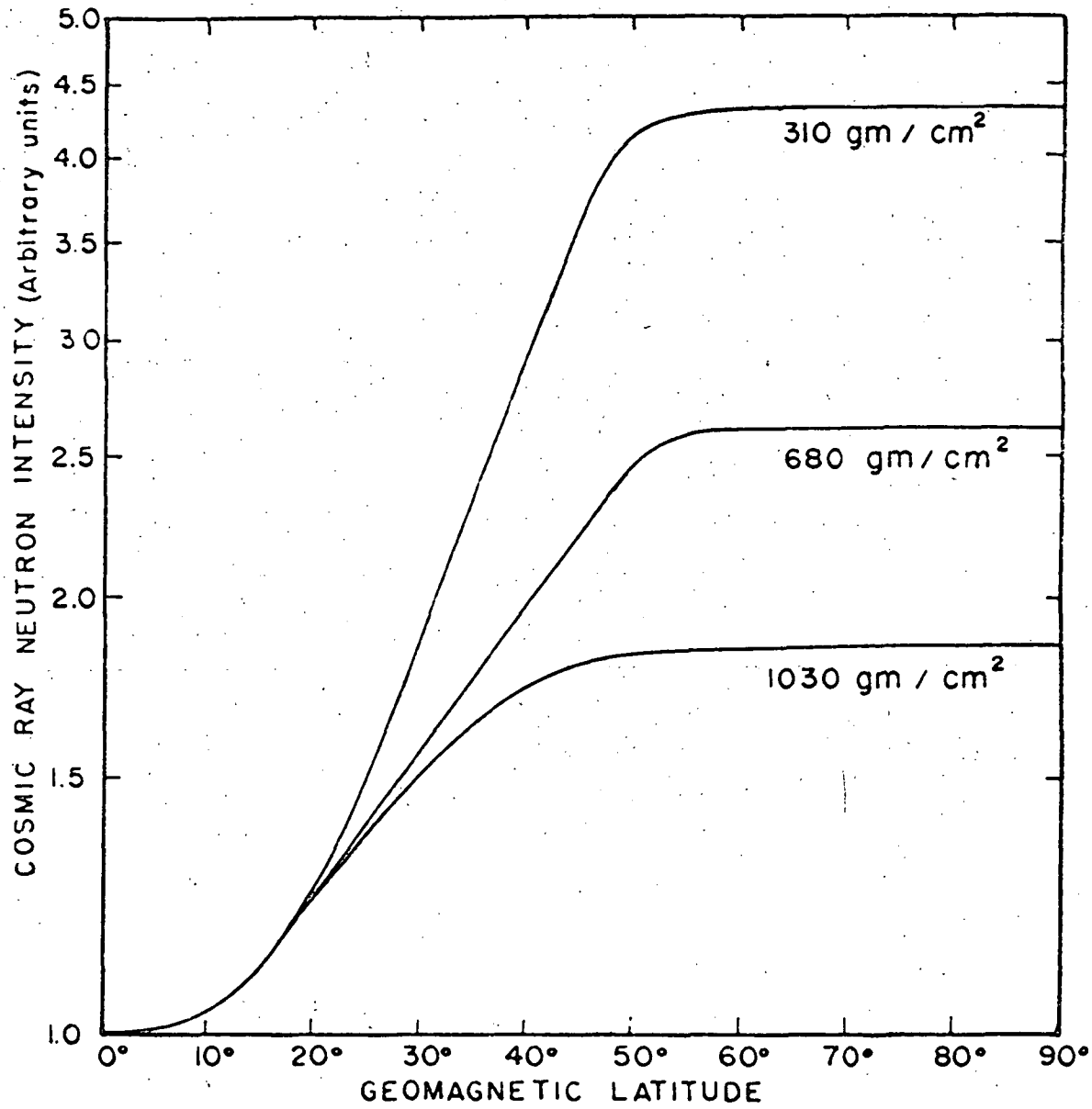

Figure 1.1. The latitude variation of the solar minimum cosmic-ray neutron intensity at 1030, 680 and 312 gm cm^{-2}. Copied from Lingenfelter (1963).

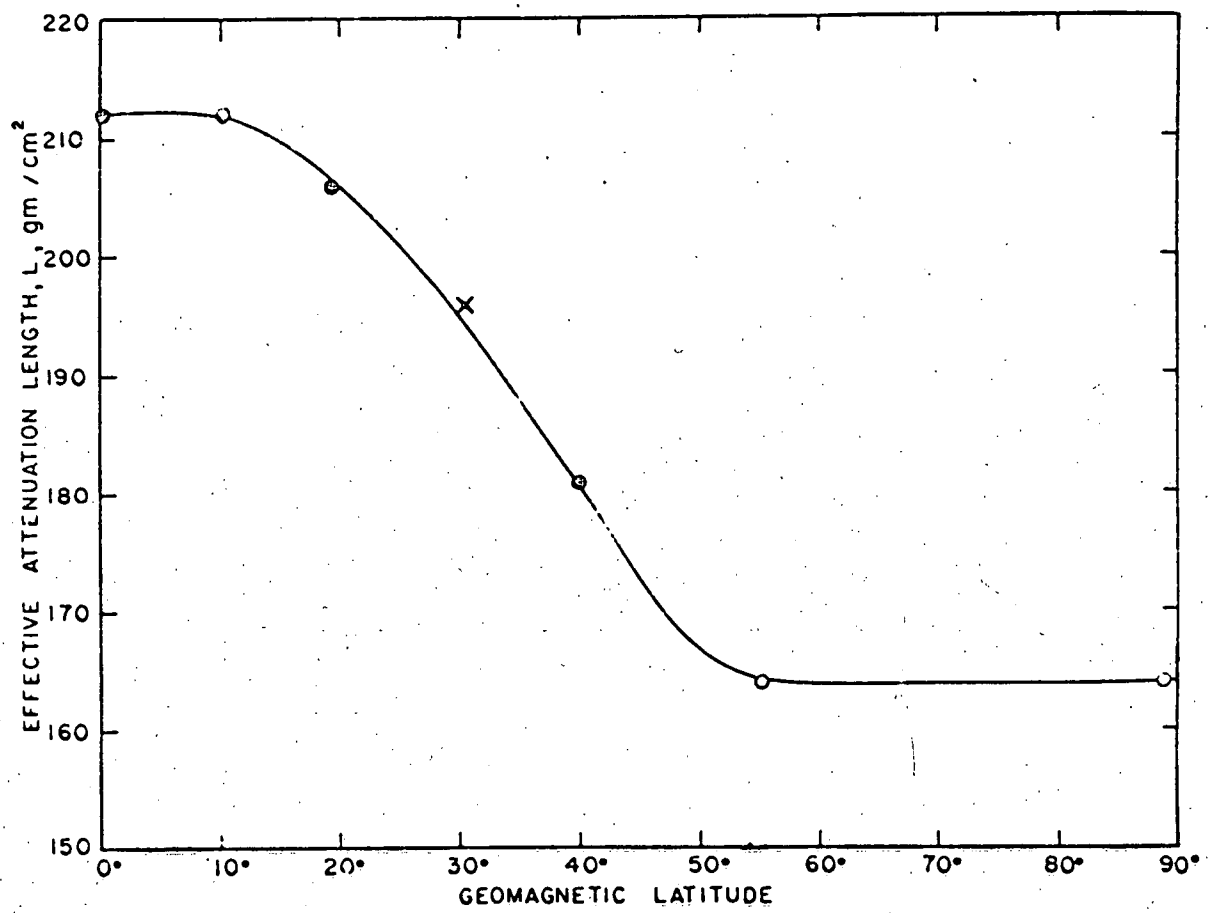

Figure 1.2. The effective attenuation length L of the cosmic-ray neutron intensity from 200 to 1033 gm cm^{-2}. Copied from Lingenfelter (1963).

fore on solar activity. Consequently we might also expect the absorption length to vary during the solar cycle. We will discuss the evidence on this subject in a later chapter but it would appear that the variation is small (Lingenfelter 1963) and can be ignored for most purposes.

(ii) Scattering and absorption at the earth's surface

In the region within about 100 gm/cm^2 of the earth's surface reflection and absorption by the surface materials destroy the balance between neutron production and absorption. The effect of this on the neutron energy spectrum depends on the properties of the surface materials and on the distance from the surface. Bethe et al (1940) estimated a 5:1 reduction in the fast neutron flux immediately above an extended water surface. Consequently the N radiation distribution can only be measured with detectors such as the neutron monitor which are insensitive to neutrons below about 10 Mev.

(iii) The upper atmosphere

At atmospheric depths less than about 200 $gm.cm^{-2}$ leakage of neutrons into space causes an increasing divergence with altitude of the neutron flux distribution from the neutron source. Many neutrons leak out of the atmosphere before being slowed down, and the mean neutron energy increases with altitude. Consequently the production rate distribution must be obtained by direct measurement. Unfortunately there is very little information on the production rate in this region. The only direct measurements are those of Lord (1951) who obtained the altitude variation in the production rate of three to five pronged stars at geomagnetic latitudes between 52° and 56° N.

In addition Addario and Tamburino (1949) have measured the relative frequency of star sizes in nuclear emulsions at an altitude of 29,000 meters. There is unfortunately, no information on the altitude dependence of the neutron production rate at other latitudes or times during the solar cycle. Lingenfelter (1963) has estimated the distribution by interpolating from the known production rate at 200 $gm.cm^{-2}$ to the observed variation of the primary cosmic ray intensity at the top of the atmosphere. This distribution is normalised to the production rate of three to five pronged stars at 0 $gm.cm^{-2}$ and $55^{o}N$ geomagnetic, obtained from the measurements of Lord (1951) by extrapolation from 15 $gm.cm^{-2}$.

Similar curves were obtained for periods other than the time of Lord's measurements, by using the relevant latitude distributions at 0 and 200 $gm.cm^{-2}$ and assuming that the shape of the altitude distribution at the equator is independent of solar activity. The solar minimum neutron production curves for various geomagnetic latitudes are illustrated in figure 1.3 (copied from Lingenfelter 1963).

There is some doubt about the reliability of these curves however, since the high altitude data are based partly on the latitude variation of the primary intensity. Lingenfelter and Flamm (1964a) have shown that the neutron production cross-sections increase rapidly with primary energy and consequently the latitude variation of the neutron production rate will be significantly less than that of the primary cosmic ray intensity. This effect will be most pronounced at low rigidities where the production rate per gram of air changes most rapidly. The data of Lingenfelter and Flamm (1964a)

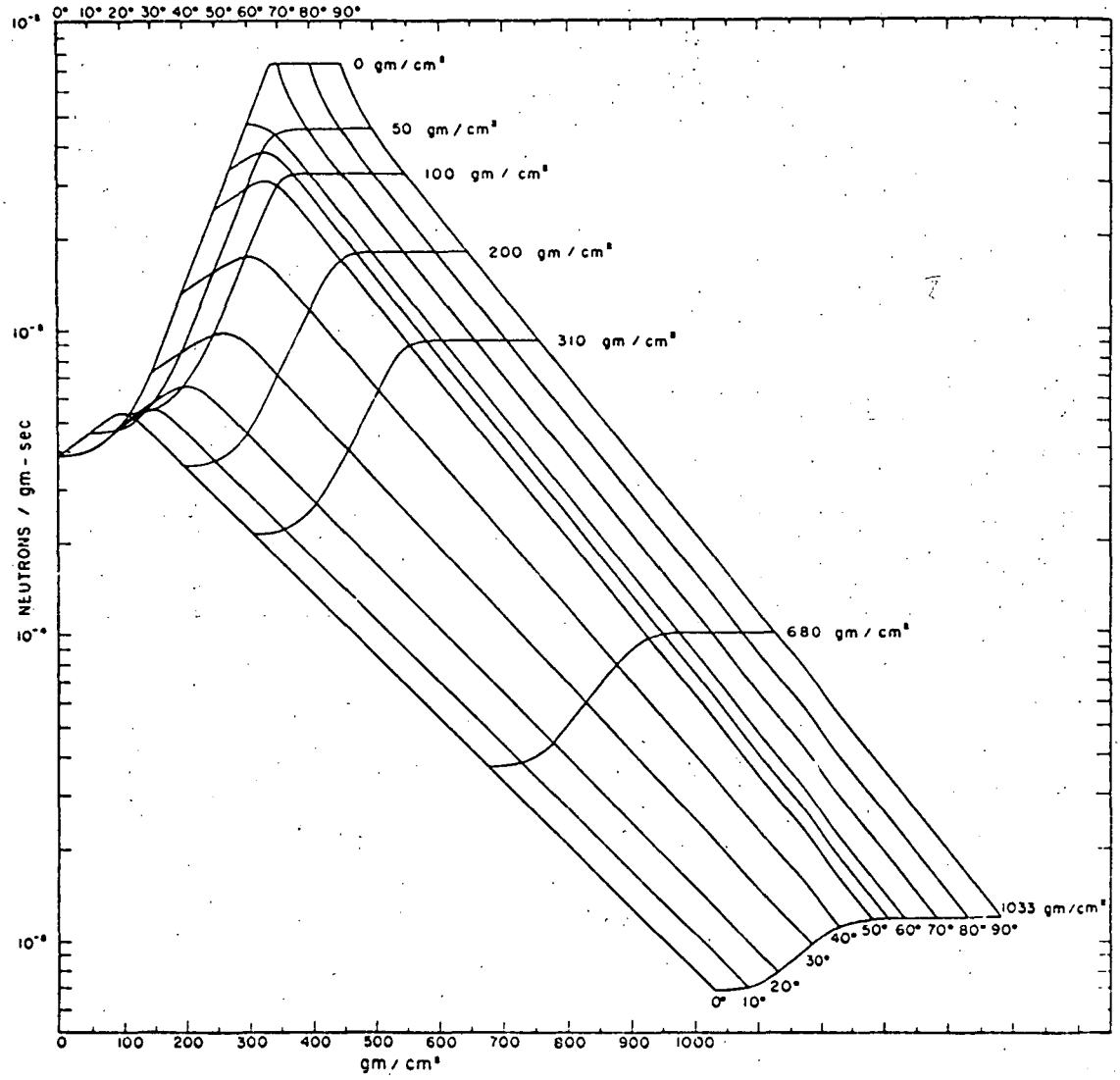

Figure 1.3. The solar minimum cosmic-ray neutron production rate in neutrons/g sec as a function of altitude, g/cm^2, and geomagnetic latitude, normalized to a total production rate of one neutron per square centimeter column of air per second at the geomagnetic pole.

show for example that the neutron production rate of 1.5 Bv protons is at least five times that of 0.5 Bv protons.

The production cross-sections are not sufficiently well known at high energies to enable us to evaluate the neutron source in this way and further measurements of the production distribution would be helpful in checking the results of Lingenfelter (1963).

1.6 The Neutron Transport Equation.

Many analytic solutions of the spatial and energy distribution of neutrons in the atmosphere have been published (Bethe et al 1940, Flügge 1943, Fujimoto and Tamura 1952, Galli 1953 and others). Recently Hess et al (1961) and Lingenfelter (1963) have obtained more detailed numeric solutions using high speed electronic computers. All these calculations are based on the age diffusion approximation to the rigorous neutron transport equation (Marshak 1947, Sneddon 1951, Davison 1957).

The time dependent form of the transport equation is

$$\frac{\partial N}{\partial t}(r,\Omega,u,t) + v\Omega \cdot \text{grad } N(r,\Omega,u,t) = -\frac{vN}{l(u)}(r,\Omega,u,t) + \int_0^u du' \int \frac{v'N}{l_s(u')}(r,\Omega,u',t)F(\mu_o,u-u')d\Omega' + S(r,u,t) \quad \ldots (1.3)$$

where: $N(r,\Omega,u,t)d\Omega du$ is the density at time t and position r of neutrons with u lying between u and u + du and directions between Ω and $\Omega + d\Omega$. r is the position vector.

$u = \log(E_o/E)$ is called the lethargy of the neutron. In elastic scattering by a nucleus the

change in lethargy per collision is independent of E.

E is the neutron energy and E_o is some arbitrary value of E.

Ω is the unit direction vector of the neutron velocity.

v is the neutron speed.

l(u) is the neutron total mean free path given by $\frac{1}{l(u)} = \frac{1}{l_s(u)} + \frac{1}{l_c(u)}$ where $l_s(u)$ and $l_c(u)$ are the scattering and capture mean free paths respectively.

$F(\mu_o, u-u')$ is the scattering probability function and is the relative probability of a neutron being left with direction and energy (Ω, u) as a result of a collision before which it had the parameters (Ω', u'). It is normalised so that

$$\int_o^u \int F(\mu_o, u-u')du'd\Omega = 1$$

$\mu_o = \Omega . \Omega'$

S(r,u,t) is the source function and is the number of neutrons being produced per unit time and volume at the point whose position vector is r. The source is assumed here to be isotropic but it is of course not necessarily so.

The left hand side of equation (1.3) is the time rate of change of the distribution function N moving with the neutron stream in the direction Ω and is derived in a manner analagous to the derivation of the equation of continuity in hydrodynamics. In the steady state condition $\frac{\partial N}{\partial t}$ is zero and $v\Omega.\text{grad } N$ represents the change, per unit time, in the number of neutrons (with direction Ω and lethargy u) in a unit volume element at r, due to particles

streaming through the volume element without collision.

The first term $\frac{vN}{l(u)}$ on the right hand side of (1.3) represents the number of neutrons with velocity $v\Omega$ which are removed, per unit time, from the volume element due to scattering and capture changing their velocity and/or direction. The second term gives the number of neutrons having other directions and (higher) energies which are scattered into the volume element with direction Ω and lethargy u. The third term is the source function.

1.7 The Age Equation.

The age equation may be derived from the time independent form of the transport equation under certain restricted conditions by making several simplifying approximations. It may also be derived directly by simple arguments involving the conservation of neutrons (Fermi 1950). The former method has the advantage of making evident the nature of the limitations of age theory. In appendix I we derive the age equation from the neutron transport equation (1.3) following the method of Marshak (1947), Marshak et al (1949) and Sneddon (1951).

In deriving the age equation we assume that neutron scattering is spherically symmetrical in the centre of mass system. This assumption is justified provided:

(i) Inelastic scattering may be neglected. Neutrons may make inelastic collisions with nitrogen at energies as low as 2.3 Mev but elastic scattering dominates at energies up to at least 4 Mev (Fujimoto and Tamura 1952).

(ii) The effects of chemical binding may be neglected. In air most neutrons are captured before reaching energies at which chemical binding has any significant effect on scattering (Bethe et al 1940).

(iii) Elastic scattering is isotropic in the centre of mass system. This implies S wave scattering which adequately describes the interaction provided the De Broglie wavelength of the neutron is large by comparison with the nuclear diameter. In air this corresponds to the condition that $E << 1.6$ Mev. However, deviations from S-scattering are usually insignificant by comparison with the effects of inelastic scattering (Marshak 1947).

In spite of the limitations noted above, scattering in nitrogen and oxygen is not highly anisotropic at energies below 10 Mev (Lingenfelter 1963) and age diffusion theory may be used.

The age equation without capture may be written:

$$\frac{\partial \chi}{\partial \tau}(z,\tau) = \frac{\partial^2 \chi}{\partial z^2}(z,\tau) + T(z,\tau) \qquad (1.4)$$

where τ is called the symbolic age and is defined by

$$= \frac{1}{3}\int_0^u \frac{l^2(u')}{\xi(1 - \langle\cos\theta\rangle_{AV})}\,du' \qquad (1.5)$$

$\langle\cos\theta\rangle_{AV}$ is the average value of $\cos\theta$ where θ is the scattering angle in the laboratory system. In appendix I we show that

$$\langle\cos\theta\rangle_{AV} = \frac{2}{3M}$$

where M is the atomic weight of the scattering nucleus.

ξ is the average logarithmic energy loss or change in lethargy per collision

$$\xi \simeq 2/M \text{ for large M.}$$

$\chi(z,\tau)$ is called the slowing down density and

represents the number of neutrons per unit volume per unit time which reach the age τ .

$$\chi(z,\tau) = \xi \frac{vN}{l(u)} (z,u) \qquad (1.7)$$

The source function $T(z,\tau)$ is related to the source function in (1.3) by

$$T(z,\tau) = 4\pi S(z,u) \frac{\partial u}{\partial \tau}$$

1.8 The Age Equation with Capture

If the neutron capture cross section is small and a slowly varying function of energy we may derive the age equation with capture following the same procedure as for the capture free case. Then

$$\frac{\partial \chi}{\partial \tau}(z,\tau) + \frac{3}{l_a l_t}(z,\tau) = \frac{\partial^2 \chi}{\partial z^2}(z,\tau) + \delta(z)\delta(\tau) \qquad (1.8)$$

where l_a is the absorption mean free path,

l_t is the transport mean free path defined by

$$l_a = \frac{l(u)}{1 - \langle \cos\theta \rangle_{AV}}$$

and δ is the Dirac delta function implying a plane neutron source at $z = 0$.

Equation (1.8) may be simplified by putting

$$\chi = \chi' \exp\left[- \int_0^u \frac{\sigma_a}{\xi\sigma} du' \right] \qquad (1.9)$$

where σ, σ_a are the total and absorption cross sections respectively. Then (1.8) becomes

$$\frac{\partial \chi'}{\partial \tau} = \frac{\partial^2 \chi'}{\partial z^2} + \delta(z)\delta(\tau) \qquad (1.10)$$

Thus the linear absorption term may be factorised out and the solution is of the form

$$\chi(z,\tau,h) = \chi(z,\tau)H(h) \qquad (1.11)$$

where $h = \sigma_s/\sigma$ is a function of energy and

$$H(h) = \exp\left[-\int_0^{\tau} \frac{\sigma_a}{l_t}\, d\tau'\right]$$

$$= \exp\left[-\int_0^{u} \frac{\sigma_a}{\xi\sigma_s}\, du'\right] \qquad (1.12)$$

We may therefore include the effects of absorption simply by multiplying the solution for no absorption by the factor H(h) defined by equation (1.12). This method is valid only for single element moderators or mixtures for which $\sigma_a/\xi\sigma_s$ is the same for all elements. This is not true of air since the capture cross section for oxygen is insignificant by comparison with that for nitrogen. However, the effects of capture are relatively small in air except at near thermal energies and this condition can be ignored in analytic solutions of the cosmic ray neutron distribution.

1.9 The Limitations of Age Theory

The assumptions made in deriving the age equation lead to five restrictions on its range of applicability. We require that

(i) The mean free path does not vary appreciably within any collision interval of energy.

(ii) The number of collisions experienced by the neutron is large.

(iii) The distance from the source is not too great.

(iv) The neutron capture cross section is small and varies slowly with energy.

(v) The distance from boundary regions is large compared with the mean free path.

Conditions (i) and (iv) are well satisfied for neutrons in the atmosphere. In appendix II we show that condition (ii) is satisfied for atmospheric neutrons having initial energy $\gtrsim$ 1 Mev provided $\tau \gg 110$ gm^{2}cm^{-4}. We also show that condition (iii) implies that age theory is satisfactory for $z \lesssim 90$ gm.cm^{-2} from the point of production. Marshak (1947) has shown that at greater distances from the source age theory tends to underestimate the neutron flux. Consequently calculations based on age theory will underestimate the neutron flux at large z for solar cosmic rays where neutron production is confined to a thin layer near the top of the atmosphere. Age theory will, however, be more reliable for neutrons from galactic cosmic rays because of the distributed nature of the neutron source.

Condition (v) limits the reliability of the age equation within one or two mean free paths of the top of the atmosphere. The neutron flux decreases towards the boundary and a linear extrapolation of the distribution in this region requires the flux to vanish at some definite extrapolation distance beyond the boundary. In appendix III we show that the condition that the incoming neutron current across the z = 0 plane be zero is given by

$$\chi(z,\tau) - \frac{2}{3} l_t \frac{\partial \chi}{\partial z} = 0 \qquad (1.13)$$

at z = 0 for all .

Equation (1.13) implies that the extrapolated value of the slowing down density is zero at $z = -\frac{2}{3} l_t(u)$. This value of z is called the extrapolated end point z_o of the slowing down density. It can be shown from transport theory (Glasstone and Edlund 1952, p.104) that in order to make the results more nearly correct at reasonable distances from the boundary we should use an extrapolated end point

$$z_o = 0.71\, l_t \qquad (1.14)$$

The actual distribution and the diffusion theory results using the two different end points are illustrated for the boundary region in figure (1.4) (copied from Glasstone and Edlund 1952, p.105). The ratio of the actual flux at $z = 0$ to the flux calculated by diffusion theory (using (1.14) as boundary condition) is 0.81 (Glasstone and Edlund 1952, p.403).

1.10 Analytic Solutions of the Atmospheric Neutron Distribution.

(i) Plane neutron source.

To illustrate some of the problems involved in evaluation of the neutron flux in the atmosphere we will discuss the analytic method of Fujimoto and Tamura (1952). They calculate the Green function $G(\tau,z,z')$ for the age equation; that is the solution for a mono-energetic delta function neutron source at z'. Then

$$\frac{\partial G}{\partial \tau}(\tau,z,z') = \frac{\partial^2 G}{\partial z^2}(\tau,z,z') \qquad (1.15)$$

and $G = \delta(z - z')$ at $\tau = 0$

Using the boundary conditions

(i) $G(\tau,z) \to 0$ as $z \to \infty$ for all τ

(ii) $G(\tau,z) - \frac{2}{3} l_t(u) \frac{\partial G}{\partial z} = 0$

at $z' = 0$ for all τ

it may be shown (Marshak 1947) that

$$G(\tau,z,z') = \frac{1}{\sqrt{2\pi\tau}}\left[\exp - \frac{(z-z')^2}{4\tau} + \exp - \frac{(z+z')^2}{4\tau}\right]$$

$$- \frac{3}{2l_t} \exp\left[\frac{9\tau}{4l_t^2} + \frac{3(z+z')}{2l_t}\right]\left[1 - \operatorname{erf} \frac{3\sqrt{\tau}}{2l_t} + \frac{z+z'}{2\sqrt{\tau}}\right]$$

. . . . . (1.16)

where erf x is the error function.

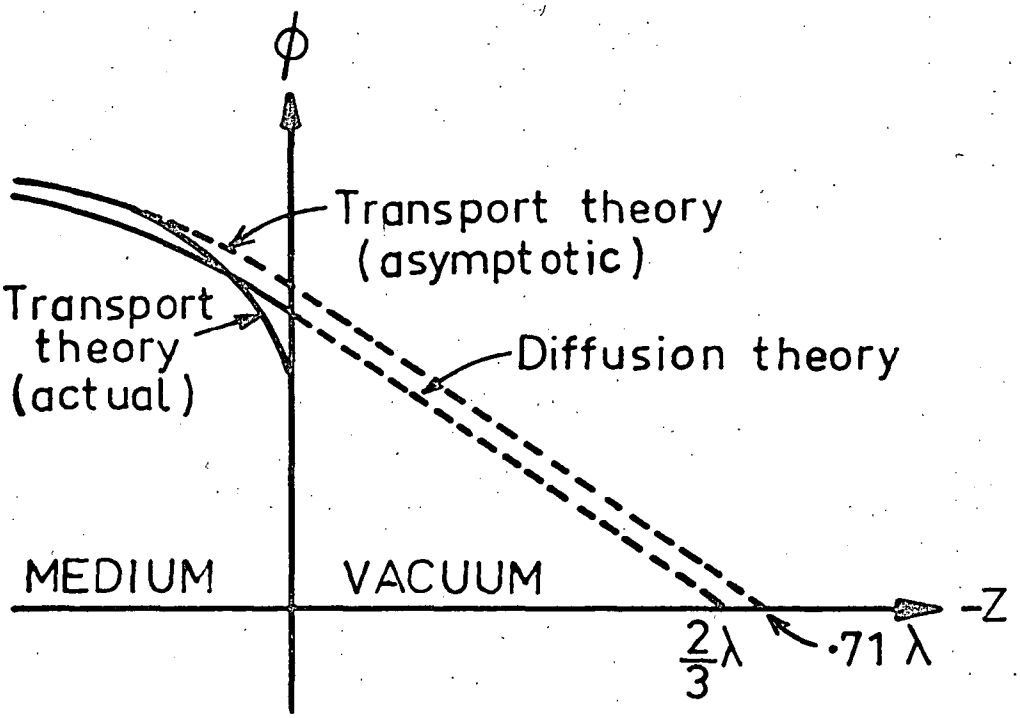

Figure 1.4. Transport theory and diffusion theory extrapolations. (from Glasstone and Edlund 1952).

Fujimoto and Tamura (1952) have assumed that $l(u)$ may be approximated by

$$l(u) = \begin{cases} 18 \text{ gm.cm}^{-2} & \text{for } 570 \text{ Kev} < E < 4 \text{ Mev} \\ 2.8 \text{ gm.cm}^{-2} & \text{for } 0.26 \text{ ev} < E < 570 \text{ Kev} \end{cases}$$

They also assume that all neutrons have initial energy 4 Mev and are captured at 0.26 ev with no capture at intermediate energies. Then, provided $A^2\tau \gg 1$, equation (1.16) may be written

$$G(\tau,z,z') = \frac{1}{\sqrt{2\pi\tau}}\left[\exp - \frac{(z-z')^2}{4\tau} - \frac{2A\tau - z - z'}{2A\tau - z + z'} \exp -\frac{(z+z')^2}{4\tau}\right]$$

where $A = 3/2l_t$ . . . . . (1.17)

Figure (1.5) shows the slowing down density at 570 Kev ($\tau = 1570$ gm^{2}cm^{-4}) for neutrons from a 4 Mev plane source at $z' = 0.2\sqrt{\tau}$, $0.6\sqrt{\tau}$, $\sqrt{\tau}$ and $3\sqrt{\tau}$ (8, 24, 40 and 120 gm.cm^{-2}). It will be noted that, for sources near the top of the atmosphere, the peak in the density distribution is not much dependent on the position of the source. The area under the curves (that is the integrated slowing down density) decreases for sources near the top of the atmosphere (small z'). This is a consequence of neutron leakage into space: many neutrons are lost before being slowed down to 570 Kev. This results in an increase in the mean neutron energy; that is a hardening of the neutron energy spectrum. The loss is small at depths greater than about $2\sqrt{\tau}$ (80 gm.cm^{-2}) so the neutron energy spectrum above 570 Kev is not much affected by leakage.

The Green function $G(z,z')$ is symmetrical with respect to z and z'. Thus it also represents the contribution to the slowing down density at z' of a plane neutron source at z. It is apparent from figure (1.5) that most of the neutrons near the

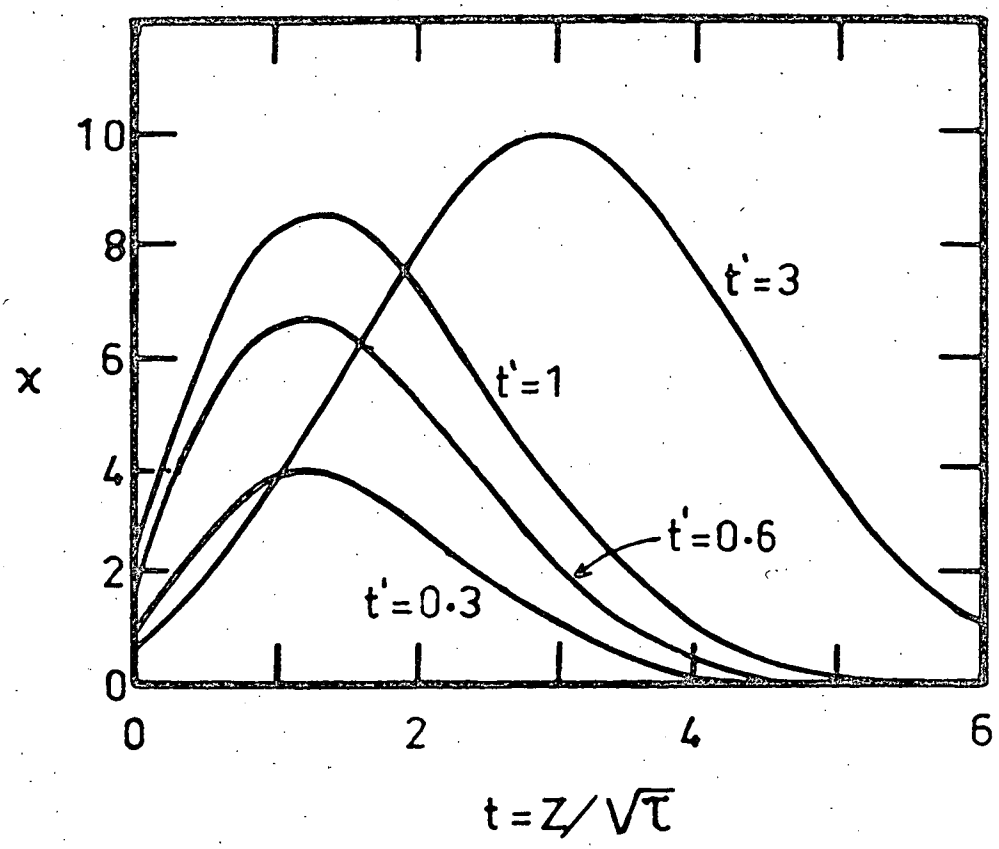

Figure 1.5. Slowing down density distributions at 570 Kev (τ = 1600 gm cm^{-2}) for neutrons from a 4 Mev plane source at various altitudes t'. t & t' are atmospheric depths measured in units of τ_1 (40 gm cm^{-2}).

boundary (for example at $z' = 0.2\sqrt{\tau} = 8$ gm.cm^{-2} in figure 1.5) come from lower in the atmosphere at depths of the order of $\sqrt{\tau}$ (40 gm.cm^{-2} in this case). There is therefore a net upward flux of neutrons in the boundary region.

At $z' = 3\sqrt{\tau}$ (120 gm.cm^{-2} in this example) $G(z,z')$ is almost symmetrical about $z = 3\sqrt{\tau}$ and the flux is therefore almost isotropic. A non uniform source distribution will affect this isotropy however, and may even result in a net downward movement of neutrons in this region.

It should be noted that the numerical values given above apply only to neutrons produced with an energy of 4 Mev. Many neutrons have higher initial energy and their age at 570 Kev will consequently be greater.

The age of neutrons slowing down from 570 Kev to 0.26 ev (the mean energy for capture by N^{14}) is 280 gm^{2}cm^{-4}, which is much less than that from 4 Mev to 570 Kev. Consequently the slowing down density distribution at 0.26 ev does not differ much from that calculated above except within about $2\sqrt{\tau}$ (~30 gm.cm^{-2}) of the top of the atmosphere.

(ii) Distributed neutron source.

The slowing down density for a mono-energetic source function $S(z')$ is

$$\chi(z,\tau) = \int_0^\infty G(\tau,z,z')\, S(z')\, dz' \qquad (1.18)$$

Fujimoto and Tamura use a source function similar to that measured by Lord (1951)

$$S(z') = \begin{cases} J_o \exp - a/L & \text{for } z' < a \\ J_o \exp - z'/L & \text{for } z' > a \end{cases} \qquad (1.19)$$

where $a = 100$ gm.cm^{-2} and $L = 140$ gm.cm^{-2}.

Then, assuming constant mean free path

$$\chi/J_o = \tfrac{1}{2}\left\{2 \text{ erf } \frac{z}{2\sqrt{\tau}} - \text{erf } \frac{z-a}{2\sqrt{\tau}} - \text{erf } \frac{z+a}{2\sqrt{\tau}}\right\} e^{-a/L}$$
$$+ \tfrac{1}{2} e^{\tau/L^2}\left\{1 + \text{erf } \left(\frac{z-a-2\tau/L}{2\sqrt{\tau}}\right)\right\} e^{-z/L}$$
$$+ \tfrac{1}{2} e^{\tau/L^2}\left\{\frac{LA+1}{LA-1}\right\}\left\{1 - \text{erf } \left(\frac{z+a+2\tau/L}{2\sqrt{\tau}}\right)\right\} e^{z/L}$$
$$+ \frac{2\sqrt{\tau}e^{-a/L}}{\sqrt{\pi}} \cdot \frac{e^{-z^2/4\tau}}{2A\tau + z} + \frac{2\sqrt{\tau}e^{-a/L}}{\sqrt{\pi}}\left\{\frac{1}{LA-1}\right\}\frac{e^{-(z+a)^2/4\tau}}{2A\tau + a + z}$$
. . . . . (1.20)

This equation represents the distribution in space and energy of neutrons with 570 Kev < E < 4 Mev for the neutron source specified by equation (1.19). We may evaluate the spatial distribution of 570 Kev neutrons by inserting numerical values into this equation and use this distribution as a source function $S(z')$ in a similar integration to determine the distribution of 0.26 ev neutrons.

(iii) <u>The Altitude Distribution of Slowed Down Neutrons</u>.

Inserting numerical values into equation (1.20) we can show that, to within a few per cent, for $z > 20$ gm.cm^{-2} and $E = 570$ Kev ($\tau = 1600$ gm^{2}cm^{-4}).

$$\frac{\chi}{J_o} = A(z,a,L) + B(z,a,L)e^{-z/L} + D(z)e^{-z^2/6400}$$
. . . . . (1.21)

The first term is a strong function of z but becomes

insignificant at about 200 gm.cm^{-2}. B(z) is also strongly dependent on z and tends to unity as z increases. It becomes essentially constant at about 250 gm.cm^{-2}. D(z) is only slightly dependent on z and the whole of the third term becomes insignificant for z > 100 gm.cm^{-2}. Thus, for z > 200 gm.cm^{-2}

$$\chi \propto J_o\, B(z,a,L)\, e^{-z/L} \qquad (1.22)$$

which reduces to a simple exponential function of z and L at z > 250 gm.cm^{-2}. In other words the slowing down density (and hence the flux) is directly proportional to the neutron production rate as noted in section (1.5).

(iv) Neutron Energy Spectrum.

The energy spectrum of E > 570 Kev neutrons may be evaluated from equation (1.20) using the relation

$$\phi(z,E)dE = \frac{l_t}{\xi}\, \chi(z,\tau)\, \frac{dE}{E} \qquad (1.23)$$

where $\phi(z,E)$ is the neutron flux $N(z,u)v$. Fujimoto and Tamura's calculations show that for z > 220 gm.cm^{-2}, $\phi(z,E)dE \propto E^{-1}$ except for z > 1 Mev when age theory breaks down. This distribution is normal for any moderator in the absence of capture provided the scattering cross sections are independent of energy (Newkirk 1963). Fujimoto and Tamura's equations could be improved if the effects of capture were included using the method outlined in section (1.8). Measurements by Hess et al (1959) and recent calculations (Newkirk 1963) which allow for capture and energy dependent scattering cross sections, indicate that, in the equilibrium region of the atmosphere, the flux spectrum is $\propto E^{-0.9}$ for 1 ev< E <10^5ev.

As $z \rightarrow 0$ more and more neutrons leak out of the atmosphere before being slowed down. Consequently the spectrum becomes harder and at $z = 0$, $\phi(z,E) \propto E^{-0.9}$ (not corrected for capture effects). This should be compared with the results of the more sophisticated theories of Lingenfelter (1963) and Newkirk (1963) for which $\phi(z,E) \propto E^{-0.8}$ at $z = 0$.

1.11 Numerical Solutions.

(i) Introduction

A serious weakness of the analytic methods discussed in the previous section is the assumption of a mono-energetic source. As a consequence of this assumption the calculated energy spectrum bears little relation to the actual spectrum in the energy region above about 100 Kev where source neutrons form a significant fraction of the total population (Hess et al 1959). The development of high speed computers has made practical the numeric solution of neutron diffusion problems. Two such methods are the Carlson multigroup S_n approximation to the transport equation and the multigroup diffusion method. The S_n method is not limited by the diffusion approximation and is therefore more accurate in boundary regions than methods based on diffusion theory (Newkirk 1963).

(ii) The multigroup diffusion equations.

The multigroup diffusion equations may be derived from the age equation using the procedure described by Erlich and Hurwitz (1954). In this method the energy range is divided into a number of discrete intervals and the age-diffusion equation reduces to a set of coupled ordinary differential

equations called multigroup equations. These may be solved in turn to give the average flux for each energy interval.

We now describe the procedure used by Erlich and Hurwitz (1954) in deriving the multigroup equations. The age equation with capture may be written in the form

$$-\frac{1}{3\xi\sigma_s\sigma_t}\nabla^2\chi(r,u)+\frac{\sigma_a}{\xi\sigma_s}\chi(r,u)=-\frac{\partial\chi}{\partial u}(r,u)+S(r,u) \qquad (1.24)$$

assuming the cross sections to be constant in a given spatial region.

We now integrate equation (1.24) with respect to u over the logarithmic energy range U_i corresponding to the i'th energy group. We then obtain

$$-U_i\left[\frac{1}{3\xi\sigma_s\sigma_t}\nabla^2\chi\right]_{i_{av}}+U_i\left[\frac{\sigma_a}{\xi\sigma_s}\chi\right]_{i_{av}}=-\chi_i^o+\chi_i^1+\int_{U_i}S(r,u)du \qquad (1.25)$$

where χ_i^o is the value of χ at the high u end of the i'th energy group and χ_i^1 is the value of χ at the low end. Thus χ_i^1 is the degradation into the group from higher energies and χ_i^o is the degradation out into the lower energy (i + 1)'th group.

We now make the assumption that the average of the products in equation (1.25) may be replaced by the product of the averages. This approximation is valid provided and the cross sections do not change radically over the energy group. This is an important condition in the choice of the energy subdivisions. Equation (1.25) now becomes

$$-\left[\frac{U}{3\xi\sigma_s\sigma_s}\right]_{i_{av}} \nabla^2(\chi)_{i_{av}} + \left[\frac{U\sigma_a}{\xi\sigma_s}\right]_{i_{av}} (\chi)_{i_{av}} + \chi_i^o = \chi_i^1 + \int_{U_i} S(r,u)du$$

. . . . . (1.26)

To solve (1.26) we must postulate some relationship between $(\chi)_{av}$, χ^o and χ^1. This is taken to be of the form

$$(\chi)_{av} = \omega_1 \chi^1 + \omega_2 \chi^o \qquad (1.27)$$

where ω_1 and ω_2 are appropriately chosen constants. Several choices of constants may be used, depending on the particular problem, but the simplest is to put $\omega_1 = \omega_2 = \frac{1}{2}$; that is to assume that χ varies linearly over each energy group. Then equation (1.27) may be written

$$-\left[\frac{U}{3\xi\sigma_s\sigma_t}\right]_{i_{av}} \nabla^2(\chi)_{i_{av}} + \left\{\left[\frac{\sigma_a U}{\xi\sigma_s}\right]_{i_{av}} + 2\right\}(\chi)_{i_{av}}$$

$$= 2\,\chi^o_{+i-1} + \int_{U_i} S(r,u)du \qquad (1.28)$$

where $\chi^o_{i-1} = \chi^1_i$ is the slowing down density at the upper energy limit of the i'th group.

(iii) Multigroup solutions of the atmospheric neutron distribution.

The multigroup diffusion method makes practical the solution of the atmospheric neutron diffusion problem with a neutron source which is a complex function of energy and atmospheric depth. The scattering and absorption cross sections need not be restricted to simple functions of energy. Being derived from the age equation the multigroup equations are subject to the same restrictions as

age-theory and are not as reliable in boundary regions as the rigorous transport equation.

Hess et al (1961) and Lingenfelter (1963) have used the multigroup method to determine the distribution of cosmic ray neutrons in the atmosphere. Hess et al (1961) used a neutron production distribution which was an exponential function of atmospheric depth and normalised their results to observations in 1956-1957 by Hess et al (1959) at a geomagnetic latitude of 44°N. The energy distribution of the source neutrons was determined on the assumption that 89% were evaporation neutrons and the remainder originated in knock-on reactions (section 1.2).

Lingenfelter (1963) used the same energy distribution for the source neutrons and calculated the atmospheric neutron flux for geomagnetic latitude from 0° to 90° in 10° steps for both solar minimum and solar maximum. The altitude and latitude dependence of the source functions were derived from equilibrium region measurements and the latitude variation of the primary cosmic ray flux in the manner described in section (1.5). Having calculated the spatial and energy distribution of the neutron flux, Lingenfelter (1963) obtained the carbon 14 production rate distribution by integrating the flux spectrum times the $N^{14}(n,p)\ C^{14}$ cross section over energy. Finally he normalised these results to data from sixteen measurements of the slow neutron density: three in 1948-1949 by Yuan (1951) at 52°N geomagnetic, seven in 1952-1954 by Soberman (1956) at 10°, 55° and 88°N, five in 1957 by Hess et al (1959) at 36°, 48° and 58°N and one in 1960 by Reidy et al (1962) at 49°N. The only data published are the latitude and altitude distributions of the carbon

14 production rate (Lingenfelter 1963) and the spectrum of the leakage flux at $\lambda = 0^{o}$, 40^{o} and 90^{o} (Lingenfelter 1963a).

Newkirk (1963) used a 7090 electronic computer to solve the neutron transport equation using the multigroup S_n method. The neutron source energy and angular distributions were assumed to be similar to the distributions measured by Miyake et al (1957) for charged particles emitted in cosmic ray reactions in nitrogen. These measurements were made in a cloud chamber at an altitude of 2840 metres and the observed energy distribution was shifted 2 Mev lower to account for the differences in neutron and proton energies that result from the Coulomb barrier. The S_n method is not limited to isotropic scattering and Newkirk (1963) was able to extend his spectrum calculations to 20 Mev. The altitude dependence of the neutron source was assumed to be exponential with absorption length $L = 160$ gm.cm^{-2} between 200 and 600 gm.cm^{-2}. At higher altitudes the cosmic ray star data of Lord (1951) and Addario and Tamburino (1949) were used. The area under this curve was normalised to an absolute production rate of 7.1 neutrons cm^{-2}sec^{-1} by means of data obtained by Smith et al (1962) at $\lambda = 57^{o}$N.

1.12 Neutron Energy Distribution.

In the equilibrium region of the atmosphere both Hess et al (1961) and Newkirk (1963) found that the neutron flux between 1 ev and about 50 Kev varies as $E^{-0.95}$. This result is in good agreement with the measurements of the spectrum by Hess et al (1959) and Miyake et al (1957) and should be compared with the $E^{-1.0}$ dependence obtained by Fujimoto and Tamura (1952) using the age equation without

capture.

At atmospheric depths less than about 200 $gm.cm^{-2}$ the effects of leakage become noticeable and the spectrum becomes harder. Thus the flux varies as $E^{-0.9}$ at 40 $gm.cm^{-2}$ and as $E^{-0.85}$ at the top of the atmosphere (Newkirk 1963).

In the energy range from 100 Kev to about 5Mev source neutrons modify the spectrum producing a pronounced "bump" on the curve. The bump is much more pronounced in the results of Hess et al (1961) than in those of Newkirk(1963). In the equilibrium region of the atmosphere, where the results are otherwise in agreement within the uncertainty limits, the fluxes given by Hess et al (1961) are greater by a factor of two or three. Differences in the source spectra used cannot account for this discrepancy since calculations by Newkirk using the source spectrum of Hess et al (1961) made only a few per cent difference to the results of Newkirk (1963). The experimental evidence is in conflict also since the results of Miyake et al (1957) agree well with Newkirk's calculations while the measurements of Hess et al (1959) support the theoretical data of Hess et al (1961).

At higher neutron energies the flux falls off more rapidly than in the 1 ev to 50 Kev region. Haymes (1964) observed an $E^{-1.3}$ dependence for the flux of 2 to 8 Mev neutrons both in the equilibrium region and at 4.5 $gm.cm^{-2}$. These measurements were made with a phoswich type scintillation detector at $\lambda = 41^{o}N$ in 1963. In 1957 Hess et al (1959) measured the spectrum up to several hundred Mev using bismuth fission chambers, nuclear emulsions and polyethylene lined proportional counters. Gauger (1964), using a similar fission chamber in an aircraft, found that the energy dependence of $E > 60$ Mev neutrons had increased from $E^{-1.4}$ as measured by Hess et al in 1957, to $E^{-2.5}$ in 1962. The flux in this energy region in 1962 was only 20% of its value in 1957 and Gauger (1964) observed a three-fold

change in intensity during a flight in July 1962. The cause of this intensity change has not been determined. Another unexplained increase was observed in the 1-14 Mev flux during a geophysically quiet period in 1963 (Haymes 1964a). It is clear that the details of the high energy spectrum are not well known.

1.13 The Absolute Value of the Neutron Flux.

There is considerable uncertainty as to the absolute value of the neutron flux. The results of Hess et al (1950) and Hess et al (1961) would appear to be in error throughout the atmosphere. In the equilibrium region Miles (1964) found that the slow neutron density estimated from the data of Hess et al (1961) was about 60% above his own measurements at $\lambda = 41^{o}N$. Measurements by Boella et al (1965) using moderated boron 10 plastic detectors, and by Haymes (1964) of the 1-14 Mev flux indicate a somewhat larger error at these energies. At higher altitudes the errors increase and at 40 $gm.cm^{-2}$ the total flux given by Hess et al (1961) is three times the flux given by Newkirk (1963). This discrepancy is borne out by the measurements of Miles (1964), Haymes (1964) and Boella (1965) and it is clear that the altitude dependence given by Hess et al (1961) is in error.

Newkirk (1963) obtained a flux at $\lambda = 57^{o}N$ and $z = 200$ $gm.cm^{-2}$ of 3.8 neutrons $cm^{-2}sec^{-1}$, which is only about 60% of the value obtained by Hess et al (1961). There are no recent high latitude measurements with which these data can be compared but if we translate the measurements of Boella et al (1965) to $\lambda = 57^{o}$ using the latitude variation of Gauger (1964), with a small correction for the difference in atmospheric depth, we obtain a flux of 4.3 neutrons $cm^{-2}sec^{-1}$. The difference between this result and that of Newkirk (1963) is probably due to the change in primary cosmic ray intensity between the time of the measure-

ments by Boella et al (1965) and those of Smith et al (1962) to which the results of Newkirk (1963) were normalised. Recent measurements (Miles, 1964) of the slow neutron density at $\lambda = 41^{o}N$ suggest that the results of Lingenfelter (1963) are in error at this latitude. Miles (1964) found that the absolute densities predicted by Lingenfelter were about 50% above the observed values which were in satisfactory agreement with the results of Haymes (1959). Inspection of the published data shows that the discrepancy increases at atmospheric depths less than 50 $gm.cm^{-2}$, (it is over 100% at 10 $gm.cm^{-2}$), presumably due to the breakdown of diffusion theory in this region.

1.14 Carbon 14 in the Atmosphere.

In section (1.11) we showed how Lingenfelter (1963) obtained the altitude and latitude distribution of the carbon 14 production rate for solar minimum in 1953-1954 and solar maximum in 1957-1958. By integrating these data over altitude and latitude, Lingenfelter (1963) obtained two values of the global average carbon 14 production rate $\bar{Q}$: 2.61 ± 0.50 $cm^{-2}sec^{-1}$ for 1954, and 2.08 ± 0.40 $cm^{-2}sec^{-1}$ for 1957-1958. Then, assuming that the deviation of $\bar{Q}$ from its solar minimum value is directly proportional to the average sunspot number, he estimated the average value of the production rate during the last ten solar cycles to be 2.50 ± 0.50 $cm^{-2}sec^{-1}$. To this must be added a small contribution (0.03 to 0.06 $cm^{-2}sec^{-1}$ according to Lingenfelter and Flamm 1964a) of carbon 14 atoms produced in the atmosphere by solar flux particles.

Other estimates of the carbon 14 production rate are based on less detailed information on the spatial, energy and time distributions of the cosmic ray neutrons. They range between 1.1 $cm^{-2}sec^{-1}$ (Soberman 1956, ~~corrected by Korff 1958~~) and 2.9 $cm^{-2}sec^{-1}$ (Hess et al 1961).

The global average carbon 14 decay rate has been calculated by Craig (1957) from the known specific activity of carbon 14 and the estimated mass of carbon in the exchange reservoir. He obtained a value of 1.8 ± 0.2 $cm^{-2}sec^{-1}$. In a similar manner Fergusson (1963) estimated a decay rate of 1.9 ± 0.2 $cm^{-2}sec^{-1}$.

There is considerable interest in the carbon 14 production-decay budget because of its bearing on the widely used carbon 14 dating technique and on the long-term constancy of the primary cosmic ray intensity. Lingenfelter (1963) finds a significant excess of production over decay and notes that the imbalance is compatible with either the several hundred year variations in solar activity suggested by Stuiver (1961) or with an exponential decay in the earth's magnetic field during the last 2,000 years (Elasser et al 1956).

1.15 The Neutron Leakage Flux.

(i) Theoretical data.

There have been many measurements and several theoretical estimates of the flux of neutrons leaking out of the atmosphere. The main interest in the leakage flux or neutron albedo lies in the possibility, first suggested by Singer (1958), that the decay of these neutrons is a source of the high energy protons and electrons in the Van Allen radiation belts.

Hess et al (1961) estimated the leakage flux at $\lambda = 44^{o}N$ from the diffusion calculations described in section (1.11). They obtained the flux at other latitudes using the latitude distribution of the neutron flux at 312 $gm.cm^{-2}$ as measured by Simpson (1951) in 1949. Lingenfelter (1963a) obtained the neutron albedo energy and latitude distribution using the procedure described in section (1.11). Newkirk (1963) has estimated the

total leakage flux and the energy distribution (for E > 1 ev) at $\lambda = 57^{o}N$ using the multigroup S_n method.

Some details of these calculations are given in table (1.2).

Geomagnetic latitude	Lingenfelter (1963a)		Hess et al (1961)	Newkirk (1963)
	solar min.	solar max.	1957	about 1961
0^{o}	0.11	0.105	0.32	-
40^{o}	0.37	0.30	0.85	-
57^{o}	0.99	0.70	1.45	0.80
90^{o}	1.37	0.71	1.45	-
Total latitude effect	12.5	6.8	4.5	-

Table (1.2) Neutron Leakage Flux ($cm^{-2}sec^{-1}$)

While the high latitude results of Hess et al are in good agreement with the solar minimum flux of Lingenfelter, the overall latitude effect is very much smaller, so that the flux at the equator is about three times that given by Lingenfelter. It is difficult to justify the assumption (Hess et al 1961) that the leakage flux has the same latitude distribution as the flux at 312 $gm.cm^{-2}$, and the results of Hess et al (1961) are therefore not likely to be as reliable in this respect as those of Lingenfelter (1963a). Nevertheless there is some doubt about the latitude variation obtained by Lingenfelter because of the uncertainty about the neutron production distribution at high altitudes (section 1.5).

The agreement between the high latitude results of

Hess et al (1961) and the solar minimum data of Lingenfelter (1963a) is of no great significance since the data of Hess et al are intended to apply to 1957 when solar activity was high. The apparent agreement is probably a fortuitous consequence of errors (section 1.13) in the high altitude distribution given by Hess et al. In any case, the absolute flux obtained by both Hess et al (1961) and Lingenfelter (1963a) is in doubt following recent measurements as noted in section 1.13.

The leakage flux estimated by Newkirk (1963) for $\lambda = 57^{o}N$ in 1961 is in agreement, within errors, with the results of Lingenfelter (1963a). The flux in 1961, predicted by Lingenfelter, was estimated by interpolation between his solar minimum and solar maximum values using the Mt.Wellington neutron monitor rate.

The shape of the energy spectrum obtained by Lingenfelter (1963a) depends on latitude and time as a consequence of the variation of the neutron source altitude curves. The mean energy is greatest when the neutron production is concentrated near the top of the atmosphere: that is in polar regions and at times of low solar activity. The spectrum obtained by Hess et al (1961) is of course independent of latitude.

There are significant differences between the spectra obtained. Thus the "source peak" in the 10^{5} to 10^{7} ev region is more pronounced in the results of Hess et al (1961) and Lingenfelter (1963). A similar effect has already been commented on (section 1.12) when comparing the results of Hess et al (1961) and Newkirk (1963) for the equilibrium region of the atmosphere. The apparent enhancement of the source peak in both diffusion theory results suggests that the difference may arise from the breakdown of the theory for

neutrons which have made few collisions: that is those neutrons with near source energies. The multi-group S_n equations used by Newkirk (1963) are derived directly from the transport equation, and are presumably not subject to this limitation. The position of the source peak is at a much higher energy in the results of Hess et al (1961) than in the other two results. Newkirk (1963) and Lingenfelter (1963a) have included the effects of inelastic scattering in their calculations (Williams and Bostrom 1964), and this results in a lowering of the neutron source peak from 800 Kev as obtained by Hess et al (1961) to about 250 Kev.

Bame et al (1963) measured the neutron energy spectrum at $\lambda = 8.7^{o}N$ and $36.5^{o}N$ using $Li^{6}I$ scintillation detectors with varying amounts of moderating material. Although their results were taken to verify the shape of the spectrum given by Hess et al (1961) (the only spectrum published at the time) they are probably not incompatible, within errors, with the spectra given by Newkirk (1963) and Lingenfelter (1963a).

(ii) Experimental results.

The interpretation of experimental results is complicated by the uncertainty in the energy spectrum, and also by the effect on the detector counting rate of neutrons produced in the materials of the detector system and of the rocket or satellite vehicle. This local production effect is difficult to measure or calculate.

There is a very large spread (as much as 30 to 1 at mid-latitudes) in the published experimental results for the absolute neutron leakage flux and also in the latitude dependence. In a recent survey of all the

measurements and theoretical results, Williams and Bostrom (1964) conclude that the absolute leakage flux is not known to better than a factor of 3 to 5 and that there is an uncertainty of 2 or 3 to 1 in the total latitude variation.

In view of the difficulties discussed above it is desirable that future measurements be made with detectors designed to minimise local production effects. More detailed measurements of the energy spectrum are also required.

II THE EQUIPMENT

2.1 Introduction.

The measurements described in this thesis were made with balloon borne equipment incorporating neutron detectors and a pressure measuring device. In many cases the flight unit also contained Geiger counters and/or a triple coincidence Geiger counter telescope. Flights were made over the three year period 1962-1964 (inclusive), at six different sites ranging from Wilkes, Antarctica to Lae in New Guinea. The measurements may be divided into three groups.

(i) Flights from Macquarie Island in 1962 and 1964 during auroral and other geophysical activity.

(ii) Measurements of the neutron and ionising particle flux distribution by means of flights at five stations, covering the latitude range from Wilkes to Lae, during a geophysically quiet period near solar minimum in 1964.

(iii) Measurements at Wilkes and at Mildura, Victoria to obtain information on the background and directional properties of the neutron detectors.

The flights will be described in more detail in a later section.

The detectors used varies from flight to flight and included one or more of the following: unmoderated BF_3 counters in pairs (one with natural BF_3 and the other enriched with the boron 10 isotope); BF_3 counters with $\frac{1}{2}$ or 1 inch of polyethylene moderator (in some flights moderated counter pairs, with natural and enriched boron, were used); Geiger counters with thin aluminium walls; Geiger counters as above but shielded with iron foil to reduce their sensitivity to low energy X-rays; triple coincidence Geiger counter telescopes.

A temperature measuring device was included in some flight units, and in the flights from Mildura, where the data was recorded magnetically with an on flight recorder, a crystal clock was also included. As mentioned above, all rigs contained a pressure measuring device.

After amplification the pulses from these detectors are scaled using binary circuits, and the binary outputs used to frequency modulate subcarrier audio oscillators operating at standard I.R.I.G. frequencies. The oscillator outputs are mixed and either telemetered to the receiving station by means of a 72 mc/s FM transmitter or (in the Mildura flights) recorded on magnetic tape or wire, using a small recorder in the flight unit. A block diagram of a typical flight unit is given in figure 2.1.

The output from the receiver in the ground station (or from the flight recorder recovered after the flight) is passed into amplifier and FM demodulator circuits which operate a high speed chart recorder. Since in general each sub-carrier channel contains the information from only one detector, the chart readout has the appearance of an irregular square-wave pattern, the two states of which correspond to the two states of the binary output for the particular detector. The pressure and temperature data are included in one of these channels as a smaller amplitude modulation superimposed on these two states. Because the telemetered rates are at times quite high, the outputs of the sub-carrier demodulators are also connected to amplitude discriminators which operate high speed pulse registers. There are two sets of registers and the discriminator outputs are switched alternately from one set to the other at intervals of one minute. Provided the telemetered signal is noise free, the scaled detector counting rates can be read directly from the registers as the data is being received. The chart record is normally used only during

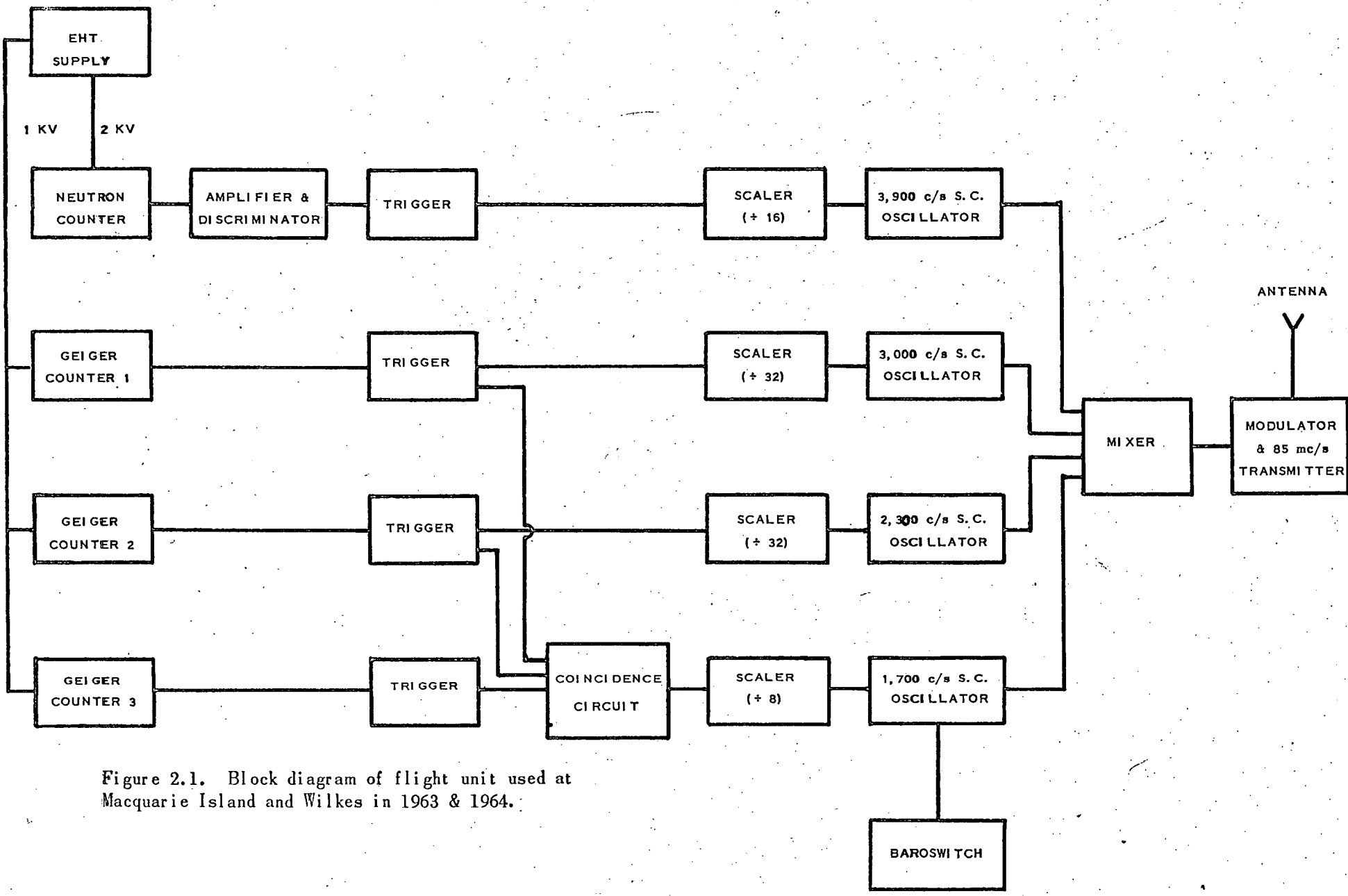

Figure 2.1. Block diagram of flight unit used at Macquarie Island and Wilkes in 1963 & 1964.

periods of noisy reception and for read-out of the pressure information.

The receiver output is also recorded on magnetic tape which may be used for checking unusual or noisy data, and as a back-up in case of difficulties with the other equipment during a flight.

The general principles of the receiving station are illustrated in figure 2.2. All circuits in the receiving station were designed by the author except when stated otherwise.

2.2 The detectors.

(i) Moderated $B^{10}F_3$ proportional counters.

The counters used in these experiments are of glass construction with an internal nickel cathode of 4.7 ± 0.1 cm. diameter and 20 ± 1 cm. long. They were designed and manufactured in this department (Fenton and Fenton 1965) and are filled with BF_3 gas to a pressure of 45 ± 1 cm. of Hg at 20°C. The boron in the "enriched counters" contains 96% of the boron 10 isotope.

In order to avoid high voltage breakdown at low ambient pressures during flight, the counters are sealed into an aluminium tube which also contains the high voltage (EHT) generator and circuits and part, or all, of the moderator sheath. Four different moderator geometries have been used:

(a) Type A in which the counter is embedded in paraffin in a 7.5 cm. diameter Al tube. This results in a sheath which is 1.25 cm. thick around the circumference of the counter and 2.5 to 4.0 cm. thick at the ends.

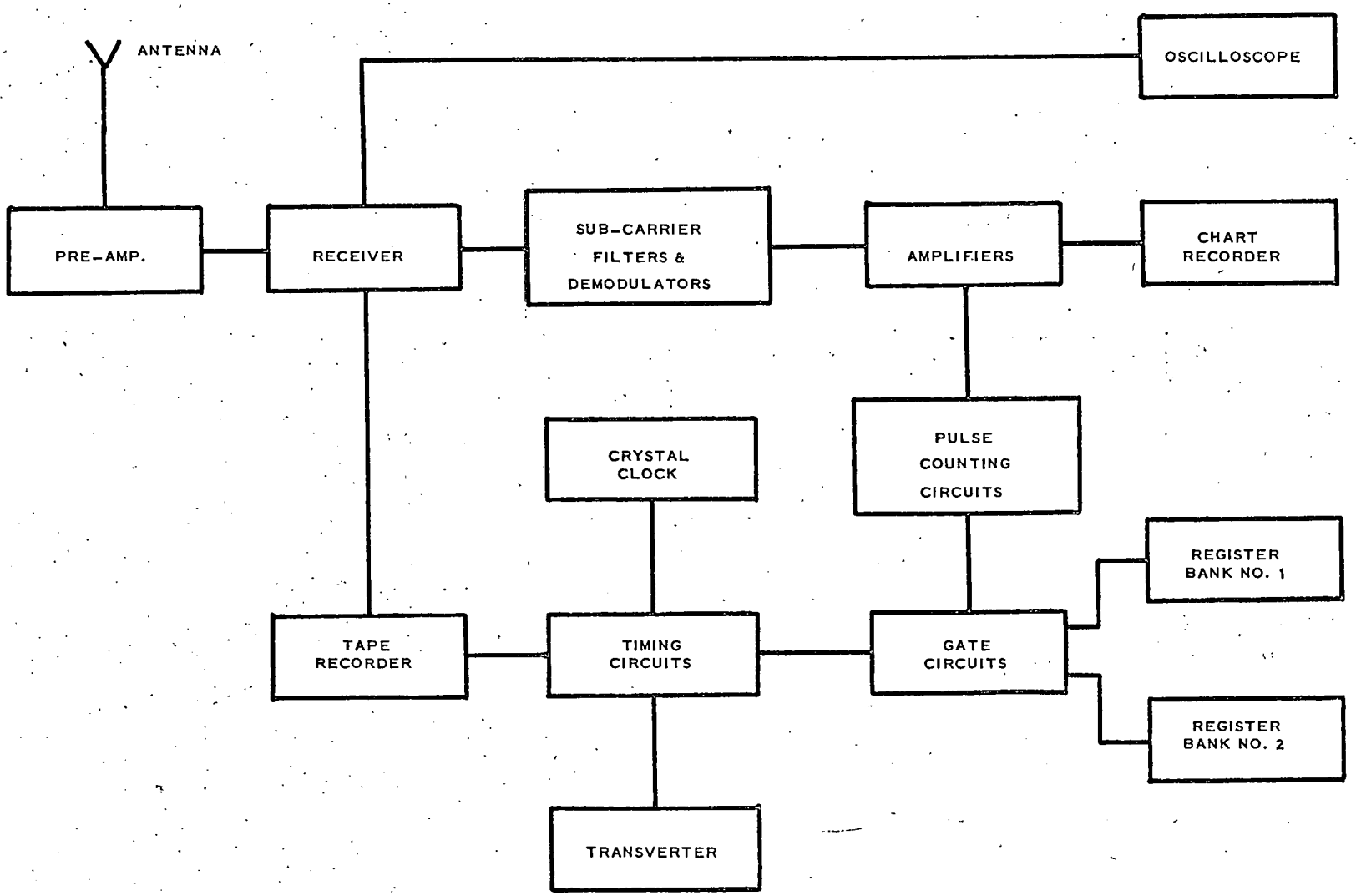

Figure 2.2. Block diagram of the receiving station.

(b) Type B which consists of a 2.5 cm. thick by 20 cm. long sheath of moulded polyethylene surrounding the counter and contained in a 10 cm. diameter Al tube.

(c) Type C which is similar to type B but with a sheath thickness of 1.25 cm. fitted into a 7.5 cm. diameter Al tube.

(d) Type D which is similar to type with a second external sheath 1.25 cm. thick and 20 cm. long. In this type both the internal and external sheaths are made up from $\frac{1}{16}$ inch polyethylene sheet.

The construction of a type D neutron detector unit is illustrated in figure 2.3. The end discs, pulse and battery lines are cemented in place with "Araldite" epoxy resin. The first batch of neutron units were tested for leaks or failure of seals to a pressure of five atmospheres, but in view of the good performance in this test, later batches were tested either by immersion in hot water or by inspection only.

The pulse output from the neutron counter is connected to a pulse amplifier and discriminator (section 2.3) in an aluminium box clamped to the detector unit. After the amplifier and discriminator have been adjusted for best operation of the counter, the detector-amplifier system is calibrated relative to a standard system by measuring its counting rate in a reference flux from a uranium 238 spontaneous fission source. This consists of 30 Kg of $U^{238}O_2$ in the form of a cylindrical sheath 44" I.D. x 10" O.D. x 15" long surrounded by 4" of paraffin. The flux from this source is over-rich in slow neutrons by comparison with atmospheric neutrons, and the calibration is therefore suitable only for comparison between detector units having the same moderator geometry.

The energy response and other characteristics of these

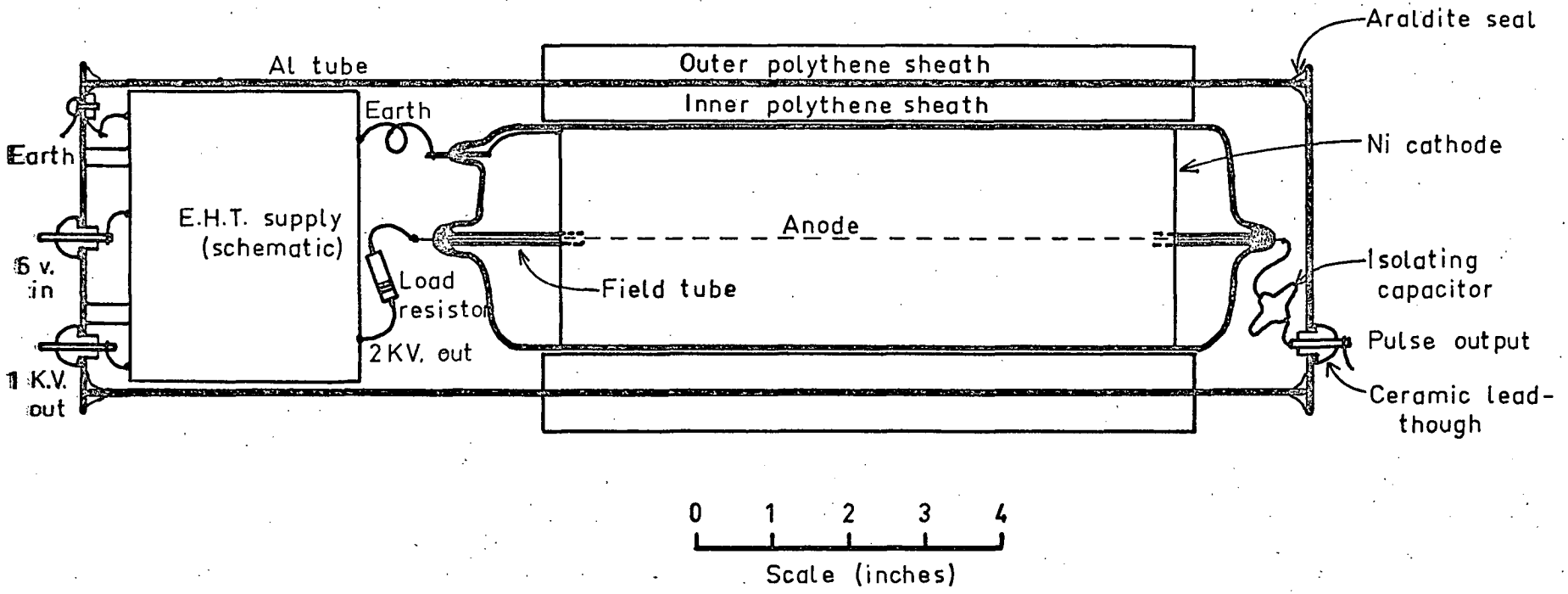

Fig. 2.3 : Type "D", BF_3 neutron counter unit

detectors are described in Chapter III.

(ii) Unmoderated BF_3 counters.

The construction of the counters and detector units is identical with that of the type C units described above, except that the moderator sheath is replaced by two mounting rings of "Coolite" polystyrene foam. These are cemented in place with epoxy resin. The units are always flown in pairs with one counter (the "unenriched" unit) containing natural BF_3 and the other (the "enriched" unit) with the boron enriched to 96% with B^{10}. Two counters are used to enable the highly ionising background rate to be determined using the difference technique (Soberman 1956, see also Chapter III). The unmoderated detectors are calibrated in the reference flux as described above.

(iii) Geiger counters.

The Geiger counters are organic quenched argon type with an operating voltage of about 950 volts and plateau slope not more than 3% per hundred volts. They are of aluminium construction, 10 cm. long by 4 cm. diameter with 0.5 mm. walls and a filling pressure of 6 cm. of Hg. The quenching agent is a propane butane mixture designed to enable low temperature operation, and the counters are individually tested to - 60°C. They were designed (by Drs. A.G. and K.B.Fenton) and constructed in this department.

In flight units containing a triple coincidence Geiger counter telescope, the middle counter is shielded with 0.1 mm. of iron foil to reduce its sensitivity to low energy X-rays. The effect of the shield is to reduce the count rate due to 25 Kev X-rays by a factor of 4 while scarcely affecting the sensitivity to 50 Kev X-rays.

(iv) Geiger counter telescopes.

Three of the Geiger counters described above are placed one above the other (each touching its neighbour) and connected to a triple coincidence circuit to form a Geiger counter telescope. These telescopes are calibrated with respect to each other by measuring their cosmic ray counting rate when standing vertically in the laboratory. Time variations of the sea level cosmic ray flux are corrected for, using the rate of the Hobart C1 one meter cubical meson telescope.

(v) Pressure measurement.

Pressure is measured using a modified version of the standard Australian Bureau of Meteorology radiosonde baroswitch. The modifications (designed by Dr.N.R.Parsons *) increase the number of contacts in the low pressure (high altitude) region, and change the order of contact read-out so that during ascent the three different contact types read out sequentially. The change in contact layout occurs only above contact number 130 (about 30 mb) and greatly reduces the risk of ambiguity about the pressure during floating flight.

Some early flights incorporated a Sprenger rotating drum type baroswitch giving three read-outs: pressure P_1 on a 0-1,000 mb scale, pressure P_2 on a 0-200 mb scale and temperature. However, large differences were observed between the pressures indicated by the P_1 and P_2 channels, and their use was discontinued.

The use of hypsometers was considered in view of their greater accuracy at low pressures (Haymes and Van Paassen 1958, Greenhill 1960). They proved to be quite

* Now at Department of Physics, University of Alberta, Calgary, Alberta, Canada.

satisfactory in previous flights from Hobart but were not used in the present experiments because of their greater complexity and weight.

2.3 The electronics in the flight units.

(i) Effects of temperature.

Balloon borne equipment must operate in extreme environments and during long night flights it is usually impractical to prevent the instrument package reaching ambient temperature which varies from -40° to $-100^{\circ}C$. During daylight hours the equipment temperature may rise to $+30^{\circ}C$.

Most electronic components are temperature sensitive but transistors and electrolytic capacitors are probably the most affected by very low temperatures. The impedance of electrolytic capacitors increases so much that they become unuseable at temperatures below about $-40^{\circ}C$. Because of the high cost of dry tantalum capacitors, which are satisfactory at these temperatures, the use of high value ($C > 1\ \mu f$) capacitors has been avoided in the present circuits.

Experiments with high frequency alloy-diffused germanium and silicon mesa transistors showed that the common emitter current gain, β, for these types is often less than 10% of the room temperature value. Lower frequency types are considerably less temperature sensitive, but all circuits must include massive DC and AC feedback if their operating conditions and gain are to remain stable over this temperature range.

(ii) EHT supply.

The EHT supply is a conventional ringing choke circuit with a bypassed emitter resistor to improve the low temperature performance. The 1 μf bypass is much below

optimum but has been used because of the poor low temperature performance of electrolytics. The staircase multiplier increases the voltage in steps of 500 to 2 Kv with a tapping at a norminal 1 Kv to supply the Geiger counters. The output voltage is stabilised by means of a shunt corona regulator tube designed (Greenhill 1960) and made up in this department. The minimum current for stable operation of this tube sets the battery end-point for the EHT supply. The minimum current varies from 1 to 5 μA, resulting in a battery end-point of about 7 volts at - 80°C. The circuit is given in figure 2.4.

(iii) Neutron amplifier and discriminator.

The amplifier circuit consists of two similar DC coupled two-transistor feedback stages similar to circuits described by Waugh (1958) and Goulding (1959). These are followed by a grounded base stage T_5 (figure 2.4) having unity current gain and operating as an impedance transformer between the amplifier and discriminator. The gain of each feedback stage is set by the 4.7 K and R_f feedback resistors in the emitter circuits of T_2 and T_4 (figure 2.4) and is approximately

$$A = \frac{R_f + 4,700}{R_f}$$

where R_f is in ohms. Feedback reduces the amplifier input impedance to a few tens of ohms and its input time constant is therefore very much less than the charge collection time for the counter. Consequently there is very little change of potential on the counter anode as the charge leaks rapidly off to ground via the base emitter circuit of the input transistor. Thus the current in the amplifier input is $^{dQ}/_{dt}$, the time rate of arrival of charge on the anode, and the amplifier is said to be operating in the current mode.

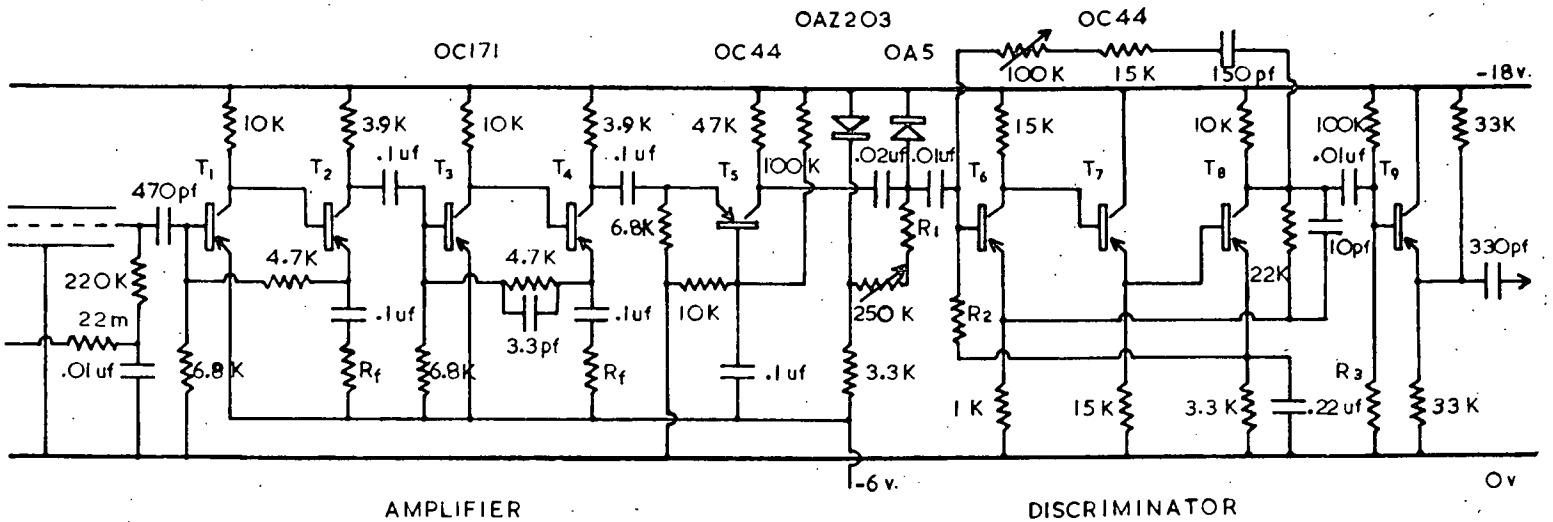
OAZ203
OC44
OC171
OC44
OA5
100K
15K
150pf
-18v.
10K
3.9K
10K
3.9K
47K
100K
.02uf
.01uf
15K
10K
100K
33K
T1
T2
T3
T4
T5
T6
T7
T8
T9
.1uf
.1uf
470pf
6.8K
R1
.01uf
330pf
4.7K
4.7K
10pf
220K
22K
22m
.1uf
.1uf
10K
250 K
R2
3.3pf
.01uf
6.8K
6.8K
Rf
Rf
.1uf
3.3K
R3
1 K
15K
3.3 K
.22uf
33 K
-6 v.
0v
AMPLIFIER
DISCRIMINATOR

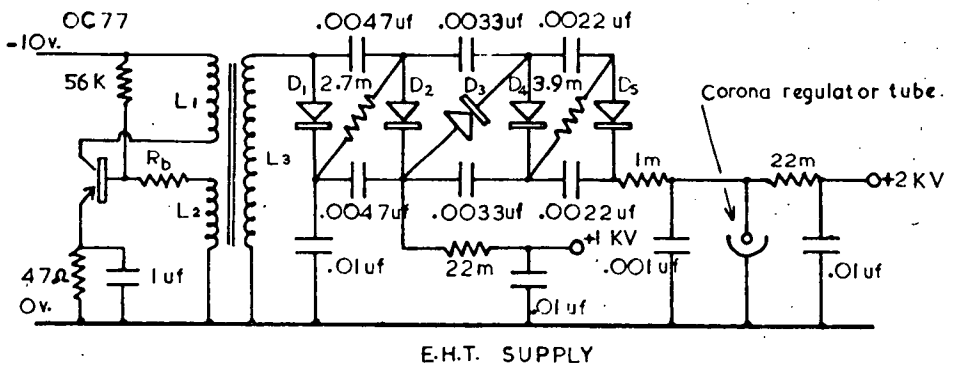
OC77
-10v.
.0047uf
.0033uf
.0022 uf
56K
L1
D1
2.7m
D2
D3
D4
3.9m
D5
Corona regulator tube.
Rb
L3
1m
22m
+2 KV
L2
.0047uf
.0033uf
.0022 uf
+1 KV
47Ω
1uf
.01uf
22m
.001uf
.01uf
.01uf
0v.
E.H.T. SUPPLY

Figure 2.4

In the present application the BF_3 counter is run at the relatively high gas gain of about 300 in order to reduce RF interference and noise problems. The short circuit current gain is set at a nominal 170 by making R_f 390 ohms, and under these conditions the output pulse amplitude is 20-80 μA for neutrons.

The discriminator (figure 2.4) is a low level Kandiah type current threshold discriminator, and is a modified version of a circuit described by Zaglio (1957). It consists of a stable direct coupled three stage amplifier with a positive feedback loop giving rise to a stable negative impedance z at the input. A forward biassed OA5 germanium diode is connected across the input and the signal pulses are injected at this point. If $|z|$ is greater than the differential resistance R_d of the diode the circuit remains quiescent. Pulses of sufficient amplitude will reduce the diode current to the point where $R_d \geq |z|$ thereby triggering the circuit and generating an output pulse of about 4 volts amplitude and several microseconds duration. The value of R_d for a given pulse depends to some extent on temperature, but this effect can be minimised by using a large standing current in the diode. The triggering level depends also on the value of $|z|$ which is proportional to the resistance in the positive feedback loop. Consequently, the setting up of the system requires adjustment of both the feedback control (100 K variable resistor) and the diode standing current (250 K variable resistor).

The discriminator operates as a linear amplifier to pulses of amplitude below the threshold, and these appear at the output as small "linear" pulses together with the much larger triggered pulses. The emitter follower stage T_9 is biassed to cut-off to discriminate against the linear pulses.

As a consequence of the relatively sharp pulse

height distribution curve of the BF_3 counters, at least a 50% change in the amplifier-discriminator sensitivity could be tolerated, provided the bias is set at the optimum value. However, tests on the present circuit show that its sensitivity is constant within 2% from + 20°C to - 70°C and decreases by less than 10% at + 30°C and - 80°C. This stability is maintained even when the amplifier gain is increased to 500. The sensitivity is virtually unaffected by a 40% reduction in battery voltages, provided the ratio of the two remains constant within about 10%. The output pulses are of about 2 volts amplitude and the minimum resolving time between two pulses is 3 microseconds. The maximum pulse rate before sensitivity is affected is about 3,000 sec^{-1}, randomly distributed in time.

(iv) <u>The Geiger counter pulse amplifier and coincidence circuits</u>.

The output from each Geiger counter is connected to a single transistor common emitter amplifier which is cut-off in the quiescent state. Counter pulses saturate the stage producing 4 volt pulses of about 10 microseconds duration.

The coincidence circuit consists of three grounded emitter transistors with a common collector load. In the quiescent state all three transistors are saturated and no output is obtained unless all three are switched off simultaneously. The resolving time is about 5 microseconds.

These circuits, like all others in the flight unit, have been tested at temperatures from + 30°C to - 80°C. The designs of the amplifier, coincidence and binary scaling (section 2.3 (v)) circuits were made available to the author by Dr.R.R.Brown of the University of California, Berkeley, California, U.S.A.

(v) Binary circuits.

The binaries are of the saturated Eccles-Jordan type employing matched pairs (common emitter current gain within 10%) of OC44 transistors. They operate from a 6 volt supply and have a resolving time of less than 4 μsec.

The total scale factor used in any channel depends on the type of detector and the geomagnetic latitude at which the measurements are being made. Usual values are 16-64 for Geiger counters, 16 for moderated BF_3 counters, 4 or 8 for unmoderated BF_3 counters and Geiger counter telescopes.

(vi) Sub-carrier oscillators.

The sub-carrier oscillators are LC Colpitts type using the common emitter configuration. They are frequency modulated with centre frequencies varying from the I.R.I.G. channel 6 (1,700 c/s) to channel 11 (7,350 c/s). The numbers of channels used in a given flight depends on the detectors used, and varies from 2 to 4.

The modulator is a simple transistor switching circuit arranged so that when the output transistor of the final binary pair is cut-off, a capacitor is switched across the sub-carrier coil, thereby reducing the oscillator frequency. When the binary transistor is saturated, the modulator switch is cut-off and the oscillator is in its undeviated (high frequency) state. The total deviation is arranged to be about 13% of the centre frequency so that the modulation is within the I.R.I.G. standard ± 7½%.

The oscillators have been tested at temperatures ranging from +30°C to - 80°C. The output amplitude changes by less than 10% and the frequency by less than 1% over this temperature range.

(vii) Mixer and transmitter.

The transmitter is of the self-excited type employing a 2N707 silicon NPN transistor in the common base configuration. The power input is about 750 mW at 24 volts and the output about 200 mW into a 50 ohm load. The carrier is frequency modulated using a biassed off OA202 silicon diode as a variable capacitor connected across the tank circuit. The carrier deviation is adjusted, by varying the input to the modulator, to suit the receiver I.F. bandwidth (35 Kc/s when the lower frequency sub-carriers are used, and 70 Kc/s for the higher ones).

The transmitter output is of the unbalanced type and drives the antenna through an L matching network and a co-axial feeder cable. The antenna is of the turnstile type and since it has a balanced input the transmission line, being unbalanced, is terminated with a balun. The radiation pattern of the turnstile is almost isotropic, and the telemetry is therefore not subject to (pendulum) fading when the natural swinging of the antenna directs a radiation null towards the receiving station. The vertical co-axial dipole is at first sight a more attractive antenna than the turnstile since its radiation pattern is concentrated at angles near the horizontal. It might therefore be expected to provide stronger signals when they are most needed: that is when the transmitter is approaching the radio horizon for the receiving station. However, experiments with this antenna showed that pendulum fading is very troublesome during the early part of the flight, when the important ascent data is being telemetered.

The transmitter is matched to the antenna by adjusting the L network for maximum power into a 50 ohm absorption power meter. It is assumed that the antenna impedance is 50 ohms and purely resistive when the antenna elements and its matching and phasing stubs are cut according

to theory. Measurements of the standing wave ratio in the transmission line give a value of 1.5 to 2, indicating a satisfactory match using this procedure.

The frequency stability of the transmitter is very variable, and while quite satisfactory for use in Antarctic regions with an uncluttered radio spectrum, some difficulties arise in city areas. The carrier frequency tends to increase by an amount which varies between 0.1 and 1.0 Mc/s after release of the balloon and consequent removal of the antenna from proximity to conducting materials. A two stage transmitter, with the oscillator isolated from the antenna by an output stage, would be more stable in this respect.

(viii) Batteries and power supplies.

A single 24 volt battery pack, with tappings at 6, 12, 18 and 24 volts, is used for all circuits. This pack is made up from types AA and C alkaline manganese dry cells which experiments have shown to have much better performance than conventional dry cells, especially at low temperatures. The low temperature performance of nickel cadmium cells is probably even better, but the alkaline cells were found to operate satisfactorily during long night flights and the extra expense of the nickel cadmium cells was not considered to be justified.

All circuits except the EHT supply and the transmitter are decoupled from the battery pack by means of simple electronic circuits. The neutron amplifier is very sensitive to noise on the battery line, and the 18 volt input requires a two stage circuit employing cascaded emitter followers with high impedance RC decoupling in their base circuits. The 6 volt line is supplied from a third (NPN transistor) emitter follower driven from a tapping on the 18 volt output. The decoupling circuit is used in preference to a separate battery pack because of the greater convenience,

lower weight and comparable materials cost.

The other amplifier, scaling and sub-carrier circuits are supplied from the 12 volt tapping on the battery via an emitter follower with base and hence output potential fixed at 6 volts by means of an OAZ203 zener diode.

(ix) Construction.

The flight unit is assembled in a light weight box, constructed of 1 inch "Coolite" (polystyrene foam) board, containing separate compartments for the detectors, circuits, batteries etc. The transmitter is built up on a copper backed circuit board and mounted in an aluminium box to reduce RF pick-up by the other circuits. The other electronic circuits are built up on matrix board with two sub-carrier channels to each board. These boards are mounted in slots cut in the "Coolite". Some details of the construction and layout can be seen in figure 2.5.

The weight of the flight unit varies according to the detectors included. Thus a rig containing two unmoderated BF_3 counters weighs about 9 lbs., and with two moderated counters and a Geiger counter telescope about 15 lbs. The Mildura flight units with a tape recorder and heavy crash resisting box weigh 35-40 lbs.

(x) Balloons.

Neoprene expansible balloons were used for many of the flights described here. Numerous attempts were made to obtain level flight with the Darex J11 2400 gm. neoprene balloon using a modified form of the valving technique first described by Laby et al (1957). A method for estimating the maximum balloon diameter and floating altitude for a given payload and safety margin in balloon skin thickness has been devised by Dr.K.B.Fenton and described by Edwards (1964). Safety margins corresponding to 20-50% in skin thickness were

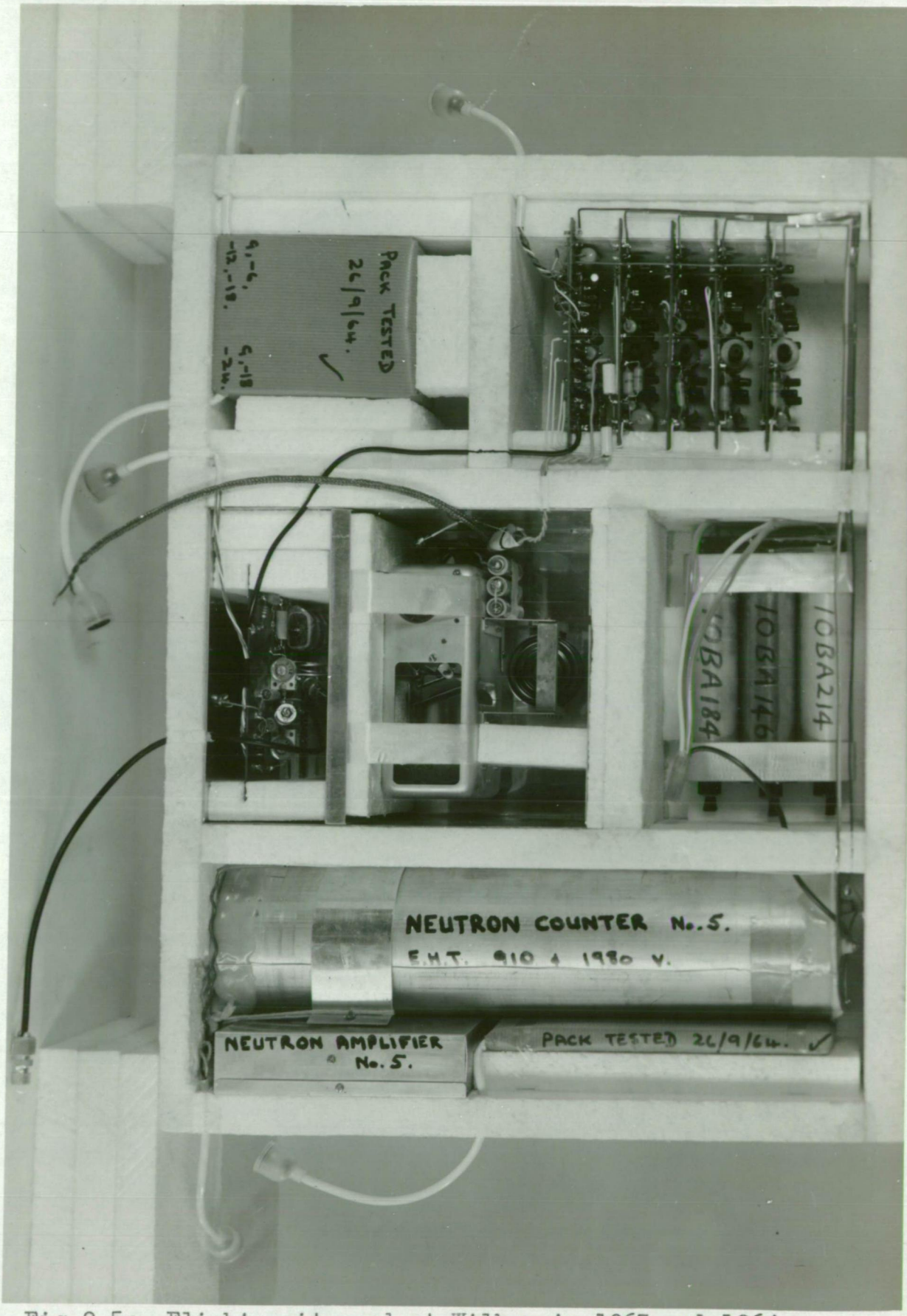

Fig 2.5: Flight unit used at Wilkes in 1963 and 1964.

used in all flights, but only about 30% of these attempts resulted in level flights lasting more than 4 hours. The remainder either burst or descended slowly after reaching the expected floating altitude. In other flights a cluster of 4 or more Darex 800 gm. J11 neoprene balloons were used, and these usually resulted in a slow descent after one of the balloons burst.

When long floating flights were required 60,000 or 80,000 ft^3 polyethylene balloons were used.

2.4 The Mildura flight units.

A number of instrument packages were flown from Mildura, Victoria, in conjunction with the air sampling equipment used in the Project Hibal flights conducted on behalf of the United States Atomic Energy Commission by the Australian Department of Supply. Since this equipment is normally recovered after each flight, the data were recorded on magnetic wire or tape with a recorder in the flight unit. A "Minifon" magnetic wire recorder was used in the first few flights, but the wow and flutter levels were unacceptably high and it was replaced by a "Philips" portable magnetic tape recorder. This was modified to operate at a tape speed of $^{15}/_{16}$ inches/sec., giving three hours recording time using "triple play" tape on 4 inch diameter spools. The maximum useable frequency is about 4 Kc/s, allowing satisfactory operation of sub-carrier channels 6 to 9. Tests indicate a better than 1% frequency stability for recorder supply battery voltages between 9 and 6.5 volts. Performance is not much affected by temperature in the range from $-10^{\circ}C$ to $30^{\circ}C$. All flights were conducted in daylight, and rig temperatures remained well within these limits.

A crystal clock (designed by Dr.A.G.Fenton of this department) was included in these rigs to give accurate time data during flight. The clock contains a binary strip with total scale factor adjusted by pulse feedback to give an

output of 1 cycle/minute from the crystal frequency of 102.4 Kc/s. The output was adjusted to produce a shallow frequency modulation of the 1.7 Kc/s sub-carrier which was also modulated with the Geiger counter telescope data.

2.5 Factors affecting the design of the telemetry system.

There are many possible methods of telemetering information, and the choice of the most suitable method (system) depends on a number of factors. These include:

(i) The number of information channels to be telemetered.
(ii) The type of information.
(iii) The information frequencies.
(iv) The minimum acceptable signal to noise ratio in the telemetry channel outputs.
(v) The power available for the transmitter.
(vi) Limitations on the cost and complexity of the modulator and transmitter.
(vii) Flexibility requirements.
(viii) Compatability with systems in use elsewhere.

Some of these factors must also be taken into account when optimising the performance of the selected telemetry system.

2.6 Characteristics of the data.

In the present application the number of information channels varies from three to five. One of these consists of infrequent (3 or 4 min^{-1}) transitions between the four possible states of a baroswitch pressure transducer. The other channels contain the scaled counts from each of the detectors in the flight unit. In order to keep the flight unit costs as low as possible, it was decided to telemeter at the highest practical information rates consistent with acceptable signal to noise ratios in the telemetry channel outputs. The scaled detector rates would be counted by electronic equipment in the receiving station, thus avoiding the laborious task of counting the pulses from the chart record.

The minimum bandwidth required to accommodate a given scaled counting rate depends on the scale factor and on the minimum acceptable efficiency of the system. The efficiency η of a telemetry system is equal to the ratio of the pulse rate at the output to that at the input. It may be shown (Alaoglu and Smith 1938) that the efficiency of a system with resolving time τ, scale factor 16, and scaled count rate R, is virtually unity provided

$$R \lesssim 0.43 \qquad (2.1)$$

When the only information required at the output is the presence or absence of a pulse, the minimum frequency response f_{min} of the system is equal to $1/\tau$. Equation (2.1) therefore corresponds to the condition

$$f_{min} \gtrsim \frac{R}{0.43}$$

Similarly, for a scale factor of 8 the minimum frequency response for a scaled rate R' is

$$f_{min} \gtrsim \frac{R'}{0.25}$$

A practical upper limit to the information rates is set by the requirement that any section of the record should be capable of being played out for visual inspection on the chart record. This facility is necessary for the study of unusual or noisy data, and for analysis of variations on a time scale less than one minute. The information frequencies are therefore required to be less than the recorder frequency limit (100 c/s) at all times. In practice the channel scale factors are adjusted to give information frequencies much lower than 100 c/s under normal conditions. The reserve capacity provides for counting rate increases during solar, auroral or other "events". Details of the information channels in a typical flight unit are given in table 2.1.

Instrument	Type of information	Scale factor	Normal scaled rate	f_{min} (c/s)
1. Neutron counter (enriched)	2 states of binary	16	2 sec^{-1}	4.7
2. Neutron counter (natural boron)	"	16	0.5 sec^{-1}	1.2
3. Geiger counter	"	16	6 sec^{-1}	14
4. Triple coincidence Geiger counter telescope	"	8	1 sec^{-1}	4
5. Baroswitch	4 states of switch	Normal rate - 3 or 4 changes of state min^{-1}.		

Table 2.1: Information channels in a typical flight unit.

2.7 Methods of Multiplexing.

The process of transmitting more than one channel of information over the same link is called multiplexing. There are two general methods of multiplexing: frequency division and time division. In the frequency division method each information channel modulates a single sub-carrier. The sub-carrier frequencies are separated in such a way that their modulation sidebands do not overlap. The outputs of all sub-carriers are mixed in a linear circuit and the resulting signal modulates the transmitter. At the receiving end the sub-carrier signals are separated using band-pass filters and then demodulated.

In the time division methods, a mechanical or electronic commutator samples each channel in a cyclic sequence, and generates a pulse or pulses for each channel. These pulses are modulated in amplitude, duration, separation or in some code in accordance with the information in each channel.

At the receiving end the pulses may be sorted by inspection or (in the case of high commutation rates) by a commutator synchronised with the one in the transmitter.

Time division multiplexing is most suited to the transmission of many channels of slowly varying information. It is capable of operating at lower signal to noise ratios in the telemetry link than are the frequency division systems (Nicholls and Rauch 1956, p.194). However, the frequency division methods are generally simpler and more flexible for small numbers ($\lesssim 10$) of channels, particularly when information frequencies are high (~ 100 c/s). Consequently we will confine our discussion to frequency division multiplexing.

2.8 Interference.

The telemetry link is subject to interference of several different kinds.

Fluctuation noise or hiss has frequency components with random phase. The main sources are receiver noise, galactic radio emissions and thermal radiation from the ground etc. The r.m.s. noise voltage is proportional to the square root of the receiver bandwidth. The noise generated in the receiver itself sets an absolute lower limit to the signal level which can be detected.

Impulse noise is generated by lightning and other natural and man made electrical disturbances. Each impulse has frequency components of related phase, and the peak noise voltage is directly proportional to the receiver bandwidth. Impulse noise may be minimised by suppression techniques, station siting and the use of high link frequencies.

Crosstalk, between channels in a multiplex, occurs when non-linearities in the system cause generation of harmonics and linear combinations of the sub-carrier frequencies. The number of crosstalk terms may be quite large ($\sim 10^3$) in

systems with many ($\sim$10) sub-carriers. Since the sub-carrier oscillators have random phase, crosstalk noise approaches the characteristics of fluctuation noise. It may be minimised by avoiding non-linearities in the system, and by the wideband techniques to be discussed later.

Telemetry links are also subject to multipath fading and distortion when the signal is received simultaneously over two or more paths of differing length. This results in destructive interference causing overmodulation in amplitude modulated (AM) links. In frequency modulated (FM) links, spurious signals of variable amplitude and frequency are generated by beating together of the R.F. signals. Multipath distortion can often be reduced by the use of directional antennas and proper siting of them.

2.9 Methods of modulation.

(i) Amplitude modulation (AM).

When a carrier $A \cos \omega_o t$ is modulated by an information component $m \cos \Omega t$, the resultant can be written

$$a = A (1 + m \cos \Omega t) \cos \omega_o t \qquad (2.2)$$

where A is the unmodulated carrier amplitude
ω is the carrier angular frequency
m is the modulation index
Ω is the modulation signal angular frequency
t is the time.

If $|m| = 1$ the carrier is said to be 100% modulated. When $|m| > 1$ the carrier is overmodulated and distortion results.

The modulated carrier has three components viz the carrier of amplitude A and two sideband components of amplitude $\frac{A|m|}{2}$ and frequencies $\frac{1}{2\pi}(\omega_o \pm \Omega)$. In a fully modulated signal the sideband power is equal to half the carrier power. This is very wasteful of power since the carrier contains no information and one of the sidebands is

redundant.

In the single sideband (SSB) technique, the carrier and one sideband are filtered out at a low level in the transmitter, with a consequent saving in power. SSB links are not subject to multipath distortion, and their performance in high noise conditions is improved because of the smaller bandwidth required. Similar advantages are obtained from the double sideband suppressed carrier (DSBSC) technique, where both sidebands are telemetered without the carrier. SSB and DSBSC receivers are much more complex and expensive than their AM and FM counterparts, and are also much more prone to non-linear distortion. The techniques are therefore not attractive for expendable flight units of the type used in the present experiments.

(ii) Frequency modulation (FM).

When a carrier $A \sin \omega_o t$ is frequency modulated by an information signal $m \sin \Omega t$, the resultant modulated carrier is given by

$$a = A \sin \left(\omega_o t + \frac{m\Delta\omega}{\Omega} \sin \Omega t \right) \qquad (2.3)$$

where $\Delta\omega$ is the full modulation frequency deviation when $m = 1$. The quantity

$$\frac{\Delta\omega}{\Omega} = D$$

is called the deviation ratio.

The frequency spectrum of the modulated carrier is made up of many components consisting of the carrier and side frequencies spaced from the carrier by integral multiples of the modulating frequency . The amplitudes of the carrier and sideband components is a complex function of the deviation ratio and significant sideband components may extend well beyond the frequency deviation limits, especially when D is small. Figure 2.6 (taken from Nichols and Rauch 1956, p.51) shows the bandwidth factor β as a function of D for a system in which all the sidebands of amplitude less

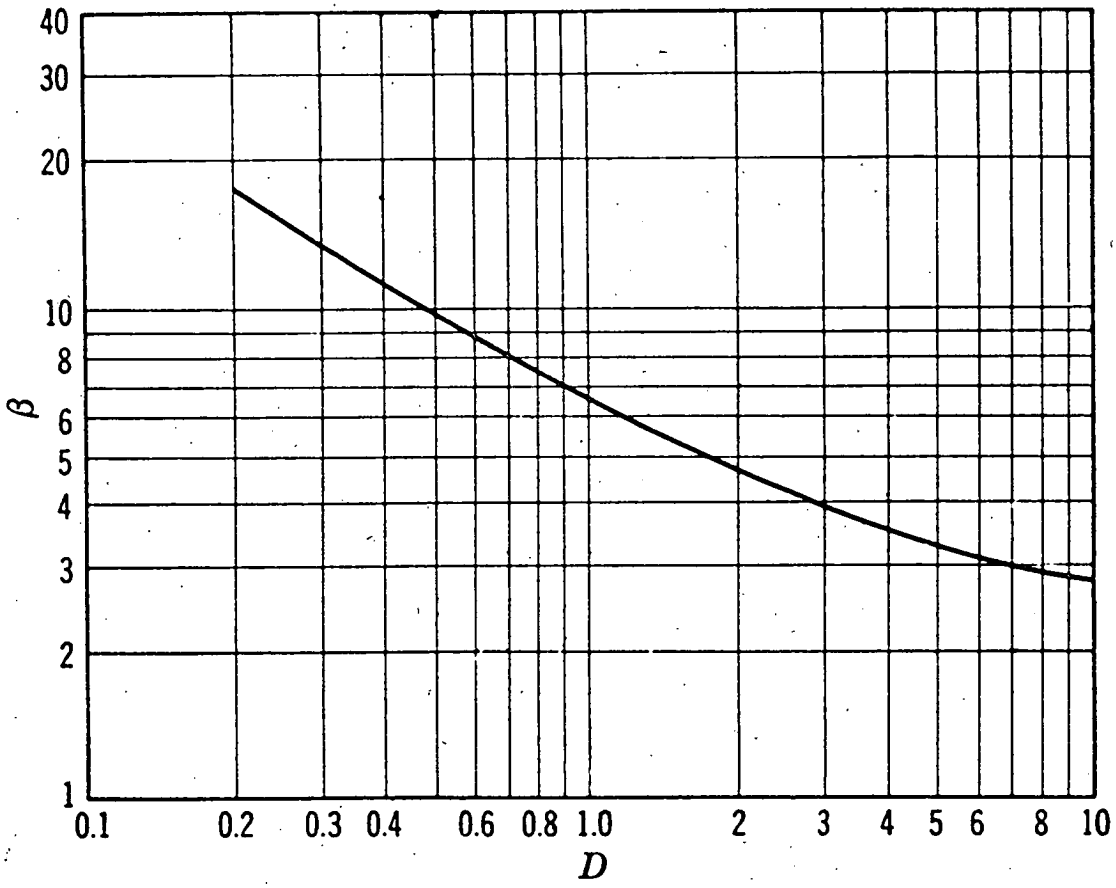

Figure 2.6. Required radio-frequency bandwidth versus deviation ratio D. The units of bandwidth are f_D so that the bandwidth is βf_D.

than 1% of the unmodulated carrier are excluded. The units of β are f_D the maximum frequency deviation so the bandwidth

$$B = \beta f_D = \beta D f_m \qquad (2.4)$$

where f_m is the modulation frequency.

The FM method results in a reduction in the signal to noise ratio of the receiver output by comparison with an AM system operating under the same conditions. In order to compare the noise improvement of various types of modulation, it is customary (Nichols and Rauch 1956,p.54) to express the signal to noise ratio of the system as a ratio to the signal to noise ratio of a fully modulated AM system, assuming the same carrier power for both systems. This ratio is called the wide band gain R_o and for FM

$$R_o(FM) = \sqrt{3}\, D \qquad (2.5)$$

for fluctuation noise and

$$R_o(FM) = 2D$$

for impulse noise.

The noise voltage per unit bandwidth in the output of an FM receiver is proportional to frequency. It is necessary, therefore, to increase the amplitude of the high frequency components of the information, before transmission, in order to obtain optimum performance from the link. This effect must be taken into account when adjusting the relative amplitudes of the sub-carriers in a multiplex employing an FM carrier.

The wideband noise improvement of equation (2.5) is not realised in FM systems when the signal to noise ratio in the link falls below a certain "improvement threshold". This threshold occurs when the amplitude of the carrier signals equals approximately four times the r.m.s. noise voltage in the carrier pass band. The r.m.s. carrier threshold voltage S_t is given (Nichols and Rauch 1956, p.55) by

$$\sqrt{2}\, S_t = 4k_1(\beta D f_m)^{\frac{1}{2}} \qquad (2.6)$$

where k_1 is the r.m.s. noise per unit bandwidth in the carrier channel. Below the threshold the output signal to noise ratio tends to fall below that of the equivalent AM link because of the larger carrier bandwidth required for FM. The measured threshold for a typical system was found (Lawson and Uhlenbeck 1950,p.382) to decrease from 16db for D = 4 to 5db for D = 1. The decrease in the threshold with deviation ratio is an important factor in the design of a telemetry system employing frequency modulation.

(iii) Phase modulation.

When the information signal is used to modulate the phase of a carrier, a wideband gain

$$R_o(PM) = \phi_D$$

(where ϕ_D is the peak phase deviation in radians), is obtained. However, the exchange between bandwidth and noise improvement is not as favourable as with FM. Consequently a PM system, with the same value of R_o as an FM system, will have greater bandwidth and a higher noise improvement threshold. PM has certain technical advantages over FM where high carrier frequency stability is required, but none in the present application. It is not used for sub-carrier modulation where DC information must be transmitted, because a time reference would be required to detect the corresponding constant phase shift.

2.10 Sub-carrier modulation and multiplexing.

(i) Nomenclature.

In specifying the method of multiplexing and modulation used in a system, it is customary to work from the input channels towards the carrier. Thus for example, AM-FM means a frequency division multiplex with amplitude modulated sub-carriers frequency modulating the carrier. In the following discussion we restrict our considerations to the

four possible systems employing AM and/or FM, viz AM-AM, FM-AM, AM-FM and FM-FM.

(ii) Sub-carrier frequencies.

The choice of sub-carrier frequencies is limited by the need to minimise the number of important cross-modulation terms within the passband of any of the sub-carrier channels. A set of 18 channels ranging in frequency from 400 c/s to 70 Kc/s has been adopted as an international standard (Nichols and Rauch 1956,p.434) for FM sub-carriers. Details of the sub-carrier bands of interest here are listed in table 2.2.

Band	Centre frequency (c/s)	Lower limit (c/s)	Upper limit (c/s)	Maximum deviation (per cent)	Frequency response (c/s)
5	1,300	1,200	1,398	± 7½	20
6	1,700	1,572	1,828	"	25
7	2,300	2,127	2,473	"	35
8	3,000	2,775	3,225	"	45
9	3,900	3,607	4,193	"	59
10	5,400	4,995	5,805	"	81
11	7,350	6,799	7,901	"	110

Table 2.2: FM-FM sub-carrier standards.

The channel frequency responses and bandwidths correspond to a deviation ratio of 2.2 on the basis of the bandwidth factors given in figure 2.6. This is much smaller than the value of 5 normally quoted (Nichols and Rauch 1956,p.436) for the standard FM sub-carriers. If a deviation ratio of 5 is used with a maximum frequency signal, many sideband components, with amplitudes greater than 1% of the sub-carrier amplitude, will fall outside the channel passband. While this may not result in significant distortion, it would seem

desirable that a smaller deviation should be used when maximum frequency signals are being telemetered.

The frequency response of the sub-carrier channels may be increased above the standards quoted by decreasing the deviation ratio to unity or even less. Smaller deviation ratios will result, however, in lower output signal to noise ratios and increased harmonic distortion and crosstalk. In the present application the deviation ratio is variable and normally much greater than five, since the normal modulation frequency must be much less than the channel maximum to allow for possible counting rate increases.

AM sub-carrier frequencies are normally scaled down by a factor of five from the FM standards.

(iii) Sub-carrier amplitudes and thresholds.

It is necessary, for optimum performance, to adjust the sub-carrier amplitudes a_{oi} so that all channels reach the improvement threshold (FM sub-carriers) or minimum acceptable signal to noise ratio (AM sub-carriers) at the same carrier strength.

As mentioned above, it is customary, with both types of sub-carrier, to make the maximum modulation frequency f_{mi} proportional to the sub-carrier frequency f_i. The noise voltage in the sub-carrier channel increases as the square root of the channel bandwidth B_i, and therefore as $f_i^{\frac{1}{2}}$ in systems employing AM carriers where the noise output per unit bandwidth is independent of frequency. Consequently, the sub-carrier amplitudes a_{oi} are adjusted so that

$$a_{oi} \propto f_{mi}^{\frac{1}{2}} \propto f_i^{\frac{1}{2}} \qquad (2.7)$$

for AM-AM and FM-AM systems. In other words we apply an "$f^{\frac{1}{2}}$ taper" to the sub-carrier amplitudes. If S is the total amplitude of the modulating signal for a system of m sub-carriers, we make

$$\frac{a_{oi}}{S} = \frac{f_i^{\frac{1}{2}}}{\sum_n f_i} \qquad (2.8)$$

With an FM carrier the noise voltage per unit bandwidth is proportional to f_i. It is necessary, therefore, to make

$$a_{oi} \propto f_i (f_{mi})^{\frac{1}{2}} \propto f_i^{\frac{3}{2}}$$

Thus we must apply an "$f^{\frac{3}{2}}$ taper" to the sub-carrier amplitudes in AM-FM and FM-FM systems and

$$\frac{a_{oi}}{S} = \frac{f_i^{\frac{3}{2}}}{\sum_n f_i} \qquad (2.9)$$

In FM-FM systems it is desirable that the carrier threshold should be reached at the same time as the sub-carrier thresholds. Nichols and Rauch (1956,p.90) show that this condition is satisfied when

$$0.71 \left[\frac{\beta f_D}{\beta_i f_{di}}\right]^{\frac{1}{2}} \frac{f_D}{f_i} \cdot \frac{a_{oi}}{S} = 1 \qquad (2.10)$$

for all i where

β is the carrier bandwidth factor

f_D is the peak frequency deviation of the carrier

f_{di} is the peak frequency deviation of the i'th sub-carrier

β_i is the bandwidth factor of the i'th sub-carrier

and f_i, a_{oi} and S are as defined above.

(iv) Design considerations.

In order to determine the optimum carrier and sub-carrier parameters for a given system, we must first decide on a minimum acceptable signal to noise ratio $(S/N)_{it}$ in the output of the i'th sub-carrier channel.

The sub-carrier frequencies are then selected. With AM sub-carriers we choose the lowest frequency channels with sufficient bandwidth. With FM sub-carriers the bandwidths B_i must first be selected using the relation

$$B_i = \beta_i D_i f_{mi}$$

where D_i is the sub-carrier deviation ratio estimated from

$$D_i = \left[\frac{0.28}{\beta^{\frac{1}{2}}} \left(\frac{S}{N} \right)_{it} \right]^{\frac{2}{3}} \qquad (2.11)$$

and the relation between β and D in figure 2.6. The sub-carrier frequencies can then be selected from table 2.2.

The sub-carrier amplitudes are adjusted using the appropriate taper for the system as given in equations 2.8 and 2.9. $(S/N)_{it}$ will then be the same for all i.

Having selected the sub-carrier parameters, we may obtain the optimum carrier deviation f_D using figure 2.6 and the following equations

$$f_D = \left[0.7 f_1 \frac{S}{a_{oi}} \left(\frac{S}{N} \right)_{it} \right]^{\frac{2}{3}} \left[\frac{f_{mi}}{\beta} \right]^{\frac{1}{3}} \qquad (2.12)$$

for AM-FM systems and

$$f_D = \left[f_i \frac{S}{a_{oi}} \right]^{\frac{2}{3}} \left[\frac{2\beta_i f_{di}}{\beta} \right]^{\frac{1}{3}} \qquad (2.13)$$

for FM-FM systems.

It is important to compare the performance of the various systems under weak signal conditions. To do this we estimate the value of the parameter $\frac{S_t}{k_2}$ for each system for a given $(S/N)_{it}$. The parameter S_t/k_2 is the r.m.s. signal to noise per unit root bandwidth in the output of the standard comparison AM link (section 2.9 (ii)) when the output ofthe given system reaches the prescribed value

of $(S/N)_{it}$. The system having the lowest value of S_t/k_2 will obviously give the best performance (for a given $(S/N)_{it}$) under these weak signal conditions.

S_t/k_2 may be calculated using equations (2.14), (2.15) and (2.16). In the case of AM-AM systems no improvement threshold is involved, and we write the parameter as S_v/k_2.

AM-AM

$$\frac{S_v}{k_2} = \sqrt{2}\,\frac{S}{a_{oi}}\left(\frac{S}{N}\right)_{it}(f_{mi})^{\frac{1}{2}} \qquad (2.14)$$

FM-AM

$$\frac{S_t}{k_2} = 2.8\,\frac{S}{a_{oi}}(\beta_i f_{di})^{\frac{1}{2}} \qquad (2.15)$$

AM-FM and FM-FM

$$\frac{S_t}{k_2} = 2\,(\beta D f_h)^{\frac{1}{2}} \qquad (2.16)$$

where f_h is the highest sub-carrier frequency.
The derivation of equations 2.11 to 2.16 is described by Nichols and Rauch (1956).

(v) Comparison of Multiplexing methods.

For the purpose of comparison of telemetry systems, we assume a minimum useful peak signal to noise voltage ratio of three. It may be shown (Tibbs 1947,p.48), that if N is the r.m.s. fluctuation noise voltage, the peak fluctuation noise voltage will, on the average, exceed 4N only 0.0063% of the time. The factor of four is called the fluctuation noise "crest factor". The minimum r.m.s. signal voltage S, for the above condition, is given by the relation

$$\sqrt{2}\,S = 3\,(4N)$$

Hence $(S/N)_{it} = 8.5$ for all i.

Multiplexing methods for a three channel system (using the detectors in table 2.1) and $(S/N)_{it} = 8.5$, are compared in table 2.3.

System	D	D_h	f_h (Kc/s)	S_t/k_2	Carrier bandwidth (Kc/s)
AM-AM	-	-	1.7	320	3.5
FM-AM	-	0.95	3.0	205	6
AM-FM	1.2	-	1.7	220	11
FM-FM	0.64	0.95	3.0	255	16

Table 2.3: Comparison of multiplexing methods for a three channel system with $(S/N)_{it} = 8.5$. The subscript h refers to the highest frequency sub-carrier.

Although the FM-AM and AM-FM systems reach threshold at a slightly lower carrier strength, there are no very significant differences at this value of $(S/N)_{it}$. If, however, we use the standard sub-carrier deviation ratios of five, $(S/N)_{it}$ becomes 72.5 (equation 2.11) with a quite small increase (except in the case of AM-AM) in carrier threshold. Details are given in table 2.4.

System	D	D_i	f_h (Kc/s)	S_t/k_2	Carrier bandwidth (Kc/s)
AM-AM	-	-	1.7	2,840	3.5
FM-AM	-	5	7.35	315	15
AM-FM	2.7	-	1.7	275	19
FM-FM	0.63	5	7.35	395	40

Table 2.4: Comparison of multiplexing methods for a three channel system with standard sub-carriers, corresponding to $(S/N)_{it} = 72.5$.

Again the FM-AM and AM-FM systems are slightly superior to FM-FM. However, these results do not include the effects of crosstalk which will generally be smallest in the FM-FM multiplex. With the simple circuits used in expendable balloon borne equipment, crosstalk may be of considerable importance, especially in systems employing large numbers of sub-carriers. In view of this, and its widespread use elsewhere, the FM-FM method was adopted for the Hobart Group cosmic-ray balloon program.

It is apparent from tables 2.3 and 2.4, that by increasing the sub-carrier deviation ratio from 1 to 5, a gain of nearly 10:1 in $(S/N)_{it}$ is obtained with only a small (about 50%) increase in carrier threshold. The increased deviation ratio will also reduce crosstalk interference and make the linearity requirements of the radio link less stringent. Consequently, all flight units have been designed to have a minimum deviation ratio of five.

2.11 The receiving station.

(i) The antenna and receiver.

The optimum frequency for telemetry from balloon borne equipment has been discussed in some detail by Edwards (1963). The 72 mc/s link, used in these experiments, is somewhat lower than the optimum frequency; the choice being dictated by the desire to use all solid state circuits, and the limited range of frequencies available. The fully transistorised receiver was designed to our specifications by Mr. Ian Bird, in the laboratories of the Antarctic Division, Department of External Affairs, Melbourne. It is a single conversion superhet designed to tune from 68-100 Mc/s, and is supplied with three plug-in I.F. strips providing I.F. bandwidths of 35, 70 and 200 Kc/s. Other features include automatic frequency control, amplified AGC and a noise figure of 5db at 80 mc/s. Four of these receivers have been constructed for the Hobart Cosmic-ray Group by "Laboratory

Electronics", Michelton, Brisbane, Queensland.

The range of I.F. bandwidths specified for the receiver makes possible the use of near optimum carrier deviation ratios for any given multiplex. Many FM receivers do not have this facility, and rely on a low pass filter in the audio section to suppress the noise level. Consequently, they must be operated at a carrier deviation ratio well above optimum for most multiplexes, and their weak signal performance must suffer accordingly.

The receiving station antenna is a twelve element yagi, with a masthead, wide-band television pre-amplifier. At the Antarctic stations two stacked five element yagis are used, because of their ability to withstand high wind velocities.

(ii) Sub-carrier filter and demodulator circuits.

The receiving stations have demodulating equipment for the six standard FM-FM bands 5-11. The circuits for these bands are very similar in design. Each contains a linear common emitter input amplifier followed by a commercially made, standard FM-FM bandpass filter. The filter output drives an LC tuned amplifier-limiter, which in turn drives the sub-carrier demodulator stage. This consists of a common emitter amplifier with the primary of an FM discriminator transformer as load. This circuit is tuned to the centre frequency of the band, and is adjusted to operate as a second limiter stage. The transformers are commercially made to FM-FM standards, and have two secondary windings, closely coupled to the primary and tuned to the upper and lower limits of the channel passband. The outputs are rectified and smoothed with high impedance RC circuits operating silicon transistor emitter follower amplifiers. The difference voltage generated operates a balanced, two stage, power amplifier circuit driving the 12/12 ohm, 1.6 watt pen coils

of the "Both" chart recorder. The amplifier contains gain controls and circuits providing adjustable RC smoothing to reduce the output bandwidth.

(iii) Pulse recording circuits.

The demodulator outputs also operate the automatic pulse recording circuits. There are four of these circuits of identical design. The principle is illustrated in the block diagram (figure 2.7). The input stage is a DC coupled circuit designed to convert the balanced output of the demodulator to a "single ended" (common ground) signal. This operates a Schmitt trigger, with a sensitivity control which can be adjusted to trigger on any point of the signal waveform. It is normally set to trigger on the centre of the balanced signal output (as viewed on the chart record), to minimise the effect of noise. The Schmitt trigger changes state each time the corresponding output binary circuit, in the flight unit, changes state. Consequently, by taking outputs from both sides of the Schmitt circuit and inverting the pulses from one side, we obtain pulses of the same polarity for each change of state of the corresponding binary. These pulses operate a train of binaries with a scale factor of 64. A rotary switch enables selection of scale factors varying from an effective $\frac{1}{2}$ to 64.

The scaled pulses operate a register driving circuit. This consists of a monostable multivibrator , giving an output pulse of 20 milliseconds duration, driving a saturating power stage with the register coil as collector load. The registers are 4 figure, manual re-setting, with a maximum operating rate of 25 p.p.s. There are two registers and power stages per channel, and the multivibrator output is switched alternately from one to the other, at intervals of one minute, by means of a gate circuit. Since one pulse may be lost or gained in the switching proceds when the register circuit is "on", there is an uncertainty of $\pm$ 1 in

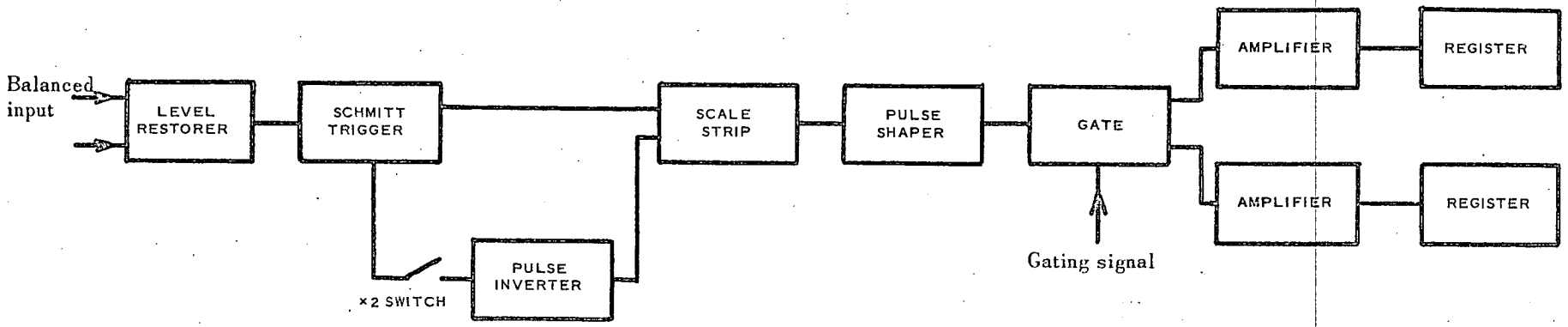

Figure 2.7. Pulse counting circuits.

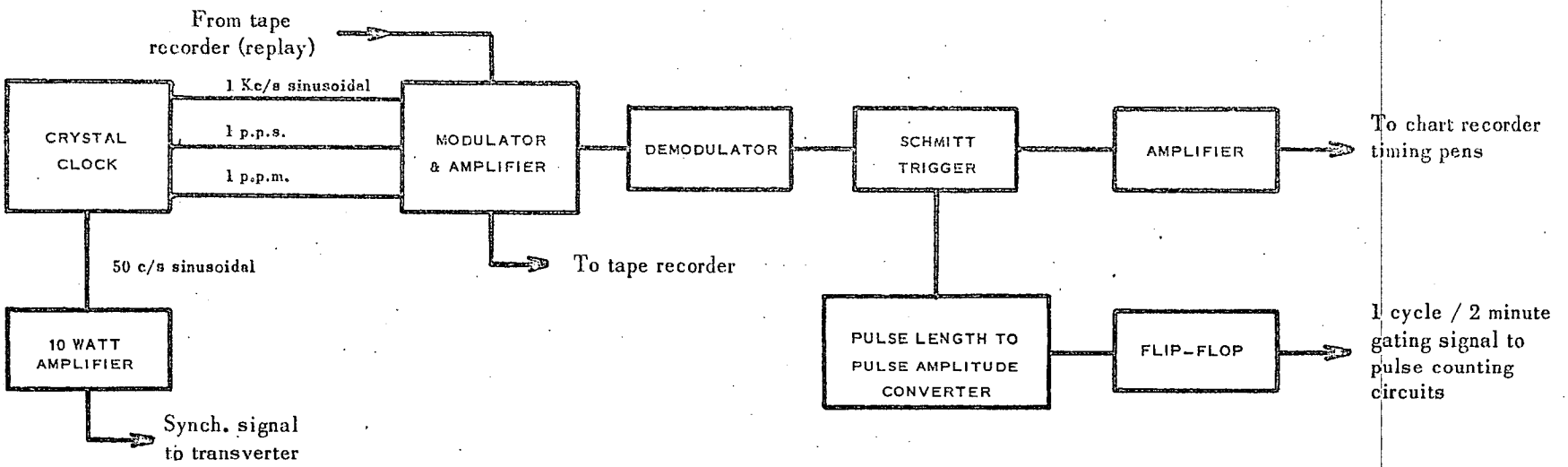

Figure 2.8. Timing circuits.

the number of pulses recorded.

The gate driving signal is generated in a circuit driven by the one minute pulses from the timing circuits. It will be described in the next section.

(iv) Timing circuits.

The general design of the timing circuits is illustrated in the block diagram (figure 2.8). The crystal clock (designed and constructed by Dr. A.G.Fenton of this Department) generates crystal controlled signals at frequencies of 800 c/s and 50 c/s. Timing relays generate pulses at the rate of 1 sec^{-1} ($\sim$100 ms duration) and 1 min^{-1} ($\sim$300 ms duration).

The timing circuits perform several functions. The 50 c/s signal is used, after amplification, to synchronise the transverter which provides power for the tape recorders, and for the chart recorder motor. The pulses from the timing relays amplitude modulate the 800 c/s to produce a timing signal which is recorded, together with the telemetry signal, on a "Philips" stereo tape recorder. This modulated signal is also used to operate the chart recorder timing pens, via demodulator, Schmitt trigger and pen driving amplifier circuits. During replay, from the tape recorder, the same circuits operate the timing pens without adjustment.

The 1 sec^{-1} and 1 min^{-1} pulses have the same amplitude in the modulated signal, and differ only in their duration. The 1 min^{-1} pulses are required for the register gating signals, and are separated from the 1 sec^{-1} pulses by means of a pulse length discriminator. This consists of an integrating circuit, with a time constant of about one second, operating a Schmitt trigger. To avoid loading effects, the integrating circuit is isolated from the Schmitt trigger by a silicon transistor emitter follower stage. The triggering level of the Schmitt circuit can be adjusted so

that the circuit responds to pulses of any duration from 0.1 to 1 second. The output pulses operate a binary circuit, giving rise to a gating signal in the form of a square wave with a period of two minutes.

(v) Power supplies.

All power for the receiving station is supplied by a 13 volt, 150 amp-hour, nickel iron battery. Under normal conditions, the current drain on the battery is matched by the input from a battery charger connected to it. In the event of a power failure, the batteries have sufficient capacity to operate the station for 10 - 15 hours.

A good deal of "hash" is produced on the battery line by the charger and the transverter. The receiver, sub-carrier, timing and register circuits are therefore decoupled from the battery line by means of two stage emitter follower circuits, stabilised with zener diodes to give a 12 volt output. The commercially made transverter draws 10 - 15 amps from the battery, and provides 120 watts of power at 240 volts, 50 c/s AC for the tape recorder. The transverter is synchronised by the 50 c/s from the timing circuits, but tends to lock intermittently to the 50 c/s charger "hash" when operated directly from the battery. It is therefore decoupled from the battery by a three stage emitter follower circuit stabilised to 12 volts with a zener diode. The output frequency of the transverter may be varied, by changing the synchronising frequency, from 45 to 65 c/s. Control of the playback frequency is very useful when playing back tapes recorded on a different machine, or one operated from a mains supply of unstable or non standard frequency.

2.12 Performance of the equipment.

(i) The flight units.

The general performance of the flight units has

been satisfactory. A number of flights lasted more than 16 hours, including long periods of darkness when rig temperatures reached - 45° to - 65°C. All components performed satisfactorily throughout these flights, except during the Macquarie Island 1961-62 program when some rigs failed at low temperatures. The failures were caused by freezing up of the electrolytic capacitors used (during this flight series only), in the battery decoupling circuits to the neutron amplifier and discriminator. One flight from Hobart in 1963, and several from Macquarie Island in 1964, ended suddenly when all channels began to count very erratically. The breakdown was sometimes accompanied by an abrupt change of transmitter frequency, and it has been suggested that these effects may have been caused by the explosion of the neutron detector assembly. This could have been caused by the failure of the "araldite" seals at low temperatures and pressures. Facilities for simulating the balloon environment have recently become available, and it is hoped that the detector assemblies will be tested under these conditions in the near future. A new detector assembly has been designed in the Physics Department workshops, and in this design the "araldite" is replaced by O ring seals.

The oscillator in the EHT supply generates large "spikes" on the battery line, especially when the battery internal impedance is high. It is sometimes necessary to decouple the transmitter from the battery, in order to avoid modulation of the telemetry signal with these "spikes". The effect varies from one rig to another, and decoupling is usually only necessary for rigs intended for long night flights when battery impedances are likely to increase considerably.

The performance (section 2.3 (x)) of the neoprene balloons, fitted with a level flight device, has been very disappointing. This is surprising in view of the high percentage of successes achieved by Laby et al (1957), but may

perhaps be due to the much larger payloads (10 - 15 lbs) used in our flights.

(ii) The telemetry system.

The telemetry system has performed very satisfactorily. Many long flights have been achieved, and in Antarctic regions it has frequently been possible to obtain good signals until the balloon reached the radio horizon. Many flights have had to be terminated after nearly 24 hours when the balloon descended at sunset.

Deep fading has sometimes been observed, and this is presumed to have been caused by multipath effects, since it was considerably reduced by re-siting of the receiving antenna.

The need for a more stable transmitter, in flights from city areas, has been noted in section 2.3 (vii). Recent reductions in the price of high frequency transistors has made this more practical.

It has not always been possible to completely eliminate the effects of crosstalk between sub-carrier channels. However, the problem has never been serious enough to affect the performance of the equipment. Its origin is still under investigation.

(iii) The ground station.

No serious difficulties have been encountered with the ground station. The register read-out system is sometimes triggered by impulse noise, but this has rarely been troublesome, except during long floating flights from Hobart. The interference can easily be recognised on the chart record, thus allowing rejection of the relevant minute totals. Under conditions where this interference is likely to be troublesome, the use of larger scale factors in the flight units would be desirable. This would facilitate the reading of the chart records for periods when impulse noise affected the register read-out.

III THE MEASUREMENTS

3.1 Introduction.

As mentioned in Chapter II, the experimental work may be divided into three main sections: observations from Macquarie Island during auroral and other geophysical activity; neutron and ionising radiation distribution measurements and experiments concerning the characteristics of the neutron detectors. These measurements will be described in more detail in this chapter. Test flights and other measurements which do not fit into any of the above categories, will also be discussed.

3.2 Measurements in auroral and polar regions.

It was suggested (K.B.Fenton, private communication 1960) that the acceleration mechanism, responsible for the frequent precipitation of energetic electrons in auroral regions, may also accelerate protons. The electrons have energies of a few tens of ~~10~~ Kev and a Fermi mechanism would, in principle, accelerate protons to energies of the order of 10 Mev; although the effectiveness of the process would undoubtedly be limited, at these energies, by losses from the trapping region. Protons of these energies would not penetrate to the altitudes accessible to low cost balloons. Some would, however, produce neutrons by interaction with air nuclei and these could be detected at lower altitudes as a result of diffusion. The precipitation of low energy protons in auroral events was well known (McIlwain 1960, Davis et al 1960, McDiarmid et al 1961) and there was some evidence (Korff and Haymes 1960) that higher energy protons may sometimes be precipitated into the atmosphere.

During the southern summer of 1961-1962 an auroral X-ray group, led by Dr.R.R.Brown of the University of California, Berkeley, California, made a series of balloon flights from

Macquarie Island (50°30'S, 158°57'E) during periods of auroral activity. Neutron detectors were hitch-hiked on several of these flights, and a total of 70 hours of neutron count rate data was obtained. Details of the flights are listed in table 3.1. The scintillator and riometer data have been made available by courtesy of Dr.Brown.

Flight no.	Detectors	Time of release	Maximum altitude (mb)	Total flight time (hrs)	X-ray and/or riometer activity
1	N_a,S	2030Z 21/12/61	9	8½	nil
7	N_a	2039Z 13/1/62	13	16	nil
9	N_a	1901Z 23/1/62	14	18	nil
11	N_a,S	1112Z 5/2/62	230	1	-
12	N_a	0246Z 12/2/62	59	1½	-
14	N_a,S	1010Z 15/2/62	12	20½	7x increase in X-rays
21	N_a,S	1000Z 6/3/62	14	3	4x increase in X-rays

Table 3.1: Details of flights from Macquarie Island in 1961-62. The detectors are type A neutron detectors (N_a) and sodium iodide X-ray scintillation detectors (S). The X-ray events are given as the increase above cosmic ray background in the NaI scintillation counting rate.

Flights 1,12 and 21 ended suddenly as a result of amplifier instability caused by freezing up of the electrolytic capacitors in the battery decoupling circuits. The

breakdown was abrupt in all cases, and there is no indication of any effect prior to the failure. Flight 11 was cut short by loss of radio contact due to damage to the antenna during balloon launching. Abnormal increases in neutron counting rate were observed during flights 1 and 21, and these are discussed in detail in chapter V. The results are ambiguous and further flights were considered to be desirable. It was decided that further measurements of this kind should be combined with a long term program to monitor the solar cycle variation of the atmospheric neutron flux over Wilkes, Antarctica.

Seven flights were made from Wilkes during a short summer program in January and February 1963. Expansible neoprene balloons fitted with a level flight device (section 2.3 (x)) were used. Only two performed satisfactorily, and the total flight time at atmospheric depths less than 20 $gm.cm^{-2}$ was about 28 hours. Two more floated for long periods: F6 at 90 $gm.cm^{-2}$, and F8 at 240 $gm.cm^{-2}$. Details of the flights are given in table 3.2.

Flight	Date	Time of release	Altitude reached (mb)	Total flight time (hrs)	Mt.Wellington neutron rate
F1	19/1/63	0327Z	33	1½	607.7
F5	29/1/63	1552Z	7	8	609.5
F6	5/2/63	1517Z	9	23	609.7
F7	10/2/63	1616Z	650	½	612.5
F8	12/2/63	1420Z	9	9½	609.6
F9	16/2/63	1733Z	18	2½	609.3
F10	22/2/63	1316Z	13	2	610.6

Table 3.2: Details of flights from Wilkes, Antarctica in 1963. All rigs included two Geiger counters with differing X-ray sensitivity, a triple coincidence Geiger counter telescope and a type B neutron detector.

The neutron counter in flight F1 failed as a result of RF pick-up. All other rigs performed satisfactorily and flights were terminated as a result of balloon failures. Flights 2, 3 and 4 were balloon test flights without detectors. Geophysical activity was low at the time of the flights and no abnormal effects were observed. Valuable information on the neutron altitude distribution was obtained, and these data will be discussed later.

The Hobart Cosmic-Ray Group and the University of California co-operated in a further series of X-ray measurements from Macquarie Island early in 1964. Neutron and geiger counter measurements were also made in a number of flights, and the results are available to the author by courtesy of Dr.N.R.Parsons and Mr.J.Phillips *. Details of the relevant flights are given in table 3.3.

Flights 5, 6 and 21 were cut short by sudden erratic counting in all channels. The origin of the breakdown is uncertain, but is suspected (section 2.12) to be the failure of the "araldite" seals on the neutron counter assembly. A total of 86 hours at atmospheric depths less than 20 $gm.cm^{-2}$ was achieved in the 8 flights. Intense auroral X-ray bursts were observed during several flights, but there is no evidence of any increase in the neutron flux. The results are discussed in more detail in chapter V, and neutron count rate data from representative flights are listed in table 3.8.

3.3 Measurements of the neutron and ionising radiation distribution in the atmosphere.

The atmospheric neutron flux and ionising radiation were measured in a series of balloon flights during 1964. These flights were made during a short period (August - October) when solar activity was low. No significant changes occurred in the rate of the Mt.Wellington neutron monitor during this

* Present address: c/- Physics Dept.,University of Tasmania.

time, and the results are therefore directly comparable. Details of the flights are given in table 3.4.(p.75).

Flight	Time of release	Maximum altitude reached (mb)	Total flight time (hrs)	Geophysical activity during flight
1	1023Z 5/1/64	12	17	Nil
5	1037Z 16/1/64	11	7½	Intense earth current activity. No X-rays.
6	0929Z 18/1/64	13	7½	Nil
7	1015Z 27/1/64	12	21	Nil
8	1033Z 29/1/64	18	21½	Earth current activity and X-ray events.
10	1743Z 31/1/64	11	19	Slight earth current activity.
15	0910Z 13/2/64	11	3½	Strong earth current and X-ray activity.
21	0953Z 2/3/64	11	5	Nil

Table 3.3: Details of neutron counter flights from Macquarie Island in 1964. For details of the detectors see table 3.2.

Neoprene balloons were used in all cases, and no attempt was made to obtain level flight. The balloon used in Ll burst prematufely. The scaled neutron count rates during each flight are given as a function of pressure in figs. 3.1, 3.2 and 3.3. The smoothed curve values of counting rate at various atmospheric depths are listed, after correction for counter sensitivity, in table 3.5 (p.76). These data will be discussed later in this thesis.

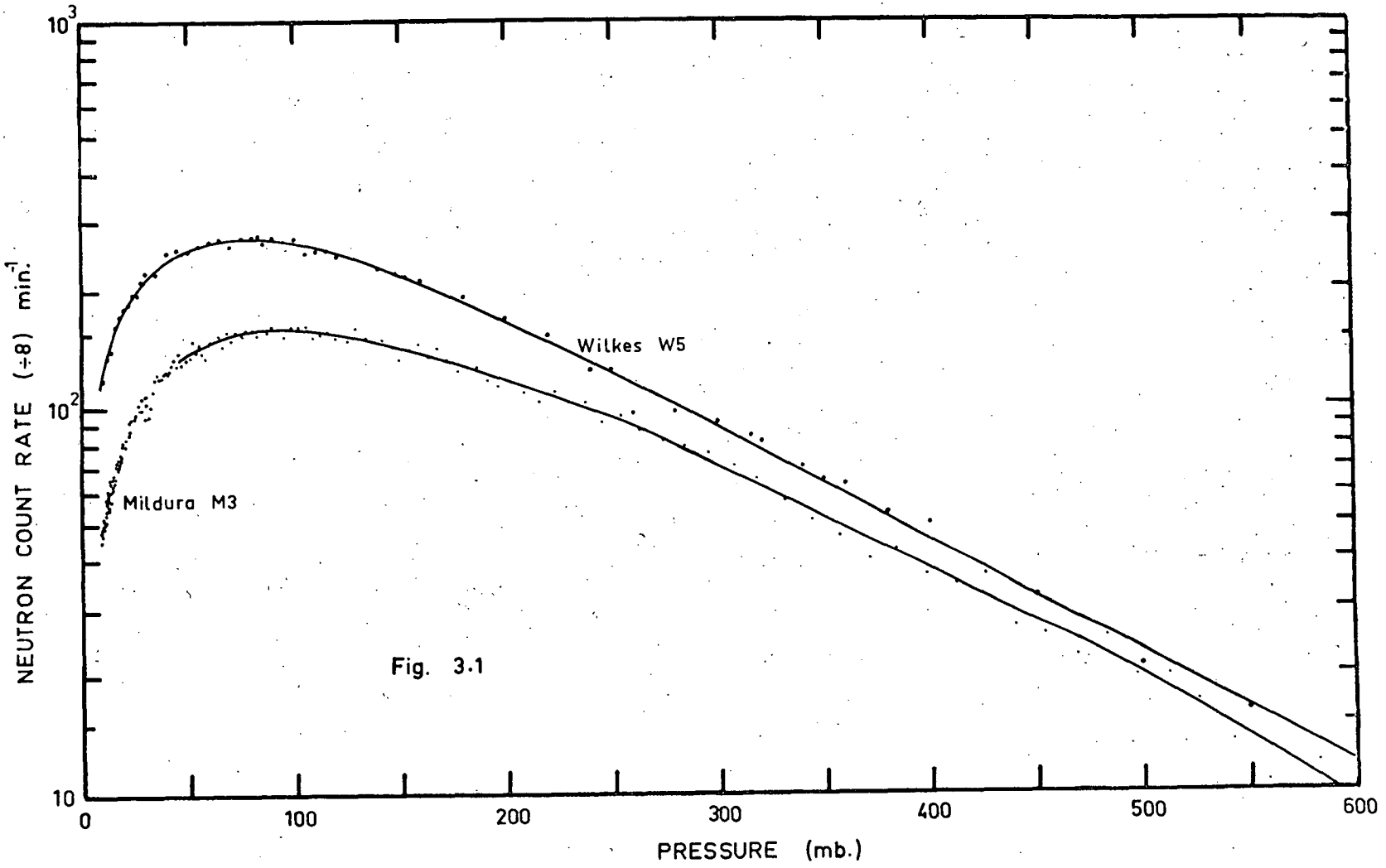
NEUTRON COUNT RATE (±8) min.$^{-1}$
10^3
10^2
10
0
100
200
300
400
500
600
PRESSURE (mb.)
Wilkes W5
Mildura M3

Fig. 3.1

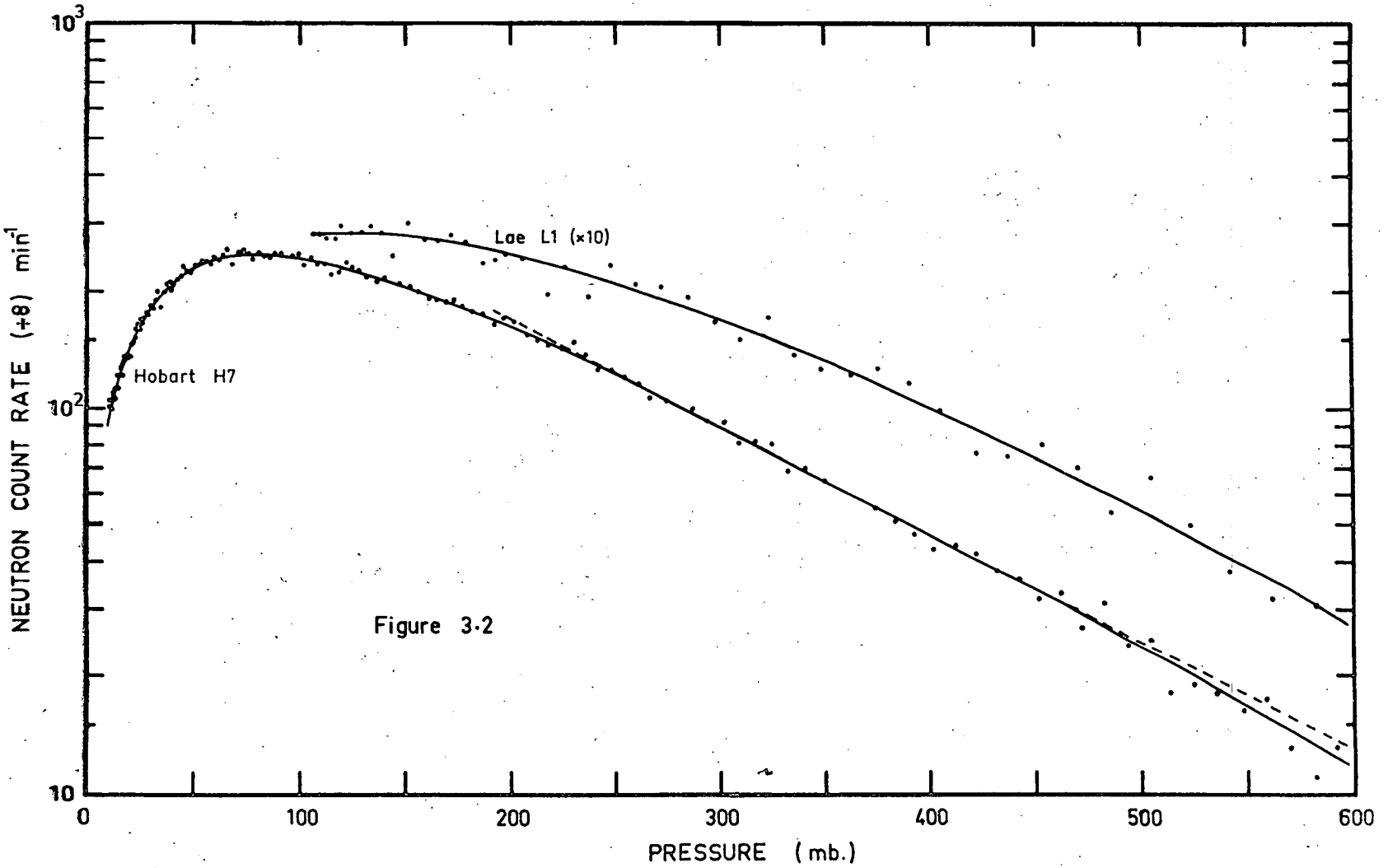
NEUTRON COUNT RATE (+θ) min⁻¹
10³
10²
10
Lae L1 (×10)
Hobart H7
0
100
200
300
400
500
600
PRESSURE (mb.)

Figure 3·2

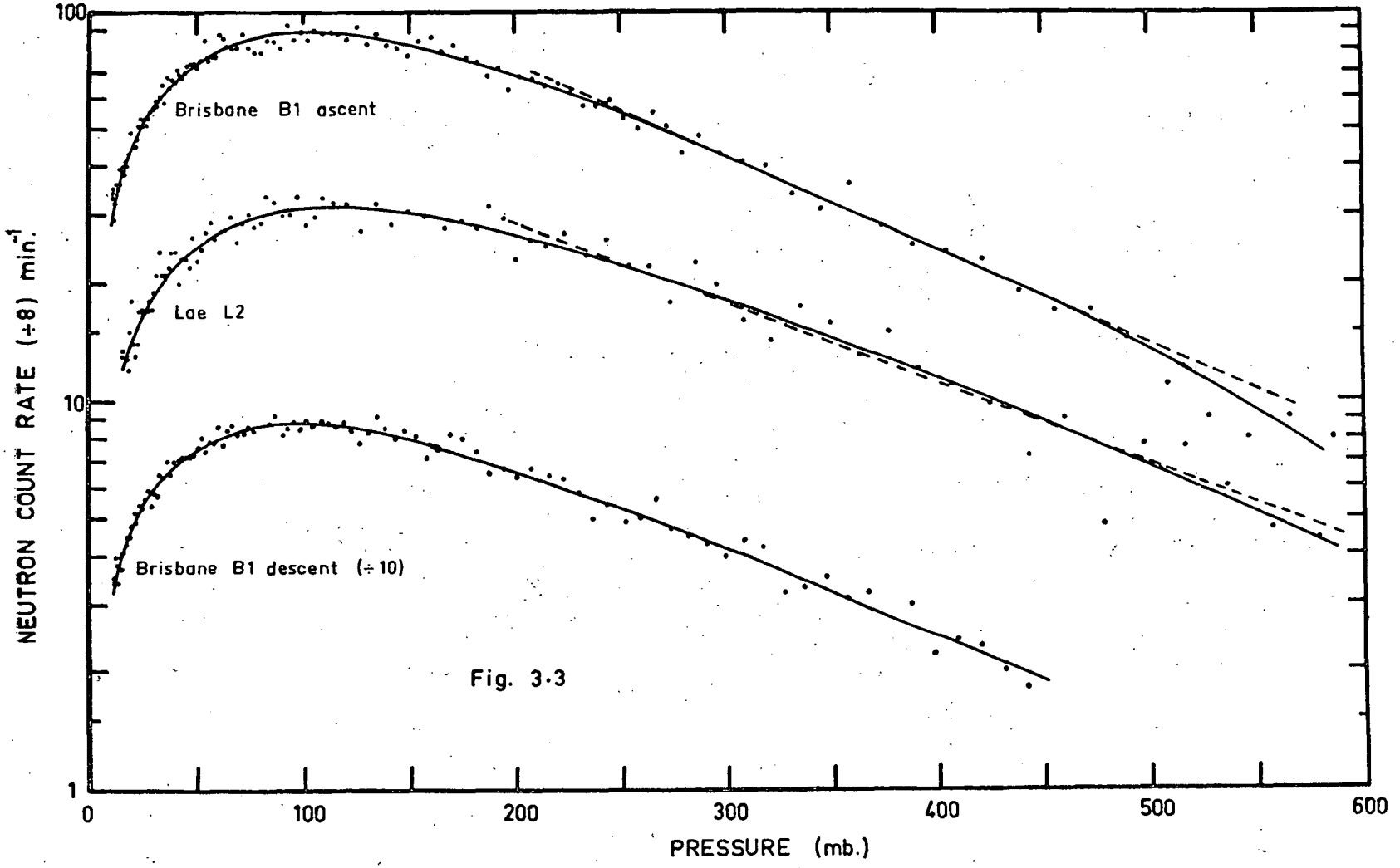
100
10
1
NEUTRON COUNT RATE (÷8) min.⁻¹
Brisbane B1 ascent
Lae L2
Brisbane B1 descent (÷10)
0
100
200
300
400
500
600
PRESSURE (mb.)

Fig. 3.3

Station and flight no.	Geographic Coordinates	Cut-off rigidity (BV)	Detectors	Date	Maximum altitude reached (mb)	Mt.Wellington neutron rate
Wilkes W5	66.6°S 109°E	<0.02	G_1, G_2, T, N_b	20/9/64	10	630.5
Hobart H7	42.9°S 147°E	1.79	G_1, T, N_d	14/10/64	9	631.7
Mildura M3	34.1°S 142°E	4.0	T, N_a, N_b	25/9/64	9	631.3
Brisbane B1	27.4°S 153°E	7.0	T, N_d	22/8/64	11	633.4
Lae						
L1	6.8°S	15.8	T, N_d	29/8/64	109	631.5
L2	147°E		T, N_d	1/9/64	16	631.1

Table 3.4: Details of the latitude and altitude distribution measurements. The values of the cut-off rigidity are from Quenby and Wenk (1962).
The detectors are:

G_1 - geiger counter
G_2 - shielded geiger counter
T - triple coincidence geiger counter telescope
N_a - type A neutron assembly
N_b - type B neutron assembly
N_d - type D neutron assembly.

3.4 Experiments concerning the neutron counter characteristics.

The BF_3 proportional counter responds to all events which leave more than about 2 Mev of ionisation energy in it. Consequently a "background", due to nuclear stars and other highly ionising events, exists in the counting rate. This background may be eliminated by the difference technique (Staker 1950) in which two counters, differing only in the

FLIGHT	R(cal)	PRESSURE (mb)									
		400	306	240	200	150	100	50	25	15	10
Wilkes W5	145.0	49.6	94.9	144	184	243	296	287	223	167	131
Hobart H7	156.6	48.1	87.9	131	166	210	250	234	167	123	98
Mildura M3	157.1	38.2	69.2	98.8	119	145	161	141	97.8	69.3	51.7
Brisbane B1	156.3	24.9	41.9	58.5	70.1	83.9	91.6	76.3	52.2	38.6	33.2
Lae L1	150.7	10.8	17.6	23.2	26.5	30.2	-	-	-	-	-
L2	160.3	11.4	17.7	22.9	26.4	30.4	31.2	24.5	16.7	11.8	-

TABLE 3.5 : Neutron count rate (± 8 min^{-1}) normalised to a detector sensitivity given by R(cal) = 160 min^{-1}. Underlined data has been obtained by an extrapolation over not more than 1 mb.

boron 10 isotopic concentration of the BF_3, are used. Details of the method are given in chapter IV. Two flights, designed to give information on the background, have been made. One of these (Mildura M6) employed moderated counters. The other (Wilkes DN3) employed unmoderated counters, and was part of a series of measurements (section 3.2) of the neutron distribution at Wilkes. Details of M6 and DN3 are given in table 3.6.

The neutron flux is isotropic in the lower atmosphere but becomes increasingly anisotropic at higher altitudes (section 1.10 (i)). The neutron detection efficiency of cylindrical counters depends on the angle of incidence of the neutrons (Hess et al 1959), and the counting rate at high altitudes will therefore depend on the orientation of the detector. In order to determine the magnitude of this effect, two counters, one standing vertically and the other horizontally, were flown in the same rig during Mildura flight M8 (table 3.6).

Because of the limited time and number of flights available, this experiment was combined with an experiment designed to check the relative calibration of the B and D type neutron detectors. Since these detector types have essentially the same geometry, their sensitivity, relative to each other, should be independent of neutron energy. Type B and D counters with the same calibration sensitivity would therefore be expected to give the same counting rate during a flight in the same rig. In order to check this, one detector in flight M8 was of the B type and the other of the D type.

The use of different detector types should not affect the anisotropy experiment described above, since their geometric sensitivity patterns should be very similar. It is also unlikely that the energy response of the two counter types will be sufficiently different to affect the results. This matter will be investigated in chapter IV when the results of the experiment are analysed.

Station and flight	Date	Detectors	Counter calibrations		Maximum altitude reached (mb)
			Enriched	Unenriched	
Wilkes DN3	/3/65	T, N_s, N_{su}	66.7	15.46	108
Mildura M6	19/1/65	G_1, N_d, N_{du}	149.4	45.03	19
			Vertical	Horizontal	
Mildura M8	8/4/65	$G_1, N_a(V), N_b(H)$	149.4	157.1	19

Table 3.6: Details of flights giving information on the characteristics of the neutron detectors. N_s represents an unmoderated (slow neutron) detector, and the subscript u indicates an unenriched counter. The other detector symbols are given in table 3.4.

The reason for the failure of flight DN3 at 109 mb is not known. The RF signal strength remained strong until the balloon burst at 7 mb, but the sub-carriers gradually faded out and were lost at 109 mb. The data at lower altitudes do not appear to have been affected, however. Severe "wow" in the wire recording of flight M6 made readout of the enriched (N_d) neutron counter data very difficult, and very little data have been obtained from this channel. Several hours of level flight results were obtained in flights M6 and M8.

3.5 Other flights involving neutron detectors.

In addition to the flights described in the preceding sections, data are available from a number of other flights. These results have been useful in determining the relationship between the counting rates at high altitudes and the rate of the Mt.Wellington neutron monitor.

There have been 7 flights from Hobart employing moderated neutron detectors. One of these, H6, failed as a result of transmitter breakdown. Only geiger counter and a little neutron data have been obtained from another, H1, because of overmodulation of the AM carrier used in the flight. Flight H7 has been described in section 3.3. Details of the other flights from Hobart are given in table 3.7. One of the balloons used in flight H5 burst prematurely at 76 mb. In addition, the neutron counter calibration was affected to an unknown extent by a Ra-Be neutron source inadvertently left near the calibration set-up.

Four of the eight neutron flights from Mildura failed as a result of difficulties with the on-flight wire recorder which has since been replaced (section 2.4) by a tape recorder. Three of the remainder have been described (section 3.4), and details of the other, M2, are given in table 3.7. Flight M2 has provided useful information on the time variations of the neutron flux over Mildura.

Data from flight W2 at Wilkes early in 1964 have been made available by Mr.M.Bowthorpe of the Antarctic Division, Department of External Affairs, Melbourne. Details are given in table 3.7.

Two flights have been made from Hyderabad, in India, by courtesy of the organisers of the IQSY-EQUEX cosmic ray balloon program. Details of the flights are given in table 3.7. Dr.K.G.McCracken of the Southwest Center for Advanced Study, Dallas, Texas, conducted these experiments on our behalf using flight units constructed in this department. All signals were tape recorded for analysis at a later date but unfortunately difficulties with the tape recorder have delayed the readout of the data. Some portions of the flights were recorded on a chart recorder during flight, and it is clear that RF pick-up caused oscillation of the unenriched neutron counter (N_{du}) amplifier. All other channels functioned correctly, and it is hoped that the data will be avail-

able in the near future.

Station and flight		Date	Detectors	Maximum altitude reached (mb)	Mt.Wellington neutron rate
Hobart	H2	20/11/63	G_1, N_a	12	606.3
	H3	2/3/64	T, N_c	9	620.9
	H4	9/3/64	T, N_c		
	H5	29/8/64	G_1, T, N_d	76	631.5
Mildura	M2	20/2/64	T, N_a, N_b	10	618.1
Wilkes	W2	2/3/64	G_1, G_2, T, N_b	8	620.9
Hyderabad	Hd 1	30/3/65	G_1, T, N_d, N_{du}	4.5	644.6
	Hd 2	9/4/65	"	3.5	644.8

Table 3.7: Details of flights described in section 3.5.

3.6 Tabulation of neutron counting rate data.

The smoothed curve values of the scaled neutron counting rates at various atmospheric depths are given in table 3.8 for representative flights from sections 3.2, 3.4 and 3.5. Except where noted otherwise, these data have been corrected to a standard counter sensitivity.

Table 3.8: Smoothed curve values of the neutron counting rates. All results, except those from flights H5 and M6, have been corrected to a standard counter efficiency. Macquarie Island flight MQ26/64 (not described previously) was released at 1029Z March 9th, 1964.

Flight		Mt. Wellington neutron rate	R(cal)	Pressure (mb) 400	306	240	200	150	100	50	25	15	10
Wilkes (1963)	6	609.7	153.4	45.2	85.5	131	170	219	267	250	184	129	104
	9	609.3	159.2	44.2	82.5	126	164	211	253	243	185	-	-
	10	610.6	151.5	45.7	83.9	127	162	210	259	252	181	131	-
Wilkes (1964)	2	620.9	103.3	50.3	93.4	139	175	229	272	274	204	163	138
Macquarie (1964)	5	623.0	108.0		91.9	138	173	226	282	268	187	133	-
	6	621.7	109.3		91.5	133	173	225	272	250	174	121	-
	7	621.9	131.3		96.9	138	174	230	271	248	187	132	-
	8	617.1	99.9		89.6	135	171	221	268	252	174	-	-
	10	616.8	112.3		88.3	137	175	228	272	250	187	132	-
	15	622.4	109.8		91.9	133	165	222	262	254	181	129	-
	21	620.9	124.8		89.1	140	180	233	274	267	187	142	-
	26	618.8	123.6		90.7	139	175	229	272	268	193	-	-

(continued on next page)

Table 3.8 (continued).

Flight		Mt. Wellington neutron rate	R(cal)	Pressure (mb) 400	306	240	200	150	100	50	25	15	10
Hobart													
	H2	606.3	156.3	40.9	77.3	117	147	184	219	201	143	104	79.3
	H5	631.5	-	41.3	78	118	150	191	217	-	-	-	-
Mildura													
	M2	618.1	157.1	37.5	65.5	92.6	110	134	154	137	92.4	63.8	47.7
	M6	640.4	45.0	9.9	17.2	25.3	32.1	39.5	43.5	39.5	27.3	-	-
	M8H	645.5	157.1	-	-	103	124	149	169	148	103	-	-
	M6V	645.5	149.4	38.3	68.8	100	124	150	167	148	102	-	-

IV THE CHARACTERISTICS OF THE NEUTRON DETECTORS

4.1 Introduction.

A number of factors, affecting the altitude and latitude dependence of the counting rate, must be considered in the evaluation of the measurements. These include:

(i) the variation of the counter efficiency with energy
(ii) the variation of the atmospheric neutron energy spectrum with altitude and latitude
(iii) the background counting rate due to highly ionising particles and nuclear stars produced in the gas and walls of the counter
(iv) the production of neutrons in the materials of the flight unit
(v) the variation of the neutron detection efficiency with the angle of incidence of the neutron.

The variation of the atmospheric neutron energy spectrum and its effect on the count rate will be discussed later in this thesis. The other factors will now be considered in more detail.

4.2 The energy dependence of the neutron counter sensitivity.

The efficiency of moderated neutron counters varies slowly with neutron energy over the range from thermal energies to about 1 Mev, but decreases rapidly thereafter. Details of the shape and absolute value of the counter response curve are essential for the interpretation of many experiments. Unfortunately, it has not, as yet, been possible to obtain these details for our detectors. We have been forced, therefore, to rely on the response curves of other detectors as published (Hess et al 1959, Fraeki et al 1963, Boella et al 1963, Bame et al 1963).

The relative response depends largely on the thickness and geometry of the moderator sheath, and our detectors differ in this respect from all the detectors referred to above.

Consequently, we have made use of a number of different response curves in our analyses, in order to obtain some indication of the sensitivity of the results obtained to the details of the response curve used. In future we will denote these curves by $\eta_n(E)$ where

$\eta_1(E)$ represents the response of a system (Fraeki et al 1963) employing plane geometry with a $\frac{1}{2}$ inch thick polyethylene moderator.

Corresponding details for the others are:

$\eta_2(E)$: spherical geometry, 0-2" moderator, Boella et al (1963)

$\eta_3(E)$: plane geometry, 1" moderator, Fraeki et al (1963)

$\eta_4(E)$: cylindrical geometry, $\frac{1}{2}$" moderator with cadmium sheath, Hess et al (1959)

$\eta_5(E)$: cylindrical geometry, 1" moderator with cadmium sheath, Hess et al (1959)

$\eta_6(E)$: cylindrical geometry, 1" moderator sheath, Hame et al (1963).

These curves are illustrated in figure 4.1. The great variability of the curves, particularly at high energies, indicates the need for careful measurement of the response of our detectors. This information would be particularly useful in the study of the neutron events in the Macquarie Island data (chapter V). Fortunately, however, the analysis of most of our results does not depend significantly on the energy response of the neutron detector. The counting rate R of a neutron detector with relative efficiency $\eta(E)$ in a neutron flux $\phi(E)$ is

$$R = k\int_0^\infty \eta(E)\,\phi(E)\,dE \qquad (4.1)$$

where E is the neutron energy and k is the normalisation constant for the absolute efficiency $k\eta(E)$ of the neutron detector.

In section 1.12 we noted the pronounced "bump" in the

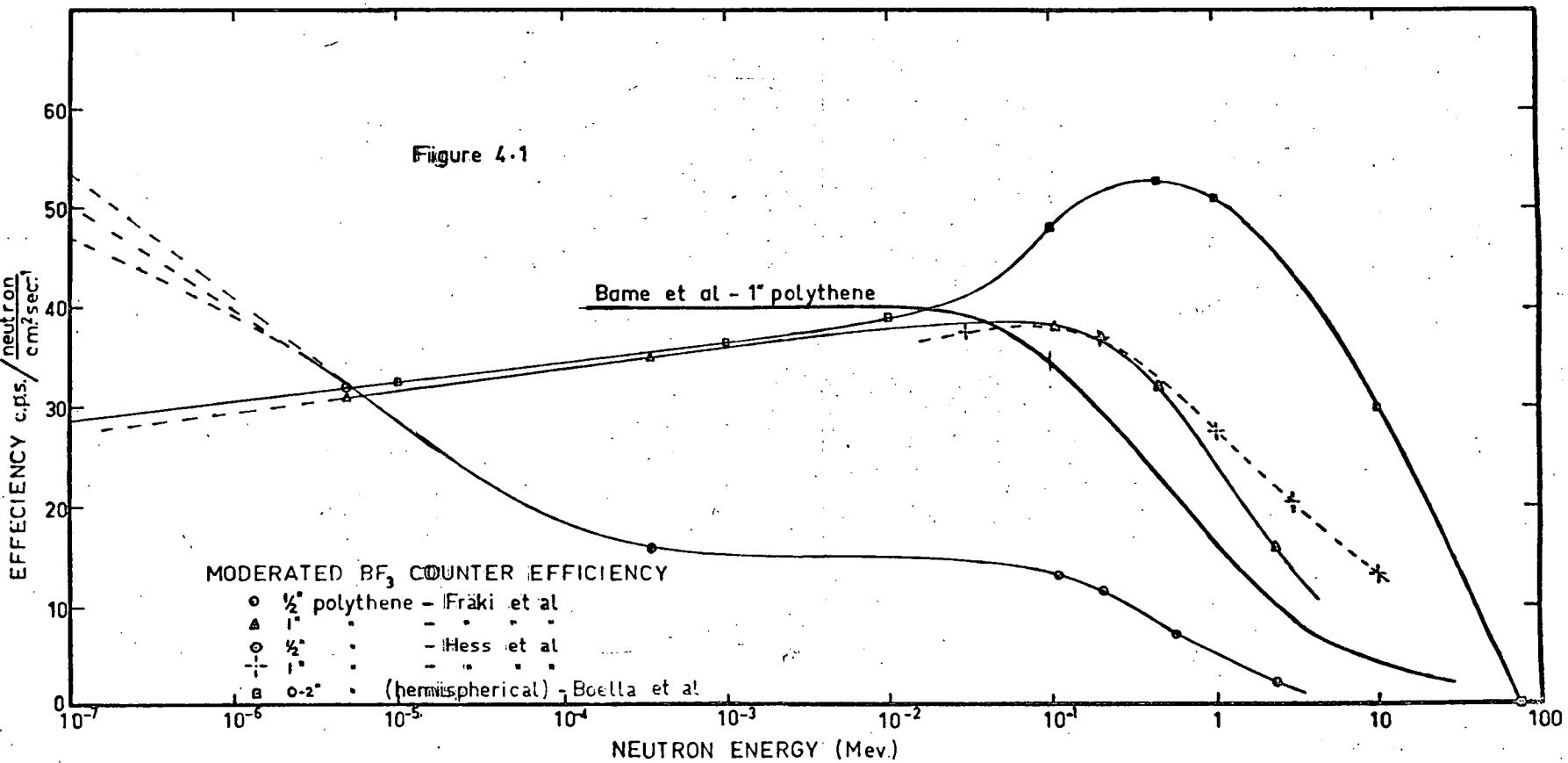
Figure 4.1
Bame et al - 1" polythene
EFFECIENCY c.p.s./neutron/cm².sec⁻¹
MODERATED BF₃ COUNTER EFFICIENCY
½" polythene - Fräki et al
1" " - " " "
½" " - Hess et al
1" " - " " "
0-2" " (hemispherical) - Boella et al
NEUTRON ENERGY (Mev.)
0
10
20
30
40
50
60
10⁻⁷
10⁻⁶
10⁻⁵
10⁻⁴
10⁻³
10⁻²
10⁻¹
1
10
100

neutron energy distribution, caused by source neutrons. These make an important contribution to the counting rate of moderated neutron detectors. In figure 4.2 we have divided the atmospheric neutrons into groups, corresponding to various energy ranges, and evaluated the fraction of the counting rate due to neutrons from each group. The calculations are based on the energy spectrum of Hess et al (1959) and the $\eta_4(E)$ and $\eta_5(E)$ counter response curves. The relatively large contribution by 0.1 to 1.0 Mev neutrons is apparent in figure 4.2. $E > 10$ Mev neutrons have little effect on the counting rate. Figure 4.2 would undoubtedly be somewhat different for our counters which have no cadmium sheath and are therefore more sensitive to low energy neutrons than are counters with the $\eta_4(E)$ or $\eta_5(E)$ responses. Nevertheless, the conclusions reached above will probably still be valid.

To obtain some idea of the absolute efficiency of our counters, we make use of the neutron flux calculations of Newkirk (1963) and the counting rate observed during flights from Macquarie Island and Hobart. Small corrections were required, to allow for the time and latitude differences between our measurements and those of Smith et al (1962) to which Newkirk's measurements were normalised. The corrections were based on the time and latitude variations described later in this thesis. The normalisation constant k_i corresponding to the relative counter response $\eta_i(E)$ may be evaluated using equation (4.2)

$$k_i = \frac{R \text{ (observed)}}{\int_0^\infty \eta_i(E)\, \phi(E)\, dE} \qquad (4.2)$$

The value of k_i has been evaluated for $i = 1$ and 2 using the count rate at 200 $gm.cm^{-2}$ during Macquarie Island flight 14 in 1962, and for $i = 3$ and 6 using the count rate at the same depth during Hobart flight H2 in 1963. The results are listed, together with the corresponding value for the absolute efficiency, in table 4.1.

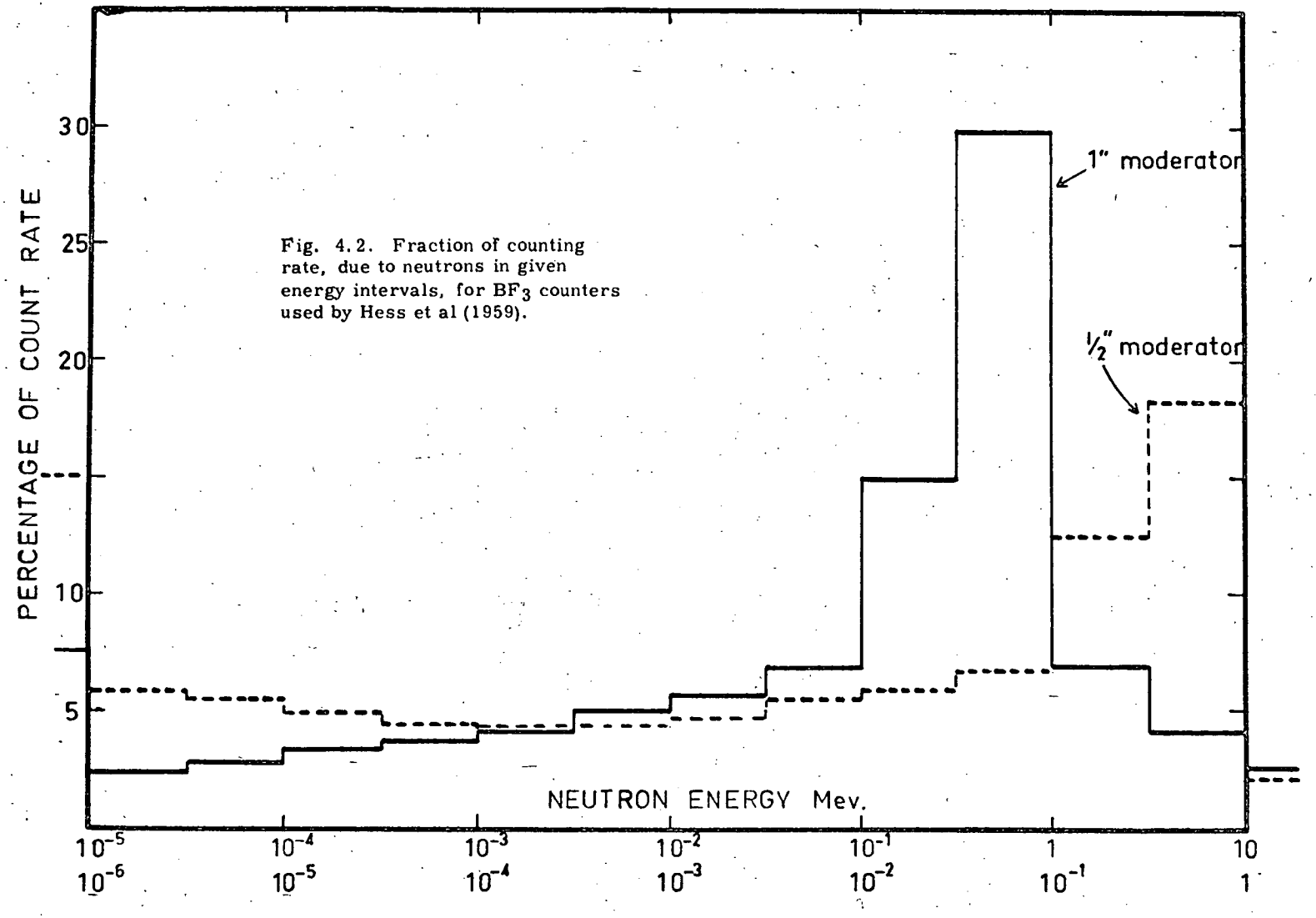

Fig. 4.2. Fraction of counting rate, due to neutrons in given energy intervals, for BF_3 counters used by Hess et al (1959).

	Counter response curve $\eta_1(E)$	$\eta_2(E)$	$\eta_3(E)$	$\eta_6(E)$
Counter assembly type	A	A	B,D	B,D
Normalisation constant k	0.23	0.11	0.17	0.17
Absolute efficiency (counts/unit flux) at 1 Kev	3.6	3.3	6.1	6.9
1 Mev	1.2	4.6	4.1	2.8

Table 4.1: Details of the absolute efficiency of type A and types B and D neutron counters.

The efficiency of the type A counter differs markedly at high energies depending on the response curve used. The $\eta_1(E)$ curve is undoubtedly a much closer approximation to the actual response than is the $\eta_2(E)$ curve. The latter is useful, however, in estimating the sensitivity of a particular result to the response curve used.

4.3 The highly ionising background.

In section 3.4 we described flights designed to measure the highly ionising event "background" in our detectors. These measurements involved flying two counters differing only in the boron 10 isotopic concentration of the BF_3. If the concentrations are known, it is a matter of simple algebra Staker 1950) to calculate the fraction of the total rate caused by highly ionising events. Because of the variability of our detector units, we have instead made use of the calibration system to determine their relative sensitivity. This is possible because the neutron flux in the calibration system is of such a magnitude that we can ignore the background during calibration. If the counting rates during calibration are respectively $N_e(cal)$ and $N_u(cal)$ for the enriched and unenriched counters, their relative efficiency is

$$K = \frac{N_e(cal)}{N_u(cal)} \qquad (4.3)$$

Since the geometry of the counters and moderators is very similar and we can ignore self screening effects, the ratio K will be independent of the neutron energy spectrum.

At any atmospheric depth z the counting rates $R_e(z)$ and $R_u(z)$ of the two counters will be

$$R_e(z) = N_e(z) + B_e(z) \qquad (4.4)$$

$$R_u(z) = N_u(z) + B_u(z) \qquad (4.5)$$

where $B_e(z)$ and $B_u(z)$ are the background rates in the two counters. These are virtually independent of moderator geometry and isotopic concentration and are therefore equal, to a first approximation.

Consequently we can show from (4.3), (4.4) and (4.5) that the ratio of the neutron rate to the total rate in the enriched counter is

$$\frac{N_e}{R_e}(z) = \frac{K}{K-1} \cdot \frac{R_e(z) - R_u(z)}{R_e(z)} \qquad (4.6)$$

The ratio of the background to the total rate is

$$\frac{B}{R_e}(z) = 1 - \frac{N_e}{R_e}(z) \qquad (4.7)$$

Data from the relevant flights (DN3 and M6) are listed in table 3.8. As mentioned in section 3.4, the rates of the enriched counter in flight M6 could not be read out from the flight recording, and we have been forced to use the enriched counter rates from flights M3 and M8. Using these results and equations (4.6) and (4.7), we have evaluated the background as a percentage of the enriched counter rate. In figure 4.3, the variation of the background with atmospheric depth is given for flight DN3 and for flight M6 using the M3 and M8 enriched counter data. The background rate for DN3 is illustrated as a percentage of the moderated counter rate in Wilkes W5 (table 3.5) in figure 4.4.

It is clear from figure 4.3 that the results from flight

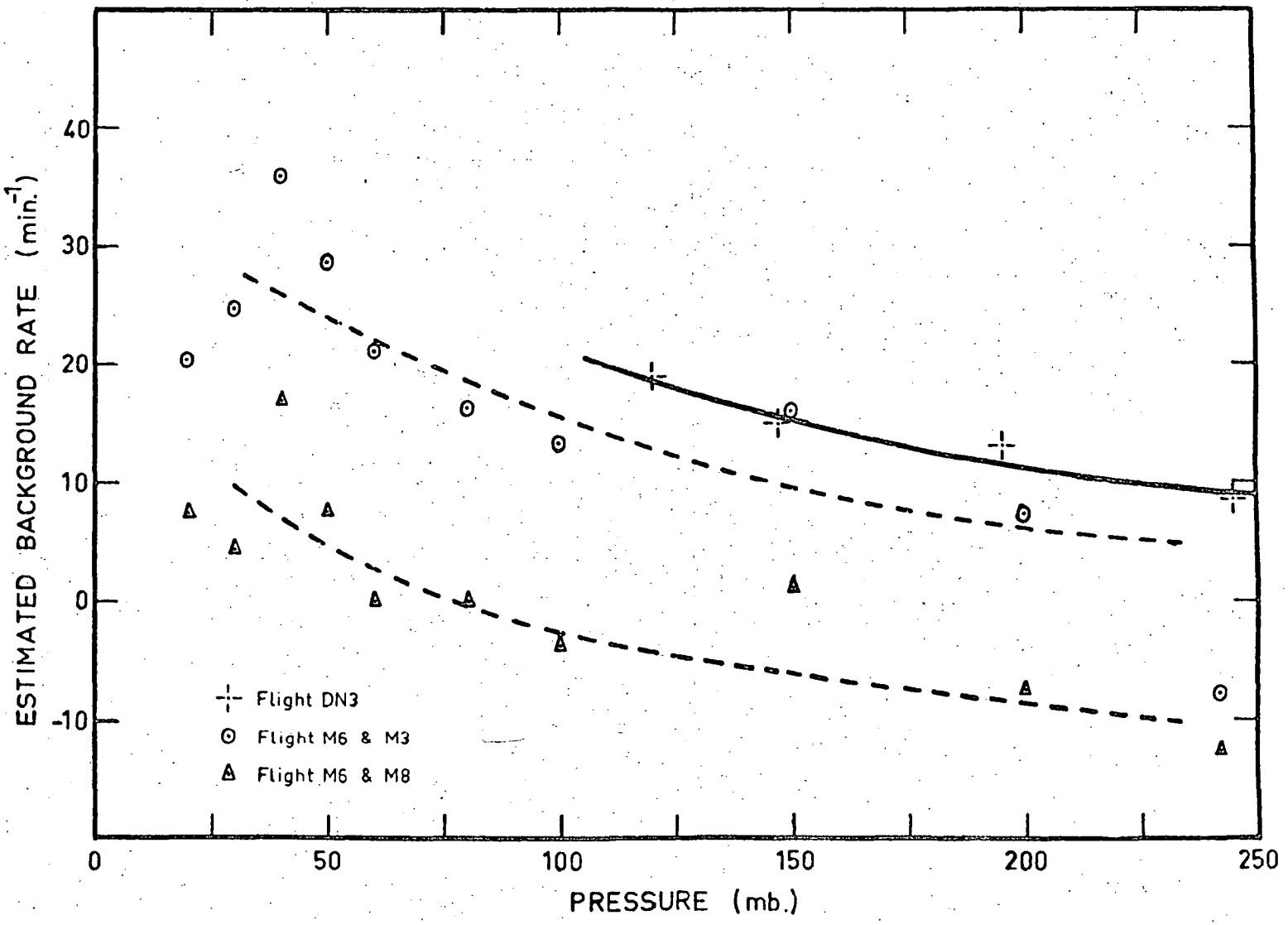

Fig. 4.3. Estimated ionising event background in BF_3 counters during flights DN3 and M6. The latter rates have been estimated using enriched counter rates during flights M3 and M6.

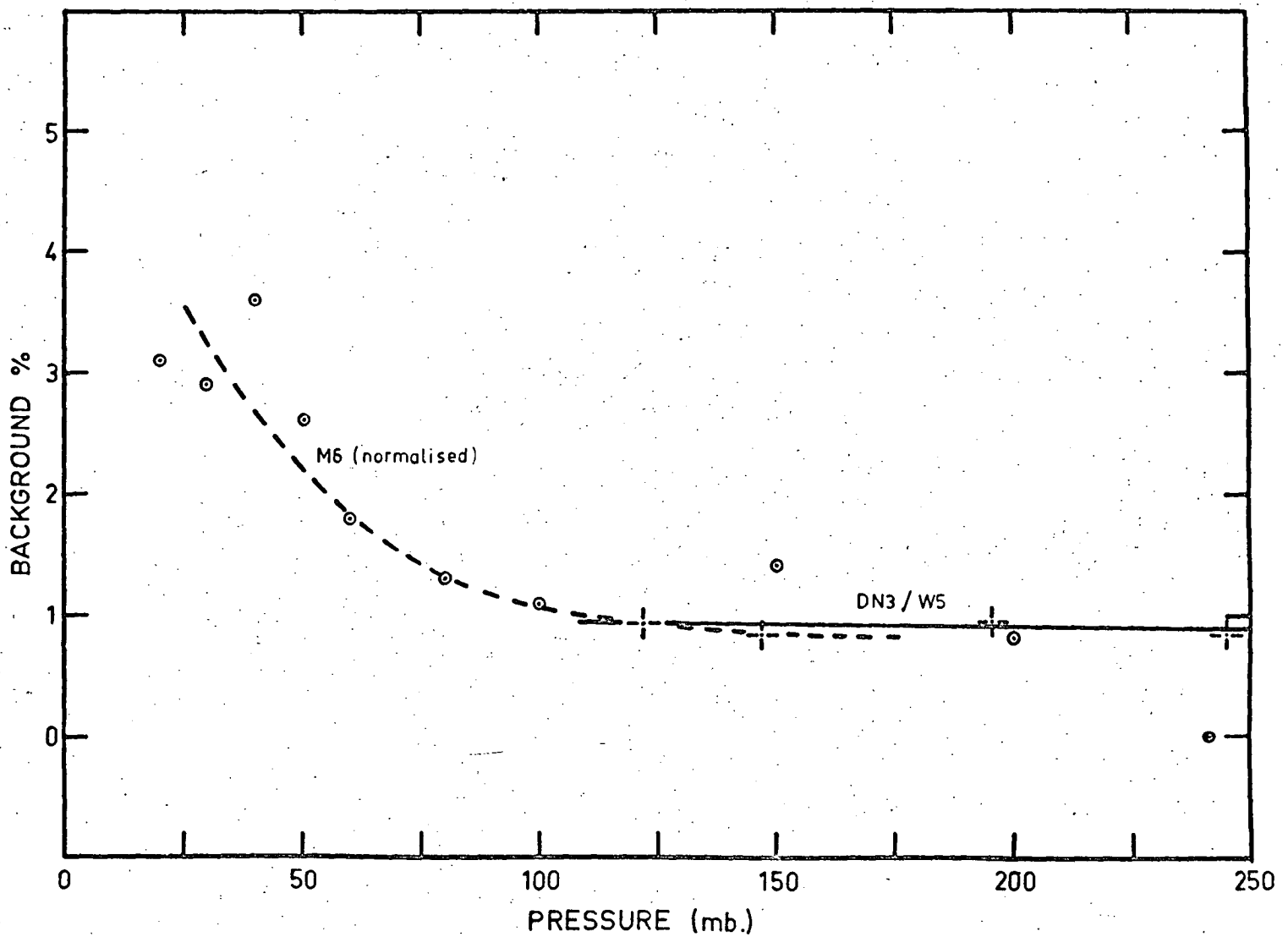

Fig. 4.4. Estimated background rates during flights DN3 and M6. The rates are expressed as percentages of the enriched counter rates during flights W5/64 and M8 respectively.

M6 are in error. Assuming the calibration of the unenriched counter in M6 to be incorrect, we have adjusted its value to normalise the percentage background at 200 mb to the results from Wilkes flight DN3 (figure 4.4). The calibration rate for the M6 unenriched counter then becomes 39 min^{-1}. Unfortunately the counter was lost in a subsequent flight from Mildura and the new figure for the calibration cannot be checked.

The background, obtained in the manner described above, is illustrated in figure 4.4. While there is considerable uncertainty in this result, it is clear that it forms a relatively small fraction of the total rate to the highest altitudes (20 $gm.cm^{-2}$) reached in the experiments. This conclusion is supported by the measurements of Bame et al (1963). The background will increase rapidly at higher altitudes as the neutron flux decreases, and more measurements in this region are desirable. It had been hoped that the measurements from Hyderabad would assist in this regard, but the failure (section 3.5) of the unenriched neutron channel makes this impossible.

4.4 Production of neutrons in the materials of the flight units.

Neutrons produced in the condensed materials of the flight unit, detector and moderator contribute significantly to the counting rate, especially at altitudes above the transition maximum. Trainor and Lockwood (1964) estimate that 20-40% of the counts in their satellite borne, moderated BF_3 counters were caused by neutrons generated in the detector system.

Precise calculations of the effect of local production would be very involved, but preliminary estimates suggest that it can be ignored for our detectors at atmospheric depths greater than 10-15 $gm.cm^{-2}$. We outline below the method used to obtain these estimates.

(1) We assume that local production is confined to the counter assembly. We may neglect the contribution from the remainder of the flight unit, since its mass is not much greater than that of the detector unit and elementary calculations indicate that less than 10% of the neutrons produced in this material are incident on the detector.

(2) Assume that the production rate in the materials of the system is the same as the production rate in air. Polyethylene $(CH_2)_n$ and aluminium are the main materials of the detector system, and Montgomery and Tobey (1949) have shown that the cosmic ray neutron production rates for these materials are not very different from that for air.

(3) Assume that the production rate is the same throughout the detector, and is equal to the rate at the balloon level. The neutron production curves of Lingenfelter (1963) indicate a manimum change of 10-15% in the production rate over an atmospheric depth interval of 10 $gm.cm^{-2}$. Since the mean path length through the detector system is about 10 $gm.cm^{-2}$, no serious error is introduced by making this assumption.

(4) We use the neutron production curves of Lingenfelter (1963) to estimate the number of neutrons L(Z) produced per second in the detector system. For the purposes of this calculation the detector system is assumed to be equivalent to 1,500 gms of air. Values of L(Z) at geomagnetic latitudes of 0^o and 90^o are given, for various atmospheric depths, in table 4.2

Geomagnetic Latitude	Atmospheric depth ($gm.cm^{-2}$) 250	100	50	25	0
0^o	3.8	7.2	6.3	5.8	5.2
90^o	18	44	62	74	101

Table 4.2: Neutron production rate (sec^{-1}) in the detector system.

(5) The counting rate R_L due to local production can be evaluated using the equation

$$R_L(Z) = k \int_0^\infty \phi_L(Z,E)\, \eta(E)\, dE \qquad (4.8)$$

where $k\eta(E)$ is the absolute efficiency of the detector at energy E. We use the values given for η_3 in section 4.2, although the actual efficiency will be reduced, especially at high energies, because of the shorter average path length in the moderator.

$\phi_L(Z,E)$ is the differential flux of locally produced neutrons. We may obtain a rough estimate of ϕ_L by assuming that all the locally produced neutrons are generated on the outside surface of the moderator and that they have directions isotropic over the inner hemisphere. The number of neutrons per second per square centimeter of the surface must be multiplied by four to obtain the equivalent flux (neutrons sec^{-1} per unit sphere)

(6) We assume that the energy spectrum of the locally produced neutrons is of the evaporation type and indepdent of Z. That is

$$1(Z,E) = L(Z)\, E \exp\left(-\frac{E}{\theta}\right) \qquad (4.9)$$

where $\theta = 1$ Mev

(7) The count rate R_L due to local production can now be evaluated. Thus, from equations (4.8) and (4.9)

$$R_L(Z) \approx \frac{4k\, L(Z)}{A} \int_0^\infty E \exp\left(-\frac{E}{\theta}\right) \eta_3(E)\, dE \qquad (4.10)$$

where A is the area of the outside surface of the moderator.

Evaluating the integral and putting A equal to 650 cm^2 we obtain

$$R_L(Z) \approx 1.5 \times 10^{-2}\, L(Z) \text{ sec}^{-1} \qquad (4.11)$$

Values of R_L are given for various atmospheric depths at $\lambda = 0^\circ$ and 90° in table 4.3. R_L can be evaluated for other latitudes and altitudes using equation (4.11) and the production rate curves of Lingenfelter (1963).

	Atmospheric depth (gm cm^{-2})					
	250	100	50	25	10	0
$\lambda = 0^\circ$						
R_L (min^{-1})	4.5	8.7	7.5	6.9	6.6	6.3
R (total)	208	288	232	157	91	-
%	2.1	3.0	3.3	4.5	7.3	-
$\lambda = 90^\circ$						
R_L (min^{-1})	24	54	75	90	110	120
R (total)	1020	2140	2080	1600	940	-
%	2.4	2.4	3.6	5.7	11.7	-

Table 4.3: Count rates R_L (min^{-1}) due to neutrons produced in the detector assembly and total count rates.

(8) As a check on the reliability of these calculations

we have estimated the value of R_L for the system used by Trainor and Lockwood (1964). Using the published detector efficiency curves and a geometric correction factor of 0.67 (given by Trainor and Lockwood 1964) we obtain $R_L = 0.07 \text{ min}^{-1}$ at the geomagnetic poles assuming the mass of the detector assembly to be 400 grams. This gives the ratio of the total to the "gated" (atmospheric neutron) rate as 1.7, a result in good agreement with the value of 1.65 estimated and 1.72 ± 0.36 measured by the authors.

(9) These results are unlikely to be in error by more than a factor of 2 and probably give an upper limit to the local production rate. Local production effects can therefore be ignored for most purposes, at atmospheric depths

greater than 25 gm.cm^{-2}, and for depths greater than about 10 gm.cm^{-2} in studies of the latitude distribution.

4.5 Directional effects in the counter response.

In section 3.4 we noted that, at high altitudes, the counting rate of our neutron detectors might be expected to depend on their orientation with respect to the vertical. Mildura flight M8 was designed to measure this effect, and the counting rates of the vertical and horizontal detectors are given, for various atmospheric depths, in table 4.4.

	Calibration rate (min^{-1})	Atmospheric pressure (mb) 200	100	50	40	25	20
Horizontal counter	157.1	122	166	143.5	130	101	87
Vertical counter	149.4	116	156	137	125	95	83
Ratio	1.051	1.051	1.063	1.048	1.040	1.063	1.048

Table 4.4: Calibration, scaled counting rates (÷ 8 min^{-1}) and count rate ratio for the neutron detectors in Mildura flight M8.

The ratio of the counting rates for the two detectors is also given, and is independent of atmospheric depth, within the limits of error. It would appear, therefore, that at these altitudes the counting rate does not depend significantly on the orientation of the detector relative to the vertical.

It is conceivable that a genuine effect does occur but that it is masked, in this experiment, by an equal and opposite effect due to a difference in the energy response of the B and D type counters used. This is very improbable, however. We would have to suppose that the two detector responses differed in such a way that the ratio of their counting rates

was the same in the very different calibration system and lower atmosphere neutron energy spectra, but that the ratio was different in the upper atmosphere.

A noteworthy feature of table 4.4 is the agreement, within errors, between the ratio of the counter sensitivities as determined by calibration and the ratio of the observed counting rates in the atmosphere. The calibration rates are therefore satisfactory for normalisation of results, irrespective of whether they are obtained with B or with D type counters.

V NEUTRON MEASUREMENTS IN AURORAL REGIONS

5.1 Introduction

In section 3.2 we discussed the possibility that protons, with energies of the order of 10 - 100 Mev, may sometimes be associated with the energetic electrons frequently precipitated into the atmosphere in auroral regions. These protons would not have sufficient range to penetrate to balloon altitudes (10 - 15 $gm.cm^{-2}$), but many would produce neutrons in interactions with air nuclei. The neutrons would diffuse down through the atmosphere and could be detected at lower altitudes.

Neutron detectors were flown from Macquarie Island, in the southern auroral zone, on a number of occasions (section 3.2) during auroral X-ray measurement programs in 1961-62 and in 1964. Bremsstrahlung X-rays, from electron precipitation, were observed during four of these flights: numbers 14 and 21 in 1961-62, and numbers 8 and 15 in 1964. Details of the neutron and X-ray detector counting rates are illustrated for ~~these~~ flights 21, 8 and 15 in figures 5.2 to 5.4. Strong earth current and magnetic activity also occurred during flight 5 in 1964; but no X-ray increases were recorded.

Abnormal neutron count rate increases were observed during two flights from Macquarie Island in 1961-62. The first increase occurred during flight 1, at a time of very low geophysical activity. The NaI scintillator rate remained normal throughout the flight. Details of the neutron and X-ray detector counting rates during this flight are shown in figure 5.5. The second event began during the balloon ascent in flight 21. It was accompanied by, but not closely correlated with, a three-fold increase in the counting rate of the $E > 25$ Kev channel of the NaI scintillator in the flight unit.

The X-ray increases during flights 8 and 15 in 1964 were quite large when we take into account the low sensitivity, for

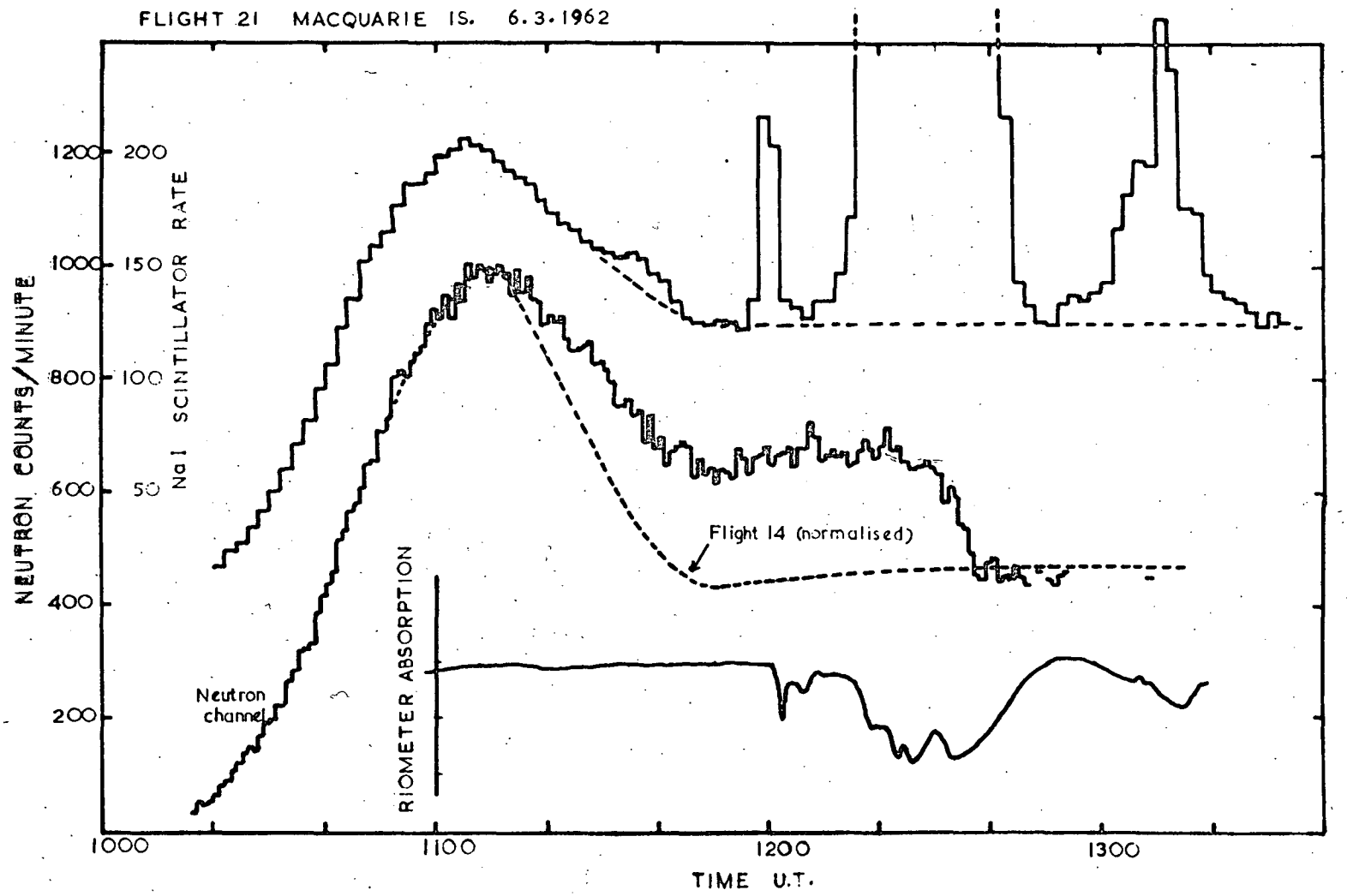

Fig. 5.2. Macquarie Island flight 21, March 6, 1962. The normal neutron and scintillator rates are indicated by the dotted lines.

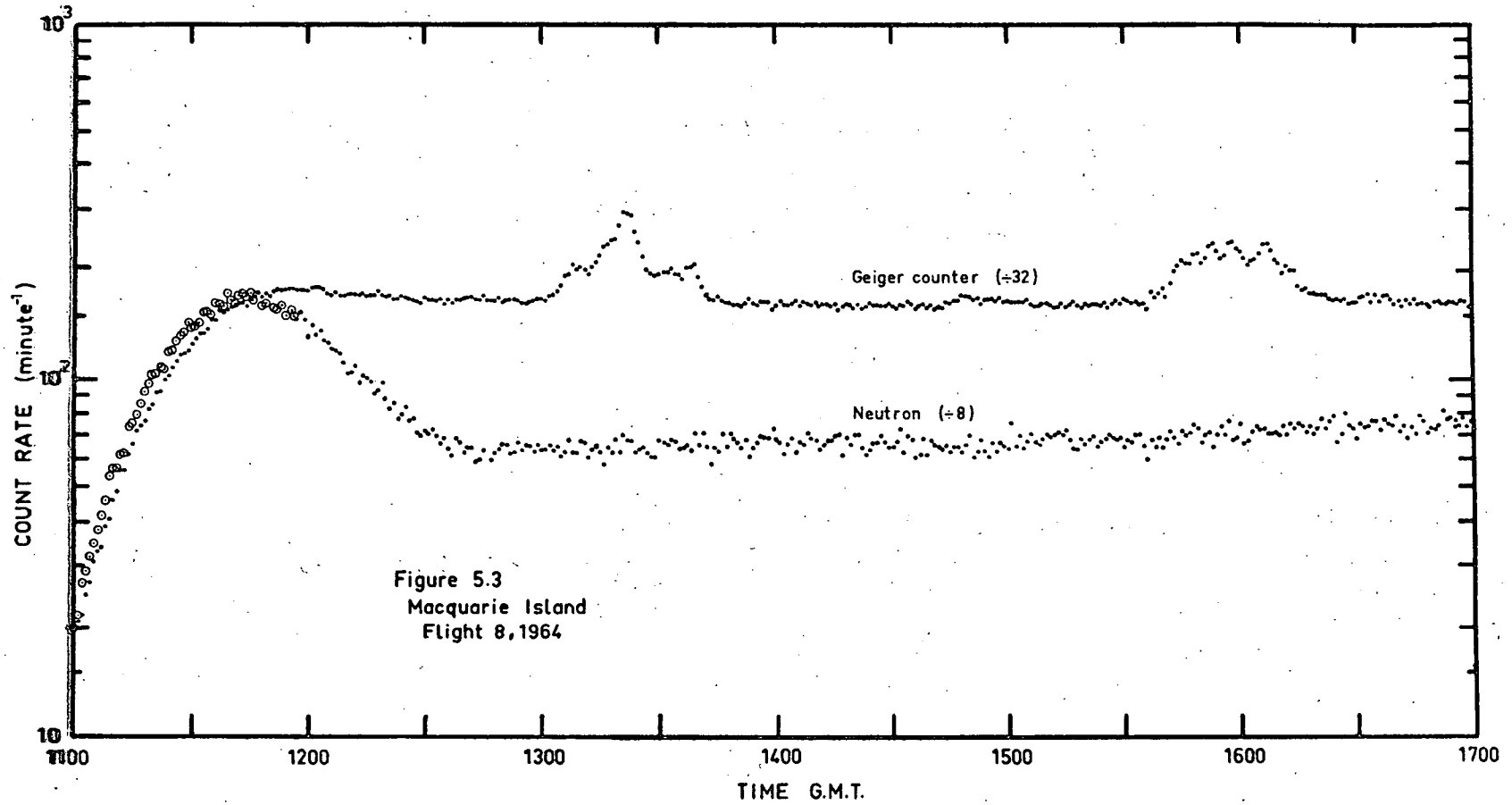

Figure 5.3
Macquarie Island
Flight 8, 1964

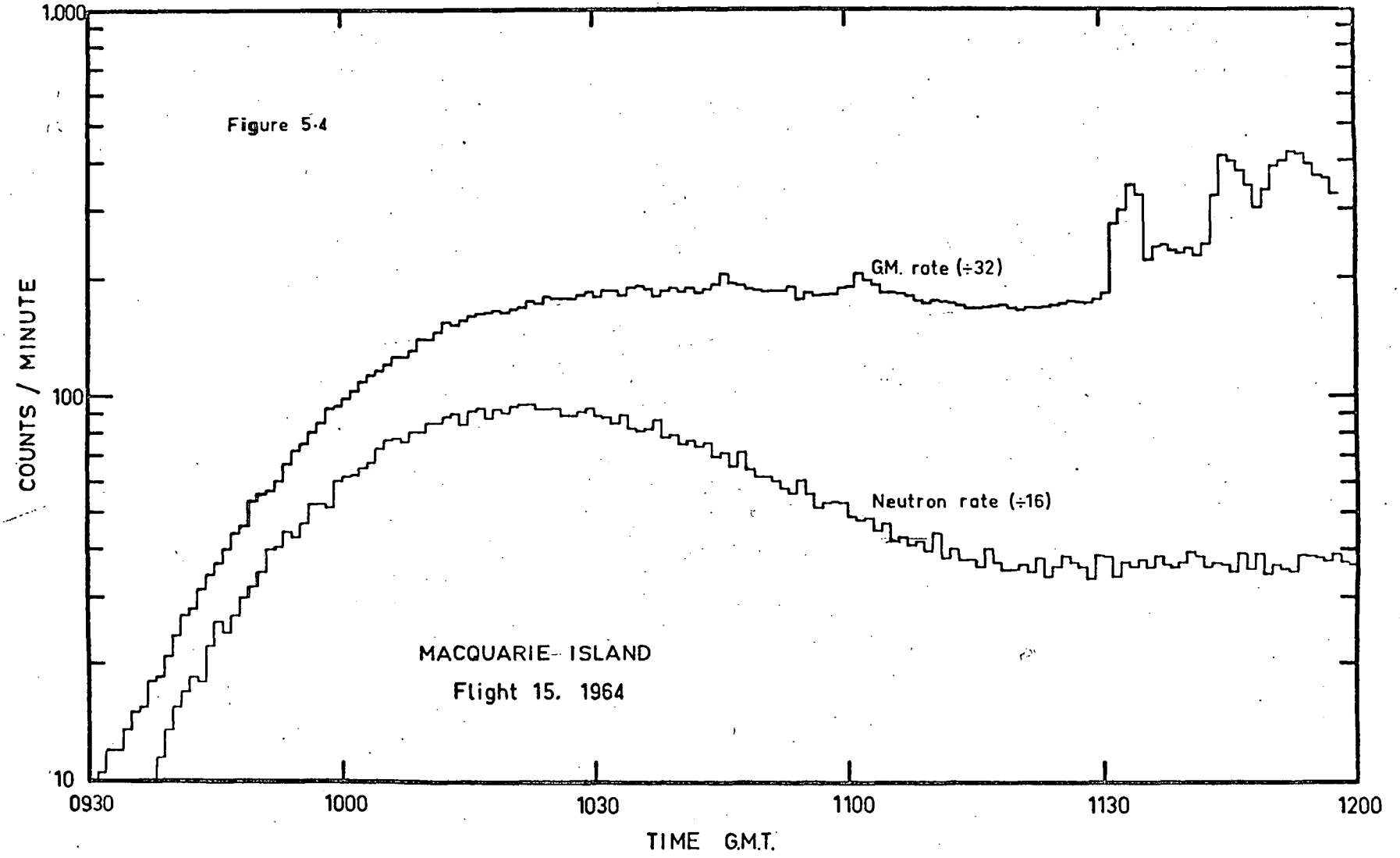
Figure 5·4
1,000
100
10
COUNTS / MINUTE
GM. rate (÷32)
Neutron rate (÷16)
MACQUARIE ISLAND
Flight 15. 1964
0930
1000
1030
1100
1130
1200
TIME G.M.T.

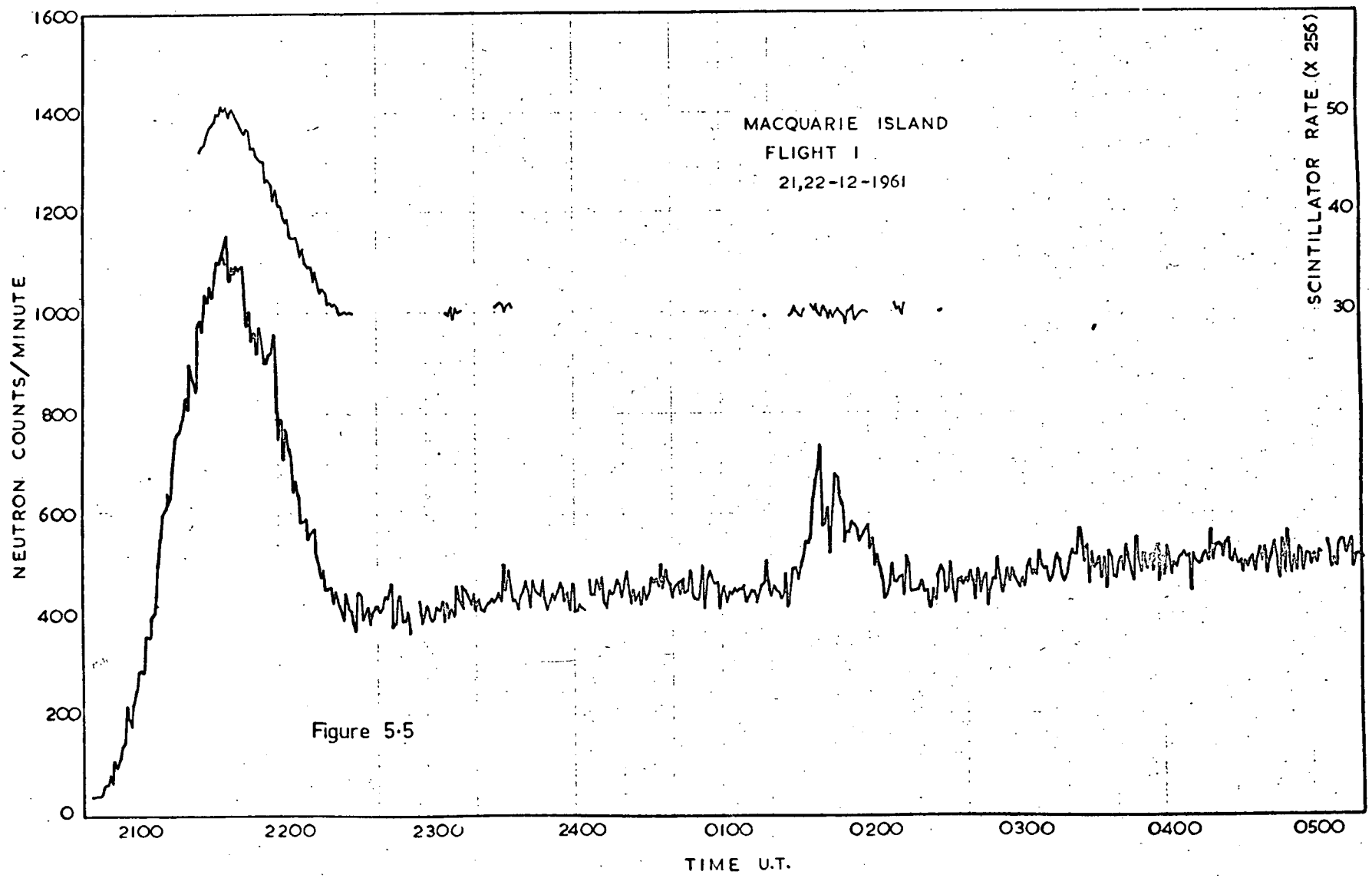
MACQUARIE ISLAND
FLIGHT 1
21,22-12-1961
NEUTRON COUNTS/MINUTE
SCINTILLATOR RATE (X 256)
TIME U.T.
0
200
400
600
800
1000
1200
1400
1600
30
40
50
2100
2200
2300
2400
0100
0200
0300
0400
0500

Figure 5·5

X-ray detection, of the Geiger counters used. In spite of these increases (about 70% during flight 8 and 270% during flight 15), no neutron count rate enhancements were observed during any of the flights in 1964.

The origin of the neutron events in 1961-62 is not clear. It is possible that both were caused by instrument malfunction, although we are unable to suggest its nature. Of the two events, the one during flight 21 seems the more likely to be genuine, and we have therefore investigated it first. These investigations will be described in the following sections and the same methods will then be applied to the flight 1 event.

5.2 Details of the flight 21 event.

(i) Description of the event.

Flight 21 was launched from Macquarie Island at 1000Z on March 6th, 1962. As can be seen in figure 5.2, the neutron flux absorption curve was normal during the ascent until the detectors reached 100 - 200 mb. As the ascent continued the rate began to diverge from the normal, as determined on flight 14 (dotted line in figure 5.2). The divergence continued until about 1140Z, when the balloon reached ceiling at 14 mb. The rate then remained enhanced and essentially constant (except for a slight increase correlated with the slow descent of the balloon to 17 mb) until 1220Z when it rapidly decreased, reaching the normal level at 1235Z. The rate remained constant for about 15 minutes and then counting ceased suddenly when the discriminator circuit began to oscillate. The oscillation continued until the end of the flight, except for a brief period at 1310Z when the count rate was again about normal. The oscillation was caused by freezing up of the electrolytic decoupling capacitors used in the battery supply line to the discriminator. Similar breakdowns occurred during flight 12 and during laboratory

operation of the circuits at low temperature. It is unlikely that there is any causal relationship between the failure of the decoupling circuits and the neutron count rate enhancement in flight 21, since no count rate increase was observed, prior to breakdown, during flight 12 or in the laboratory experiments. This conclusion is supported by the fact that the count rate was normal, during the two minute interval at about 1310Z, when the oscillation temporarily ceased.

(ii) Geophysical activity.

Geophysical activity was relatively high during flight 21. The Macquarie Island magnetometer (figure 5.6) shows magnetic activity gradually increasing from about 0200Z until 1140Z when greatly increased activity began. A geomagnetic storm was in progress and the planetary magnetic index Kp was as high as 6 during the neutron counting rate enhancement. Values of Kp are given in figure 5.7. This activity was a 27 day recurrence of a gradual storm lasting from 2100Z on February 6th to 1200Z on February 7th. 54 days previously, on January 10th, a sudden commencement geomagnetic storm occurred and was accompanied by a small (approximately 2½%) Forbush decrease in the Mt.Wellington neutron monitor rate. A slight depression of the Mt.Wellington neutron level is also apparent for March 6th (figure 5.7).

The counting rate of the sodium iodide X-ray scintillation detector in the flight unit increased in several large "bursts" during the neutron event. The largest increase was about 3 times normal in the $E > 25$ Kev channel but very small in the $E > 100$ Kev and $E > 250$ Kev channels. These events are undoubtedly due to bremsstrahlung X-rays from electron precipitation at higher altitudes. There is good correlation (figure 5.2) between the X-ray increases and cosmic noise absorption as recorded by the Macquarie Island 27 mc/s riometer, but no absorption greater than the threshold (about 0.5 db) corresponding to the neutron event. In spite of the

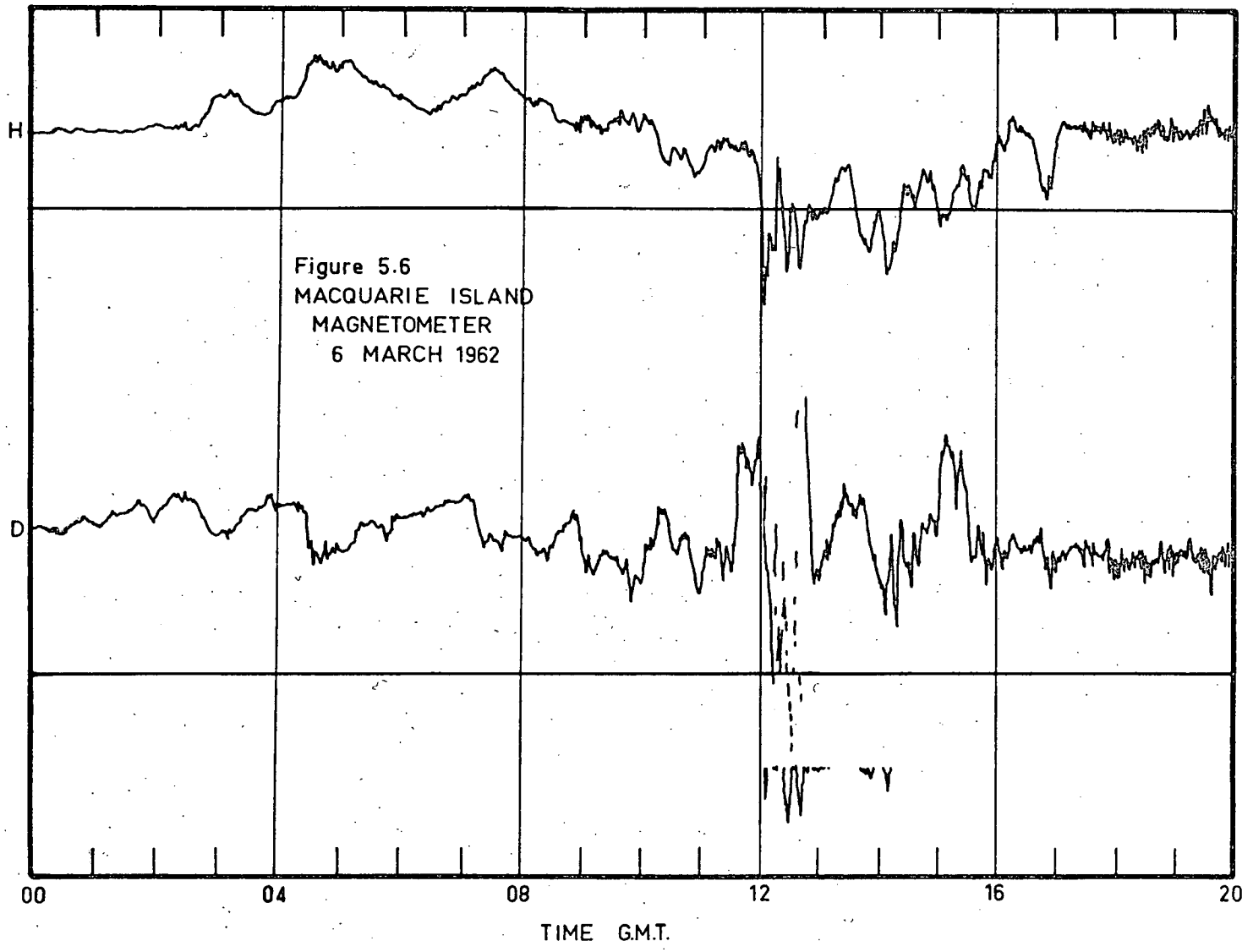
H
D
Figure 5.6
MACQUARIE ISLAND
MAGNETOMETER
6 MARCH 1962
00
04
08
12
16
20
TIME G.M.T.

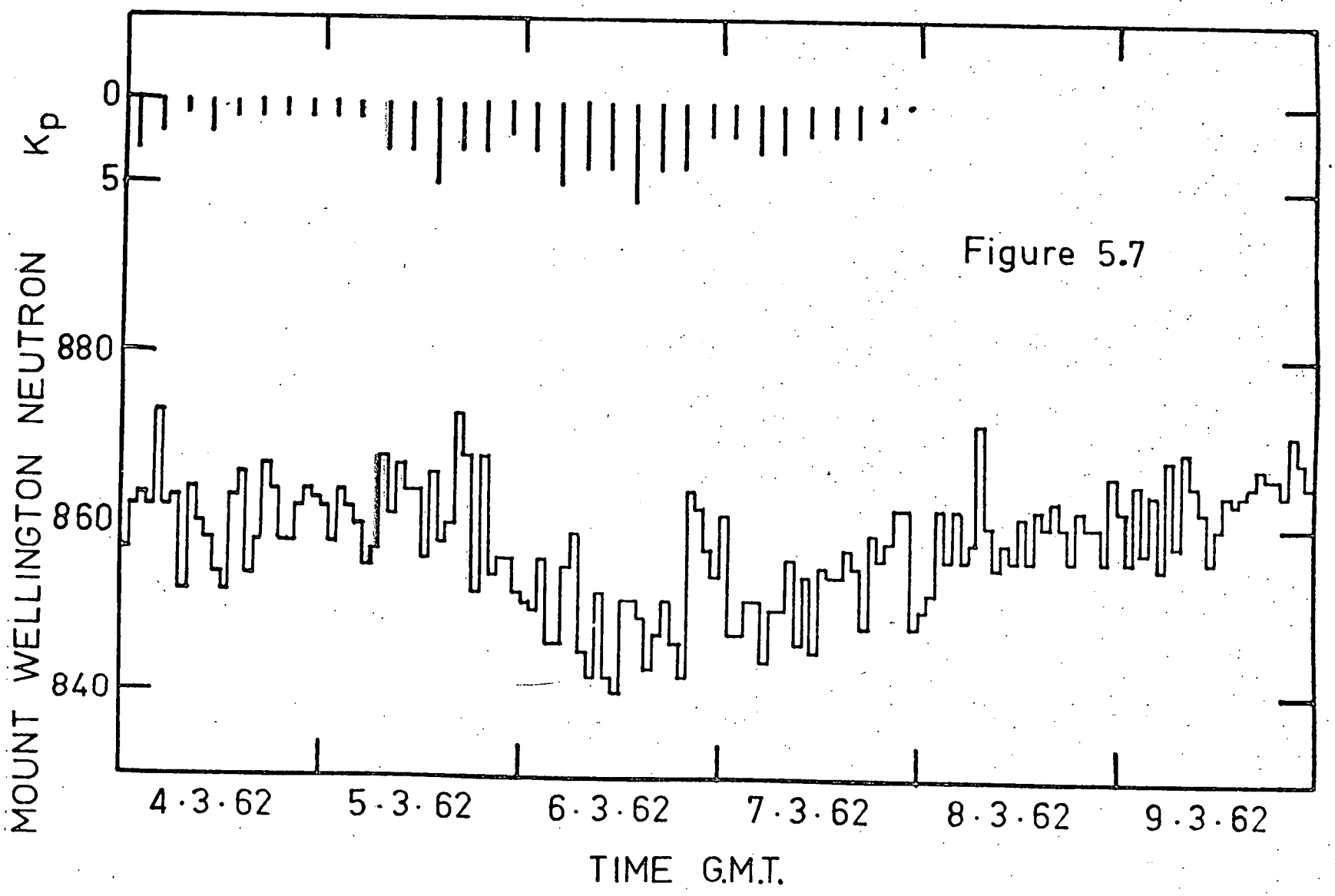
0
5
K_p
880
860
840
MOUNT WELLINGTON NEUTRON
4·3·62
5·3·62
6·3·62
7·3·62
8·3·62
9·3·62
TIME G.M.T.

Figure 5.7

considerable geophysical activity at the time of flight 21, solar flare activity was low during the preceding three days. A class 2^+ flare was observed at solar coordinates S 13°, W 56° during the period 1636 - 1730Z on March 1st. Energetic particle emission may have occurred in this flare since it was accompanied (National Bureau of Standards, Solar-Geophysical Data, 1962) by type IV and 2,800 mc/s solar radio noise bursts. There is, however, no evidence of other geophysical effects, and no further solar flares greater than class 1 occurred in the period between this flare and the magnetic storm on March 6th. This storm has been ascribed (Preliminary report of solar activity, Boulder Observatory, March 9, 1962) to an M1 region.

The significance of the simultaneity of the X-ray and neutron events should not be over-emphasised. X-ray events occur frequently in auroral regions even at times of relatively low solar activity and the flights were made, whenever possible, during geophysically disturbed periods.

(iii) Estimation of count rate excess.

In order to determine the excess count rate as a function of time and pressure, we have normalised the count rate versus pressure data from flight 14 and subtracted it from the flight 21 data. The normalisation factor has been obtained by determining the smoothed curve values of count rate versus pressure, for the two flights, and plotting the ratio of the flight 21 rate to the corresponding flight 14 rate, as a function of pressure. This is shown in figure 5.8 and it can be seen that the ratio remains essentially constant for atmospheric depths greater than about 200 $gm.cm^{-2}$. The count rate excess has been estimated using the normalisation factor of 1.435 obtained in this way. The excess rate and the atmospheric pressure are plotted, as a function of time, in figure 5.9. (The rates illustrated were inadvertently reduced by a factor of 1.435. This error does not apply to

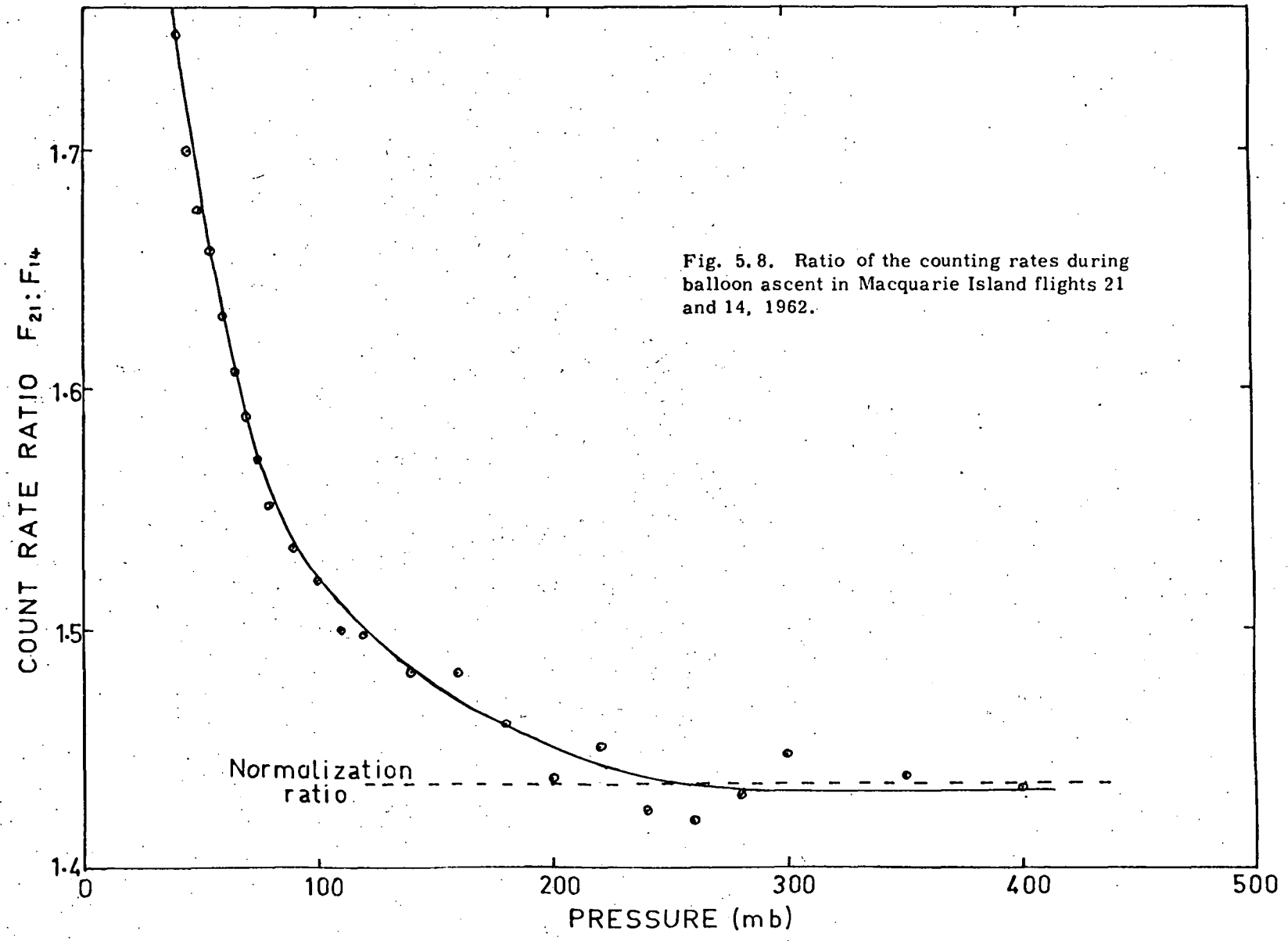

Fig. 5.8. Ratio of the counting rates during balloon ascent in Macquarie Island flights 21 and 14, 1962.

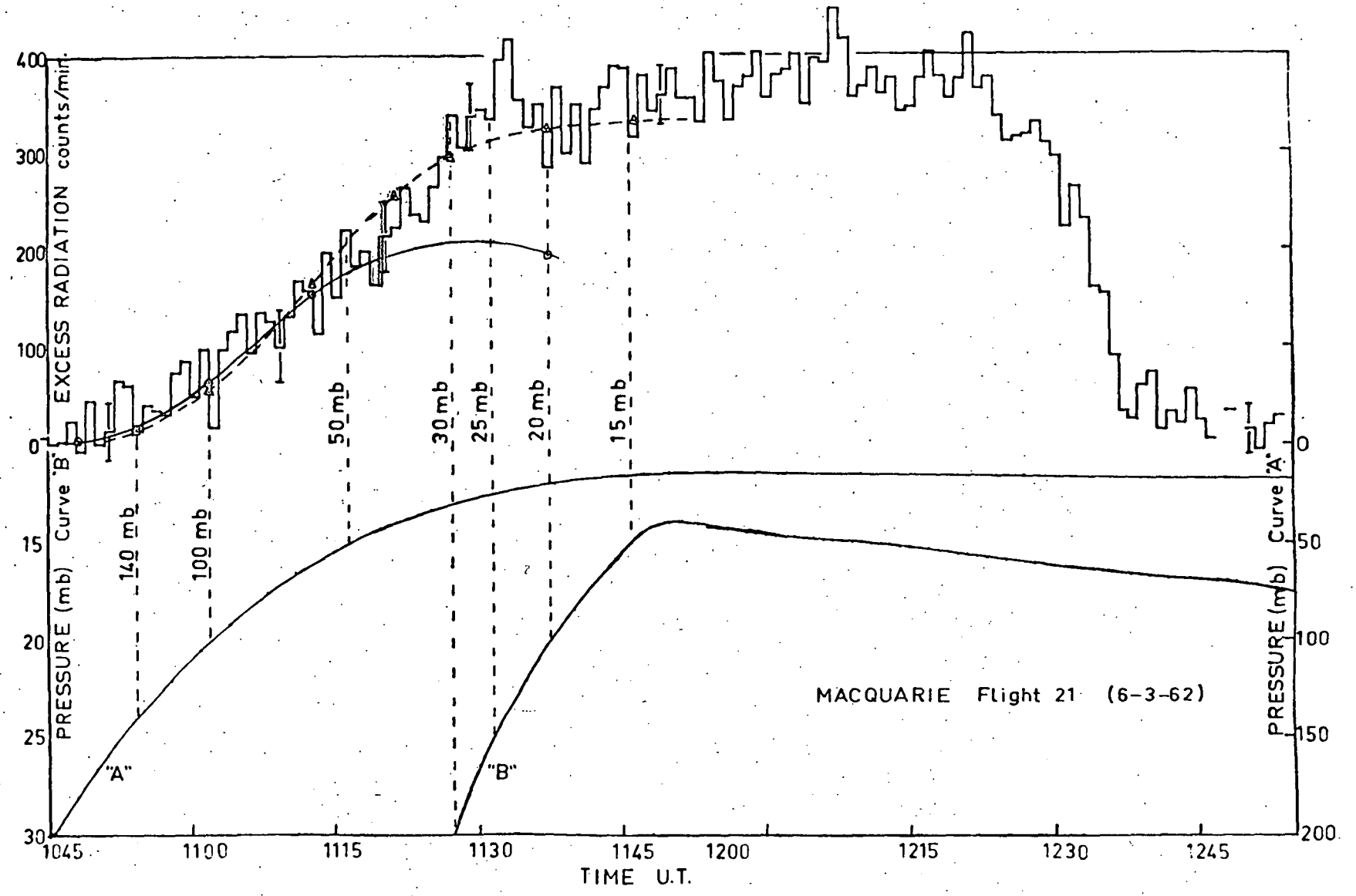

Fig. 5.9. Pressure and count rate excess as a function of time during Macquarie Island flight 21, 1962.

the results given elsewhere in the text.)

(iv) Reliability of the results.

There are several aspects of the count rate enhancement which increase our confidence in the reliability of the data. It will be noted that the excess rate remains essentially constant, for a period of over half an hour commencing from about the time the rig reached altitude. This "plateau rate" is about 60% above normal, whereas the malfunction of a binary in the scale strip would, most probably, produce either a very erratic increase or else a doubling of the counting rate. The absorption curve for this flight was normal at atmospheric depths greater than about 200 $gm.cm^{-2}$. The absorption length between 200 and 600 $gm.cm^{-2}$ was 156 ± 3 $gm.cm^{-2}$, indicating correct equipment performance in this region.

Failure of high voltage components, such as decoupling or isolating capacitors, or the voltage regulator tube, can cause spurious counts due to intermittent breakdown. Such an effect is, however, obvious from the records, since each breakdown produces a long string of pulses followed by a normal period. No such effect was observed.

It is possible that temperature effects caused spurious counting by increasing the sensitivity of the circuits. These effects would have to be rather unusual, however, since the rig temperature was about $-30^{\circ}C$ and decreasing monotonically during the event, whereas the count rate increase has a much more complex time dependence. It is possible that two opposing temperature effects may, over a limited temperature range, increase the amplifier-discriminator sensitivity to ionising particles and thereby increase the count rate in the manner observed. However, the temperature effects in a normal flight unit are very small (section 2.3 (iii)) and the simultaneous occurrence of two abnormal effects in the one unit is

improbable. In addition, any rate increase caused by increasing sensitivity to ionising radiation would show a positive correlation with the normal background rate, which has an altitude dependence somewhat similar to the neutron flux (Korff and Haymes 1960). Consequently, in spite of the obscuring effects of time dependent sensitivity, we would expect some change of slope, in the excess rate, corresponding to the transition maximum in the normal neutron count rate. No such correlation can be detected in the flight 21 data.

The most plausible source of spurious counts is electrical noise pickup from the DC electric motor in the baroswitch. This form of interference has been observed during laboratory tests but precautions were taken to avoid it during flight. It is also necessary to postulate a mechanism capable of producing the time variations observed. A temporary increase in sensitivity induced by two opposing temperature effects, as proposed above, would probably provide the mechanism, but seems improbable for the reasons already mentioned.

The counting rates during the normal parts of flight 21 were over 40% greater than the rates during flight 14. This implies a difference in counter sensitivity of over 40%, since the cosmic ray intensity was similar during the two flights. The sensitivity of the flight 14 counter was unusually low, but it would seem, from the counting rates during the other flights, that the flight 21 counter sensitivity was about 25% greater than that of the average counters.

Unfortunately, we have no pre-flight information on the relative sensitivities of the counters used in these flights. The flight data indicates, however, that the type A counters are, as a consequence of the method of construction, much more variable in sensitivity than are the B, C and D types. While the flight 21 counter sensitivity lies somewhat outside the normal range for this type, there is no reason to suppose that this implies incorrect counter performance. The fact that the

ascent curve and post event count rate were normal, indicates the reverse.

(v) Possible geophysical origins for the event.

The neutron detector will respond to any event which releases more than about 2 Mev of ionisation energy in the BF_3. It is possible for electrons or X-rays to produce counts by pile-up, but very large fluxes are required and these would have been detected by the NaI scintillator.

High energy γ-rays may produce neutrons by the (γ,n) reaction with air nuclei, but large fluxes would be required to account for the flight 21 event and these would have been detected by the scintillator. In any case, the sun, which has been suggested as a possible source of such γ-rays (Maeda 1961) was below the horizon at the time of the neutron event. Solar neutron production can also be eliminated for this reason.

The production of neutrons by low energy protons appears to be the most probable cause of the count rate increase. It is clear that very few of these protons had sufficient energy to reach the balloon level since the scintillator count rate after the neutron event was the same, within errors, as it was (between X-ray bursts) during the event. This rate was about 120 sec^{-1} and it is unlikely that more than about 5 counts per second were caused by the hypothetical protons. This limit will also include the contribution, to the scintillator rate, of γ-fays produced above the balloon by interaction between the protons and air nuclei.

The NaI scintillator is a cylindrical crystal with axis vertical and dimensions 2.5 cm diameter by 2.5 cm long. The counting rate R of this detector, in a flux J ($cm^{-2}sec^{-1}ster^{-1}$), assumed isotropic over the upper hemisphere and zero over the lower, is derived in appendix IV.

We find that

$$R = 2\pi J \left(\frac{\pi r^2}{2} + \frac{\pi r l}{2} \right) \qquad (5.1)$$

$$= 2\pi J \times 7.4 \text{ sec}^{-1}$$

Consequently, the limitation on the count rate increase of 5 sec^{-1} corresponds to a maximum permissable flux of protons and γ-rays at the balloon level of 0.11 $cm^{-2}sec^{-1}ster.^{-1}$, if we assume the flux to be isotropic over the upper hemisphere. Assuming the flux to be vertical, the limit becomes $\sim$1.0 cm^{-2} sec^{-1}.

The limit which this places on the flux at the top of the atmosphere will depend on the energy spectrum of the incident particles. This will determine the number of particles with range sufficient to reach the detector, and also the cross-sections for production of nuclear γ-rays capable of influencing the scintillator rate. We will postpone further discussion of this subject until we have investigated the magnitude of the proton flux required to account for the neutron increase.

5.3 Estimation of hypothetical proton flux.

(i) Introduction

Many factors are involved in the estimation of the flux and energy spectrum of the protons required to produce the flight 21 neutron event. We must first estimate the neutron production distribution, as a function of altitude, for a unit proton flux at the top of the atmosphere. The production rate and distribution will, of course, depend on the proton energy spectrum chosen.

Having evaluated the neutron source distribution, we can use diffusion theory to calculate the equilibrium neutron flux energy spectrum and altitude distribution. The effect on the neutron detector counting rate can then be evaluated from this result using equation (4.1). Finally, having calculated

the relationship between the counting rate and the neutron production rate, we can normalise the production rate and from this obtain the initiating proton flux.

(ii) Neutron production calculations.

The altitude and latitude dependence of the source neutrons may be calculated from the equation

$$N(z,\lambda) = \int_{P_c(\lambda)}^{\infty} \pi(P,z) \frac{dJ}{dP} dP \qquad (5.2)$$

where: $N(z,\lambda)$ is the number of neutrons produced per gram and second at latitude λ (with cut-off rigidity $P_c(\lambda)$) and atmospheric depth z

$\frac{dJ}{dP}$ is the differential rigidity spectrum of the incident protons

$\pi(P,z)$ is the probability that a proton of initial rigidity p will produce a neutron in unit atmospheric depth at z.

This latter function has been evaluated for various values of z by Lingenfelter and Flamm (1964) using the expression

$$\pi(E,z) = \int_{1}^{z/R(E)} \sigma_{1n}(E') \exp \frac{-z}{\mu L(E')} dz\, d\mu \qquad (5.3)$$

where: E is the initial energy of the proton at z = 0

R(E) is the range in air of the proton

μ is the cosine of the zenith angle of the incident proton

L(E') is the attenuation length of protons of energy E' in air

$$E'(E,z,\mu) = E - \int_{0}^{z/\mu} \frac{dE}{dr} dr$$

$\frac{dE}{dr}$ is the differential energy loss of protons in air

$\sigma_{1n}(E')$ is the macroscopic cross-section for the production, in air, of one neutron by a proton of energy E'. This function is derived from the excitation function curve (figure 5.10) given by Lingenfelter and Flamm (1964).

(iii) Spectrum of Incident Protons.

In order to evaluate $N(z,\lambda)$ from equation (5.2), we must choose a proton spectrum $\frac{dJ}{dP}$ and a cut-off rigidity $P_c(\lambda)$. The undisturbed period cut-off rigidity for Macquarie Island ($\lambda = 66.6^{o}S$) is 370 MV (Quenby and Wenk 1962). However, this cut-off may be reduced at times of high geophysical activity, and there have been numerous satellite observations of 1-15 Mev (50-170 MV) protons at latitudes as low as 65^{o} during relatively quiet periods (Zmuda et al 1963, Fan et al 1964).

The energy spectrum of the protons will depend on their origin and method of acceleration. Freier and Webber (1963) have shown that the energy distribution of solar protons is best described in terms of rigidity P using an exponential function

$$\frac{dJ}{dP} = \left(\frac{dJ}{dP}\right)_o \exp -\left(\frac{P}{P_o}\right) \qquad (5.4)$$

where J is the proton flux

$\left(\frac{dJ}{dP}\right)_o$ is the flux per MV at P = 0

P_o is the characteristic rigidity of spectrum. It changes from one event to another, and sometimes during an event. Values of P_o from 45 MV to 375 MV have been observed during the last solar cycle.

The distributions in other proton events are more accurately described by an expression of the form

$$\frac{dJ}{dE} \propto E^{-\gamma} \qquad (5.5)$$

where E is the proton energy and γ is a constant which may

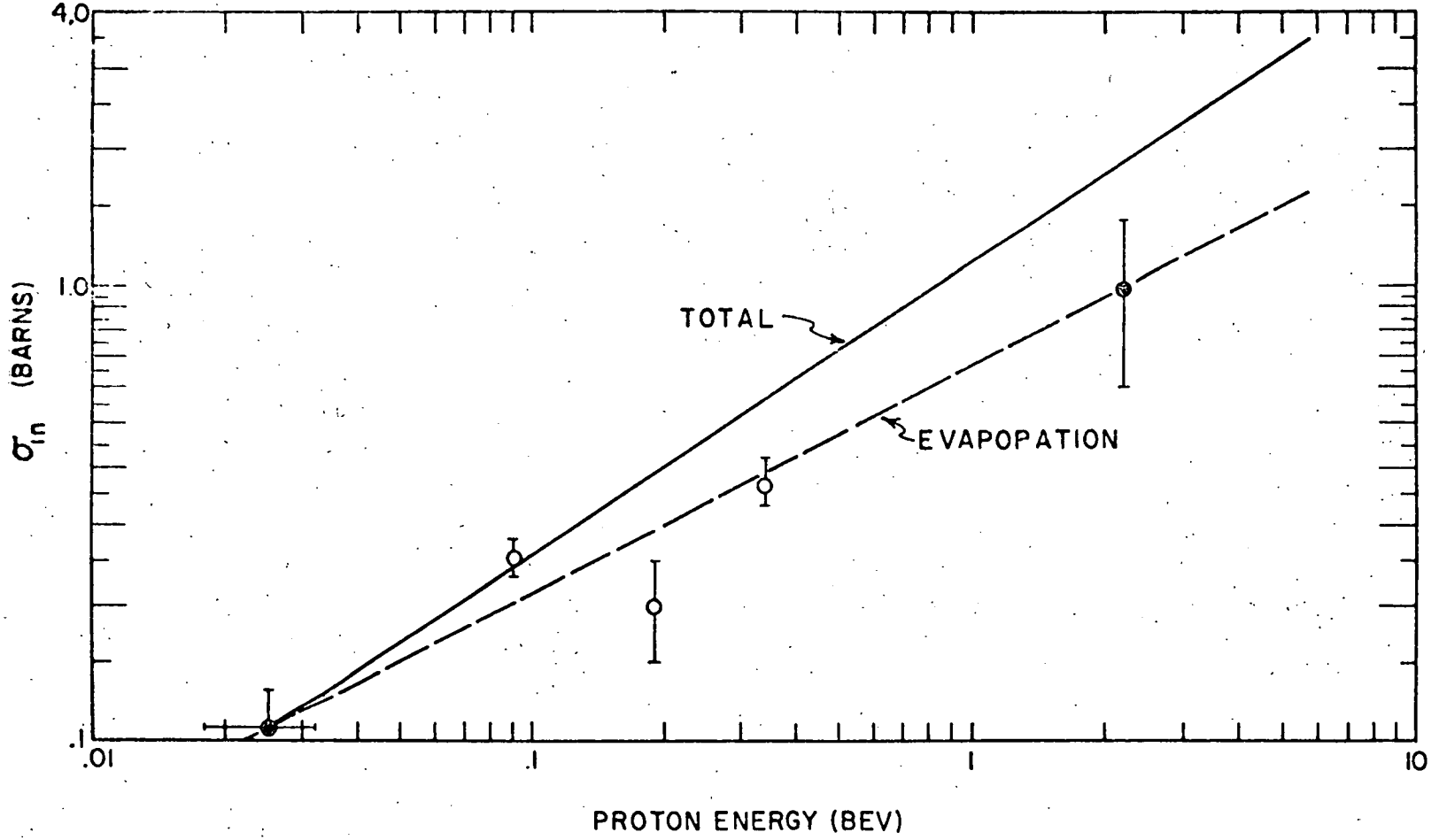

Fig. 5.10. Excitation functions for production of evaporation neutrons (broken curve) and for total neutron production (solid curve) by protons on nitrogen 14.

vary during an event and from one event to another. Typical values of γ range from 3 to 5 or more.

It is obvious, from the fact that very few protons penetrated to the balloon level, that the spectrum must have been very steep. Fortunately, the altitude distribution of the neutron flux is relatively insensitive to the depth dependence of any source function which is confined mainly to the top few gm.cm^{-2} of the atmosphere. This follows from the fact that the characteristic diffusion lengths are longer than the attenuation length of the parent neutron producing radiation. Consequently, the details of the proton energy spectrum have little effect on the neutron flux altitude distribution.

(iv) Evaluation of the neutron production distribution.

In order to estimate the altitude dependence of the neutron source, it is necessary to know the value of the neutron production probability function $\pi(P,z)$ for the relevant range of atmospheric depth z. Curves of $\pi(P,z)$ for several values of z have been published (Lingenfelter and Flamm 1964, figure 3), and using this data we have drawn a family of isometric lines for $\pi(P,z)$ on the (P,z) plane (figure 5.11). From these lines we can construct a series of curves relating $\pi(P,z)$ to rigidity P. Curves of $\pi(P,z)$ for various values of z are given in figure 5.12.

We can now evaluate the neutron production rate $N(z,\lambda)$ (equation 5.2), for various values of z, using graphical methods. First we evaluate the differential production rate $\pi(P,z)\frac{dJ}{dP}$ at various values of z. We have used exponential rigidity spectra (equation (5.4)) with characteristic rigidity P_o = 50 MV and 125 MV. Curves of the differential production rate (normalised to $\frac{dJ}{dP}$ = 2 protons cm^{-2}sec^{-1}MV^{-1} at P = 200 MV) are given in figures 5.13 and 5.14. Then by measuring the area under the curves we obtain the neutron production rate $N(z,\lambda)$ (figure 5.15) as a function of atmospheric depth.

Curves are given for cut-off rigidity $P_c = 0$ and 370 MV. It is obvious from figures 5.13 and 5.14 that the neutron production rate is virtually independent of cut-off rigidity for $P_c \lesssim 250$ MV. As the value of P_c increases beyond this value the production rate decreases more rapidly, especially in the first few grams of the atmosphere. Figure 5.15 shows that most of the neutrons are produced in the first few grams of the atmosphere when the proton spectrum has a characteristic rigidity P_o of 50 MV. Production extends somewhat further into the atmosphere when $P_o = 125$ MV.

Calculations (not described here) indicate that similar results are obtained with a power law spectrum (equation 5.5) with $\gamma = 5$.

(v) Diffusion calculations.

Lingenfelter and Flamm (1964, 1964b) have used multi-group diffusion theory to calculate the energy and spatial distribution of neutrons produced in the atmosphere by low energy protons. The results are subject to errors due to the breakdown of diffusion theory in boundary regions (section 1.9). The magnitude of these errors is not known. Lingenfelter and Flamm's results are, however, probably the most accurate available. Calculations based on the multi-group S_n method would undoubtedly be more reliable, but the effort involved in special calculations is probably not justified in the present problem because of the many other uncertainties in our data. We have therefore used Lingenfelter and Flamm's diffusion results in our calculations.

Lingenfelter and Flamm (1964, 1964b) used a proton rigidity spectrum, in their calculations, with characteristic rigidity $P_o = 125$ MV and a cut-off rigidity $P_c = 0$. In our calculations we assume that the neutron flux and energy spectrum at 20 gm.cm^{-2} is the same for $P_o = 50$ MV as for 125 MV, provided the total number of neutrons $\int_0^\infty N(z,\lambda)dz$

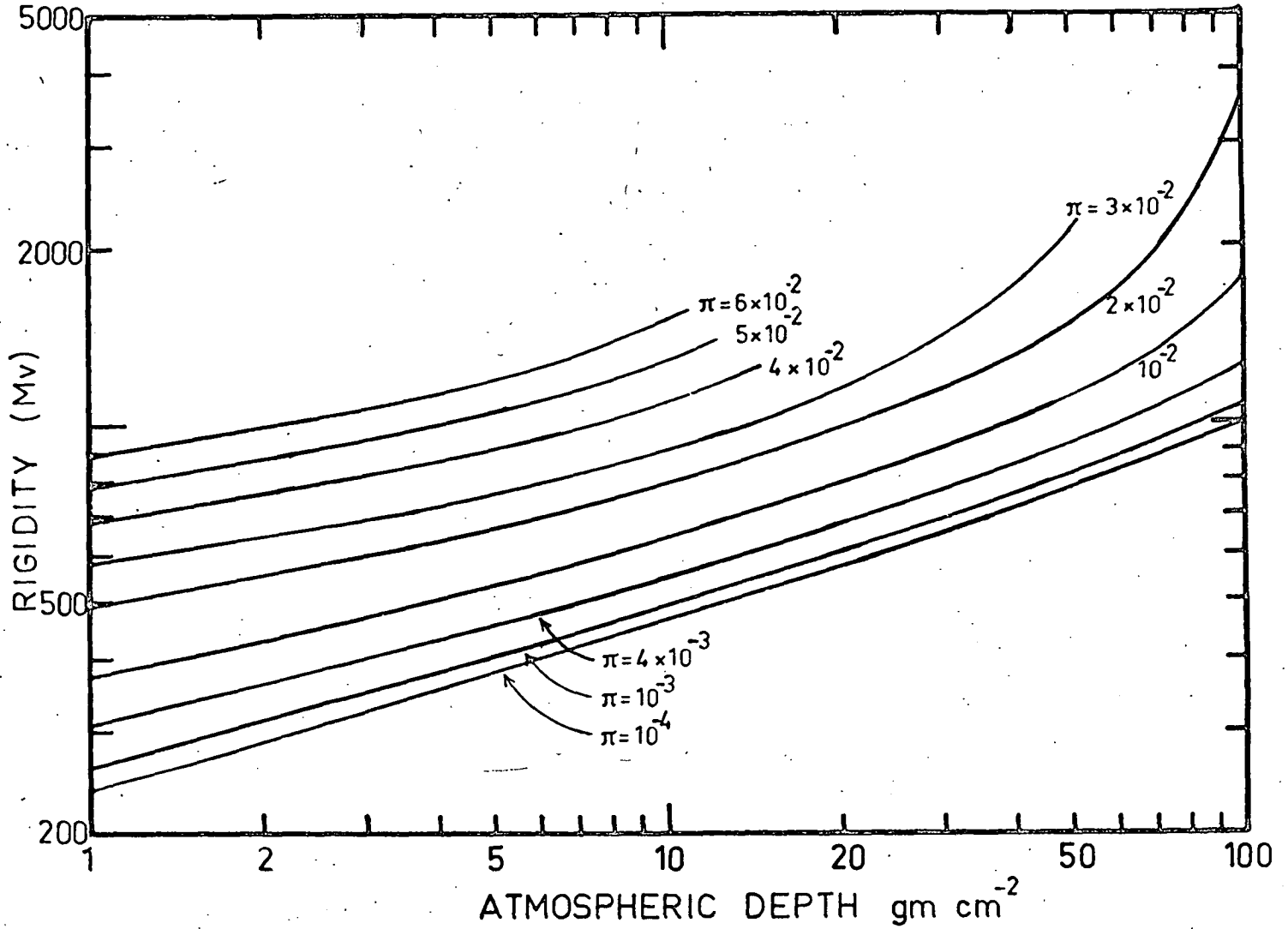

Figure 5.11. Isometric lines of $\pi(P, Z)$ – the probability of neutron production at atmospheric depth Z by protons having initial rigidity P.

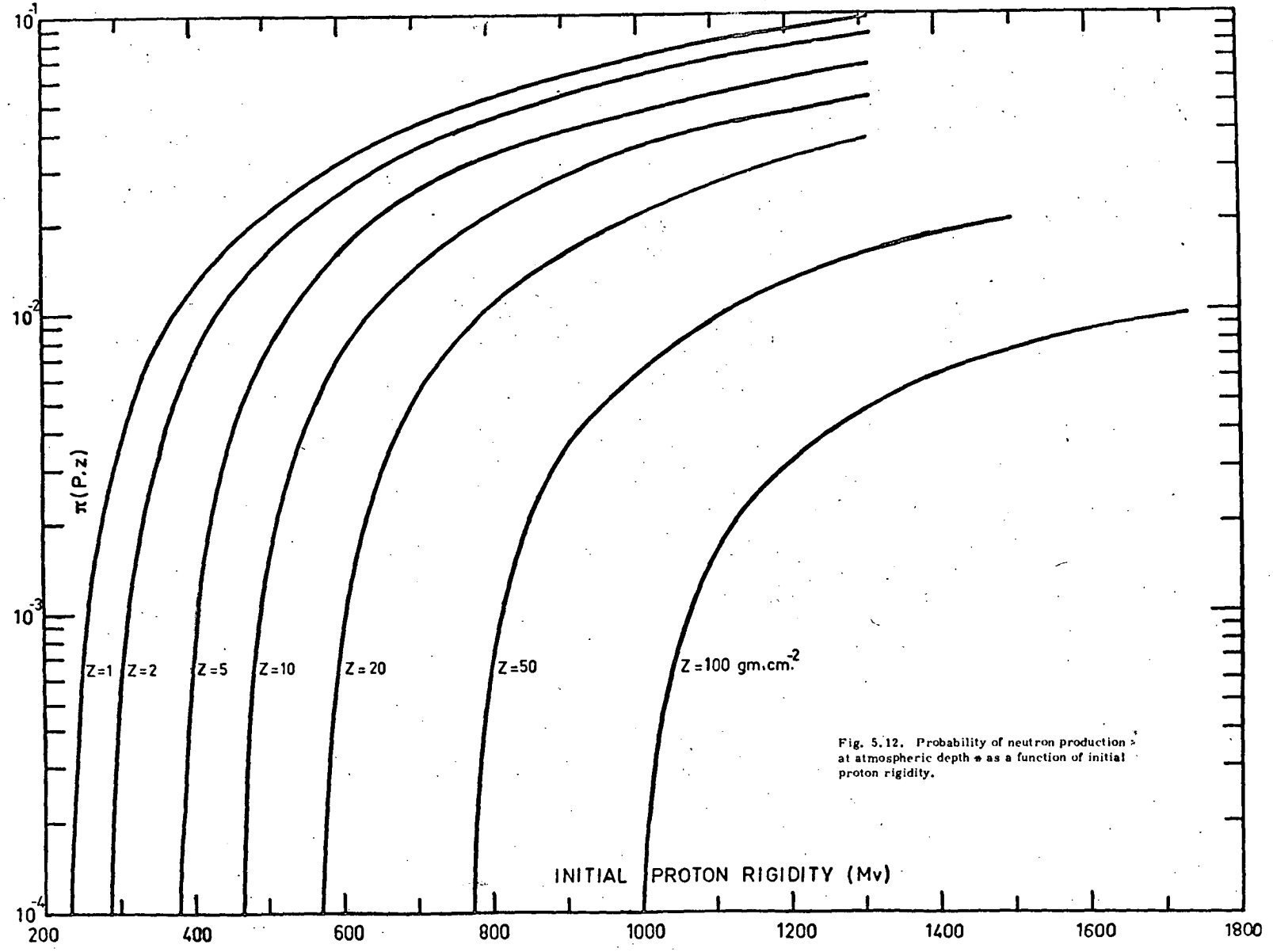

Fig. 5.12. Probability of neutron production π at atmospheric depth z as a function of initial proton rigidity.

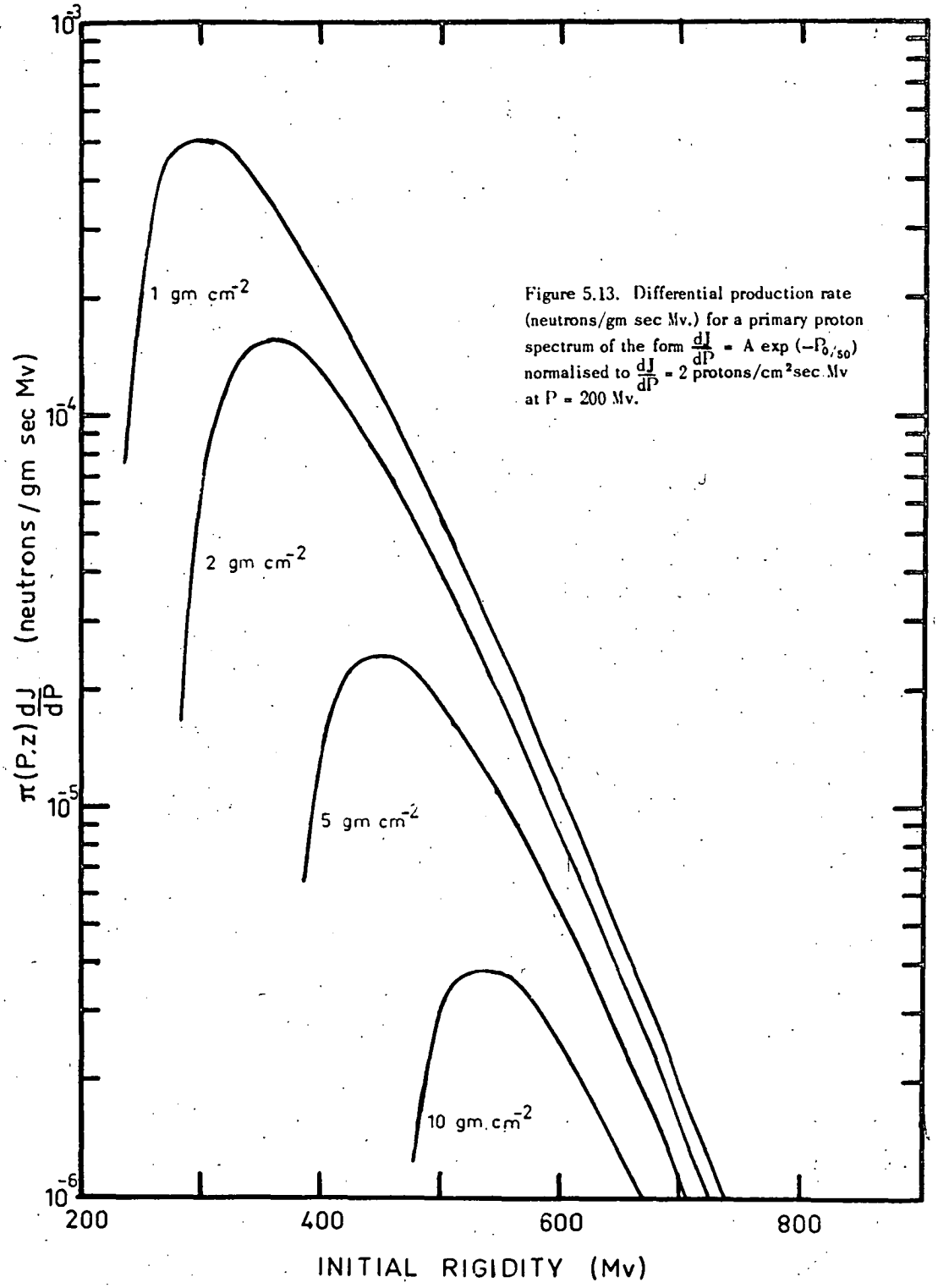

Figure 5.13. Differential production rate (neutrons/gm sec Mv.) for a primary proton spectrum of the form $\frac{dJ}{dP} = A \exp(-P_{0/50})$ normalised to $\frac{dJ}{dP} = 2$ protons/cm^{2}sec Mv at P = 200 Mv.

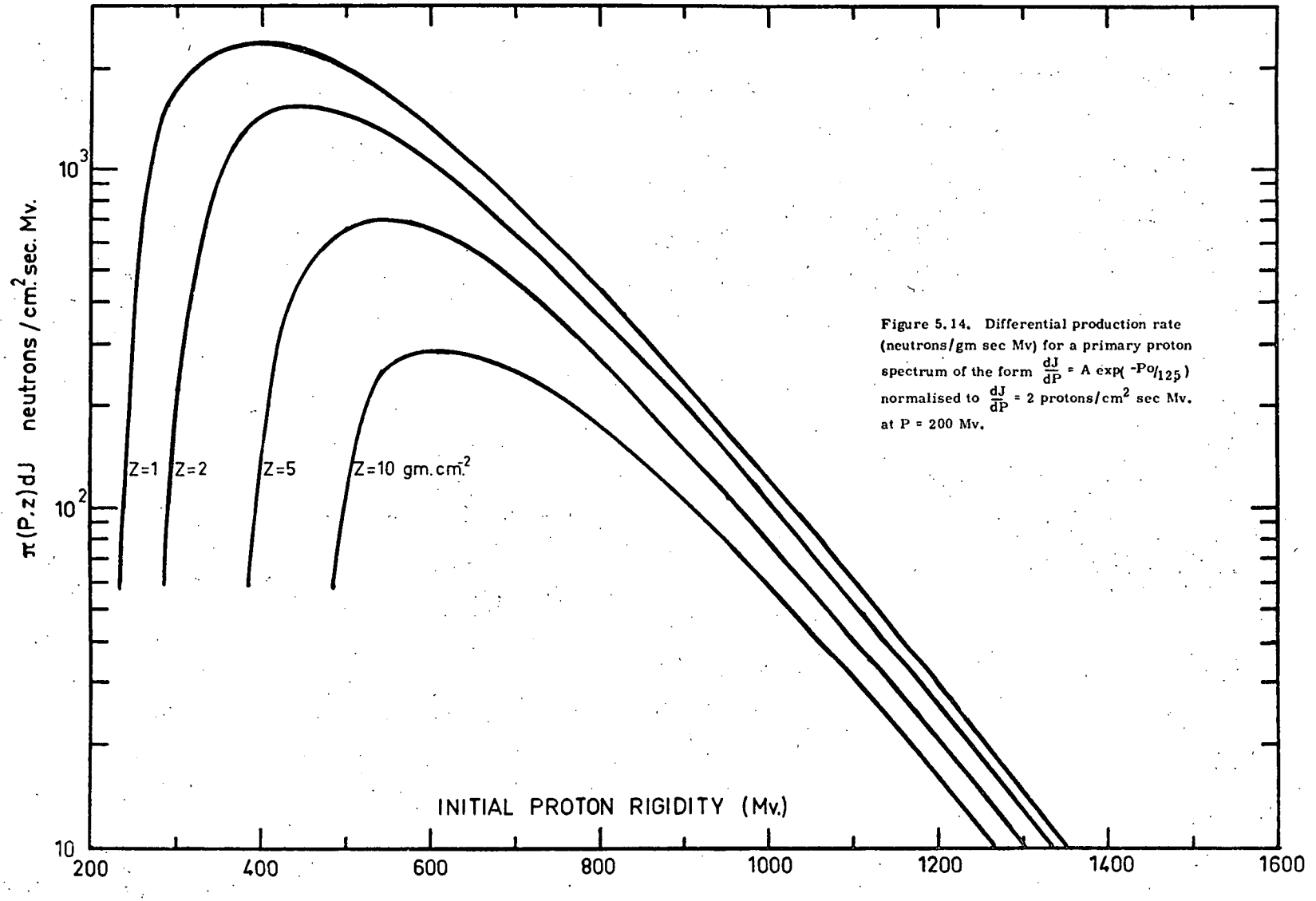

Figure 5.14. Differential production rate (neutrons/gm sec Mv) for a primary proton spectrum of the form $\frac{dJ}{dP} = A \exp(-P_{o}/_{125})$ normalised to $\frac{dJ}{dP} = 2$ protons/cm^2 sec Mv. at P = 200 Mv.

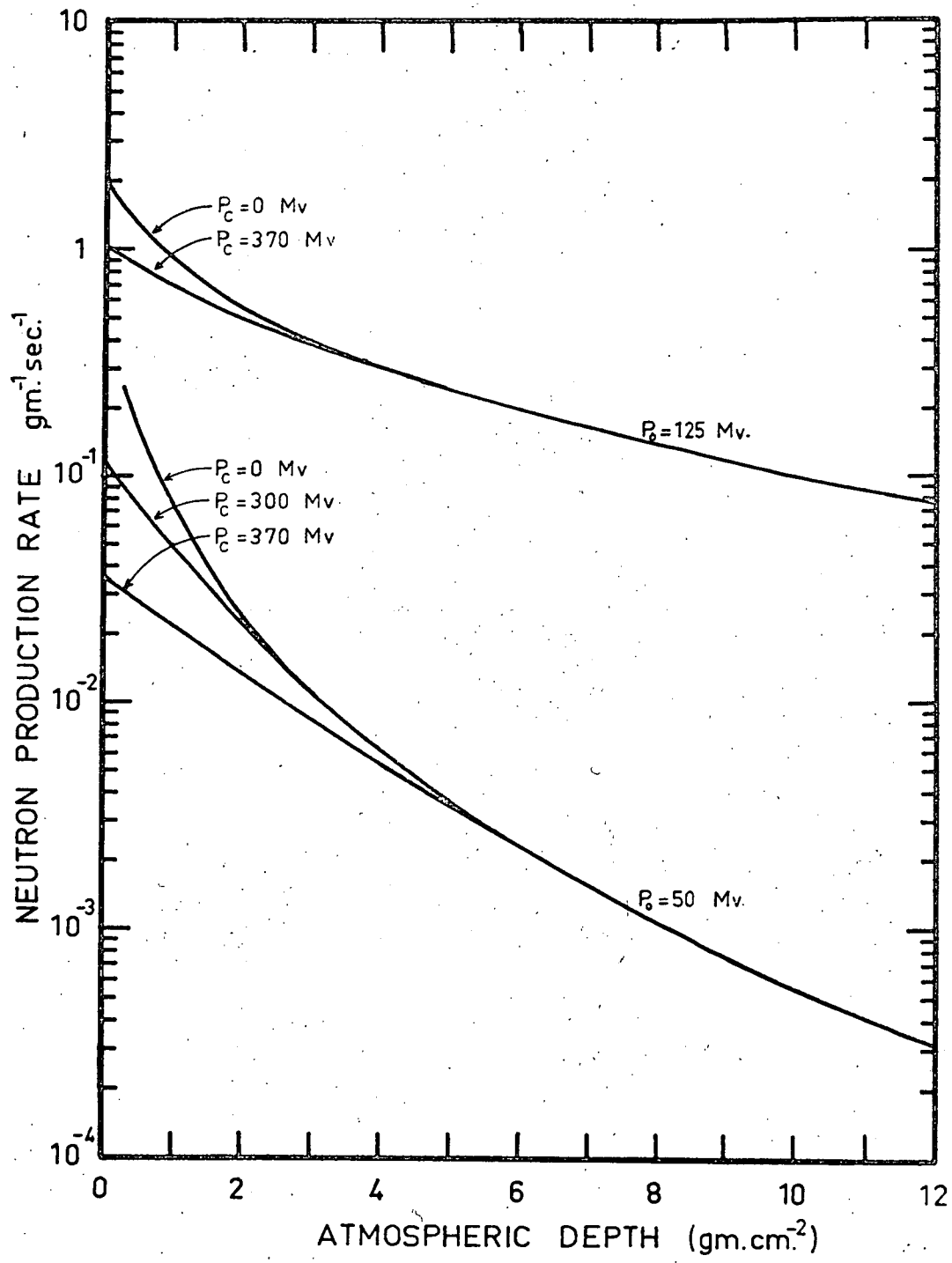

Figure 5.15. Neutron production rates for primary protons having exponential rigidity spectra with characteristic rigidities P_0 = 50 and 125 Mv. and fluxes normalised to dJ/dP = 2 cm^{-2} sec^{-1} Mv^{-1} at P = 200 Mv.

produced in the atmosphere is the same. A small error will be introduced here. It is obvious from figure 5.15 that leakage effects will be greater for the P_o = 50 MV spectrum than for P_o = 125 MV. The error will, however, be small be comparison with other errors involved in these calculations.

Outlined below is the procedure used to estimate the proton flux required to produce the flight 21 neutron count rate increase.

(1) The results of section 5.3 (iv) have been used to calculate the integrated neutron production rate for both spectra normalised to $\left(\frac{dJ}{dP}\right)_o$ = 2 protons $cm^{-2}sec^{-1}MV^{-1}$. (We follow Lingenfelter and Flamm in normalising to 2 rather than 1). The results are given in table 5.1.

Characteristic rigidity P_o	50 MV	125 MV
Normalised production rate	4.8×10^{-2}	0.99

Table 5.1: The integrated neutron production rate (neutrons sec^{-1} per cm^2 atmospheric column) for incident protons having a rigidity spectrum given by $\frac{dJ}{dP} = 2 \exp -\left(\frac{P}{P_o}\right) cm^{-2}sec^{-1} MV^{-1}$.

(2) The neutron count rate excess R_E for this normalised flux is given for P_c = 0 and the P_o = 125 MV spectrum at 20 $gm.cm^{-2}$ by the formula

$$R_E = \int_o^\infty \phi(E) k_i \eta_i(E) dE - k_i \sum_j N_j(E) \eta_{ij}(E) dE \qquad (5.6)$$

where $\phi(E)$ is the excess neutron flux estimated by Lingenfelter and Flamm (1964,1964b) at 20 $gm.cm^{-2}$.

$N_j(E)$ is the total flux at 20 $gm.cm^{-2}$ in the j'th energy group as determined by Lingenfelter and Flamm.

$k_i \eta_i(E)$ is the absolute counter efficiency as determined in section 4.2. The values of $k\eta(E)$ in table 4.1 apply to the counter used in flight 14. We have increased these values by a factor of 1.435 to allow for the greater sensitivity (section 5.2 (iv)) of the flight 21 counter.

$\eta_{ij}(E)$ is the mean value of $\eta_i(E)$ for the j'th energy group.

In these calculations we make use of the $\eta_1(E)$ and $\eta_2(E)$ counter response curves (section 4.2). These have been used as they represent the extremes of the probable counter response. The actual response will undoubtedly be more like the $\eta_1(E)$ curve but the sensitivity at high energies ($\sim$1 Mev) will be somewhat greater because of the 1 - 2 inches of paraffin at the ends of the counter.

The excess count rate $R_E(P_o = 50$ MV) for the normalised, $P_o = 50$ MV, proton spectrum can be estimated from the value of $R_E(P_o = 125$ MV), obtained above, by multiplying by the ratio of the integrated neutron production rates given in table 5.1. The results are given for the $\eta_1(E)$ and $\eta_2(E)$ responses and $P_o = 50$ and 125 MV in table 5.2.

Counter response curve	Characteristic rigidity P_o	
	50 MV	125 MV
$\eta_1(E)$	3.2×10^{-2}	6.4
$\eta_2(E)$	6.1×10^{-2}	12

Table 5.2: The counting rate (sec^{-1}) of a neutron detector at 20 $gm.cm^{-2}$ due to incident protons with rigidity spectrum $\frac{dJ}{dP} = 2 \exp -\left(\frac{P}{P_o}\right)$ cm^{-2} $sec^{-1}MV^{-1}$.

(3) The observed count rate excess at 20 $gm.cm^{-2}$ was 8.1 sec^{-1} (figure 5.9) and we use the results of table 5.2 to estimate the proton flux required to produce this excess.

This is given by the relation

$$\left(\frac{dJ}{dP}\right)_o = \frac{\text{Observed excess rate}}{\text{Estimated rate for unit } \left(\frac{dJ}{dP}\right)_o} \qquad (5.7)$$

Values of $\left(\frac{dJ}{dP}\right)_o$, obta ined on the assumption that the incident proton flux was isotropic over the upper hemisphere and zero over the lower, are given in table 5.3.

Counter response curve	Characteristic rigidity P_o	
	50 MV	125 MV
$\eta_1(E)$	81	0.41
$\eta_2(E)$	43	0.21

Table 5.3: Differential proton flux $\left(\frac{dJ}{dP}\right)_o$ ($cm^{-2}sec^{-1}MV^{-1}$ $ster^{-1}$) at 0 MV required to produce the observed count rate excess at 20 $gm.cm^{-2}$.

(4) The integral proton flux will depend on the geomagnetic cut-off rigidity P_c at the time of the measurements. If $P_c \gtrsim 200$ MV the neutron production rate will also be affected and the differential spectrum must be adjusted to maintain the same integrated neutron production rate. To make these corrections we have estimated the integrated production rates for various values of P_c. Table 5.4 gives the integral flux for both spectra with P_c = 0, 200, 300 and 370 MV, the latter figure being the vertical cut-off rigidity for Macquarie Island as calculated by Quenby and Wenk (1962).

Characteristic rigidity P_o	Cut-off rigidity P_c (MV)			
	0	200	300	370
50 MV	2.1-4.1 x 10^3	41-78	9-17	4.3-8.2
125 MV	24-46	4.9-9.3	2.3-4.4	1.4-2.7

Table 5.4: The integral proton flux $J(>P_c)$ $cm^{-2}sec^{-1}ster^{-1}$ for proton spectra having characteristic rigidities of 50 and 125 MV. The two values given

correspond in each case to the $\eta_1(E)$ and $\eta_2(E)$ counter response curves used in the calculations.

(vi) Probable errors.

It is very difficult to estimate the limits of error in these results. The counter sensitivity cannot be known to an accuracy greater than the ± 25% uncertainty of the flux used in its calibration (section 4.2, Newkirk 1963). The errors introduced by the assumptions about the shape of the counter energy response curve are also unknown. It is probable, however, that the two curves used will give the upper and lower limits to the flux if all other errors are eliminated. Lingenfelter and Flamm (1964, 1964b) do not give any estimate of the errors involved in their neutron production and diffusion calculations, but claim the results to be "in good quantitative agreement" with measurements by Smith et al (1962). Our results are, of course, subject to the same errors together with others introduced (section 5.3 (v)) by assuming that the neutron flux, for a given total production rate, is independent of the proton energy spectrum.

The most probable values of the proton flux can be obtained by taking the mean of the two values given in each case in table 5.4. The actual values are unlikely to be less than half or more than twice these means.

It is clear, in any case, that the results are strongly dependent on the shape of the proton energy spectrum. Since this must remain unknown, we can at best obtain only an order of magnitude estimate of the flux required.

5.4 Compatibility of hypothesis with other observations.

(i) Altitude dependence.

An obvious test of our hypothesis is to use diffusion theory to determine the excess counting rate altitude dependence

$$R_E(z) = k_1 \int_{P_c}^{\infty} \phi(E,z)\eta_1(E)dE \qquad (5.8)$$

which we would expect for a neutron counter with detection efficiency $k_i \eta_i(E)$ rising through the atmosphere while the hypothetical proton flux remained constant.

R(z) has been evaluated for the P_o = 125 MV proton spectrum and both counter response curves using the diffusion calculations of Lingenfelter and Flamm (1964). The results (not normalised) are shown as the dotted and solid curves in figure 5.9. Although the $\eta_2(E)$ curve gives a good fit to the data we do not attach much significance to this because the high energy response given by this curve is undoubtedly greater than for our counter (section 5.3 (v)). It is largely the high energy component of the neutron flux which is responsible for the strong altitude dependence of $R_E(z)$ (for the η_2 curve) in the 20 - 50 gm.cm^{-2} region. The true altitude dependence for the P_o = 125 MV proton spectrum probably lies somewhere between the two curves in figure 5.9.

A P_o = 50 MV proton spectrum would give rise to a somewhat steeper altitude dependence because of the correspondingly steeper altitude distribution of the neutron production (figure 5.15). Thus, over 95% of the neutrons are produced in the first 5 gms of the atmosphere when P_o = 50 MV, whereas about 15% are produced at depths greater than the balloon level ($\sim$15 gm.cm^{-2}) when P_o = 125 MV. However, diffusion is the dominating factor in the neutron flux distribution and the altitude dependence is unlikely to be greatly dependent on P_o.

Two features of the absorption curve for the excess radiation which support our hypothesis are the tendency towards a levelling off in the 15 - 25 mb region and the fact that the excess radiation first becomes significant at about 150 mb.

The altitude dependence of the excess radiation is therefore not incompatible with our hypothesis. No stronger conclusion can be reached because of the uncertainty about the counter energy response and the possibility of time variations of the incident proton flux, during the event.

(ii) Riometer absorption.

Freier and Webber (1963) have published curves relating cosmic noise absorption, for a 30 Mc/s riometer, to solar proton flux, for various integral spectra and cut-off rigidities, during daylight hours. In calculating these curves the authors made use of electron and ionic recombination parameters evaluated by Webber (1962), who combined these to obtain a single effective parameter α_{eff} which he has calculated for various heights and electron densities for mid-day and mid-night. The electron density n_e is obtained from the electron production rate q by the equation

$$n_e = \left(\frac{q}{\alpha_{eff}}\right)^{\frac{1}{2}} \qquad (5.9)$$

Recombination rates are considerably higher during darkness, due mainly to the elimination of photodetachment effects. Riometer absorption for a given flux is consequently much lower at night than during daylight hours. Webber (1962) has used data from a large number of polar stations and many different events to obtain the ratio A_D/A_N between day-time and night-time absorption. This tends to decrease with increasing A_D. However, for daylight absorption A_D less than about 5 db, the ratio is essentially constant at about 5, for geomagnetic latitudes $\leq 65^\circ$, under relatively undisturbed magnetic conditions. In table 5.5 we have given the riometer absorption as predicted by Freier and Webber (1963), using the flux given in table 5.4. The absorption estimated from Freier and Webber's graph has been divided by a day-night ratio $A_D/A_N = 5$, since the Macquarie flight 21 event occurred near local midnight. Also shown in table 5.5 are riometer absorption figures for the $P_o = 50$ MV spectrum, estimated from the graphs of Van Allen et al (1964) with the same day-night correction factor. These authors give curves relating absorption per unit flux against particle kinetic energy, for protons and alpha particles. The total absorption has been estimated by numerically integrating for the exponential fluxes as before.

Riometer absorption for P_o = 50 MV	Cut-off rigidity P_c (MV) 0	200	250	300	370	MV
Freier and Webber						
$\eta_1(E)$	1.84	0.92	0.60	0.44	0.26	db
$\eta_2(E)$	1.36	0.68	0.44	0.30	0.20	"
Van Allen et al						
$\eta_1(E)$	-	1.60	0.96	0.70	0.40	"
$\eta_2(E)$	-	1.20	0.70	0.50	0.30	"
Riometer absorption for P_o = 125 MV						
Freier and Webber						
$\eta_1(E)$	0.36	0.24	-	0.15	0.11	"
$\eta_2(E)$	0.26	0.18	-	0.11	0.08	"

Table 5.5: Estimated absorption (db) for a 30 mc/s riometer, due to the proton fluxes given in table 5.4. The calculations are based on the results of Freier and Webber (1963) and Van Allen et al (1964). A day-night absorption ratio of 5 is assumed.

In these calculations we have ignored the effect of α-particles present in the particle stream. The absorption per unit flux of α-particles is about twice that of protons (Van Allen et al 1964). The p/α abundance ratio is very variable in solar events (Biswas and Fitchel 1965). This results in a further uncertainty of ~50% in the results in table 5.5.

Although the exact sensitivity of the Macquarie Island riometer is not known, the minimum detectable absorption would probably be about 0.5 db for this event. Since there is no obvious correlation between the neutron flux increase and the Macquarie riometer record, we conclude, from table 5.5,

that the cut-off rigidity P_c was $\gtrsim$ 300 MV if the event was initiated by protons having an exponential rigidity spectrum with characteristic rigidity $P_o \sim$ 50 MV. If, on the other hand, $P_o \gtrsim$ 125 MV, riometer absorption would not be expected even for P_c = 0 MV.

The postulated fluxes would, however, have produced detectable cosmic noise absorption in polar regions, especially at stations in Northern Europe which were in daylight at the time. No such absorption has been reported, and if we assume that none occurred, we conclude either that the event was confined to auroral regions or that the characteristic rigidity was greater than 125 MV. A proton spectrum very flat below $\sim$ 200 MV and becoming steeper at high rigidities would also be compatible with the observations, but such ad hoc assumptions are unattractive.

(iii) Scintillator count rate.

(a) Introduction.

The count rate of the NaI scintillator would be affected in two ways by the hypothetical protons. A small fraction (depending on the spectrum and angular distribution) would penetrate to the balloon level and directly increase the scintillator count rate. Some protons would make inelastic collisions with air nuclei, and some of the secondaries (chiefly nuclear gamma rays) would have sufficient energy to reach the balloon level and produce an output in the scintillator channel. We have already shown in section 5.2 (v) that no significant increase was observed in the scintillator rate, and consequently that the flux of such protons and secondaries was less than 0.11 $cm^{-2}sec^{-1}ster^{-1}$. We will now estimate the scintillator rate increase arising from the proton fluxes given in table 5.4 to check the compatibility of our hypothesis with these observations.

(b) Nuclear γ-ray production.

Protons making inelastic collisions with air nuclei may produce nuclear γ-rays by several reactions. The most important are the (p,p') and (p,n) reactions. The latter give rise to unstable isotopes decaying by positron emission, and to excited nuclear states which reach the ground state by γ-ray emission. The positrons give rise to further γ-rays in annihilation reactions. Hoffmann and Winckler (1963) have made a survey of the experimental data on the cross-sections for these reactions and have estimated the theoretical γ-ray production ratio $\frac{dN_\gamma}{dN_p}(E)$ (gammas per proton) as a function of energy E.
They obtain an expression

$$\frac{dN_\gamma}{dN_p} = 7 \times 10^{-5} E^{1.92} \qquad (5.10)$$

for E >3 Mev. This is in reasonable agreement with the theory of Colgate (1955), who predicts a production ratio of $10^{-5}E^2$ gammas proton^{-1} in the 3 - 30 Mev range. Hoffmann and Winckler's data were based on the estimate of an average 3 ± 1 γ-rays per reaction in the 1.5 - 17 Mev range, and should be compared with the value of 4 γ-rays per reaction estimated by Bhavsar (1962) for protons of 30 - 300 Mev. The γ-ray production cross-section is the product of the number of γ-rays per reactions and the total reaction cross-section. Since this changes only slowly with energy in the range of interest (30 - 150 Mev), so does the γ-ray production cross-section. Consequently the γ-ray production ratio is directly proportional to the range of the protons which varies as a power law with energy. H ence we are justified for the present purposes in extrapolating equation (5.10) beyond the 40 Mev for which it was calculated by Hoffmann and Winckler (1963) to several hundred Mev.

To estimate the total γ-ray production rate in a 1 cm^2 atmospheric column, we solve the integral

$$N_\gamma = \int_{E_c}^{\infty} \frac{dN_\gamma}{dN_p}(E)\,\frac{dN_p}{dE}\,dE \qquad (5.11)$$

(1) P_o = 50 MV proton spectrum.

For ease of calculation we approximate the power law expression of equation (5.10) by the exponential function

$$\frac{dN_\gamma}{dN_p} = 7.9 \times 10^{-3}\, e^{P/106} \qquad (5.12)$$

This function is equal to the power law expression at 300 and 500 MV and differs from it by not more than ± 15% in the interval 300 MV < P < 600 MV. The contribution to γ-ray production of P > 600 MV protons is insignificant.

Using the exponential expression equation (5.4), previously assumed for the proton spectrum, we find for P_o = 50 MV

$$N_\gamma = 7.9 \times 10^{-3} \left(\frac{dJ}{dP}\right)_o \int_{P_c}^{\infty} e^{-P/95}\,dP \qquad (5.13)$$

Evaluating this integral using the differential proton fluxes $\left(\frac{dJ}{dP}\right)_o$ corresponding to the integral fluxes in table 5.4 we obtain the values of N_γ given in table 5.6.

	Cut-off rigidity P_c (MV)	
Counter response curve	300	370
$\eta_1(E)$	27.5	25.5
$\eta_2(E)$	14.5	13.5

Table 5.6 : Integrated γ-ray production rate per cm^2 atmospheric column per second for a proton spectrum with characteristic rigidity P_o = 50 MV.

(2) P_o = 125 MV proton spectrum.

The evaluation of the γ-ray production rate is difficult

since the integral (equation 5.11) converges slowly and particles having energies in the 0.5 - 1 Bev range make a significant contribution to the nuclear γ-ray production. However, N_γ is unlikely to exceed 20 $cm^{-2}sec^{-1}$ for a cut-off rigidity of 300 MV.

The γ-ray production rate is not very sensitive at these rigidities to the value of P_c. This applies to both the P_o = 50 and 125 MV proton spectra.

(c) Attenuation of the γ-rays in the atmosphere.

The gamma ray intensity I(z) at depth z due to a flux of strength I_o at the top of the atmosphere (z = 0) is given by the Gold integral

$$\epsilon_1(\mu z) = \frac{I(z)}{I_o} = \mu z \int_{\mu z}^{\infty} \frac{e^{-s}}{s^2}\, ds \qquad (5.14)$$

where μ is the gamma ray absorption coefficient

$s = \frac{\mu z}{\cos \theta}$

θ is the zenith angle.

This integral is derived (Appendix V) on the assumption of a flux at z = 0 isotropic over the lower and zero over the upper hemisphere. It is also assumed that the rays are propagated in straight lines (no scattering).

Since most nuclear gamma rays are produced in the first few grams of the atmosphere (assuming a P_o = 50 MV proton spectrum), we can use equation (5.14) to determine the attenuation of the flux at the balloon level. Solving this integral using the curves given by Rossi (1952) and values of μ (Davisson and Evans 1952) for 0.1, 0.5 and 1.0 Mev gamma rays, we find that at 14 $gm.cm^{-2}$ the attenuation of the total intensity is 30, 9 and 5.6 respectively. The average intensity over the upper hemisphere at 14 $gm.cm^{-2}$ can now be determined for the values of N_γ in table 5.6. The results are given in table 5.7 for a cut-off rigidity of 300 MV.

Gamma ray energy		
0.1 Mev	0.5 Mev	1.0 Mev
0.04 - 0.07	0.13 - 0.25	0.21 - 0.38

Table 5.7: Estimated average γ-ray intensity ($cm^{-2}sec^{-1}ster^{-1}$) at 14 $gm.cm^{-2}$ for cut-off rigidity P_c = 300 MV and proton spectrum characteristic rigidity P_o = 50 MV. In each case the upper and lower values are for the $\eta_1(E)$ and $\eta_2(E)$ neutron counter response curves respectively.

To evaluate the flux at 14 $gm.cm^{-2}$ for the P_o = 125 MV proton spectrum it would be necessary to determine the altitude variation $\frac{dN_\gamma}{dz}$ of the gamma ray production and integrate $\epsilon_1(z - 14)\frac{dN_\gamma}{dz}$ over all z. However the average flux at 14 $gm.cm^{-2}$ is unlikely to differ greatly from that given in table 5.7.

Hoffmann and Winckler (1963) have measured the absorption in the atmosphere of γ-rays produced by low energy protons. Their results are most compatible with a mean γ-ray energy of about 0.5 Mev.

(d) Residual proton flux at the balloon level.

In order to estimate the residual proton flux at the balloon level we will assume, following Freier and Webber (1963), that the proton absorption mean free path is the same as the interaction mean free path λ and that this is 100 $gm.cm^{-2}$ for the proton energies of interest here. We can make these assumptions because the range of secondary particles produced by protons of a few hundred Mev is only a few $gm.cm^{-2}$ and in any case, most of the attenuation of the proton flux, at these energies, is due to ionisation. Using a similar procedure to that adopted for the attenuation of γ-rays (Appendix V), we obtain the following expression (Edwards 1964) for the flux J(z,P) at atmospheric depth z due to an isotropic flux J(P) of

of protons of rigidity P at z = 0.

$$J(z,P) = \int_0^{\theta_o} J(P)\, e^{-z/\lambda \cos\theta} \sin\theta\, d\theta \qquad (5.15)$$

where θ is the zenith angle

$\theta_o = \arccos z/R(P)$

and $R(P)$ is the range in air of protons of rigidity P.

Integrating equation (5.15) we find

$$J(z,P) = J(P)\left\{\varepsilon_1\left(\frac{z}{\lambda}\right) - \frac{z}{R(P)}\ \varepsilon_1\ \frac{R(P)}{\lambda}\right\} \qquad (5.16)$$

where $\varepsilon_1(\bar{x})$ is the Gold integral (Rossi 1952).

This is then integrated over energy to obtain the flux J(z).

$$J(z) = \int_{P(z)}^{\infty} \left\{\varepsilon_1\left(\frac{z}{\lambda}\right) - \frac{z}{R(P)}\ \varepsilon_1\ \frac{R(P)}{\lambda}\right\} \frac{dJ}{dP} \cdot dP \qquad (5.17)$$

where P(z) is the rigidity of a proton with range z.

This integral must be solved numerically.

By a similar method, Freier and Webber (1963) have obtained the altitude dependence of the counting rate of an omnidirectional counter for various incident proton energy spectra. They have also evaluated the ratio A(z) of the flux of protons with $P > P(z)$ at the top of the atmosphere to the flux J(z) at z.

$$A(z) = \frac{1}{J(z)} \int_{P(z)}^{\infty} \frac{dJ}{dP} \cdot dP \qquad (5.18)$$

At 14 gm.cm^{-2} with an exponential rigidity spectrum (equation 5.4): $A(z) = 5$ for $P_o = 50$ MV

and $A(z) = 3$ for $P_o = 125$ MV.

The residual proton flux at 14 gm.cm^{-2} is given for various values of P_c and $P_o = 50$ and 125 MV in table 5.8.

Characteristic rigidity P_o	Cut-off rigidity P_c (MV) ≤ 200	300	370
50 MV	0.012-0.022	0.02-0.038	0.066-0.13
125 MV	0.11 -0.22	0.12-0.23	0.13-0.25

Table 5.8: Residual proton flux $J(z)$ $cm^{-2}sec^{-1}ster^{-1}$ at 14 $gm.cm^{-2}$ averaged over the upper hemisphere for various values of cut-off rigidity. In each case the upper and lower values are for the two neutron counter response curves $\eta_1(E)$ and $\eta_2(E)$.

The total flux capable of influencing the scintillator count rate may be estimated by combining the data in tables 5.7 and 5.8. The resulting fluxes are given in table 5.9 for three different values of the γ-ray energy. We assume that the values of N_γ are independent of the cut-off rigidity P_c and of the characteristic rigidity P_o of the proton spectrum (section 5.4 (iii b)).

Characteristic rigidity P_o	γ-ray energy (Mev)	Cut-off rigidity P_c (MV) 200	300	370
50 MV	0.1	0.05-0.09	0.06-0.11	0.11-0.20
	0.5	0.14-0.27	0.15-0.29	0.20-0.38
	1.0	0.22-0.40	0.23-0.42	0.28-0.51
125 MV	0.1		0.16-0.30	
	0.5		0.25-0.48	
	1.0		0.33-0.61	

Table 5.9: Total flux ($cm^{-2}sec^{-1}ster^{-1}$ averaged over the upper hemisphere) at 14 $gm.cm^{-2}$, capable of influencing the scintillator counting rate. In each case the upper

and lower limits correspond to the $\eta_1(E)$ and $\eta_2(E)$ counter response curves used in the calculations. The results for P_o = 125 MV have not been calculated for P_c = 200 and 370 MV.

The uncertainty in these results is determined, principally, by the errors in the proton fluxes given in section 5.3 (vi) and by the errors in the γ-ray production cross-sections and the γ-ray and proton flux attenuation in the atmosphere. The actual fluxes at the balloon level probably lie within a factor of 3 of the values given in table 5.9.

(e) Conclusions.

The scintillator counting rates corresponding to the fluxes given in table 5.9 may be evaluated (assuming the flux to be isotropic over the upper hemisphere) using equation (5.1). These rates vary from < 2% of the background (assuming P_o = 50 MV, P_c = 200 MV and E_γ = 0.1 Mev) to about 12% for P_o = 125 MV and E_γ = 1 Mev. The rates would be reduced by about 25% if we assume a $\cos^2\theta$ (where θ is the zenith angle) distribution for the flux at the detector.

Assuming a γ-ray energy of 0.5 Mev (Hofmann and Winckler 1963) and the error limits discussed above, we estimate that the scintillator rate would have increased by 2 - 16%, during the neutron event, if the proton spectrum had characteristic rigidity P_o = 50 MV. If P_o = 125 MV the increase would have been about three times as large.

These results depend strongly (particularly in the case of the P_o = 50 MV spectrum) on the absorption of the nuclear γ-rays in the atmosphere. Thus the estimated scintillator rate increase is more than halved if the mean γ-ray energy is reduced from 0.5 Mev to 0.1 Mev.

In section 5.2 (iv) we noted that the scintillator rate changed very little, if at all, at the end of the neutron channel event during flight 21. The rate could have decreased

by, at most, about 4%. Our predictions, based on the calculations in section 5.4 (iii), are probably not compatible with this observation and the proton-neutron hypothesis is probably incorrect. We cannot be any more dogmatic than this since it is possible, within the limits of error given, that the event could have been produced by protons having a very steep energy spectrum.

5.5 Proton Acceleration Mechanisms.

In the preceding section we have shown that the Macquarie Island flight 21 event was probably not caused by low energy protons. The proton flux required would probably have caused an increase in the rate of the NaI scintillator in the rig, and none was observed. There is some uncertainty about this conclusion and it is of interest to consider methods by which protons may be accelerated to the energies required to produce the neutron count rate increase.

(i) Solar flare acceleration.

Direct solar flare production of the protons seems very unlikely since solar activity was very low, with no flares greater than class 1 observed during the 4 days prior to the neutron count rate increase. The time scale of the increase was much shorter than is normal for solar proton events which decay with a time constant of the order of one day.

(ii) Long-lived solar particle streams.

Bryant et al (1963), Gregory and Newdick (1964) and others, have reported long-lived streams of solar particles which give rise to proton flux increases at the earth up to two solar rotations after the originating solar flare. These increases occur at the beginning of a magnetic storm and a Forbush decrease near the time of the central meridian passage of the original flare and solar proton production. Recurrences may also occur during geomagnetically quiet periods (Gregory

and Newdick 1964). The time scale of these events is typically only a few hours.

The flight 21 increase has a certain resemblance to these events in that it occurred during a recurrent type magnetic storm which may be associated with a small decrease (figure 5.7) in the Mt. Wellington neutron monitor rate. The storm 54 days previously was accompanied by a Forbush decrease and a short-lived increase (Zmuda et al 1963), in the flux of 1 - 15 Mev protons, occurred during the magnetic storm 27 days prior to March 6th. However, the flux of $E > 40$ Mev protons did not rise above the detection threshold of 10 $cm^{-2}sec^{-1}$ during the increase reported by Zmuda et al (1963). This raises the difficulty in supposing the flight 21 event to be produced by long-lived solar protons, namely, the steep energy spectrum of these particles. According to Bryant et al (1963), these have a differential energy spectrum of the power law type with exponent between -4 and -5 in the 3 - 10 Mev range. If the flight 21 event was caused by protons with a spectrum of this type, the low energy flux would have been very large and would certainly have caused riometer absorption at high latitude stations. No such observations have been reported, and we conclude that the flight 21 event was not caused by an event of this kind, unless the proton energy spectrum was considerably harder than that reported by Bryant et al (1963).

(iii) Local acceleration.

It has been suggested (K.B.Fenton - private communication) that the protons assumed responsible for the flight 21 event were accelerated from low energies in the vicinity of the earth. There is little doubt (Galperin 1963) that local acceleration processes play an important part in the production of the large fluxes of particles precipitated into the atmosphere in the auroral regions. This precipitation frequently includes protons with energies in the tens and hundreds of Kev (McIlwain 1960, Davis et al 1960, McDiarmid et al 1961)

but the energy spectrum is steep ($J(>E) \propto E^{-\gamma}$ where $\gamma = 3 - 4.5$) and there is little evidence for auroral protons with energies in the 10 - 100 Mev range. Davis et al (1960) observed a count rate increase which could have been produced by 50 - 120 Mev protons, but bremsstrahlung from ~100 Kev electrons seems a more probable explanation.

Korff and Haymes (1960) observed large increases in the count rate of moderated BF_3 counters during a balloon flight from Sioux Falls ($\lambda = 53^{o}N$) on September 3rd, 1959. This was a period of intense auroral and geomagnetic activity, with K_p reaching 7^{+} during the count rate increases, and strong riometer absorption was also recorded. The authors suggest that the increases were caused by large fluxes (about 500 $cm^{-2}sec^{-1}ster^{-1}$) of E > 140 Mev protons. This flux was required to account for the increase in the highly ionising particle "background" rate, (detected by the difference technique - section 4.3) which they assumed was produced by stopping protons having path lengths greater than 15 cm in their counter. The authors rejected an alternative hypothesis that the increase in background was caused by ionisation from X-rays because of the large fluxes required ($\sim 10^{5}$ $cm^{-2}sec^{-1}$ with E > 30 Kev). However, fluxes of this and even larger magnitudes have since been observed during auroral events (Winckler et al 1962), and this explanation now seems more acceptable.

If this theory is correct we would expect the riometer and neutron count rate peaks to coincide, provided the two instruments were in the same locality. The proton flux required to produce the neutron increase would be very much less than that estimated on the stopping proton hypothesis. We need not, however, postulate the existence of energetic protons since, in the main increase at 0350 U.T., both the unenriched and the enriched counter channels were swamped, and no difference in their rates could be detected. The other two increases were very small and were detected only in the enriched counter channel, in spite of the unenriched counter's sensitivity to neutrons. We

are inclined to believe, therefore, that the first two "events" were statistical in nature and that the swamping event was produced by a very intense burst of auroral X-rays.

Recent satellite measurements (Fan et al 1964, Frank and Van Allen 1964) have given direct evidence for electron acceleration in the transition region between the magnetosphere and the solar wind. Frank and Van Allen observed large bursts of $E > 40$ Kev electrons in this region. During magnetically disturbed periods, $E > 1.6$ Mev electrons were also detected, but only at large sun-earth-satellite angles (i.e. near local dawn and sunset). It has been suggested (Jopikii and Davis 1964) that a Fermi acceleration mechanism operates between the earth's hydromagnetic shock front and irregularities in the solar wind. There is, however, no evidence for acceleration, in this region, of protons to the energies required to produce the flight 21 neutron increase.

Kaufmann (1963) has investigated all acceleration mechanisms likely to be effective in the vicinity of the earth. He finds that protons are unlikely to be accelerated to energies greater than a few hundred Kev, except perhaps for those trapped on field lines lying within one or two earth radii of the surface.

The proton energies produced by Fermi acceleration, near the boundary of the magnetosphere, are restricted by the limited dimensions and weak fields of the trapping region and by the small energy increments (a few Kev) per collision. Hydromagnetic waves may accelerate trapped protons, but not beyond a critical energy above which the magnetic moment is not conserved in the proton - hydromagnetic wave interaction. This critical energy is $\ll 1$ Mev for protons on field lines passing through Macquarie Island. In the betatron process the fractional energy increase is equal to the fractional increase in field strength produced in the magnetosphere,for example by increased solar wind pressure during magnetic storms. These field changes are, however, relatively small.

(iv) Acceleration in interplanetary regions.

Axford and Reid (1962) have suggested that protons may be accelerated to tens of Mev in interplanetary regions. The acceleration is produced by repeated reflections from magnetic field lines, bent by the shock wave associated with the advancing solar plasma which is responsible for sudden commencement magnetic storms on earth. This theory was developed to explain the observation on several occasions of a sudden increase in riometer absorption, minutes or hours before a sudden commencement magnetic storm. The decay time of the particle flux varies from minutes to days. Observations from Explorer XII on September 30th, 1961, of protons which may have been accelerated in this way (Bryant et al 1962), indicate an integral spectrum, above 10 Mev, of the power law type with exponent ~ 3.

Parker (1965) shows that acceleration of charged particles is a normal feature of any tenuous ionised gas in a state of vigorous agitation. He argues that energetic particles should normally be produced in violent interplanetary plasma phenomena. The 9-14 Mev protons observed by Bryant et al (1962) were accelerated in the region at the front of a blast wave produced by a sudden increase in the solar wind, following a large scale solar flare several days previously.

The energy spectrum, flux and time dependence of these events are compatible with the Macquarie Island flight 21 data. However, interplanetary acceleration would be expected to produce riometer absorption at high latitudes, and as we have noted, none has been reported for this time. In any case, the lack of solar activity and the slow commencement nature of the March 6th magnetic storm suggest that interplanetary conditions were not suitable for this type of acceleration to occur.

(v) Count rate increases during geophysically quiet periods.

There have been a number of reports of neutron

and other counting rate increases observed at times of very low solar and geophysical activity. The origin of these events has not, as far as is known, been satisfactorily explained. We mention them here because of the similar obscurity concerning the origin of our flight 21 event.

Neher and Anderson (1960) reported two flux increases recorded with balloon borne ionisation chambers at Bismarck ($\lambda = 56^{o}N$), in 1954 and 1958. Both occurred during geophysically quiet periods and could not be related to any solar, magnetic or ionospheric activity.

Gauger (1964) observed a three-fold increase in the $E > 60$ Mev neutron flux at $\lambda = 50\text{-}55^{o}N$, during an aircraft flight at 245 $gm.cm^{-2}$, on July 21st, 1962. A class 2 flare was observed on the east limb of the sun ($5^{o}N$, $75^{o}E$) several hours before the flight, but solar and geophysical activity were otherwise very low.

Haymes (1964) observed an approximately two-fold increase in the flux of 1-14 Mev neutrons during a balloon flight at $\lambda = 43^{o}N$, on May 7th, 1963. The measurements were made with a phoswich type neutron detector at an atmospheric depth of 4.7 $gm.cm^{-2}$. The increase lasted about 1½ hours, and was accompanied by an increase in the flux of 0.47 - 3.5 Mev γ-rays. No significant change was observed in the rate of a channel sensitive to charged particles and $E > 15$ Kev γ-rays. Solar and geomagnetic activity were low for several days prior to and following the flight.

Haymes was unable to explain the origin of these increases, but suggested that the γ-ray burst was similar to fluctuations observed by Duthie et al (1963). This group reported an approximately 50% increase in the $E > 60$ Mev γ-ray intensity at 4 mb, during a balloon flight on October 4th, 1962, over New Mexico. The increase lasted about 90 minutes and was accompanied by a small increase in the relativistic ($\beta > 0.7$) charged particle flux. Magnetic activity was very low ($K_p \leq 1^{+}$) at the time, and no solar flares greater than class 1 have been

reported for the preceding four days.

Recently, Gauger (1965) has reported an increase in the flux of atmospheric neutrons at aircraft altitudes (39,000 feet) in the region of the South Atlantic magnetic anomaly. The increase was observed in the counting rate of bare, moderated and cadmium shielded BF_3 neutron counters and was accompanied by an increase in the intensity of the night airglow measured by photometric equipment on board the aircraft. The neutron increase, which lasted about 20 minutes, occurred at a time of low solar and geophysical activity, on January 21st, 1964.

5.6 Other flights from Macquarie Island.

(i) Flight 1, December 1961.

Macquarie Island flight 1 was made during a geophysically quiet period on December 21st and 22nd, 1961. The neutron count rate (figure 5.1) was normal throughout the balloon ascent and for the first three hours of level flight at about 9 mb. Then, about local noon (0130Z), a count rate increase began. The increase reached a peak of about 70% at 0140Z and thereafter decayed very erratically, reaching the normal level shortly after 0200Z. Apart from statistical fluctuations and a slow increase due to decreasing balloon altitude, the rate remained steady until 0521, when neutron counting stopped abruptly. The reason for this failure is not known, but failure of a soldered joint seems the most probable explanation.

The count rate of the NaI scintillator remained normal throughout the flight and there is no indication of any change during the neutron count rate increase. Magnetic conditions were very quiet during the flight, with $K_p = 1$ at the time of the increase, and only one solar flare (of class 1) occurred in the preceding three days. There have been no reports of satellite observations of solar protons at this time, and no increase in cosmic noise absorption was detected by the 27 mc/s Macquarie Island riometer.

We have little confidence in the reliability of these data in view of the erratic nature of the event and the low level of geophysical activity. We will, however, consider the possibility that the increase was caused by low energy protons incident on the atmosphere in the same way as has been proposed for flight 21.

Using the methods described in the preceding sections we find a nuclear γ-ray and residual proton flux excess, at the balloon level of roughly 0.15 - 1.4 $cm^{-2}sec^{-1}ster^{-1}$ (for P_o = 50 MV). This corresponds approximately (equation 5.1) to a 4 - 35% increase, in the scintillator channel rate, which would almost certainly have been detected. Because the event occurred at local noon, riometer absorption would probably have been detected also. We cannot be dogmatic about this, as absorption depends critically on geomagnetic cut-off which is uncertain for Macquarie Island. Absorption would, however, have been detected at high latitude stations, unless we make the improbable assumption that the protons were mono-energetic, or that the event was confined to auroral regions. There have been no reports of riometer absorption at this time, and auroral protons, although sometimes precipitated at geomagnetically quiet times (Galperin 1963) do not have sufficient energy to produce neutrons. The assumption that the event was initiated by low energy protons would appear therefore to be untenable. As the increase occurred near local noon, the possibility arises that it was produced by solar neutrons. However, solar activity was very low at the time, and in any case, the rapid counting rate variations are inconsistent with the long transit time from the sun.

In view of the lack of solar and geophysical activity, the absence of any increase in the scintillator count rate and the erratic nature of the neutron count rate increase, we are inclined to believe that the event was spurious and caused by instrument malfunction.

(ii) Flights during auroral activity.

Flight 14 (1962) was released from Macquarie Island at 1010Z on February 15th, 1962, and the balloon reached floating level (12 mb) at 1210Z. The neutron and scintillator rates remained normal until about 1700Z when the neutron channel slowed and stopped, due, apparently, to the failure of the EHT supply at low temperatures. (This circuit was decoupled with electrolytic capacitors which become useless at temperatures below about -40°C, - section 2.12 (i).) Rig temperatures began to rise at about 1800Z and the neutron channel started to count again at 1920Z.

A large riometer absorption event began at 1700Z, and sporadic increases in the scintillator rate were recorded throughout the remainder of the flight. The count rate of the E > 25 Kev channel varied from 2 to 8 times normal, during almost continuous X-ray activity, from 2130Z on February 15th to 0130Z on the following day. Apart from the period from 1700 - 1920Z, when the channel was out of action, the neutron count rate remained normal throughout the flight.

Counting rate increases were observed with the geiger counters on flights 8 and 15 from Macquarie Island in 1964 (Table 3.3). Two events with peak intensities 75% and 50% above normal were recorded during flight 8, on January 29th, (Figure 5.3). These occurred during level flight at 18 mb at a time of high earth current and magnetic activity. A small sudden commencement magnetic storm began late on the 28th, and K_p was 4 at the time of the events. No increases were observed in the rates of the neutron counter or geiger counter telescope and it is obvious that the geiger counter increases were caused by auroral region X-rays.

The increase during flight 15 showed greater time variations (figure 5.4) and reached a peak intensity (in minute totals) of 2.7 times normal. Both geiger counters went into continuous discharge at 1356Z, presumably as a result of the high counting rates and low rig temperatures. There is no doubt,

however, about the reliability of the data prior to this failure and a coincident X-ray increase was observed, at a magnetically conjugate point in Alaska, by the group from the University of California with whom the flights were co-ordinated (Dr. N.R.Parsons - private communication). Earth current activity was intense during this event but no increase was observed in the counting rates of the neutron counter or of the geiger counter telescope.

The X-ray events, during these three flights, correspond to larger fluxes at the top of the atmosphere than the corresponding flux during the flight 21 (1962) X-ray event. This is obvious for the scintillator rate increase during flight 14 (1962) since similar detectors were used and the balloon altitudes were about the same. In the case of flights 8 (1964) and 15 (1964) we must allow for the low efficiency ($\sim$1%) for X-ray detection of the geiger counters used, and for the greater atmospheric depth during flight 8 (1964).

It is obvious, from these results, that $E \gtrsim 20$ Mev protons do not often accompany the energetic electrons frequently precipitated into the atmosphere in auroral regions. This is scarcely surprising since there is little evidence (section 5.5 (iii)), apart from our Macquarie Island flight 21 results, that they ever do.

5.7 Conclusions.

(i) The small erratic increase in neutron counting rate observed on flight 1 (1962), during a geophysically quiet period, is almost certainly due to instrument malfunction.

(ii) The atmospheric neutron flux has been measured at balloon altitudes on four flights during auroral X-ray events. No significant change was observed in the neutron flux during three of these flights, and the count rate increase during the fourth was probably caused by instrument malfunction (see subsection (iii) below). There is therefore no convincing evidence, from our measurements, for acceleration of protons to

energies in the tens of Mev range, during auroral events. The upper limit to the number of such protons depends on their energy spectrum, but the flux excess of $E > 40$ Mev protons must have been less than about 1 $cm^{-2}sec^{-1}ster^{-1}$ during our flights.

(iii) The increase in the neutron count rate during the auroral X-ray event on flight 21 (1962) remains unexplained. We believe that instrument malfunction is unlikely for the reasons set out in sections 5.2 (iv) and 5.4 (i). We are unable, however, to suggest any method involving geophysical phenomena by which the increase could have been produced, which is also compatible with the other observations during the flight.

An increase produced by neutrons, generated by protons with insufficient energy to reach the balloon level, requires a proton flux of ~ 10 $cm^{-2}sec^{-1}ster^{-1}$ with $E > 40$ Mev. These protons would produce a considerable flux of nuclear γ-rays which would almost certainly have caused a detectable increase in the rate of the scintillator channel. No such increase was observed. It is just possible that the increase in the scintillator rate would have been unobservable provided the proton energy spectrum was very steep. A spectrum of this type implies large fluxes ($\sim 10^3$ $cm^{-2}sec^{-1}ster^{-1}$ with $E > 1$ Mev) of low energy protons. These would have produced 2 - 10 db of riometer absorption in high latitude stations, and none has been reported for the time of the event. This difficulty could be accounted for by assuming that the protons were locally accelerated, perhaps in the same process that produces the energetic, X-ray generating, electrons. The scale and energy densities of the local accelerating regions do not appear, however, to be sufficient for this purpose. We note, also, that neutron events did not occur during any of the other, and larger, X-ray events reported in section 5.6 (ii).

We are forced to the conclusion that the event was very probably produced by instrument malfunction.

(iv) A balloon borne neutron counter is a sensitive instrument for the detection of solar protons. Its sensitivity,

relative to that of a nuclear γ-ray detector, depends on the proton energy spectrum and the altitude at which the measurements are made. At altitudes accessible to inexpensive balloons (10 - 15 mb) and a characteristic rigidity (section 5.3 (iv)) P_o = 125 MV, the neutron counter is about 5 times as sensitive as a nuclear γ-ray detector.

It is also more sensitive than a riometer for all but the steepest solar proton energy distributions. Thus 1 db of riometer absorption, at a high latitude station, corresponds to a five-fold increase in the rate of a neutron detector at an atmospheric depth of 10 - 20 gm.cm^{-2}.

VI NEUTRON COUNTING RATE DISTRIBUTIONS

6.1 Time variations

The neutron flux in polar regions changes rapidly during the solar cycle and appropriate corrections must be made when comparing data obtained at different times. In figures 6.1 and 6.2 we compare the count rates at 20, 50 and 240 mb over Wilkes and Mildura with the rate of the Mt.Wellington neutron monitor. We use Mt.Wellington data since they are available for the full period since last solar maximum, and are closely comparable with the data from the Chicago neutron monitor which has been operating since 1952.

The exact relation between the balloon and neutron monitor rates is difficult to determine because of the limited amount of data. We have assumed the relationship to be linear and calculated the ratio $T(z,P_c)$ of the fractional increment $\frac{\Delta R}{R}$ in the balloon count rate R at depth z to the fractional increment $\frac{\Delta C}{C}$ in the neutron monitor rate C. That is

$$T(z,P_c) = \frac{C}{R}\frac{dR}{dC} \qquad (6.1)$$

Values of $T(z,P_c)$ at 20, 50 and 242 mb are given, for Wilkes and Mildura, in table 6.1.

Station	Pressure (mb)		
	242	50	20
Wilkes	3.2	4.5	6.4
Mildura	2.2	2.0	2.9

Table 6.1: Values of the time variation factor $T(z,P_c)$ relating increases in the balloon counting rate to increases in the rate of the Mt.Wellington neutron monitor. The values given are accurate to within $\pm$ 20%.

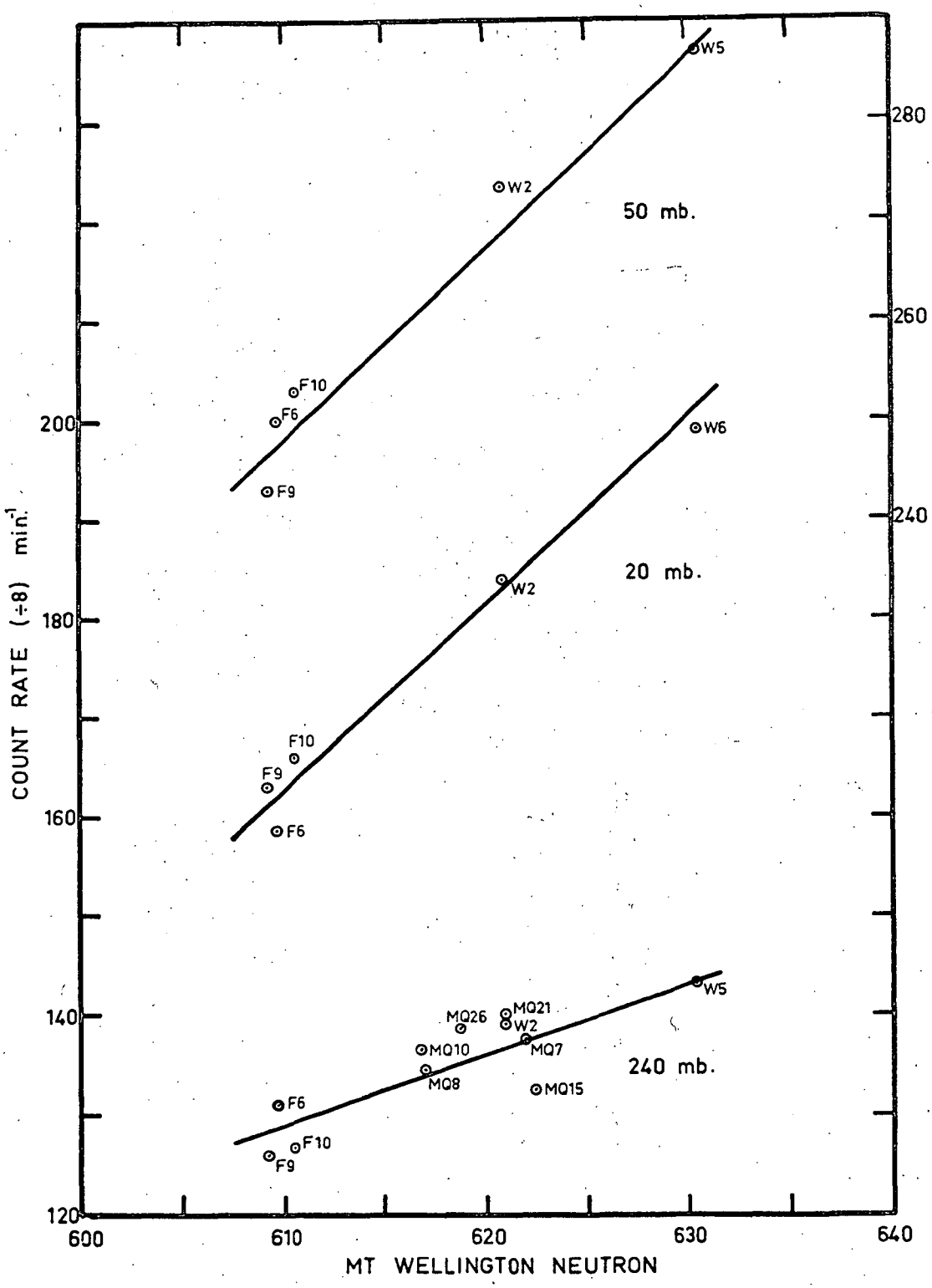

Fig. 6.1. Time dependence of the neutron flux at high altitudes over Wilkes, Antarctica.

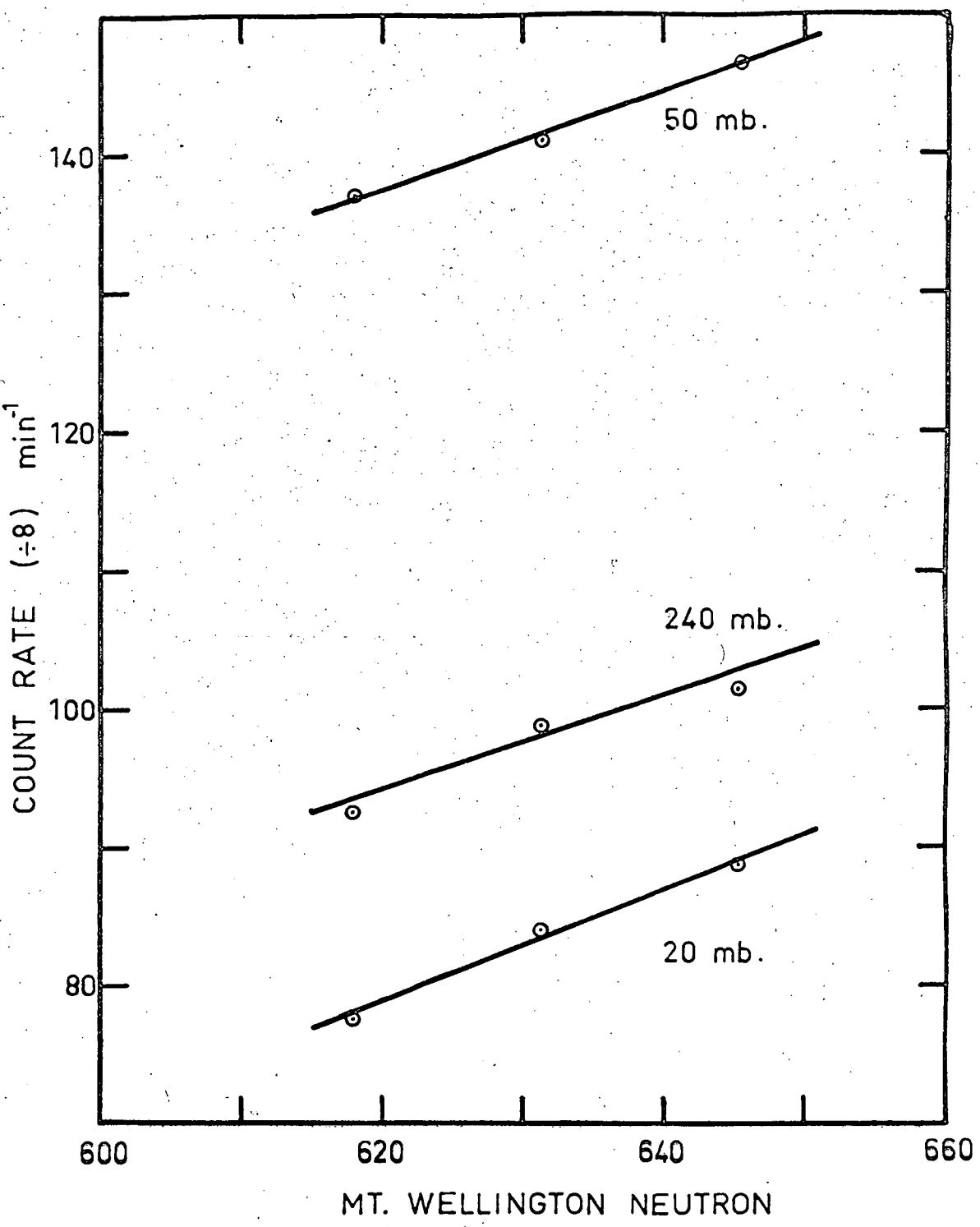

Fig. 6.2. Time dependence of the neutron flux at high altitudes over Mildura, Victoria.

Since T is a strong function of z at Wilkes, it follows that the count rate absorption curve varies during the solar cycle. This is apparent in figure 6.3, where the data for Wilkes flights F6 (February 1963) and W5 (September 1964) are compared. The flight W5 rates have been normalised to the flight F6 rate at 240 mb. The curves diverge from the point of normalisation but more rapidly for $z < 50$ mb, indicating an increased flux of low energy particles during flight W5. At 20 mb the normalised W5 rate is 13% greater than the F6 rate. The actual rates during flight W5 are also illustrated in figure 6.3, and it can be seen that the rate at 20 mb increased by about 25% between February 1963 and September 1964. It is obvious that solar modulation effects must be taken into account when comparing high altitude neutron data separated by even quite short intervals in time.

The counting rates (normalised at 240 mb) during Mildura flights M2 (February 1964) and M8 (April 1965) are also illustrated in figure 6.3. The altitude distribution has not changed significantly during this period.

While the time interval covered by the measurements is small, the results are at least qualitatively in keeping with the predictions of Lingenfelter (1963) that the altitude distribution, at mid and low latitudes, does not change much during the solar cycle.

6.2 Variation of counting rate with latitude.

Information on the global distribution of atmospheric neutrons was obtained in the measurements described in section 3.3. Some of these results are illustrated in figure 6.4, where the variation of counting rate is given, for various pressure levels, as a function of vertical cut-off rigidity. We use cut-off rigidity, rather than geomagnetic latitude, to facilitate comparisons with other measurements. The latitude parameter is not suitable for comparisons between data obtained at different longitudes.

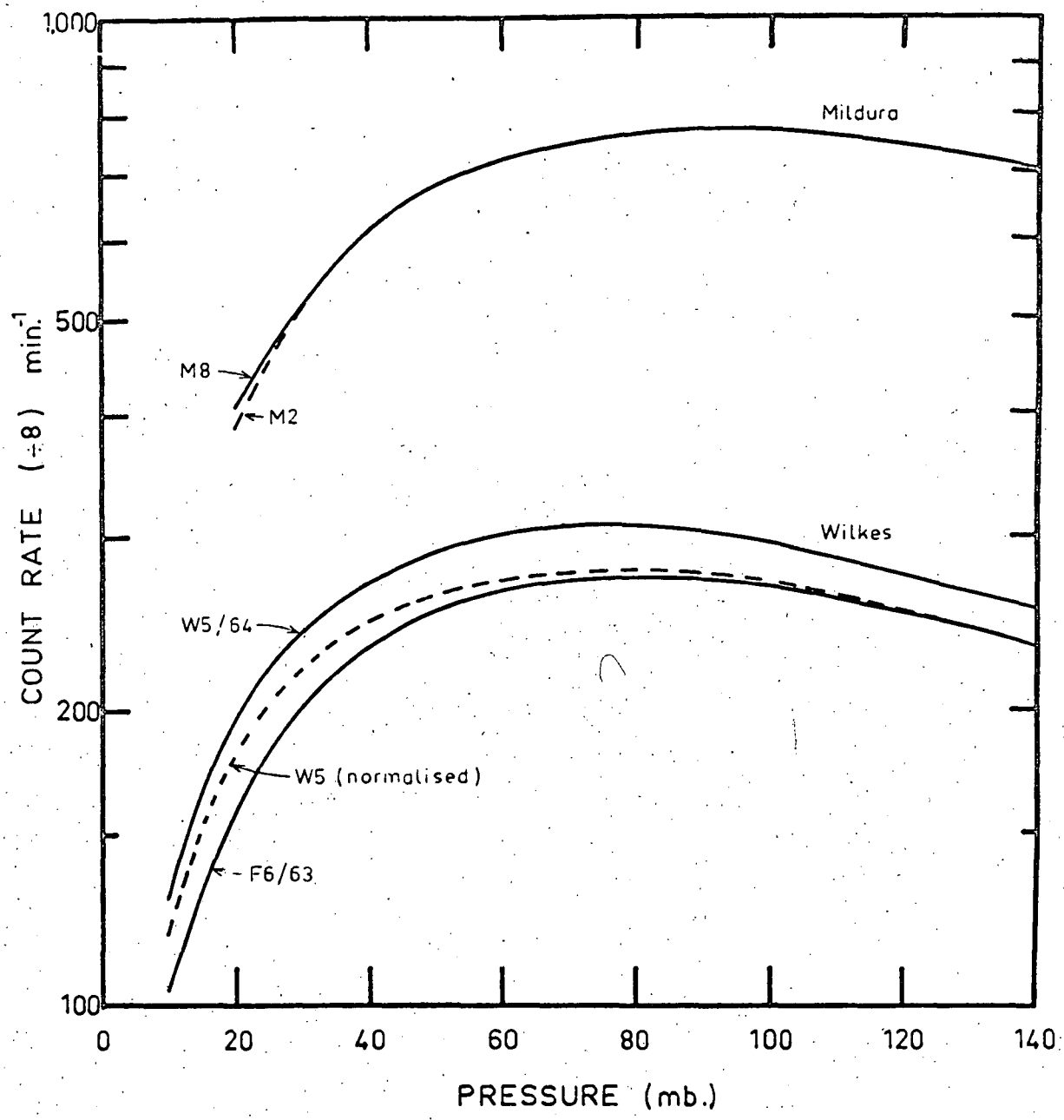

Fig. 6.3. Altitude dependence of the neutron counting rates at Wilkes and Mildura.

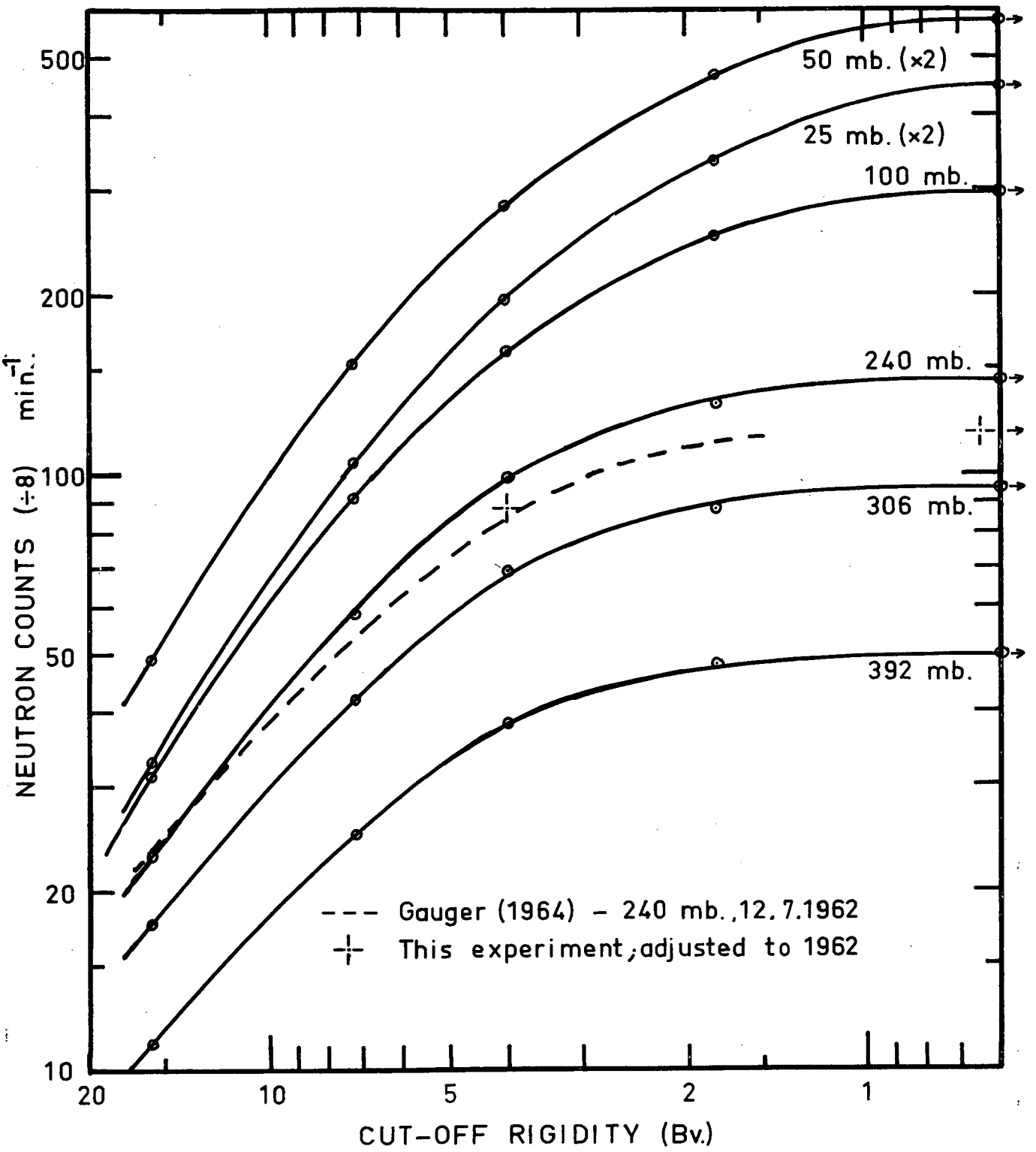

Fig. 6.4 Neutron counting rate distributions.

The results in figure 6.4 have not been corrected for background or local production effects. These corrections are relatively small (sections 4.3, 4.4) and would result, even at 25 mb, in only a few percent reduction in the counting rates and in the overall latitude variation.

Random errors in the results are very small because of the high counting rates of the detectors, and errors due to incorrect counter calibration amount to only 1 or 2%. Other errors arise from errors in pressure measurement and in the cut-off rigidity figures used. The pressure data are accurate to within about 1 mb at all levels in the atmosphere. We can estimate the effect of this on counting rate using the equation

$$\gamma = \frac{100}{R} \frac{dR}{dz} \qquad (6.2)$$

where γ is the percentage change in count rate R per unit pressure change. It varies from about 0.6% mb^{-1} in the equilibrium region of the atmosphere to about 2% mb^{-1} at 25 mb and 5% mb^{-1} at 10 - 15 mb.

No corrections have been made for changes in cut-off rigidity due to the drift of the balloon during flight. The effect of drift would be most pronounced at Mildura and Brisbane. Fortunately the upper atmosphere winds are mostly westerly at these stations and the balloons tend to drift along a line of constant geomagnetic latitude. Consequently, changes of cut-off rigidity are relatively small.

An interesting feature of figure 6.4 is the variation in the latitude distribution with altitude. Thus the ratio of the counting rate at Wilkes to that at Lae increases from 4.5 at 392 mb (400 $gm.cm^{-2}$) to 13.5 at 25 mb. The altitude dependence of this ratio, which we call the "total latitude variation", is illustrated in figure 6.5. The ratio increases monotonically to the highest altitudes reached (about 15 mb). Thus Hess et al (1961) were in error in assuming the latitude variation of the leakage flux to be similar to the variation at 306 mb.

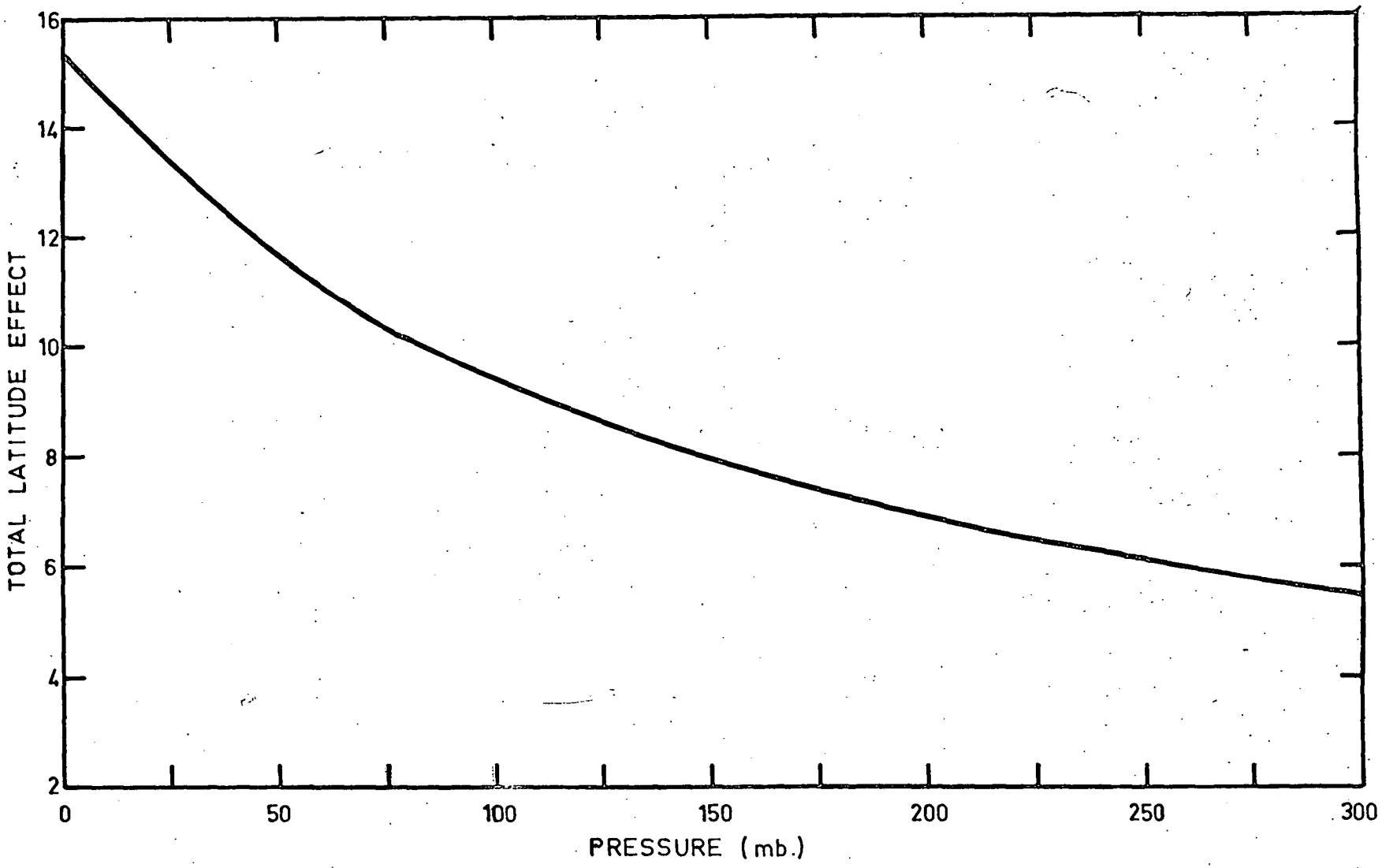

Fig. 6.5. Ratio of the neutron count rate at Wilkes, Antarctica to the rate at Lae, New Guinea.

6.3 Comparison with other measurements in the equilibrium region of the atmosphere.

The energy spectrum below 10 Mev is generally assumed to be independent of latitude, altitude and solar cycle phase in the equilibrium region of the atmosphere. Consequently, we may directly compare the spatial distributions in the counting rates of various detectors which respond to neutrons with energies in this range.

(i) Simpson (1951) and Meyer and Simpson (1955).

In figure 6.6 we compare the results of Simpson (1951) with our own measurements at 312 gm.cm^{-2} (30,000 ft). All curves have been normalised at $P_c = 0$. Simpson (1951) measured the latitude variation of the fast neutron flux with an aircraft borne BF_3 counter with a $1^{3/4}$ " paraffin moderator sheath surrounded by cadmium foil. The measurements in May-June 1948 near solar maximum, differ from ours by as much as 70%, indicating the very strong influence of solar modulation of galactic cosmic rays on the atmospheric neutron flux. The rate of change of counting rate with rigidity is less for Simpson's data than for our own at $P_c \lesssim 8$ BV, but greater for $P_c \gtrsim 8$ BV. This is surprising since we would expect the slope to be everywhere less for Simpson's data because of the harder primary rigidity spectrum at solar maximum. There is a substantial longitude effect in the region where Simpson's measurements were made, and it is possible that the differences arise from errors in the cut-off rigidities used in plotting his data.

The latitude effect on October 31st, 1949 is greatly increased as a consequence of lower solar activity, and Simpson's data differ from ours by less than 15%. However, the effects of solar modulation are still apparent since the "knee rigidity" (maximum rigidity for which the slope is zero) of 1.5 BV is significantly higher than the value (< 1 BV) for our data. The irregular changes of slope in the curve for

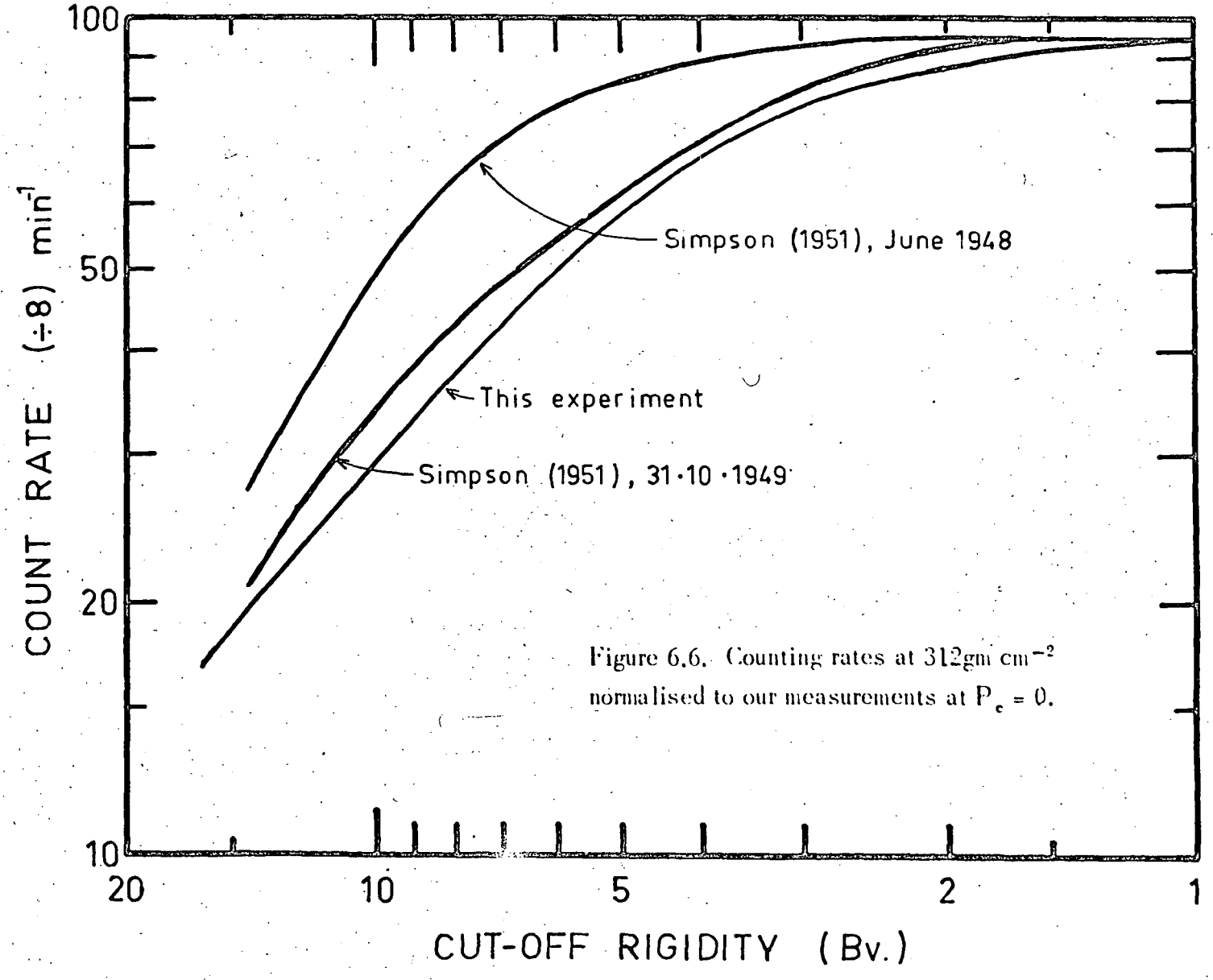

Figure 6.6. Counting rates at 312gm cm^{-2} normalised to our measurements at $P_c = 0$.

October, 1949 are probably caused by intensity variations during the period of measurement. The high latitude counting rate changed by more than 5% between October 27th and 31st, 1949 (Simpson 1951).

The measurements by Meyer and Simpson (1955), illustrated in figure 6.7, were made with an airborne neutron monitor in November, 1954 and cover the geomagnetic latitude range 40 - 65°N at 90°W geographic longitude. In spite of the very low level of solar activity in 1954 the latitude effect is everywhere less than for our own data or for Simpson's October, 1949 measurements. It would seem that neutron monitor data are not directly comparable with moderated BF_3 counter measurements because of the effects of diffusion on neutrons produced above the equilibrium region of the atmosphere. Many more neutrons are produced above the equilibrium region at high latitudes than at lower latitudes, and some of these diffuse down to the detector level. These neutrons will contribute to the counting rate of moderated BF_3 counters but not to the neutron monitor rate.

(ii) Soberman (1956).

Soberman (1956) measured the slow neutron density using unmoderated BF_3 counters in a series of balloon flights at λ = 10°, 55° and 88°N during the period 1952 - 1954. The latitude effect at 306 mb is about 25% less than for our data (illustrated by the three points, normalised at P_c = 0, in figure 6.7). The difference is partly due to the variation in solar activity during the time of the measurements. Soberman's flights at λ = 88°N were made in August, 1954 when the measurements at λ = 55° were made. If we adjust the rates to 1954 using the method described in section 6.1, (assuming the spectral response of the Mt.Wellington and Chicago neutron monitors to be identical) the overall latitude effect is increased by about 15% and is in satisfactory agreement with our own measurements.

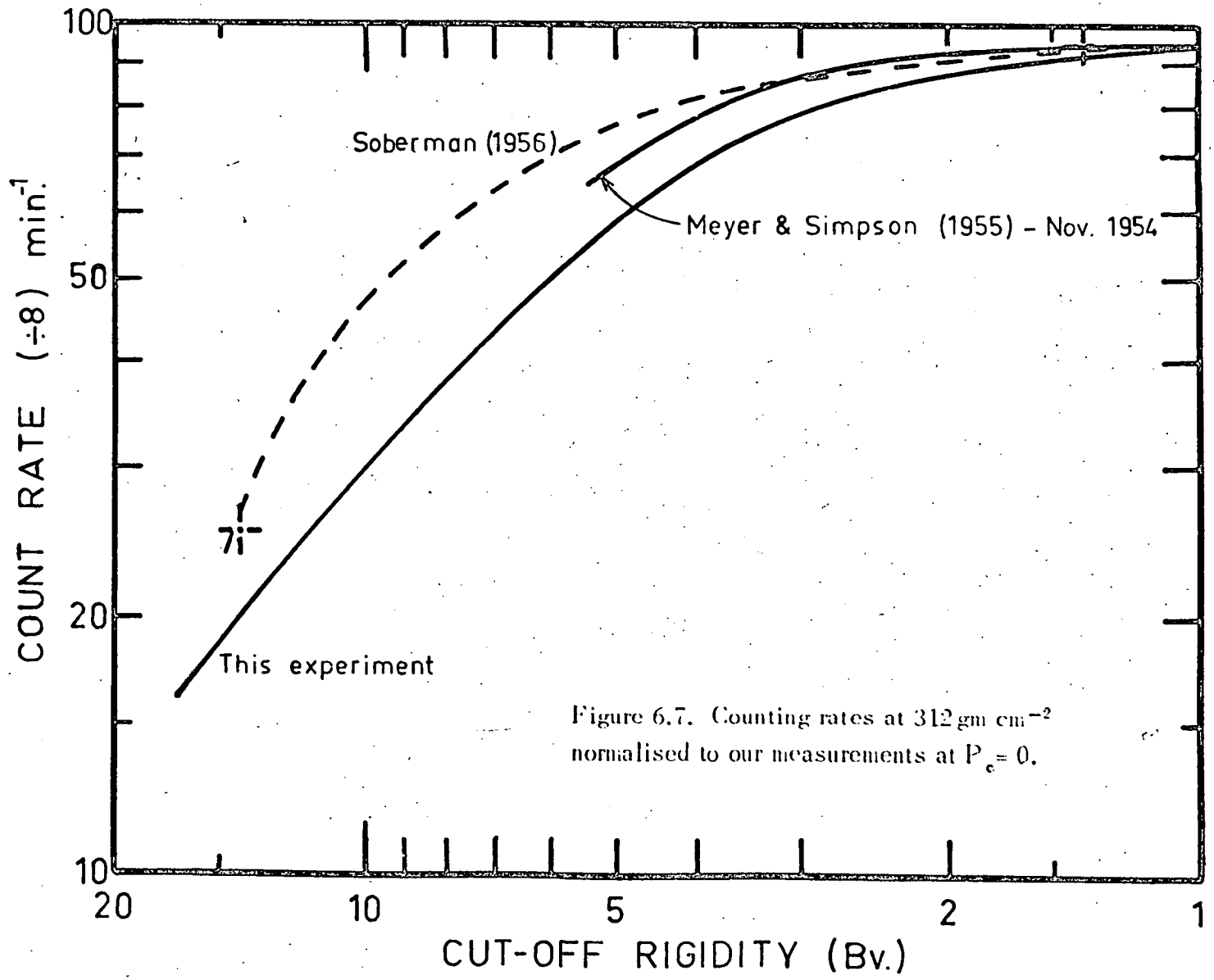

Figure 6.7. Counting rates at 312 gm cm^{-2} normalised to our measurements at $P_c = 0$.

Soberman (1956) used the measurements described above, in conjunction with data on the latitude variation of the absorption length (Simpson 1951, Staker 1950, Staker et al 1951, Yuan 1951) and the latitude variation of the neutron flux at 306 mb, as measured by Simpson (1951) in 1948, to estimate a series of curves for the slow neutron density as a function of altitude and latitude. The latitude variation at 306 mb is illustrated in figure 6.7. It is identical with Simpson's 1948 data (figure 6.6) which, as we have already seen, differs from our own data by up to 70%. These discrepancies would appear to be largely a consequence of Soberman's use of solar maximum (1948) data to determine the latitude variation.

(iii) Gauger 1964.

Gauger (1964) has measured the latitude dependence of the neutron flux at 245 gm.cm^{-2} (240 mb) during two aircraft flights on July 12th and 21st, 1962. These measurements were made using a BF_3 counter with a 2 inch paraffin moderator sheath surrounded by a thin cadmium shield. Because of the difference in energy sensitivity between our counters and Gauger's it is not possible to make a comparison of the absolute flux. We have instead normalised Gauger's counting rate to ours at a vertical cut-off rigidity of 15 BV. We have estimated the cut-off rigidity for Gauger's data by converting from the given geomagnetic latitude to geographic co-ordinates with the aid of the published flight path. The vertical cut-off rigidity figures were then determined using the tables of Quenby and Wenk (1962). The results are illustrated in figure 6.8.

The rate of change of count rate with P_c for Gauger's July 12th data is everywhere less than for our data, with greatest divergence at low rigidities. The overall latitude effect is about 15 - 20% less than for our measurements. It seems very likely that the difference is a consequence of the

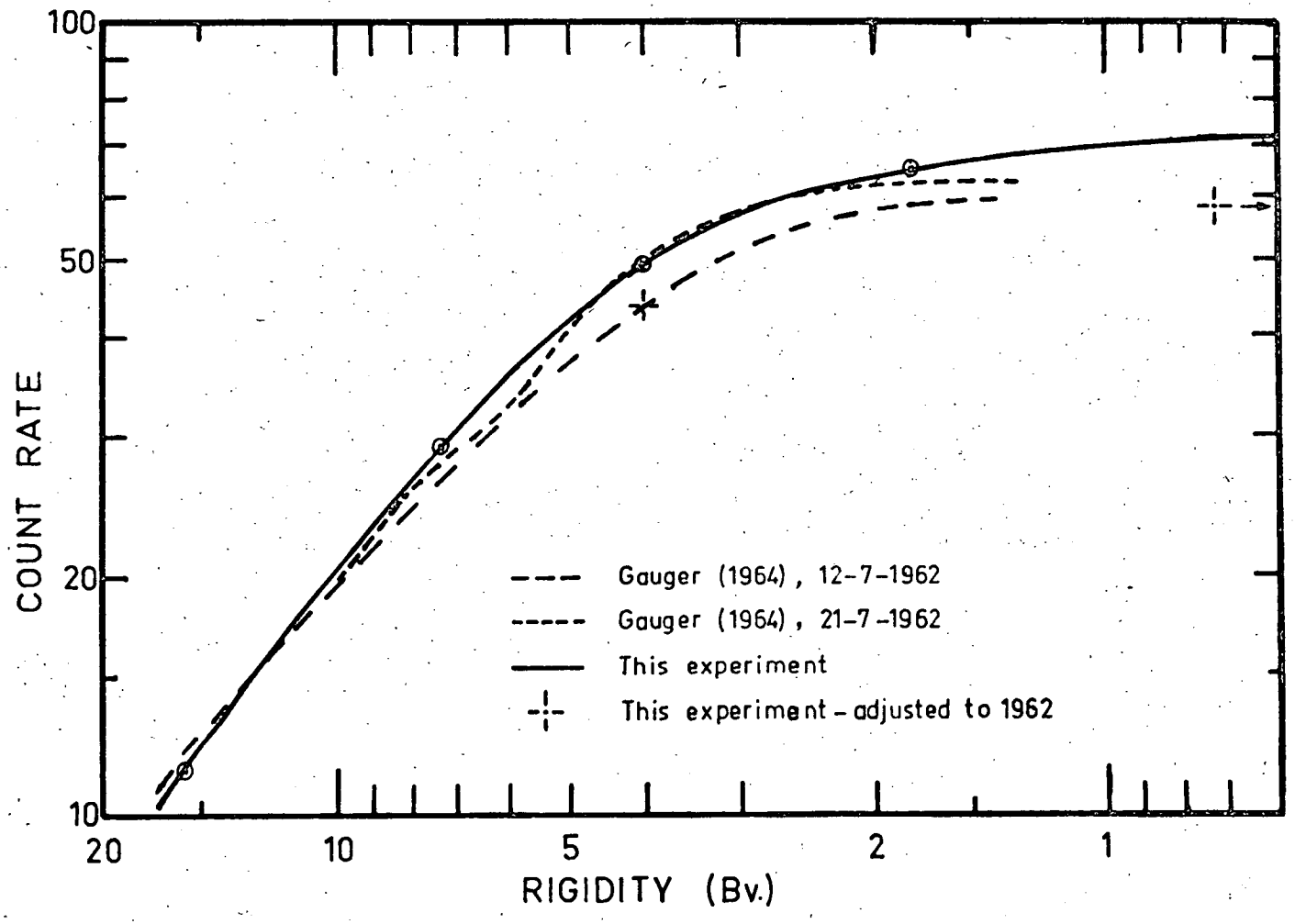

Fig. 6.8. Neutron flux distributions at 245 gm cm^{-2}. The results of Gauger (1964) have been normalised to this experiment at P_c = 15 Bv.

harder primary spectrum at the time of Gauger's measurements. We have estimated the counting rate at Wilkes and Mildura for July, 1962 from the Mt.Wellington neutron monitor rate using the factors derived in section 6.1. The Mt.Wellington monitor rate was 5.2% below the level in September, 1964. Consequently the counting rate at 245 gm.cm^{-2} would be ~11% lower at Mildura and ~17% lower at Wilkes in July, 1962. These two points lie close (figure 6.8) to the line of best fit to Gauger's data, thus confirming our belief that the difference in the two sets of data is largely a consequence of the softening of the primary spectrum since July, 1962.

Gauger's data from the flight of July 21st, 1962 are more variable and parallel our own measurements in the 3 - 5 BV rigidity interval, although the overall latitude effect is about the same as for July 12th. The good agreement between our measurements and Gauger's for July 12th, 1962 suggests that Gauger's July 21st data were abnormal. The cause of the increased counting rate on this flight remains unexplained (Gauger 1964).

6.4 Altitude distributions.

(i) Absorption length.

It is obvious from the atmospheric absorption curves (figures 3.1, 3.2 and 3.3) that the frequently assumed linear relation between the logarithm of the neutron flux and atmospheric depth is valid over only a very limited region of the atmosphere. This is particularly apparent in the Mildura, Brisbane and Lae flight data where the linear relation is restricted to atmospheric depths between about 250 and 450 gm.cm^{-2}.

A similar effect was noted by Simpson and Fagot (1953) in a series of measurements of absorption length for moderated BF_3 counters at $\lambda = 0^\circ$, 41° and 52°N. In the 200 - 300 gm.cm^{-2} region the absorption length $L(z,\lambda)$ decreased from 212 gm.cm^{-2} at the equator to 160 gm.cm^{-2} at $\lambda = 52^\circ$. At $z > 600$ gm.cm^{-2}

the value of L was independent of latitude and altitude and equal to about 140 gm.cm^{-2}. They suggest that the variation of L with z is due to the development of the nucleon cascade in the atmosphere. The average nucleon energy is degraded by collisions, nuclear disintegrations and ionisation as the cascade spreads down through the atmosphere. The effective absorption length decreases with nucleon energy because of the energy sensitivity of the secondary particle cross-sections (Rossi 1952).

In figure 6.9 the dependence of absorption length on cut-off rigidity is illustrated for the region between 312 and 500 gm.cm^{-2}. These results are in satisfactory agreement with the results of Simpson and Fagot (1963). Also illustrated is the rigidity dependence of the absorption length between 200 and 312 gm.cm^{-2} and the effective absorption length between 200 and 1033 gm.cm^{-2} used by Lingenfelter (1963). The increase in L with decreasing atmospheric depth is very marked at high rigidities, illustrating the need for care in the use of this parameter.

If L decreases with increasing z because of a degrading of the average nucleon energy as suggested above, it must also be a function of the mean energy of the primary cosmic rays. Consequently it would be expected to decrease as solar activity decreases towards solar minimum. Measurements by Roederer et al (1964) indicate that the atmospheric absorption length, for balloon borne geiger counters, changes with latitude in much the same manner as that for the nucleonic component. It might therefore be expected to change during the solar cycle, and Edwards (1964) has found evidence for such a variation. He analysed the results of balloon borne geiger counter flights from Hobart and found that the absorption length between 200 and 600 gm.cm^{-2} decreased from 168 gm.cm^{-2} in 1959 to 163 gm.cm^{-2} in 1962.

Recent analyses (Phillips 1962, La Pointe and Rose 1962, Kamphouse 1963, Bachelet et al 1964, Forman 1965) of

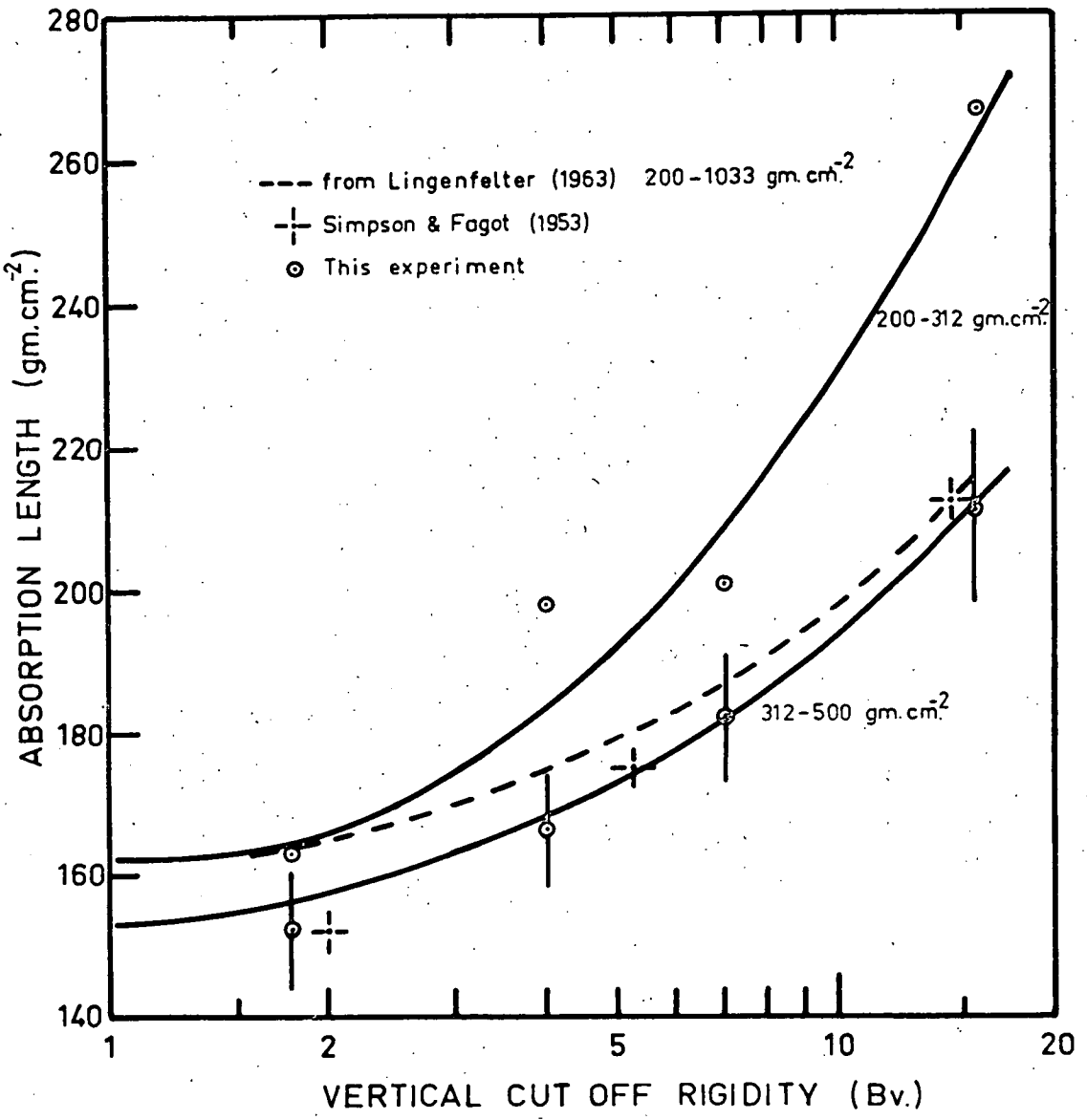

Fig. 6.9 The effective attenuation length of the cosmic-ray neutron intensity.

neutron monitor data give conflicting evidence on time variations in the absorption length of the nucleonic component at sea level. There is no obvious reason, however, why a zero or very small time variation at sea level should be inconsistent with a significant effect in the 250 - 500 mb region.

The absorption length between 250 and 500 mb has been estimated for a number of flights from Wilkes and Macquarie Island, covering the period December, 1961 to October 1964. The results were obtained using a method of computation devised by Dr.N.R.Parsons. This gives a least squares fit using a simple exponential expression, but the significance of each data point, in the analysis, is weighted according to the statistical significance of the point. The method also gives the 95% confidence limits on the value of the absorption length obtained. The calculations were performed using the Elliot 503 electronic computer in this University. The results are listed in table 6.2 and illustrated as a function of the daily mean Mt.Wellington neutron monitor rate in figure 6.10. The error tails in the diagram give the standard deviation.

There appears to be a trend towards smaller values of L with decreasing solar activity. Thus, the mean value of L at Macquarie Island decreased from 157.9 $\pm$ 3.9 mb (95% confidence limits) in early 1962 to 149.0 $\pm$ 2.5 mb in 1964. Although the energy sensitivity of the detectors used in 1962 was different (section 3.2) from those used in the other flights, it is very unlikely that this had any effect on the absorption length.

A notable feature of the results is the variability of the values of L obtained in the flights from Macquarie Island. This is much greater than would be expected on a statistical basis. Instrumental effects seem unlikely. The efficiency of moderated BF_3 counters is known to be temperature sensitive (Fenton and Fenton 1965) but the magnitude of this

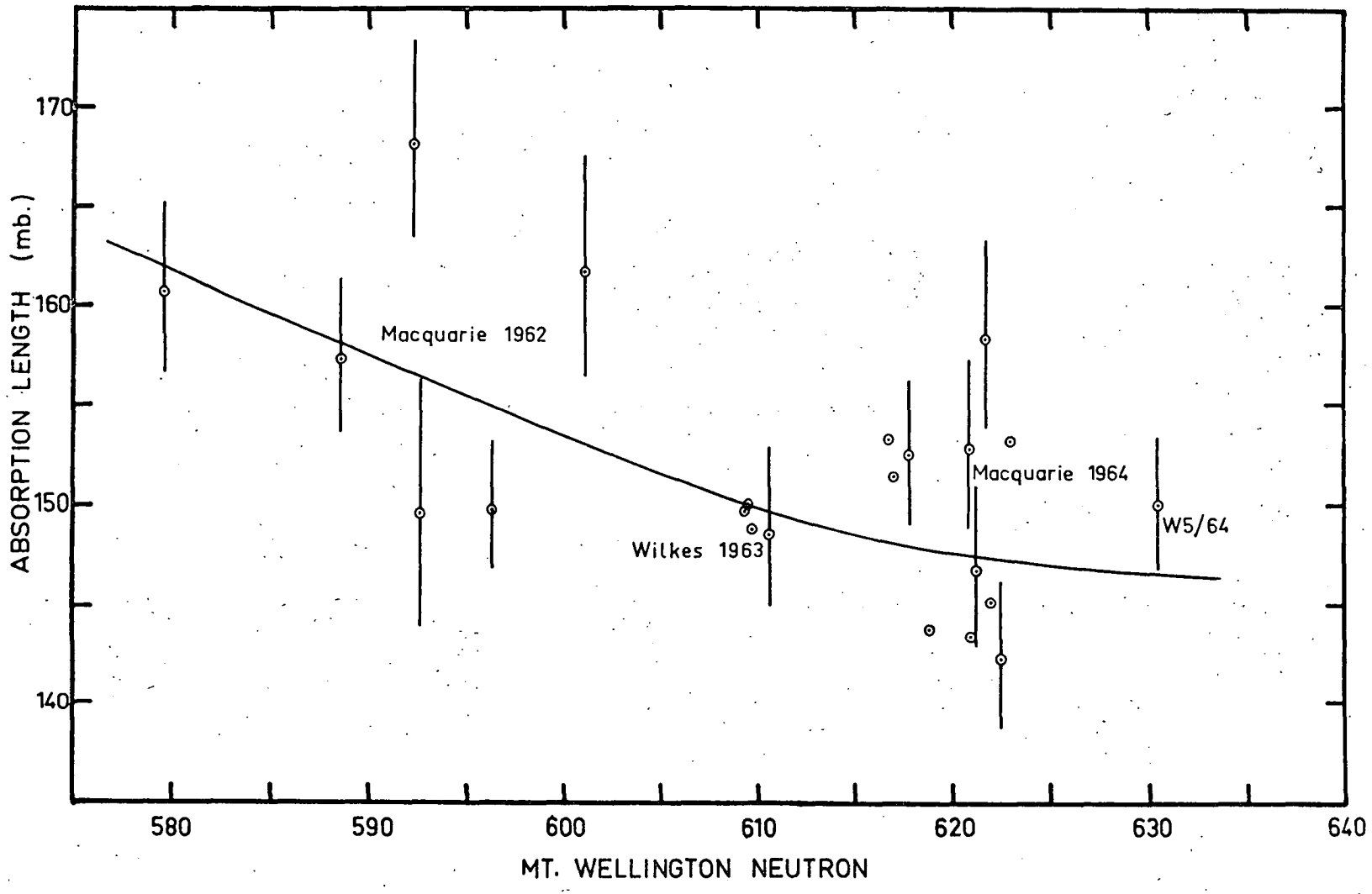

Fig. 6.10. Counting rate absorption length between 250 and 500 gm cm^{-2} during flights from Wilkes, Antarctica and Macquarie Island.

Station	Flight	Date	Mt.Wellington neutron rate	Absorption length (mb) L	$+\Delta L$	$-\Delta L$
Macquarie	1	21/12/61	592.6	149.6	13.5	11.4
1961-62	7	13/1/62	596.3	161.6	12.0	10.5
	9	23/1/62	601.1	149.8	6.7	6.1
	12	12/2/62	592.3	168.1	10.6	9.4
	14	15/2/62	588.5	157.3	8.2	7.4
	21	6/3/62	579.6	160.7	9.1	8.2
Wilkes	5	29/1/63	609.5	149.9	6.9	6.3
1963	6	5/2/63	609.7	148.8	5.1	4.8
	9	16/2/63	609.3	149.6	7.9	7.1
	10	22/2/63	610.6	148.5	8.8	7.9
Macquarie	1	5/1/64	615.3	152.5	7.5	6.9
1964	3	12/1/64	621.2	146.7	8.6	7.7
	5	16/1/64	623.0	153.2	10.1	8.9
	6	18/1/64	621.7	158.3	9.9	8.9
	7	27/1/64	621.9	145.1	6.8	6.2
	8	29/1/64	617.1	151.4	7.6	6.9
	10	31/1/64	616.8	153.3	7.4	6.7
	15	13/2/64	622.4	142.3	7.8	7.0
	21	2/3/64	620.9	143.3	9.5	8.4
	26	9/3/64	618.8	143.7	7.9	7.1
Wilkes	2	2/3/64	620.9	152.8	8.9	7.9
1964	5	20/9/64	630.5	150.0	7.0	6.4

Table 6.2: Absorption length L of the neutron flux between 250 and 500 mb. $\pm \Delta L$ are the 95% confidence limits.

effect is much too small to account for the observed variation. The temperature of the air in the instrument package was measured during the Macquarie 1962 and Wilkes 1963 flights, but there is no correlation between the absorption length and this temperature. There is a similar lack of correlation between L and the relative efficiency of the counters as given by the calibration rate.

The origin of the variability of the Macquarie Island results (figure 6.10) is not known. It is not reduced by plotting L against the Mt.Wellington neutron rate, averaged over the three hours of the balloon ascent, rather than over the day of the flight. Nor is there any significant correlation between L and the planetary magnetic index K_p.

These results cover only a small portion of a solar cycle, and further measurements near solar maximum are needed before any firm conclusions can be drawn.

(ii) The upper atmosphere.

In order to compare the latitude dependence of the altitude distribution, we have normalised the data from all latitude survey flights (section 3.3) at 240 mb. The results are illustrated in figure 6.11. The high latitude distributions are much steeper, above the transition maximum, than are the low latitude distributions. The altitude of the transition maximum varies with cut-off rigidity from 80 mb at Wilkes ($P_c = 0$) to 120 mb at Lae ($P_c = 15.8$ BV). This rigidity dependence is a consequence of the change in the mean energy of the primaries, and is in agreement with the observations of Soberman (1956).

Differences between the neutron flux at Macquarie Island and Wilkes are small, and it is necessary to use results from simultaneous flights in order to avoid differences due to time variations. The rapidity with which the flux, at high altitudes, can change is illustrated (table 6.3) by the difference ($\sim 8\%$) between the counting rates at 20 mb during flights

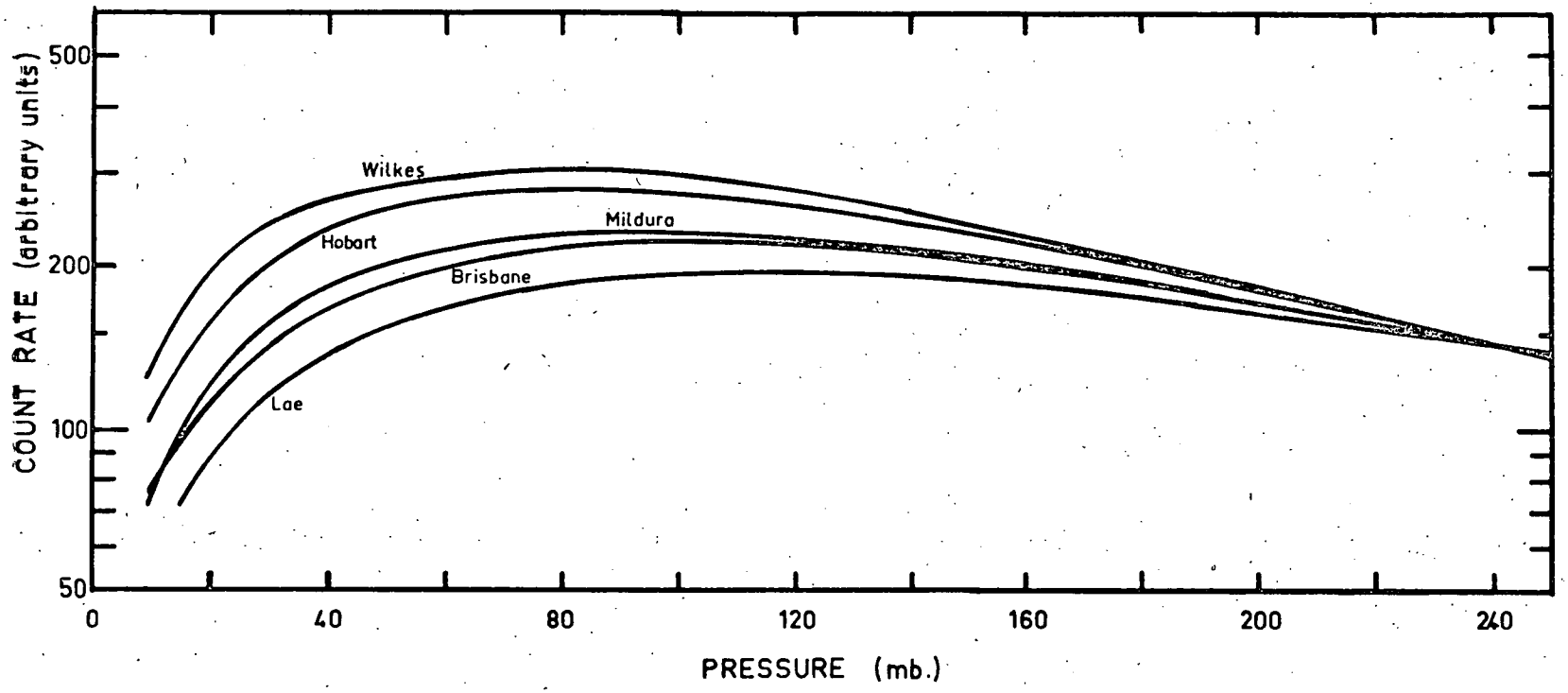

Fig. 6.11. The altitude dependence of the neutron count rate during the latitude survey measurements (August-October 1964). The rates are normalized at 240 mb.

MQ7 and MQ10 at the end of January, 1964 and during flight MQ26 early in March, 1964.

Flight	Date	R_{cal}	Pressure (mb)						
			200	150	100	50	25	20	15
MQ7	27/1/64	131.3	174	230	271	248	187	158	129
MQ10	31/1/64	112.3	175	228	272	250	187	159	132
W2/64	2/3/64	103.3	175	229	272	274	204	184	163
MQ21	2/3/64	124.8	180	233	274	267	187	167	142
MQ26	9/3/64	123.6	175	229	272	268	193	172	-

Table 6.3: Smoothed curve counting rates ($\div$ 8 min^{-1}) during flights from Wilkes and Macquarie Island early in 1964.

The altitude distributions at Wilkes and Macquarie Island were measured in the simultaneous flights W2/64 and MQ21 on March 3rd, 1964. Details of the smoothed curve counting rates during these flights, and during flight MQ26 on March 9th, 1964, are given in table 6.3. The rates at 100 - 200 mb (and deeper in the atmosphere) are essentially the same but at higher altitudes the results diverge. At 20 mb the counting rate during W2 is about 9% greater than at the same level in flights MQ21 and MQ26. The difference is even greater at 15 mb.

The efficiency of the counters used in these measurements was affected by the use (inadvertent) of a polyvinyl chloride (P.V.C.) wrapping material in the counter assembly. The P.V.C. contains chlorine which has a large (31.6 barns) cross-section for thermal neutron capture. Consequently, the efficiency and energy response of the counters varied from one unit to another, depending on the amount of P.V.C. used in the assembly. Comparison of the results obtained with a number of these counters indicates, however, that this variability has little effect on the

counting rates (when normalised to the standard detector efficiency) or altitude distribution. This is illustrated by the similarity of the results during flights MQ7 (R_{cal} = 131.3) and MQ10 (R_{cal} = 112.3), given in table 6.3. The rates of very low efficiency counters tend to be reduced by a few per cent, but the altitude dependence does not appear to be significantly affected.

It seems likely, therefore, that the difference between the Wilkes and Macquarie data is genuine. The excess counting rate could be due either to an increase in the ionising event background in our counters at high altitudes over Wilkes, or to an increased neutron flux generated by cosmic rays with rigidities below the cut-off for Macquarie Island.

The altitude dependence of the counting rate excess appears to favour the first hypothesis rather than the second. (Compare, for example, the results in table 6.3 with the theoretical altitude dependence in figure 5.9 of the counting rate due to neutrons generated by low energy primaries.) We have little information on the background in our counters at high altitudes, but a very substantial increase, relative to the rate given in section 4.3, is required to account for the observations. The geiger counter data for flights W2/64 and MQ21 have not as yet been analysed, but they should throw more light on this problem.

The alternative hypothesis also requires more investigation. The magnitude of the low energy primary flux required depends on the energy distribution and on the value of the cut-off rigidity at Macquarie Island. Preliminary estimates using a cut-off rigidity of 370 MV (Quenby and Wenk 1962) give a flux which is several orders of magnitude larger than that reported for this period by McDonald and Ludwig (1964). The discrepancy would be much smaller if the cut-off rigidity is 550 MV, as estimated by McCracken et al (1964).

(iii) Comparison with theoretical results.

In order to compare the altitude dependence of our data with the neutron flux distribution calculated by Newkirk (1963), we make use of the equation

$$R(z) = \int_0^\infty \phi(z,E)\ \eta(E)\ dE \qquad (6.3)$$

where $\phi(z,E)$ is the neutron energy spectrum given by Newkirk (1963), as described in section 1.12 and R(z) is the detector counting rate as a function of atmospheric depth, and $\eta(E)$ is the detector sensitivity function. Owing to the uncertainty as to the shape of this function we have used the very dis-similar $\eta_2(E)$, $\eta_3(E)$ and $\eta_6(E)$ curves (described in section 4.2). The counting rate at various altitudes has been estimated for both curves, and the results, normalised at 250 gm.cm^{-2}, are given in table 6.4.

Detector response curve	Atmospheric depth (gm.cm^{-2})						
	250	200	100	50	20	10	0
$\eta_2(E)$	138	194	318	303	216	138	42.1
$\eta_3(E)$	138	197	317	299	188	121	29.9
$\eta_6(E)$	138	198	318	294	182	114.5	25.5

Table 6.4: Estimated neutron detector count rate (arbitrary units) for $\eta_2(E)$, $\eta_3(E)$ and $\eta_6(E)$ counter response curves using the neutron flux distribution calculated by Newkirk (1963).

In the previous section we noted that the neutron flux altitude distribution is strongly dependent on the geomagnetic cut-off. Consequently, we cannot directly compare any of our ascent curves with Newkirk's results which are for $\lambda = 57^\circ$N (P_c = 1.2 BV). We have therefore estimated the altitude dependence for our counters at this cut-off rigidity from the curves of count rate vs rigidity in figure 6.4. The

theoretical count rates in table 6.4 are normalised to this data at 250 gm.cm^{-2}, and the four curves are compared in figure 6.12. The experimental results have been corrected for local production and background effects.

The theoretical count rates are virtually identical for the three counter response functions at atmospheric depths greater than about 50 gm.cm^{-2}, but at higher altitudes the $\eta_2(E)$ results lie consistently above the others. The $\eta_3(E)$ and $\eta_6(E)$ results are very similar, and differ by less than 5% at all depths greater than about 10 gm.cm^{-2}. Since the altitude dependence is not very sensitive to the details of the counter response, the $\eta_3(E)$ and $\eta_6(E)$ curves would appear to be satisfactory approximations to the response of our counters.

The altitude dependence given by Newkirk is in good agreement with our measurements for $250 < z < 500$ gm.cm^{-2}, but,at higher altitudes, the rates estimated from Newkirk's data are greater than the measured rates. The curves diverge from the point of normalisation (250 gm.cm^{-2}) to a constant difference of 12 - 15% for $z \lesssim 120$ gm.cm^{-2}. At higher altitudes the experimental and theoretical curves are parallel within the limits of error. Thus Newkirk's altitude dependence is identical with our measurements for all $z > 15$ gm.cm^{-2} except in the region between 120 and 250 gm.cm^{-2}.

A similar divergence is observed between the measurements of Smith et al (1962) and the rates calculated for the detectors of Smith et al by Newkirk. This is illustrated in Newkirk's figure 2 and it can be shown that if the two curves are normalised at 250 gm.cm^{-2}, the discrepancy at $z < 100$ gm.cm^{-2} is between 20 and 30%. This somewhat larger discrepancy could be due to the time difference between our measurements and those of Smith et al. The altitude dependence given by Newkirk (1963) appears to be more closely related to the distribution at solar minimum, rather than at the time of the measurements to which his data are normalised.

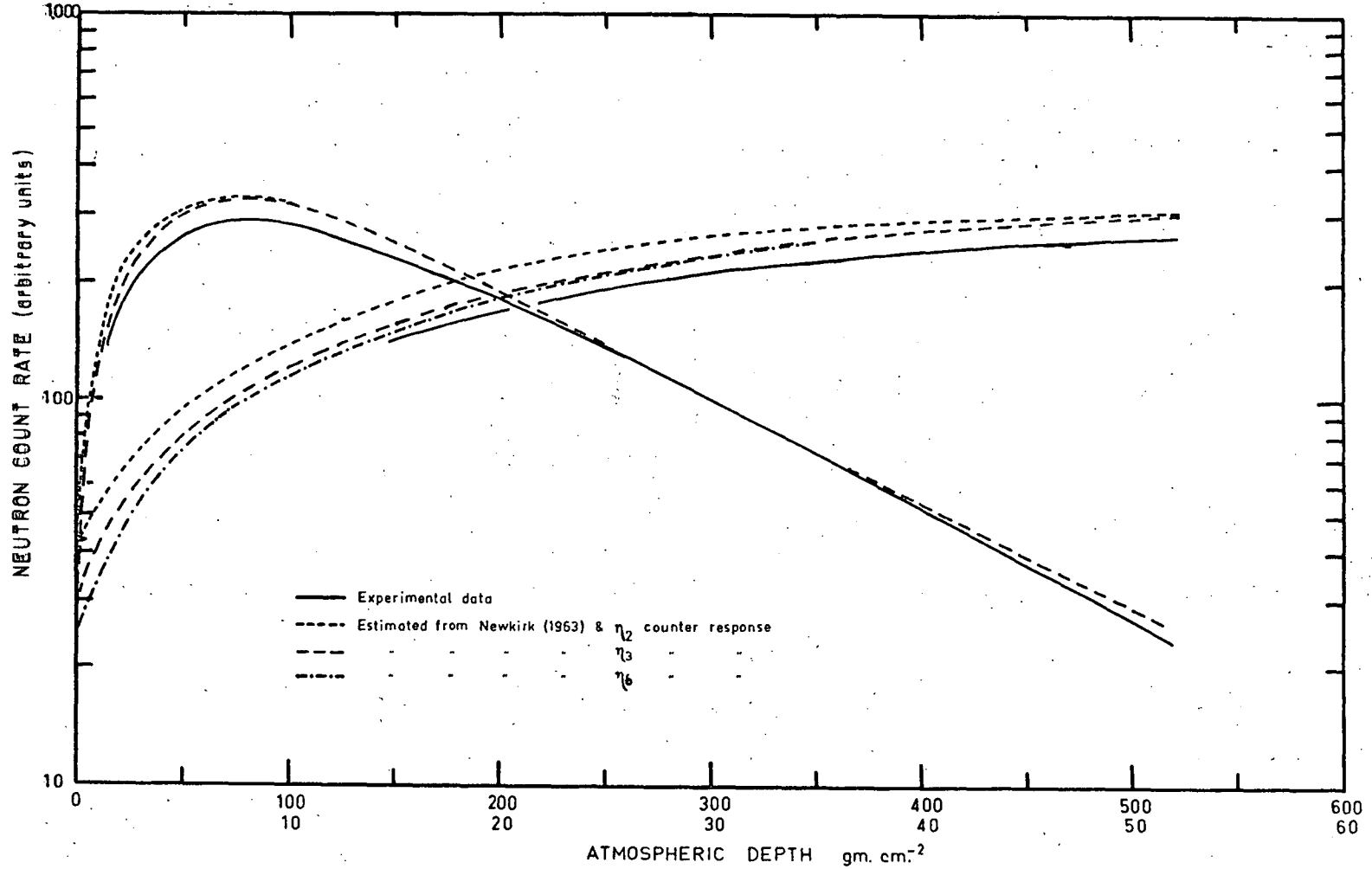

Fig. 6.12. The altitude dependence of the neutron count rate at P_c = 1.2 Bv. The experimental data was estimated from figure 6.4.

It seems probable that the neutron production altitude distribution used by Newkirk is too steep in the region $100 < z < 250$ gm.cm^{-2}. This distribution S(z) is exponential with an absorption length L of 160 gm.cm^{-2} for atmospheric depths between about 120 and 600 gm.cm^{-2}. Measurements by Simpson and Fagot (1953) and Meyer and Simpson (1955) show that the neutron production rate in lead does not have a simple exponential distribution with z at altitudes above 250 gm.cm^{-2}. They found that L increases with increasing altitude. A slight flattening of S(z) in this region could probably account for the observed divergence between our measurements and Newkirk's theory.

Boella et al (1965) determined the altitude dependence of the neutron flux, measured with boron plastic scintillators, in flights in northern Italy and in New Mexico at P_c = 4.6 BV during 1963. They report good agreement between Newkirk's theory and their results for detectors with 1", 2" and 4" of polyethylene moderator. This is somewhat surprising, since it is obvious from figure 6.11 that the altitude dependence at P_c = 4.6 BV must be significantly different from that for P_c = 1.2 BV (the cut-off rigidity for Newkirk's results). We have already obtained experimental confirmation of Newkirk's results at P_c = 1.2 BV. The reported agreement (Boella et al 1965) probably arises from the experimental uncertainty and the fact that the data were normalised at 100 gm.cm^{-2}. Normalisation at this level tends to minimise the differences between the two curves.

In section 1.13 we noted that the results of Hess et al (1961), for the neutron flux at depths less than 200 gm. cm^{-2}, are in conflict with the calculations of Newkirk (1963) and Lingenfelter (1963), and also with several recent measurements. Newkirk noted that his calculations gave a flux at 40 gm.cm^{-2} which was only a third of that estimated by Hess et al, and that the difference was largely due to the much steeper altitude dependence given by Hess et al. It is obvious, in view of the relatively good agreement between our results and

those of Newkirk, that our data do not support the calculations of Hess et al (1961).

6.5 Conclusions.

(i) The neutron flux at high altitudes in polar regions is strongly dependent on solar activity. Thus the counting rate of our detectors, at 20 mb over Wilkes, increased by about 25% between February, 1963 and September, 1964. This increase is 6.4 times as large as the corresponding increase in the rate of the Mt.Wellington neutron monitor. The temporal dependence of the counting rate is reduced at lower latitudes, and at Mildura (P_c = 4 BV) the fractional increase in counting rate at 20 mb was only 2.9 times the corresponding increase in the Mt.Wellington rate.

The altitude dependence of the counting rate is strongly dependent on solar activity at Wilkes, but no significant change was observed at Mildura between February, 1964 and April, 1965.

(ii) The latitude distribution at 306 mb is in agreement, within errors, with the measurements of Soberman (1956) and Gauger (1964), after correcting for the difference in solar activity at the times of these measurements.

The large changes in the latitude distributions during the solar cycle are illustrated by the difference between our results and those of Simpson (1951) for solar maximum in 1948. The total latitude variation between 0 and 15 BV at 306 mb was 3.8 : 1 in 1948, and 5.1 : 1 in 1964.

The slow neutron latitude and altitude distribution curves, given by Soberman (1956), differ from our results by as much as 70% when both are normalised at P_c = 0.

(iii) The difference between our measurements and airborne neutron monitor data at 306 mb in 1954 (Meyer and Simpson 1955) suggests that counter and neutron monitor data

are not directly comparable at this level. It is suggested that the difference is a consequence of diffusion of low energy neutrons from higher altitudes.

(iv) The "total latitude variation" of the neutron flux increases with altitude to the highest levels reached (about 15 mb). Expressed as the ratio of the count rate at Wilkes to that at Lae, the latitude variation was 5.4 : 1 at 306 mb and 14 : 1 at 15 mb. The atmospheric depth of the transition maximum increases from 80 gm.cm^{-2} at Wilkes to about 120 gm. cm^{-2} at Lae.

(v) The absorption length L of the neutron flux is a strong function of atmospheric depth, especially at low latitudes. Thus at Lae it increases from 210 gm.cm^{-2} between 312 and 500 gm.cm^{-2}, and 255 gm.cm^{-2} between 200 and 312 gm. cm^{-2}. The rigidity dependence of L is in satisfactory agreement with the results of Simpson and Fagot (1953).

The absorption length at high latitudes has been measured in 22 flights at Wilkes and Macquarie Island, between December, 1961 and October, 1964. There appears to be a trend towards smaller values of L with decreasing solar activity. This effect is partly obscured by day to day variations in the value of L at Macquarie Island, which are not related to the rate of the Mt.Wellington neutron monitor. The origin of these variations is not known.

(vi) Comparison of the altitude dependence at Wilkes and Macquarie Island indicates a significant flux of primaries with insufficient energy to influence the neutron count rate at depths greater than about 100 gm.cm^{-2}. Preliminary estimates suggest that the cut-off rigidity at Macquarie Island is considerably greater than the value of 370 MV given by Quenby and Wenk (1962), if our results are to be compatible with the measurements of the low energy primary spectrum by McDonald and Ludwig (1964). A more detailed analysis of these results seems

desirable.

(vii) The altitude dependence of the counting rate for our counters at P_c = 1.2 BV has been calculated, using the data of Newkirk (1963). The results are in good agreement with our measurements, except for a slight (about 12%) difference in the region between 120 and 250 gm.cm^{-2}. The altitude distribution given by Newkirk is more appropriate to solar minimum conditions than to the time (1961) of the measurements to which the data were normalised. The reported agreement between Newkirk's results and those of Boella et al (1965) is not supported by our measurements. Our results do not support the neutron flux altitude dependence given by Hess et al (1961).

VII NEUTRON LEAKAGE FLUX

7.1 Introduction.

In section 1.15 we discussed the present state of knowledge of the atmospheric neutron leakage flux. It is of interest to see if our measufements can throw any light on the present rather confused situation.

Balloon borne detectors cannot, of course, directly measure the leakage flux, and it is necessary to estimate this flux by extrapolating the counting rate curve to the top of the atmosphere. This method has been used by Boella et al (1965) to estimate the neutron albedo at 4.6 BV cut-off rigidity. There is considerable uncertainty, however, in the shape of this curve in the top few gms.cm^{-2} of the atmosphere. We have shown in section 1.9 that the neutron flux distribution in a moderating medium decreases rapidly near the boundary with a vacuum. The rapidly changing slope of the flux distribution curve makes extrapolation uncertain in this region. Some neutrons are produced in the boundary region, and this will modify the effect described above. However, we have noted in section 1.10 (i) that for a neutron source evenly distributed through the atmosphere (a condition reasonably well satisfied in the top 100 gm.cm^{-2} of the atmosphere), the majority of neutrons in the boundary region come from depths greater than 40 gm.cm^{-2}. Consequently, local production (i.e. production in the first few grams of the atmosphere) will have little effect on the flux distribution in this region.

The variation of the neutron flux in the boundary region has been measured by Bame et al (1963), using moderated BF_3 counters and LiI scintillators in rocket flights to 650 Km. The flux distribution near the boundary (figure 7.1) is in qualitative agreement with the predictions of transport theory (figure 1.4) and illustrates the difficulty of estimating the leakage flux by extrapolation from balloon altitudes.

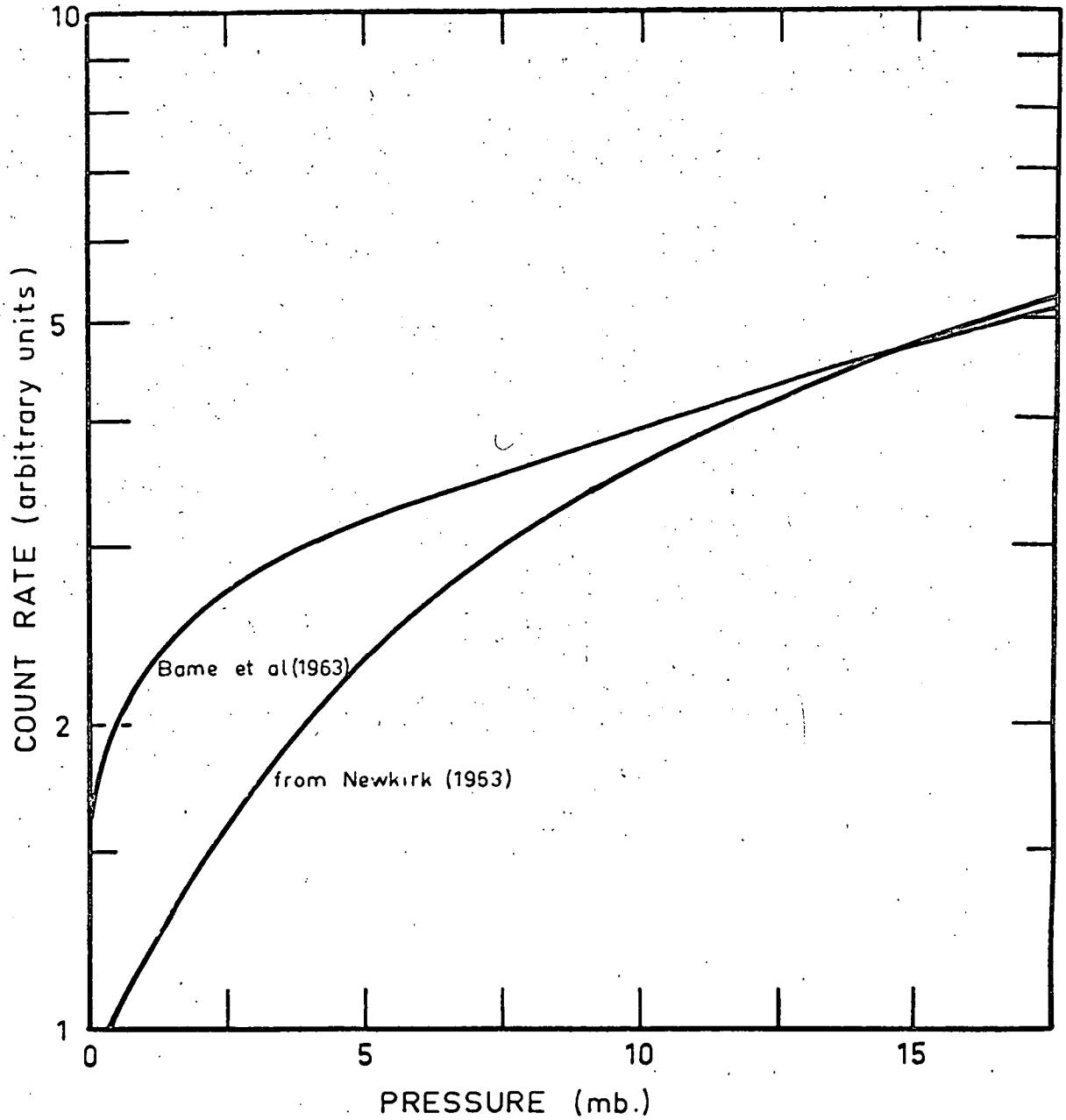

Fig. 7.1. Counting rate distributions near the top of the atmosphere.

7.2 Estimation of the leakage flux at P_c = 1.2 BV.

The main problem in interpretation of our measurements lies in the uncertainty as to the absolute efficiency of the neutron detector system. We may estimate the flux at 15 gm. cm^{-2} using the observed count rates and the efficiency data given in section 4.2. The leakage flux at P_c = 1.2 BV can then be obtained by extrapolation, using a curve parallel to the altitude dependence curve estimated (section 6.4 (iii)), for our detectors, from the data of Newkirk (1963). This method is, however, equivalent to using the leakage flux given by Newkirk (1963) with a 30% time correction to the time of our measurements, and a 12% reduction to allow for the slightly different altitude dependence observed for our data (section 6.4 (iii)). The equivalence arises from the fact that the counter efficiency was estimated in section 4.2 by relating our counting rate data to the flux at 200 gm.cm^{-2} given by Newkirk.

We could use Newkirk's leakage flux directly (with time correction), but we prefer to apply the altitude dependence correction since Newkirk's results are probably most reliable in the equilibrium region of the atmosphere.

Using Newkirk's results for 1961 with the time and altitude corrections given above, we obtain a leakage flux of 0.93 $cm^{-2}sec^{-1}$ at P_c = 1.2 BV at the time of our measurements. The accuracy of this figure depends on three main factors:-

(i) the reliability of Newkirk's value for the flux at 245 gm.cm^{-2} and of the time correction to 1964,

(ii) the reliability of the extrapolation from 15 gm.cm^{-2} to the top of the atmosphere. (The shape of the spectrum and the absolute flux given by Newkirk (1963) are in satisfactory agreement with the calculations of Lingenfelter (1963a) and with the measurements of the 1 - 14 Mev neutron flux for $z \geq 3$ gm.cm^{-2} by Haymes (1964). The altitude dependence (figure 7.1) given by Bame et al (1963) for rocket borne BF_3 counters

with polyethylene moderator, differs considerably from the data calculated for these counters using Newkirk's theory. When the two curves are normalised at 15 gm.cm^{-2}, the observed counting rate above the atmosphere is about 80% greater than the rate predicted from Newkirk's theory. It is possible, however, that the discrepancy arises from the poor statistics and the background and local production contributions to the counting rate observed by Bame et al (1963).)

(iii) the uncertainty concerning the shape of the detector efficiency function. (We have shown in section 6.4 that use of the $\eta_3(E)$ response curve should not give rise to errors greater than about 5% in the value of the flux at depths greater than 10 gm.cm^{-2}.)

Consequently, the estimated leakage flux of 0.93 cm^{-2}sec^{-1} is probably reliable to within ± 40%. The error limits could be reduced by a careful measurement of the absolute efficiency of the detector system. This would enable the flux at 15 gm. cm^{-2} to be evaluated directly.

7.3 The latitude distribution.

The boundary region flux distribution is largely determined by the scattering and absorption properties of the atmosphere. These properties vary with the neutron energy. However, the albedo neutron energy spectrum shows only a slight latitude effect (Lingenfelter 1963a), and the spatial distribution in the boundary region should not be strongly dependent on latitude. Consequently, the latitude dependence of the leakage flux should be essentia lly the same as the distribution at the maximum altitudes reached by our detectors (10 - 15 gm.cm^{-2}).

In order to determine the distribution at 15 gm.cm^{-2} from our counting rate data, we must correct for background, local production and latitude variation of the neutron energy spectrum. We have no reliable evidence on the latitude dependence of the background rate at high altitudes. It is a relatively small fraction (4.0 ± 1% at 15 gm.cm^{-2} at Mildura)

of the total rate, however, and little error is introduced by assuming that the fraction is independent of latitude at constant altitude. Since only the relative flux distribution is required, the background effect can be ignored.

The contribution to the counting rate by neutrons produced in the materials of the flight unit has been estimated in section 4.4. The total latitude variation amounts to only a few per cent of the count rate at 15 $gm.cm^{-2}$.

There is no published information on the latitude variation of the neutron energy spectrum in the atmosphere. Lingenfelter has estimated the spectrum of the leakage flux at various latitudes, and we may use these spectra to estimate the latitude variation at 15 $gm.cm^{-2}$ from our results. This method over-estimates the latitude variation of the spectrum at 15 $gm.cm^{-2}$, but provides a useful indication of the magnitude of the effect.

The total latitude variation of the neutron flux given by Lingenfelter (1963a) was 12.4 : 1. Using Lingenfelter's spectra $\lambda = 0^{\circ}$ and 90°, and the $\eta_3(E)$ and $\eta_6(E)$ counter response curves, we obtain a total latitude variation in count rate of 10.9 : 1. Thus the variation of the total flux is 14% greater than that in the counting rate after background and local production corrections. We call this ratio the "spectrum correction factor" and use it to correct the observed count rates to obtain the variation of the total flux. Since the shape of Lingenfelter's spectra at $\lambda = 0^{\circ}$ (P_c = 14.4 BV) and $\lambda = 40^{\circ}$ (P_c = 5.2 BV) are almost identical, corrections have been applied only to the Wilkes and Hobart data. In the absence of any other information we have arbitrarily assumed the correction at Hobart to be half the correction at Wilkes, i.e. we have increased the observed rates at Wilkes by 14% and at Hobart by 7%. As mentioned previously, these corrections are probably too large. Consequently, our results may slightly over-estimate the latitude variation. The error will, however, be less than 14%.

7.4 Comparison with theoretical results.

In figure 7.2 we compare the latitude variation in our results (with and without spectrum correction) with the results of Lingenfelter (1963a) and Hess et al (1961). All data have been normalised at $P_c = 0$. The cut-off rigidities for the data of Lingenfelter and of Hess et al have been estimated from the tables of Quenby and Wenk (1962), on the assumption that the geomagnetic latitudes quoted in the two papers are for 90°W geographic longitude.

Our results agree, within errors, with the results of Lingenfelter, except at low rigidities. Lingenfelter's data show a much greater latitude effect between $P_c = 0$ and 1 BV. The "knee rigidity" is about 250 MV compared with 500 - 600 MV for our data. Lingenfelter's results in this region are based largely on measurements (Neher 1956) during a short period near solar minimum in 1954, when large fluxes of low energy particles were present in the primary radiation. The difference between our results and Lingenfelter's can therefore be attributed, at least in part, to the effects of solar modulation of the primary cosmic rays. There is, in addition, some doubt (section 1.5 (iii)) about Lingenfelter's results in this region, since he did not allow for the energy dependence of the neutron production cross-sections when estimating the neutron production distribution at high altitudes.

The latitude variation given by Hess et al (1961) is very much less than the variation for our data. We obtain a total latitude effect from 0 - 15 BV of about 14.5 : 1, which is almost three times the value of 4.9 : 1 predicted by Hess et al (1961). The difference arises, in part, from solar cycle modulation. Hess et al have not specified the solar cycle phase for which their results are applicable, but they are based on measurements by Hess et al (1959) in 1956-57 and by Simpson (1951) in 1949. Solar activity was much higher during these periods than at the time of our measurements, and it is obvious (Lingenfelter 1963a) that the neutron albedo latitude

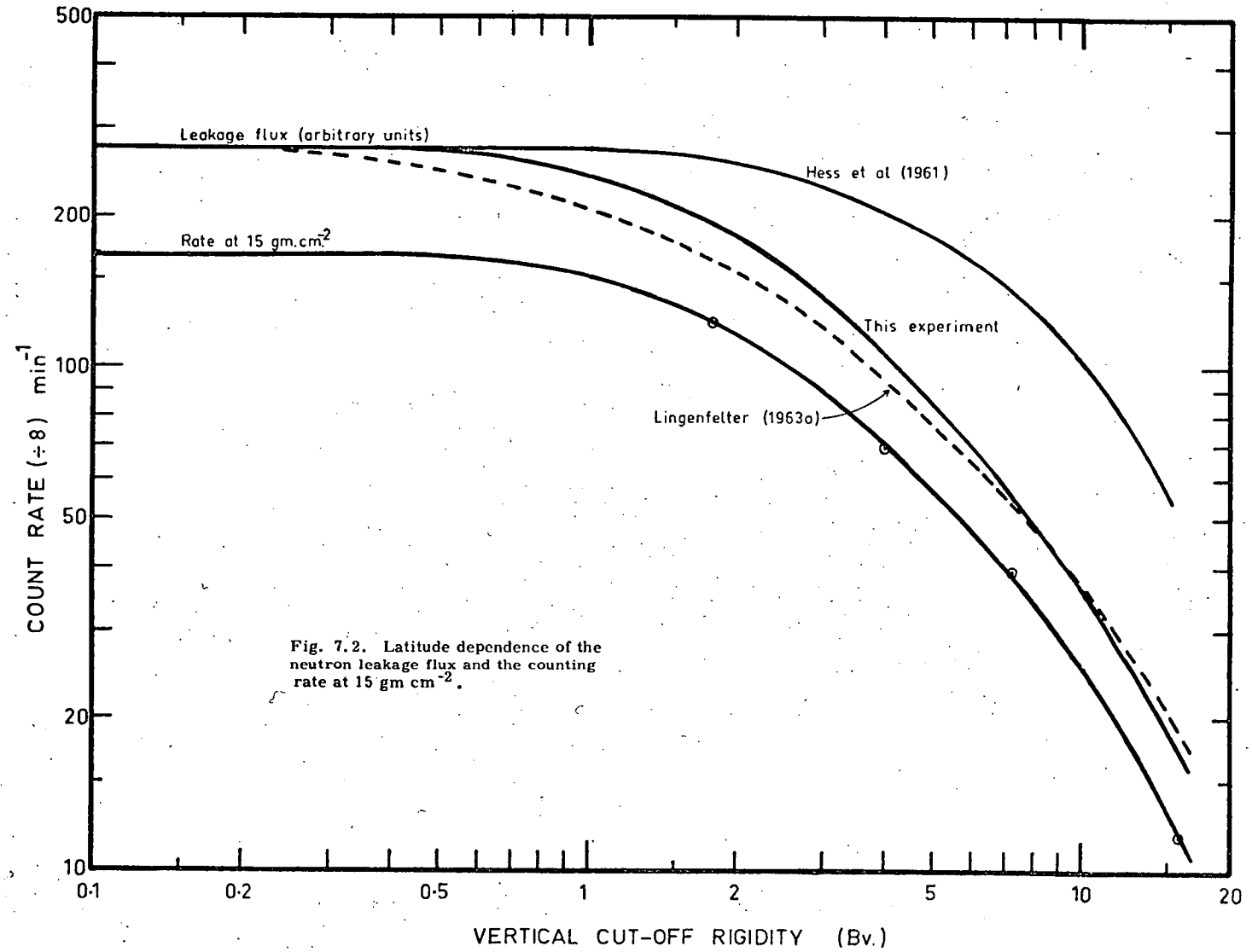

Fig. 7.2. Latitude dependence of the neutron leakage flux and the counting rate at 15 gm cm^{-2}.

variation would therefore be smaller. However, the main reason for the discrepancy is undoubtedly the assumption by Hess et al (1961) that the leakage flux has the same latitude dependence as the flux at about 312 gm.cm^{-2}. This assumption is not supported by our measurements (section 6.2) as illustrated in figure 6.5.

It is tempting to extrapolate the curve in figure 6.5 to the top of the atmosphere to obtain the total latitude effect for the leakage flux. This would give a value, before spectrum correction, of 15.5 : 1 which is 15% more than the variation at 15 gm.cm^{-2}. However, in view of the rapid reduction in the flux near the boundary (section 7.1), we believe the variation at 15 gm.cm^{-2} to be a more reliable indicator of the leakage flux latitude dependence.

7.5 Comparison with other measurements.

(i) Time corrections.

Using the value of the albedo flux at 1.2 BV estimated in section 7.2, and the latitude variation in figure 7.2, we can determine the leakage flux at all latitudes. In figure 7.3 we compare the data obtained in this way with the various experimental results and with the calculations of Hess et al (1961) and Lingenfelter (1963a). All results have been adjusted to an altitude of 300 Km, using the $R^{-3.2}$ altitude variation given by Hess et al (1961).

The experimental results have been obtained at various times during the solar cycle, and in view of the strong time dependence of the leakage flux intensity (Lingenfelter 1963a) it is desirable that all data should be corrected to the same time. Unfortunately the results of section 6.1 are not sufficiently comprehensive for the correction of these data.

Lingenfelter (1963a) has estimated the latitude variation of the neutron albedo for both solar minimum and solar maximum, and we can estimate the flux at any intermediate

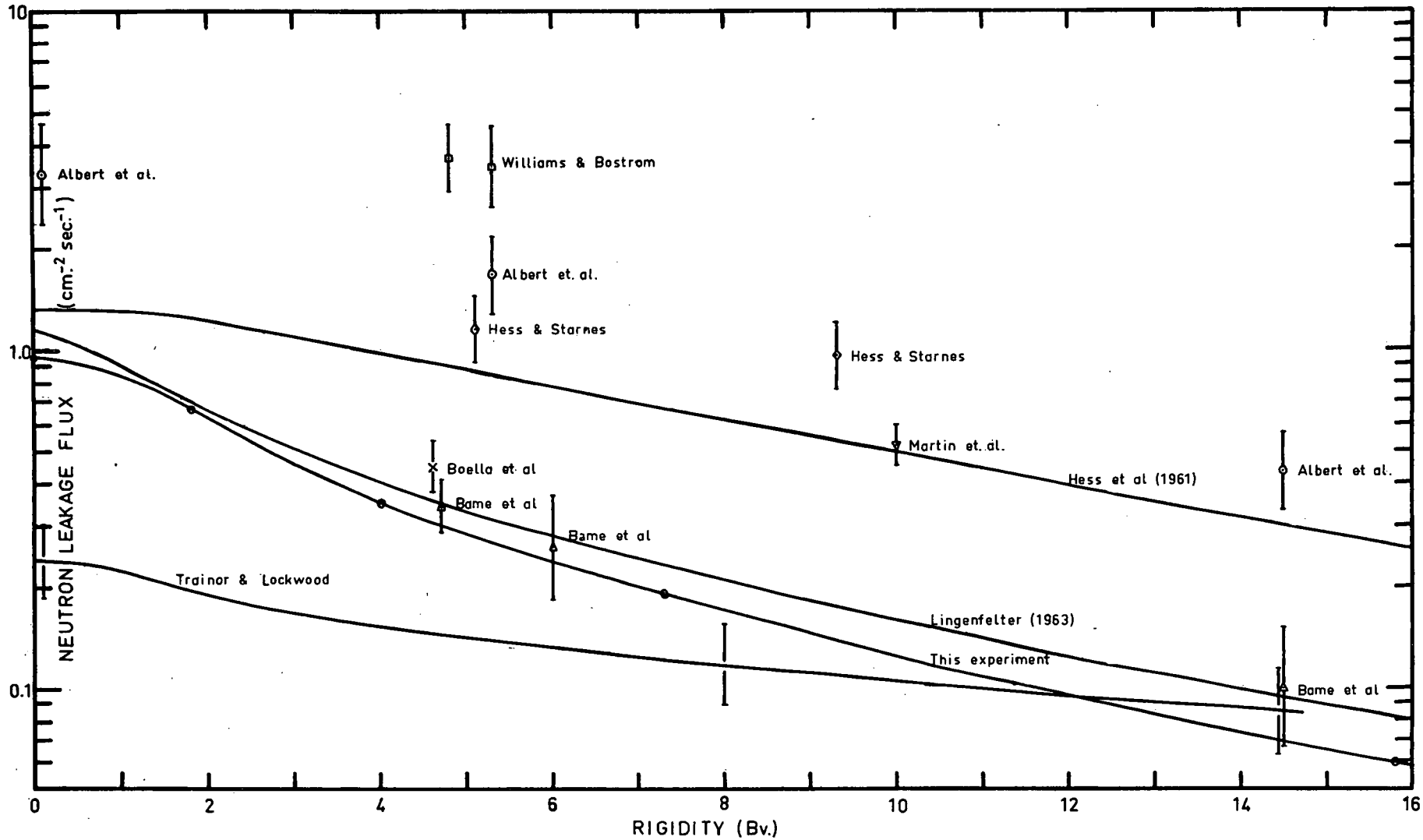

Fig. 7.3 Experimental and theoretical data on the neutron leakage flux at 300 Km based on the spectra of Lingenfelter (1963a). The data from the present experiments have been normalised to the results of Newkirk (1963).

time by interpolating between the two extremes, using the Mt.Wellington neutron rate as a guide. The leakage flux F(t) at time t is given by

$$F(t) = \left\{1 - \alpha(t)\left[1 - \beta(P_c)\right]\right\} F_1 \qquad (7.1)$$

where F_1 is the flux at cut-off rigidity P_c at solar minimum

$\beta(P_c) = \frac{F_2(P_c)}{F_1(P)}$ is the ratio of the flux at P_c (given by Lingenfelter 1963a) at solar maximum to that at solar minimum

$\alpha(t) = \frac{R_1 - R(t)}{R_1 - R_2}$ where R is the Mt.Wellington neutron rate and the subscripts 1 and 2 refer to solar minimum and solar maximum respectively.

In general the ratio of the flux at time t_a to the flux at time t_b is

$$\frac{F(t_a)}{F(t_b)} = \frac{1 - \alpha(t_a)\left[1 - \beta\right]}{1 - \alpha(t_b)\left[1 - \beta\right]} \qquad (7.2)$$

We can use this ratio to correct data obtained during one part of the solar cycle to any other time. Lingenfelter (1963) used a similar method with sunspot numbers as the solar cycle "clock" to estimate the average carbon 14 production rate. We believe, however, that the neutron monitor rate is a more direct and reliable guide to the changes in the leakage flux, especially near solar minimum when sunspot numbers are very low and, in a linear interpolation, have little effect on the ratio.

We can check this method by predicting the ratios of the flux at 15 gm.cm^{-2} for the various flights at Wilkes and Mildura. Unfortunately, the formula underestimates the change in flux at Wilkes during 1963 and 1964 by a factor of 2, and at Mildura by a factor of 3. It would seem that Lingenfelter (1963a) underestimates the change in flux over

the solar cycle since, for example, his calculations indicate a 25% increase in the leakage flux at 4 BV from solar maximum to solar minimum. Our measurements show a 20% increase in the flux at 15 gm.cm^{-2} over Mildura (P_c = 4 BV) between February, 1964 and April, 1965. The rate of the Mt.Wellington neutron monitor increased during this period by less than 25% of its total variation during the solar cycle. It is inconceivable that four fifths of the total change in leakage flux should occur in this period. Similarly, the flux at 15 gm. cm^{-2} over Wilkes changed by 43% of the total change predicted by Lingenfelter (1963a), during a period (February, 1963 to October, 1964) when the variation in the Mt.Wellington rate was less than 25% of its total solar cycle variation.

In view of the uncertainty about the time variations the experimental results in figure 7.3 have not been corrected to the time of our measurements.

(ii) Discussion.

A very large spread and a tendency towards dichotomy in the results is apparent in figure 7.3. However, closer investigation reveals that the upper group, which are consistently above but relatively close to the calculations of Hess et al (1961), are either not corrected for or insufficiently corrected for local production. The measurements of Albert et al (1962) and of Hess and Starnes (1960) are uncorrected. The results of Williams and Bostrom (1964) have been corrected for local production but there is reason to believe (Boella et al 1965, Trainor and Lockwood 1964) that their 30% correction is much too small. Williams and Bostrom point out that a local production correction of 80 - 95% is required to bring their observations into agreement with the theory of Lingenfelter. This figure does not appear to be unreasonable, however, in view of the local production measurements of Trainor and Lockwood (1964) and of the large amounts of moderator material and low efficiency for detection of external neutrons of Williams and Bostrom's flight unit. Martin et al (1963) apply

a 20% correction to their data. This correction is based on the observed increase due to local production when their equipment entered the trapped radiation zone, and the ratio of the primary cosmic ray flux to the trapped particle flux. They do not allow for the marked energy dependence of the neutron production cross-sections (Lingenfelter and Flamm 1964), and therefore undoubtedly underestimate the local production due to the primary cosmic radiation. The results of Hess et al (1961) are probably too high at low latitudes because their latitude distribution is based on the variation at 312 $gm.cm^{-2}$.

In the lower group of results, our measurements are in good agreement with the calculations of Lingenfelter (1963a) and with the measurements of Bame et al (1963) and Boella et al (1965). Bame et al used a 20% correction for local production. This would appear to be quite generous in the light of our calculations and the similarity between their detectors and ours. The data of Boella et al have been corrected using a method essentially similar to our own. Time corrections to these data will be relatively small. The correction for the data of Boella et al, estimated from our Mildura results (section 6.1), is only about 10%. This is less than the difference in the data obtained by the two methods of extrapolation used by the authors. The time corrections for the results of Bame et al will be very small for the high rigidity point, but will probably increase the fluxes at 4.6 and 6.0 BV by 20-30%.

At high rigidities our results lie consistently below the results of Lingenfelter (1963a), Bame et al (1963) and Trainor and Lockwood (1964), all of which are in good agreement. The discrepancy is within the uncertainty limits of our data (section 7.2) and may be due to incorrect normalisation of our results. In addition, the spectrum correction factor used (section 7.3) may exaggerate the total latitude effect by as much as 10%. With re-normalisation and a slight reduction in the latitude effect, our results would agree

within 20% with the results of Lingenfelter, Bame et al and Boella et al and with the low latitude results of Trainor and Lockwood.

There is a serious discrepancy between our results and the high latitude measurements of Trainor and Lockwood (1964). These measurements were made in mid-1962, and although time corrections may increase the flux at $P_c = 0$ by as much as 50% it would still amount to only about half the value obtained from our measurements. Trainor and Lockwood used a detector system designed to discriminate against neutrons produced in the detector assembly. The observed local production rate was in good agreement with the rate estimated from the primary cosmic ray flux, neutron production cross-sections and the detector mass and efficiency. In section 4.4 we showed that, when our method for obtaining the local production was applied to Trainor and Lockwood's detector system, a similar value was obtained, although with considerable uncertainty since the detector mass and composition was not known. Even without local production corrections, Trainor and Lockwood's data lies well below our own or any of the other experimental or theoretical results.

One of the most surprising features of Trainor and Lockwood's data is the very small latitude effect of less than 3 : 1 in going from the equator to the poles. It is difficult to reconcile this with our latitude variation, before spectrum correction, of 14 : 1 at 15 $gm.cm^{-2}$. It is conceivable that both results are correct, and that the altitude dependence in the top 15 $gms.cm^{-2}$ of the atmosphere is much steeper in polar regions than near the equator. This seems very unlikely, however. Qualitatively speaking, we would expect the opposite to apply because of the "harder" neutron energy spectrum in polar regions and the consequently greater diffusion mean free path.

The difference cannot be explained by the uncertainty about the latitude dependence of the leakage spectrum. Even if

the spectrum were independent of latitude, the total variation of the neutron flux between Wilkes and Lae would be reduced by only 14%. Nor would the latitude variation be significantly affected by even major changes in the detector response function (section 7.3).

7.6 Conclusions.

(i) The neutron leakage flux at P_c = 1.2 BV has been determined by extrapolating the balloon ascent data from 15 gm.cm^{-2} to the top of the atmosphere, using the altitude dependence and spectrum calculated for this region by Newkirk (1963). The estimated flux in October 1964 was 0.93 (± 40%). This result is based on the time corrected value of the flux at 250 gm.cm^{-2} given by Newkirk (1963). A more reliable value could be obtained from our results following a proper calibration of the detector system.

(ii) The latitude variation of the flux at 15 gm.cm^{-2} has been determined by correcting the count rate data for local production and for the latitude dependence of the spectrum, using the data of Lingenfelter (1963a). Assuming the latitude variation at this altitude to be similar to the variation at the top of the atmosphere, the total latitude effect between 0 and 15 BV of 14.5 : 1 is in agreement,within errors, with the calculations of Lingenfelter (1963a), but not with the 4.9: 1 variation predicted by Hess et al (1961).

(iii) Time corrections based on the theory of Lingenfelter (1963a) (with interpolation between solar minimum and maximum determined from the Mt.Wellington neutron monitor rate) consistently underestimate the change in flux at 15 gm.cm^{-2} as determined by measurements from January 1963 to April 1965. Thus the change in flux at 15 gm.cm^{-2} over Mildura (P_c = 4 BV) between February 1964 and April 1965 was almost 80% of the total change (between solar maximum and solar minimum) predicted for this rigidity by Lingenfelter. The Mt.Wellington neutron rate increased during this period by less than 25% of

its total solar cycle variation.

(iv) The leakage flux obtained from our measurements agrees (within the limits of error) with the calculations of Lingenfelter (1963a),and with the measurements of Beme et al (1963), Boella et al (1965) and the low latitude results of Trainor and Lockwood (1964). They do not support the measurements of Albert et al (1962), Hess and Starnes (1960), Martin et al (1963) or Williams and Bostrom (1964), all of which are thought to be inadequately corrected for local production of neutrons in the detector system.

(v) Our results do not support the mid and high latitude measurements of Trainor and Lockwood (1964), and we are unable to explain the discrepancy. We obtain a high latitude flux of 0.95 $cm^2 sec^{-1}$ (at 300 Km) which is four times the value obta ined by Trainor and Lockwood. Their total latitude effect of about 3 : 1 is less than one quarter the variation for our data. It is very unlikely that this difference arises from a latitude variation in the extrapolation from 15 $gm.cm^{-2}$ to the top of the atmosphere.

Notes: Two important papers were received after completion of this chapter.

(1) Martin (1965) reports polar orbiting satellite measurements of the density of slow neutrons leaking out of the atmosphere. The shape of the latitude variation is consistent with the calculations of Lingenfelter (1963a) and with our measurements after correction for the time difference and the different sensitivity of our detectors.

(2) Recent measurements by Lockwood et al (1965), using moderated He^3 proportional counters, give a latitude distribution of the leakage flux which is in good agreement with our results and with those of Lingenfelter (1963a). These measurements were made during rocket flights at geomagnetic latitudes of 0^o, 19^o and 49^o, early in 1965. The results do not support the measurements of Trainor and Lockwood (1964).

VIII THE SLOW NEUTRON DENSITY AND CARBON 14 PRODUCTION

8.1 Introduction

The only experimental evidence on the global distribution of the slow neutron density comes from the measurements of Soberman (1956). These provide little information on the latitude distributions since flights were made at only three sites and two of these were at high latitudes.

The slow neutron density cannot be obtained directly from our results. The latitude and altitude distributions of our counting rates, are however, the same as the neutron density distributions in the equilibrium region of the atmosphere. These distributions can be normalised to direct slow neutron measurements in order to obtain the absolute density distributions in this region. We shall show later that, at higher altitudes, the latitude distributions of the neutron density may be obtained from our measurements by making only minor corrections and the absolute distributions can again be obtained by normalisation to direct show neutron measurements.

8.2 Spectrum corrections for the latitude variation

(i) Corrections at $\Xi = 0$: Lingenfelter (1963a) has shown that the spectrum of neutrons leaking out of the atmosphere varies with latitude because of the latitude dependence of the neutron source altitude distribution. The

energy spectrum at high latitudes is harder than at low latitudes and although the difference is most pronounced in the leakage spectrum it will occur with decreasing effect down to an atmospheric depth of 200 or 250 gm cm^{-2}. Since the main contribution to the counting rate of our detectors comes from neutrons with energies in the tens or hundreds of Kev (figure 4.2) our measurements tend to overestimate the latitude variation of the slow neutron density for $\S < 200$ gm cm^{-2}.

In section 7.3 we calculated the relative counting rates of our detectors at $\lambda = 0^{\circ}$ and 90° using the leakage flux spectra of Lingenfelter (1963a). The estimated total latitude effect is 10.9:1.

Similarly we may obtain the total latitude variation of the slow neutron density from the results of Lingenfelter (1963a) by integrating $\phi(E).\frac{1}{v}$ over energy for $\lambda = 0^{\circ}$ and 90°. This gives a latitude effect of 9.7: 1. In order to estimate the latitude effect in the slow neutron density from our measurements we multiply the observed total latitude effect by the ratio $^{9.7}/_{10.9}$. In other words, we assume that Lingenfelter's spectrum shapes are correct but not necessarily the magnitudes. We call the ratio $100\ (\frac{10.9-9.7}{10.9}) = 11\%$, the "spectrum correction factor", S, for the total latitude effect at $\S = 0$. Comparison of the curves given by Lingenfelter (1963a) shows that the spectrum correction factor between $\lambda = 0^{\circ}$ and 40° at $\S = 0$ is very small.

(ii) Variation of the correction factor with altitude:

There is no published information on the latitude variation of the neutron energy spectrum at atmospheric depths $Z > 0$. In order to estimate the correction required at these depths we make use of the ratio $\alpha(Z)$ of the counting rate of our counters to ,that of a slow neutron detector at the same depth. $\alpha(Z)$ is normalised to unity at 250 gm cm^{-2}. The spectrum correction factor $S(Z)$ at depth Z is then estimated by assuming that

$$S(Z) = \frac{\alpha(Z) - 1}{\alpha(0) - 1} \cdot S(0) \qquad (8.1)$$

where $\alpha(0)$ and $S(0)$ are the values of α and S at $Z = 0$. In other words we assume that the spectrum correction factor $S(Z)$ at depth Z is a constant fraction of the percentage difference between the counting rate of our detectors and of slow neutron detectors when the rates are normalised in the lower atmosphere.

In order to evaluate $\alpha(Z)$ we have used counting rates estimated from the theory of Newkirk (1963) rather than experimental data which are not available for the top 10 or 20 gm cm^{-2} of the atmosphere. The estimated counting rate distributions are illustrated in figure 8.1. As Newkirk does not give the low energy distribution at $Z = 0$ we have used the altitude dependence of his group 12 (thermal to 10 ev) flux to obtain the neutron density altitude distribution. The percentage difference between the two curves decreases rapidly with atmospheric depth and the spectrum correction factor decreases correspondingly. The ratio $\alpha(Z)$ of moderated to slow neutron counter rates is illustrated in figure 8.2.

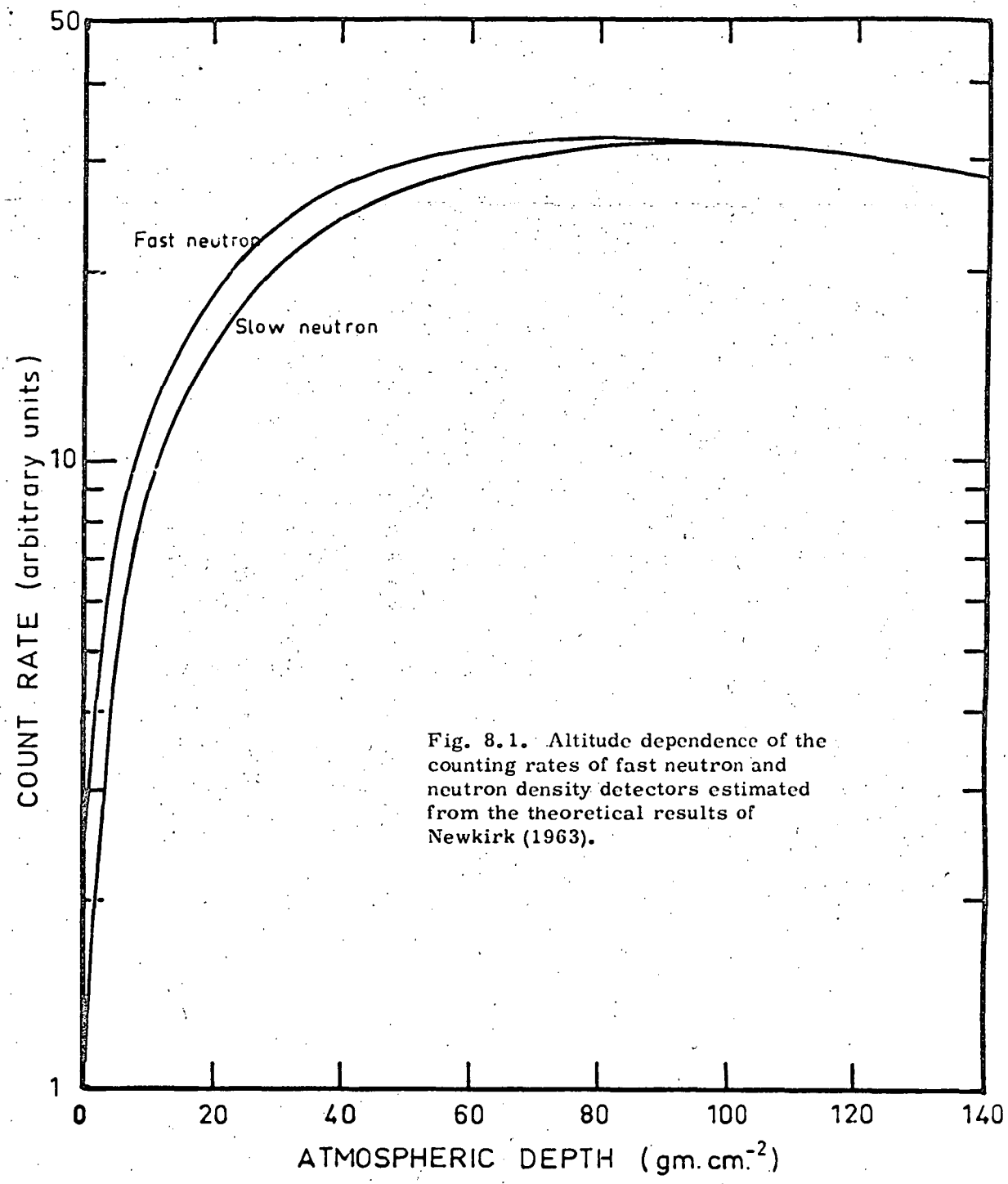

Fig. 8.1. Altitude dependence of the counting rates of fast neutron and neutron density detectors estimated from the theoretical results of Newkirk (1963).

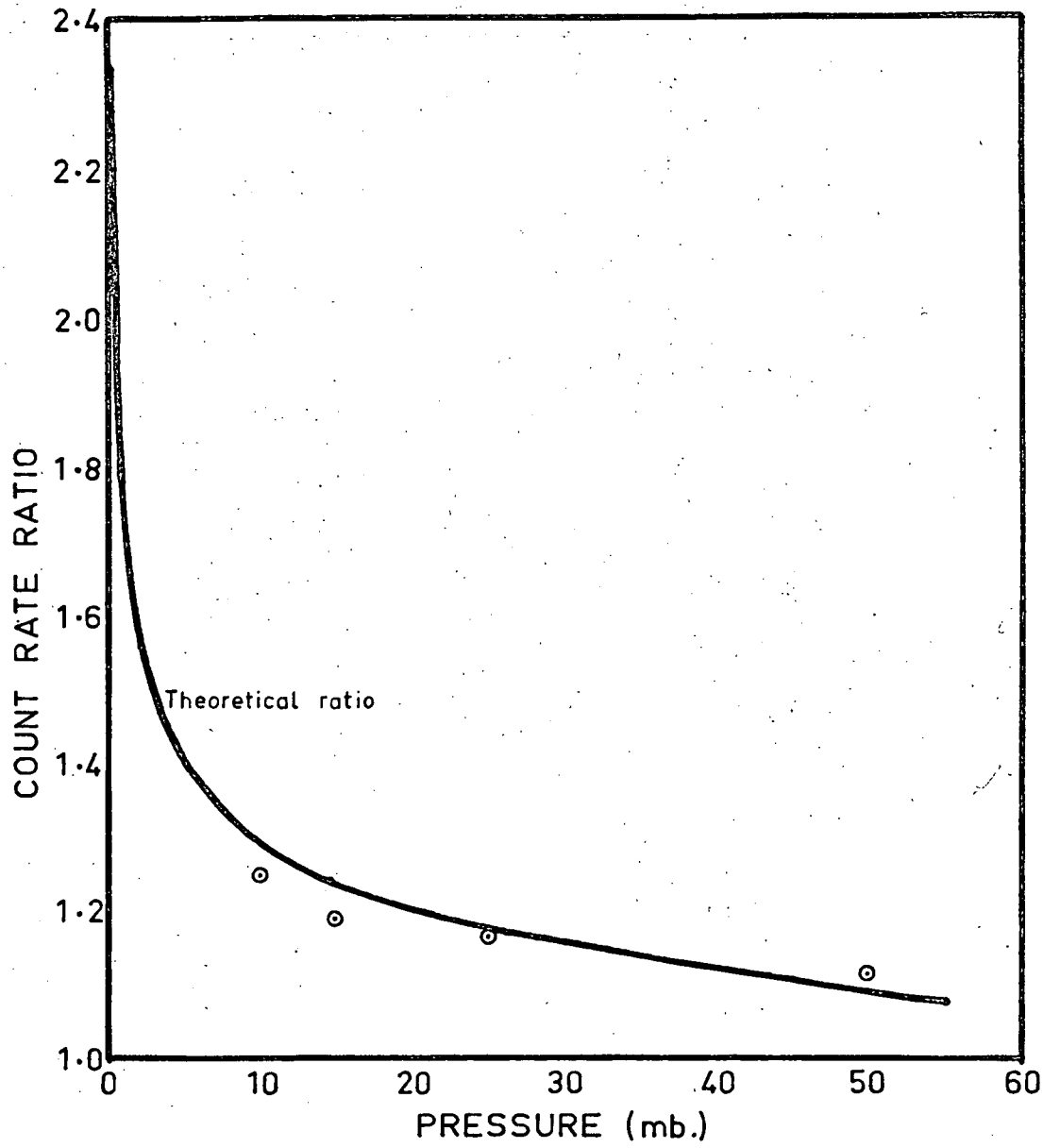

Fig. 8.2. Ratio of the count rates of fast neutron and neutron density detectors. The solid line is estimated from the theory of Newkirk (1963) and the experimental points from our measurements and the results of Miles (1963).

α remains essentially equal to unity for all $Z > 100 gm\ cm^{-2}$. It increases to about 1.2 at 25 $gm\ cm^{-2}$, 1.33 at $10 gm\ cm^{-2}$ and 2.3 at $Z = 0$. Inserting numerical values, equation 8.1 becomes

$$S(Z) = \frac{\alpha(Z) - 1}{1.3} \times 11\% \qquad (8.2)$$

At 10 $gm\ cm^{-2}$ $S = 2.8\%$ and at 25 $gm\ cm^{-2}$ $S = 1.7\%$. The uncertainty in these values is large but can have little effect on the final latitude distribution because of the small corrections involved. It is clear, in view of the other uncertainties in the results, that the latitude variation of the spectrum can be ignored at depths greater than 10 or $20 gm\ cm^{-2}$.

An indication of the reliability of Newkirk's results can be obtained by comparing the ratio $\alpha(Z)$ of the theoretical rates, for the two types of detectors, with the ratio of the rates of our detector at $P_c = 5.2$ Bv (estimated from figure 6.4) to the slow neutron rates of Miles (1964). Although the experimental ratio is for measurements at 5.2 Bv and the ratios from Newkirk's theory are for $P_c = 1.2$ Bv the two should be directly comparable at depths greater than about $25 gm\ cm^{-2}$ since little latitude variation is expected in the neutron energy spectrum at these depths. The difference in time between our measurements and those of Miles (1964) can be ignored in this case since the altitude distribution at 5.2 Bv varies little during the solar cycle (section 6.1).

The experimental ratios are illustrated by the points and the theoretical ratio by the line in figure 8.2. In both cases the data have been normalised to give a ratio of unity at 250gm cm^{-2}. There is good agreement between the experimental and theoretical results.

8.3 The latitude dependence of the neutron density

In the previous section we showed that the latitude distribution of the slow neutron density may be obtained from our counting rate distributions (section 6.2) after minor corrections for the variation of the spectrum with latitude. In figure 8.3 the density distributions obtained in this way are compared, at various atmospheric depths, with the theoretical results, for solar minimum, of Lingenfelter (1963). In each case the results have been normalised at $P_c = 0$.

It should be noted here that Lingenfelter gives carbon 14 production distributions: not neutron density distributions. We shall see later that carbon 14 is produced, in part, by resonance capture of neutrons in the hundreds of Kev. energy range. The production distributions at high altitudes will, therefore, differ in principle, from the density distributions. The differences are, however, likely to be small and will, undoubtedly, be insignificant in the case of the latitude distributions. Lingenfelter has, by normalising his carbon 14 production distributions to neutron density measurements, implicitly assumed that the altitude

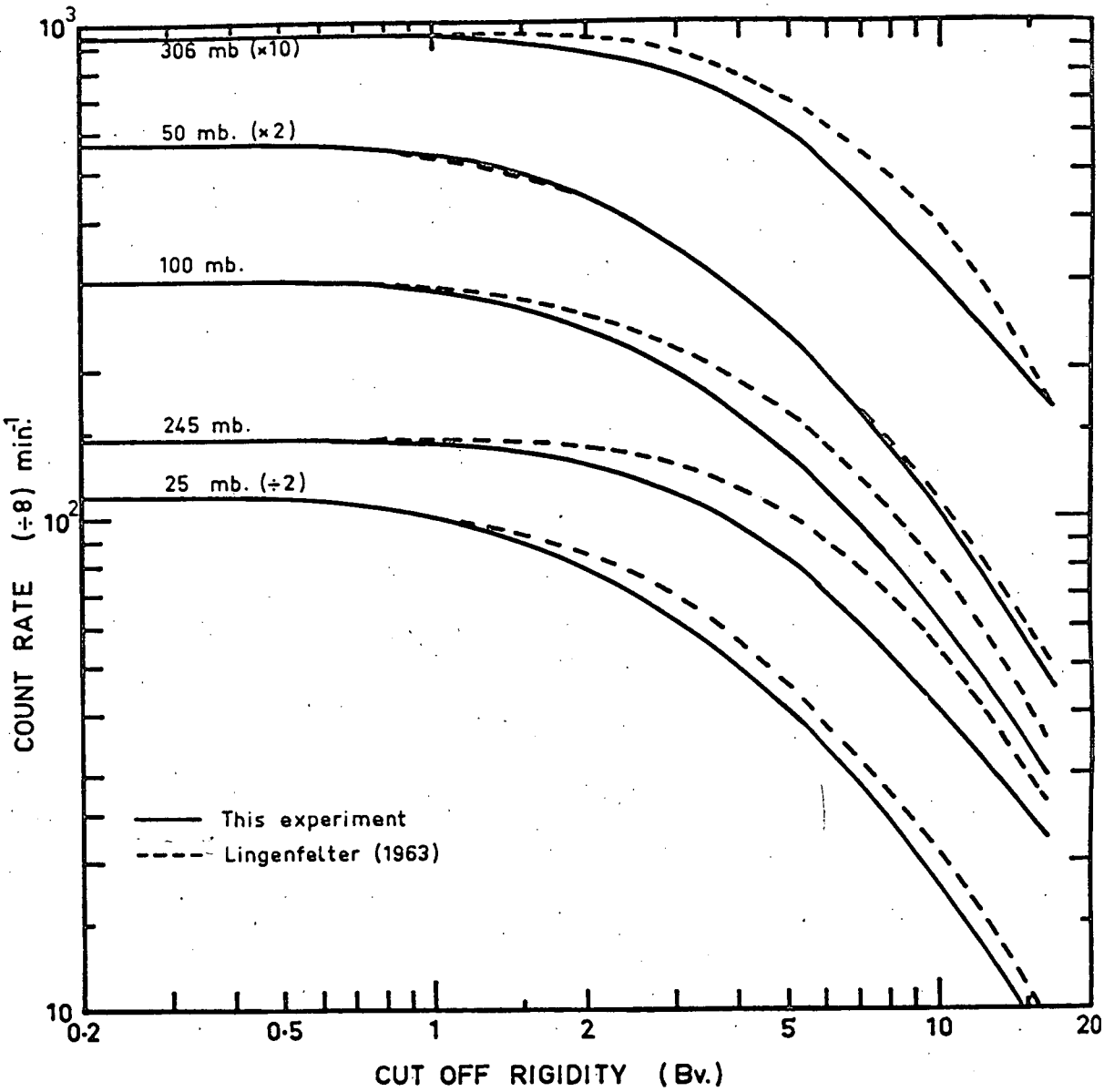

Fig. 8.3. Neutron density distributions. The results of Lingenfelter (1963) are normalised to our measurements at Pc=0.

distributions are also identical. We shall therefore assume, for the moment, that Lingenfelter's results give the neutron density distributions directly and compare them with our own data.

Significantly different latitude distributions are obtained from our measurements at most levels in the atmosphere. When normalised at $P_c = 0$, Lingenfelter's calculations give densities at 100 and 250gm cm^{-2} which are 20-35% higher than our results at P_c = 5-10 Bv. Our data at 100 and 250gm cm^{-2} give total latitude variations between 0 and 15 Bv which are about 20% greater than the corresponding variations in Lingenfelter's results.

The reason for the differences is not clear. The discrepancies are much greater than the uncertainties in our results which are, in any case, supported by the measurements at 245gm cm^{-2} by Gauger (1964). Lingenfelters calculations for the latitude distributions in the equilibrium region of the atmosphere are largely based on the neutron intensity measurements at 312gm cm^{-2} of Simpson (1951) adjusted to 1953-1954 by the data of Meyer and Simpson (1955) and Soberman (1956). It is not clear to what extent they have used Soberman's general latitude distribution in the correction to 1964. As we have shown in section 6.3(iii) this distribution differs from our measurements by as much as 70% when normalised at $P_c = 0$. Soberman's experimental data

on the other hand give no information of the distribution at mid latitudes.

Whatever the reason for the discrepancies in the latitude distributions, the significance of our results depends largely on the way the curves are normalised. In section 8.5 we shall normalise our data to the measurements of Miles (1964) since these are probably the most precise and reliable data available. There is however, some justification in normalising to Lingenfelter's results at $P_c = 0$, since these results have themselves been normalised to experimental data and the normalisation is weighted towards low rigidities.

Assuming for the moment that Lingenfelter's neutron densities are correct for all altitudes at $P_c \neq 0$ we find (figure 8.3) that he overestimates the solar minimum neutron density for $P_c > 0$ at all atmospheric depths greater than 100gm cm^{-2}. His density distribution at $P_c = 5.2$ Bv is about 25% greater than that obtained from our measurements. This is in qualitative agreement with the observations of Miles (1964) who measured the neutron densities at $\lambda = 41^{\circ}N$ ($P_c \sim 5.2$ Bv) and found Lingenfelter's results to be about 50% above the values obtained in his experiment. The apparent agreement between our results and Lingenfelter's at higher altitudes is not supported by the measurements of Miles. This agreement is based on the assumption that Lingenfelter's altitude distribution at $P_c = 0$ is correct. We shall show in the next section that this assumption is

probably not justified.

8.4 The altitude dependence of the neutron density

The neutron energy spectrum varies considerably with altitude above the equilibrium region of the atmosphere. The mean neutron energy increases with altitude as more and more neutrons escape from the atmosphere before being thermalised or captured. This is illustrated in figure 8.1 where the flux of thermal to 10 ev neutrons lies well below the flux of faster neutrons estimated from the results of Newkirk (1963) for a counter with an energy response give by the function $\eta_6(E)$. We might therefore expect that that altitude distribution of the slow neutron density given by Lingenfelter (1963) would fall below the count rate vs altitude curve for our detectors at the same latitude. The two curves for $P_c = 0$ (normalised at 250gm cm^{-2}) are illustrated in figure 8.4 and the reverse is seen to be the case. Lingenfelter's results lie as much as 35% above our own. A similar, although less pronounced discrepancy exists at higher cut-off rigidities.

Using the ratio $\alpha(\bar{z})$ of count rate to slow neutron density, obtained in section 8.2, we may estimate the altitude distribution of the neutron density from our measurements. This distribution is illustrated by the broken line in figure 8.4. It is clear that Lingenfelter overestimates the altitude dependence of the neutron density above the equilibrium region especially at high latitudes.

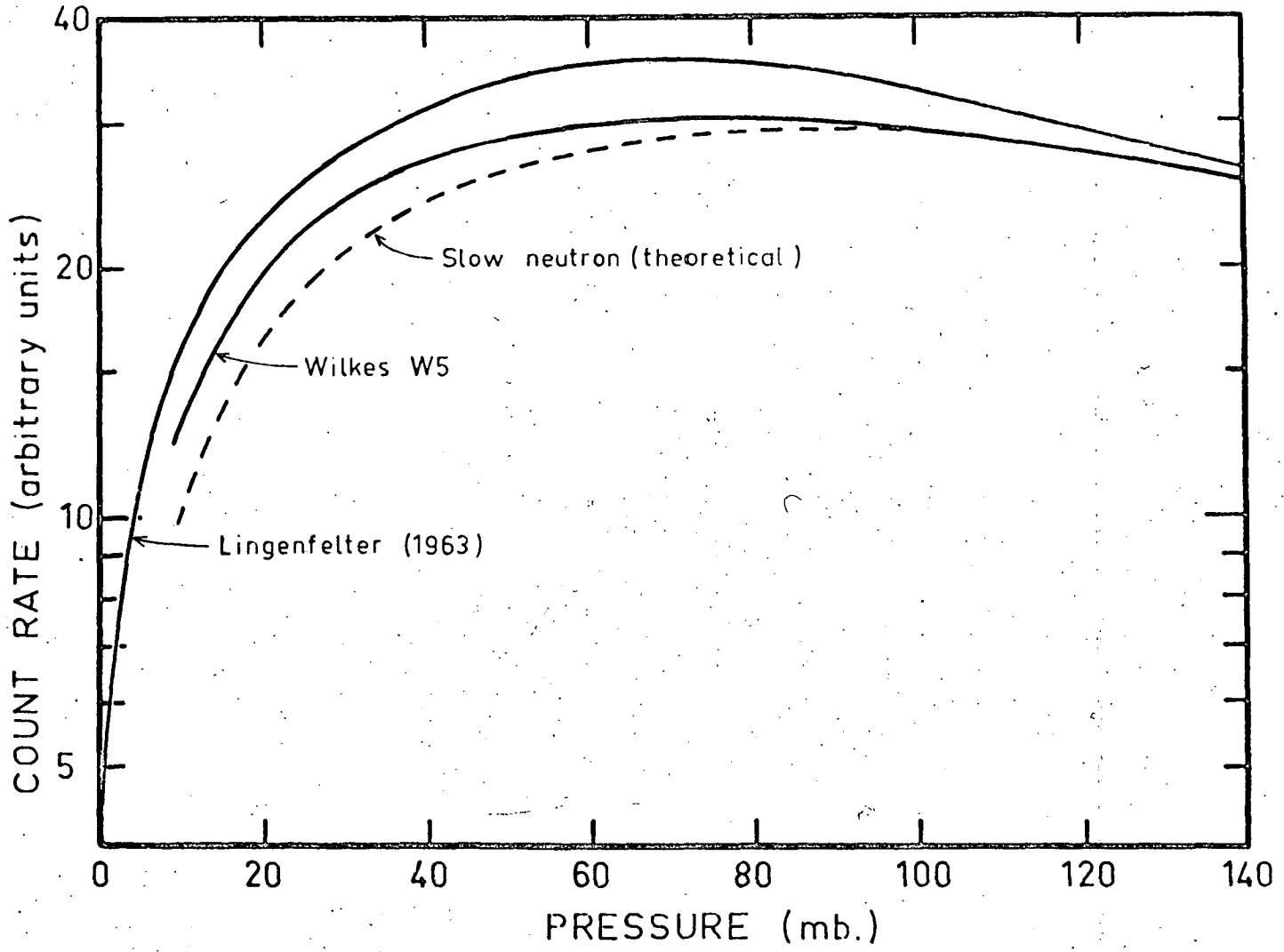

Fig. 8.4. The altitude dependence of the slow neutron density at Pc = 0 estimated from the fast neutron rates during Wilkes flight W5. The results of Lingenfelter (1963) and the theoretical rates are normalised to the W5 data at 250 gm cm^{-2}.

Relative to the neutron density at 250gm cm^{-2} he obtains a value in polar regions which is 30% too high at 50gm cm^{-2} and 60% too high at 10gm cm^{-2}. At P_c = 5.2 Bv the relative density at 50gm cm^{-2} is about 10% above our estimates. Similar results are obtained by comparing Lingenfelter's data with the slow neutron measurements of Soberman (1956) at $\lambda = 88^{o}N$. Although there is considerable uncertainty in these results it is clear that a significant discrepancy exists in polar regions. If the theoretical altitude distribution described above is combined with our latitude distribution curves, we find Lingenfelter's values for the neutron density at P_c = 5.2 Bv to be about 30% too high at all altitudes. This is in qualitative agreement with the results of Miles (1964). The remaining discrepancy is probably due to a difference in normalisation.

It is probable that the altitude distributions of the neutron production rate used by Lingenfelter (1963) is incorrect. There is little data on neutron production in this region and Lingenfelter found it necessary to use the latitude variation of the primary cosmic ray intensity to estimate the high altitude neutron production distribution. He did not, however, allow for the energy dependence of the neutron production cross-sections (Lingenfelter and Flamm 1964) in these calculations. The errors introduced in this way (section 1.5 (iii)) will undoubtedly cause the production rate at high altitudes and latitudes to be over-

estimated. Quantitative conclusions are not possible without details of the primary spectrum and the cross-sections at high energies.

The breakdown of diffusion theory in boundary regions probably contributes to the errors in Lingenfelter's results at high altitues. Close scrutiny of the slow neutron distribution of Miles (1964, figure 5) shows that the altitude dependence for $\bar{z} < 25 gm\ cm^{-2}$ is markedly different from that given by Lingenfelter.

Nitrogen 14 resonance neutron capture will affect the carbon 14 production distribution at high altitudes and this will contribute to the difference between Miles' and Lingenfelter's results. The magnitude of this effect is not known.

8.5 The absolute neutron density distribution

(i) Absolute measurements: It is impractical to obtain an absolute value for the neutron density from measurements with a moderated BF_3 counter. The bare counter is, however, an ideal instrument for this purpose.

The background corrected counting rate R_N of a bare BF_3 counter, for which self shading effects can be neglected, is given (Price 1958, p:260) by the relation.

$$R_N = N_T \int_0^\infty \sigma(E)\, \phi(E)\, dE \qquad (8.3)$$

where N_T is the total number of boron 10 nuclei in the sensitive region of the counter

$\sigma(E)$ is the $B^{10}(n,\alpha)$ cross section at energy E.

$\phi(E)$ is the flux per unit energy interval at E.

Self shielding effects in the atmospheric neutron flux are very small for our counters and can be neglected.

For energies up to at least 10Kev.

$$\sigma(E) = \frac{v_o \sigma_o}{v(E)} \qquad (8.4)$$

where v_o is the average thermal neutron velocity (2.2×10^5 cm sec^{-1})

σ_o is the $B^{10}(n,\alpha)$ thermal neutron cross section (3,820. barns - Hughes and Schwartz 1958)

If the neutron spectrum contains no neutrons with energies greater than about 10Kev. equation 8.3 becomes

$$R_N = N_T \sigma_o v_o \rho \qquad (8.5)$$

where ρ is the neutron density.

Now

$$N_T = pLV\epsilon \qquad (8.6)$$

where p is the pressure in atmosphere of the BF_3 gas in the counter.

L is Loschmidt's constant

V is the volume of the sensitive region of the counter

ϵ is the B^{10} isotopic concentration

Hence the neutron density may be obtained from the counting rate using the relation

$$\rho = \frac{R_N}{pLV\varepsilon\ \sigma_o\ v_o} \qquad (8.7)$$

Equation 8.7 may be written in the form

$$\rho = \frac{R_N}{A_o v_o} \qquad (8.8)$$

where $A_o = pLV\varepsilon\ \sigma_o$ (8.9)

is the total effective cross-sectional area of the counter for thermal neutron capture. Although many atmospheric neutrons have energies greater than 10Kev. their contribution to the counting rate of a bare BF_3 counter is very s-mall. Consequently equation 8.8 may be used for the calculation of the neutron density in the atmosphere. Many groups (Soberman 1956, Haymes 1959, Haymes and Korff 1960, Reidy et al 1962, Martin et al 1963, Martin 1965) have used these or equivalent methods to evaluate the atmospheric neutron density.

(ii) Calibration of neutron density detectors: The relationship between counting rate and neutron density may also be obtained by calibration. Yuan (1951) measured the effective cross-sectional area A_o for a BF_3 counter in the thermal neutron flux from a nuclear reactor. Others (Simpson 1951, Hess et al. 1959, Lingenfelter 1963) have used this calibration to estimate the effective cross-section

of uncalibrated counters from the ratios of their boron 10 content to that of Yuan's standard. Thus the effective cross-section A_{ox} of the uncalibrated counter

$$A_{ox} = \frac{V_x p_x \epsilon_x}{V_y p_y \epsilon_y} \cdot A_{oy} \qquad (8.10)$$

where the subscripts x and y refer to the uncalibrated counter and to Yuan's counter respectively.

There is a substantial difference between the values of A_{ox} obtained by the two different methods. Yuan obtained a value of $A_o = 10.6 \pm 1$ cm^2 for his standard counter whereas the area estimated from the dimensions, filling pressure and isotopic concentration is 24 cm^2. The origin of this anomaly is not clear but its resolution is very desirable since the interpretation of many experimental results depends upon it.

A similar discrepancy exists in the case of the BF_3 filled ionisation chamber used by Miles (1964). Miles calibrated his ion chamber in a thermal neutron flux. He found that the neutron density was related to the chamber current by the relation

$$\rho = Kn \qquad (8.11)$$

where

$$K = 2.6 \pm 0.5 \times 10^{-9} \qquad (8.12)$$

is a constant of the chamber (in units of neutrons cm^{-3}/ equivalent ion pairs) and n is the ionisation current in

"equivalent ion pairs".

The sensitivity of the chamber in terms of equivalent ion pairs per "count" of the chamber electrometer was also determined by calibration.

The theoretical relationship between neutron density and chamber current can be determined by estimating the rate of occurrence of $B^{10}(n, \alpha)$ events and calculating the mean current produced. This current can then be expressed in terms of equivalent ion pairs and K evaluated. Using this procedure we can show (Appendix VI) that

$$\rho = \frac{\Delta E\, n}{k L v_0 \sigma_0 \epsilon E} \qquad (8.13)$$

where E is the mean energy released in the $B^{10}(n, \alpha)$ reaction.

ΔE is the average energy required to produce an ion pair in BF_3

k is the ratio of the probable specific ionisation in air to that in BF_3

Inserting numerical values we find, after making a small correction for events produced near the walls of the chamber, that

$$K = 1.3 \times 10^{-9} \text{ Neutrons cm}^{-3}\text{/ equivalent ion pair} \qquad (8.14)$$

Thus we obtain a theoretical efficiency which is twice the experimentally determined value. This result is similar,

within errors, to the experimental totheoretical efficiency ratio of 2.26: for the BF_3 proportional counters of Yuan (1951).

It should be noted that Miles' result depends ultimately on the calibration of a BF_3 proportional counters which wasused to measure the neutron density in the vicinity of the ion chamber during its calibration. This counter was originally calibrated at the Lawrence Radiation Laboratory, (Patterson and Wallace, 1958). An intercalibration was made (Miles 1964) between it and a counter used by Hess et al (1959) (as reported by Lingenfelter 1963). Thus there appear to be at least three standard counters whose efficiencies have been obtained by calibration. As we have shown above, two of these calibrations agree to within about 10% but differ from the theoretical estimates by a factor of about two.

We are unable to explain the origin of this discrepancy. As mentioned previously, the theoretical procedure has been used by many different groups and has in fact been used (Larsson 1953) to calculate the efficiency of a BF_3 filled ionisation chamber used for making absolute measurements of neutron source strengths. Smith et al (1962) have measured the efficiency of an unshielded Li^6I slow neutron detector and report good agreement with the value calculated from the known lithium 6 cross-sections. It is hoped that a direct calibration of our own detectors will be possible in the near future and that this will throw more light on the problem. In the meantime we are forced to use

both methods in the interpretation of our measurements. A similar situation exists in the other experimental results. Thus, for example, Lingenfelter's (1963) interpretation of Soberman's measurements yields neutron densities more than twice those originally given by Soberman (1956).

(iii) Neutron density measurements in flight DN3: The neutron density was measured during Wilkes flight DN3 in March 1965. The flight unit contained two unmoderated BF_3 detectors differing in their B^{10} isotopic enrichment to enable estimation of the true neutron counting rate by the difference technique. Unfortunately the flight was only partially successful and no useful data were obtained above the 100mb level. The counting rates vs altitude for the two detectors are illustrated in figure 8.5. The counting rates due to neutrons have been estimated, for the enriched counter, using the smoothed curve data in figure 8.5 and the method discussed in section 4.3. The rates are listed in table 8.1.

The neutron densities during the flight may be obtained from these counting rates using equation (8.8). The value of A_o for our counters is 21.1cm^2 from the theoretical method (equation 8.9) and 9.3cm^2 from Yuan's calibration and equation (8.10). In both cases the uncertainty in A_o is $\pm$ 20% resulting largely from the uncertainty about the dimensions and pressure of the active

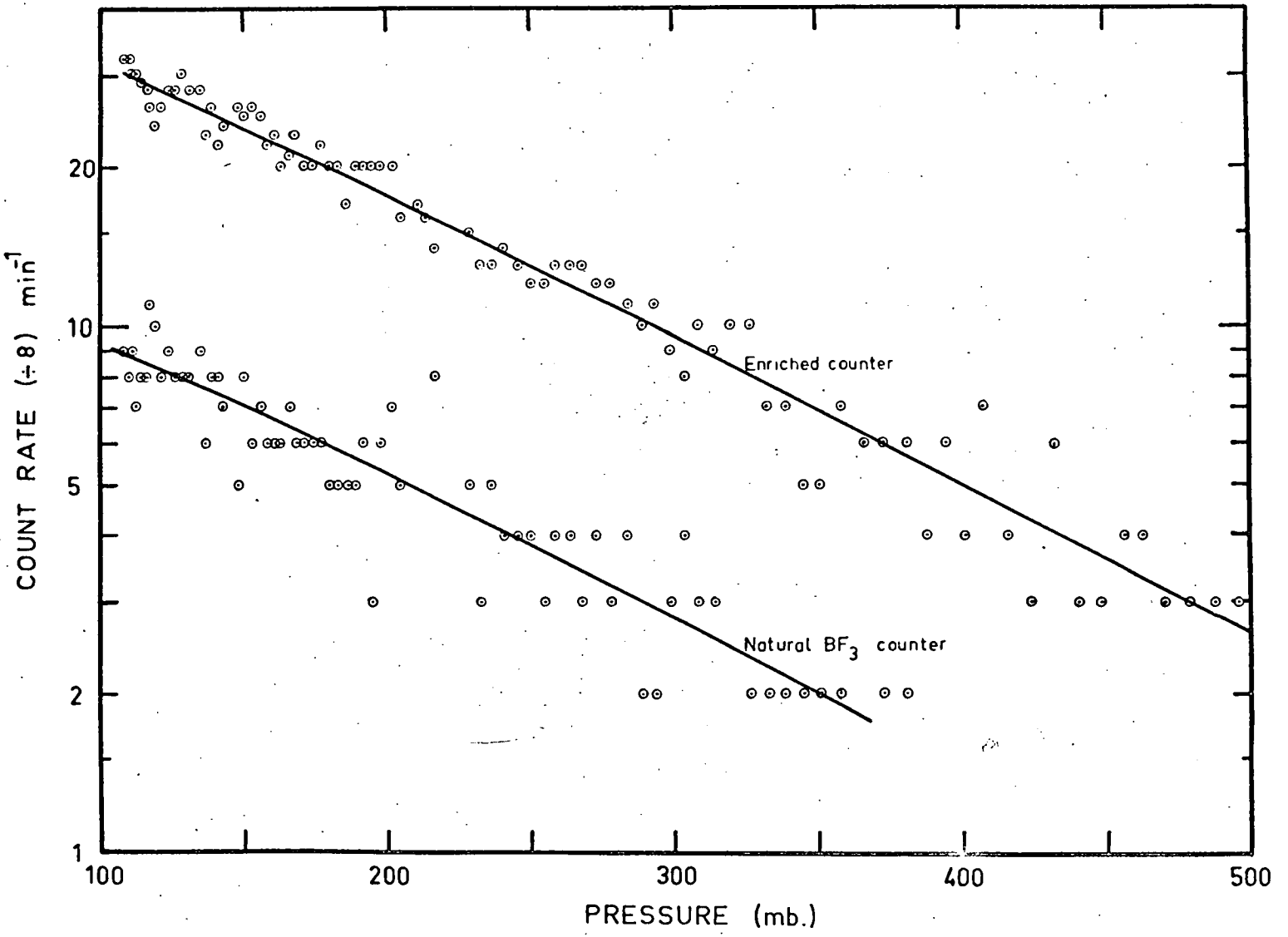

Fig. 8.5. Counting rates during Wilkes flight DN3, March 1965.

region of the counter. The densities corresponding to the two values of A_o are listed in table 8.1.

Atmospheric depth (gm cm^{-2})	Count rate due to neutrons (min^{-1})	Neutron density (cm^{-3}) (1)	(2)
312	68	2.3×10^{-7}	5.3×10^{-7}
250	99	3.4×10^{-7}	7.7×10^{-7}
200	132	4.6×10^{-7}	10.3×10^{-7}
150	179	6.2×10^{-7}	14.0×10^{-7}

Table 8.1: Counting rates (corrected for background) and neutron densities during Wilkes flight DN3, March 1965. Densities in column 1 correspond to $A_o = 22.1$ cm^2 (equation 8.9) and those in column 2 to $A_o = 9.3$ cm^2 (equation 8.10).

We will defer discussion of these results until after we have obtained the global neutron density distributions by normalising our latitude curves to the results of Miles (1964).

(iv) Normalisation to measurements by Miles (1964)

The neutron density measurements of Miles (1964) were made in 1961 and 1962 when the cosmic ray intensity was much lower than at the time of our measurements. We have therefore increased the densities given by Miles by 15% to correct them to September 1964. Fortunately, as noted in section 8.2 the altitude distribution, at the latitude of

Miles' measurements ($\lambda = 41^{o}$), changes slowly during the solar cycle and no adjustment to his altitude distribution is required.

The global neutron density distributions may be obtained from our latitude curves (section 8.3) by normalising them to the time corrected data of Miles (1964). These distributions are illustrated for the equilibrium region of the atmosphere in figure 8.6 and for the upper atmosphere in figure 8.7. We have used the altitude dependence given by Miles at all levels although our measurements are probably more accurate in the equilibrium region. When normalised at 250gm cm^{-2} the two sets of data agree throughout the lower atmosphere to within about 5%.

(v) Comparison with the results of Lingenfelter (1963) and Newkirk (1963).

In order to compare our results with those of Lingenfelter (1963) we have converted his solar minimum carbon 14 production rates to neutron densities. To do this we use the relation

$$\rho = \frac{Q}{v_o \Sigma_{ao}} \qquad (8.15)$$

where ρ is the neutron density

Q is the carbon 14 production rate in atoms per gram of air per second

Σ_{ao} is the macroscopic cross-section of air for

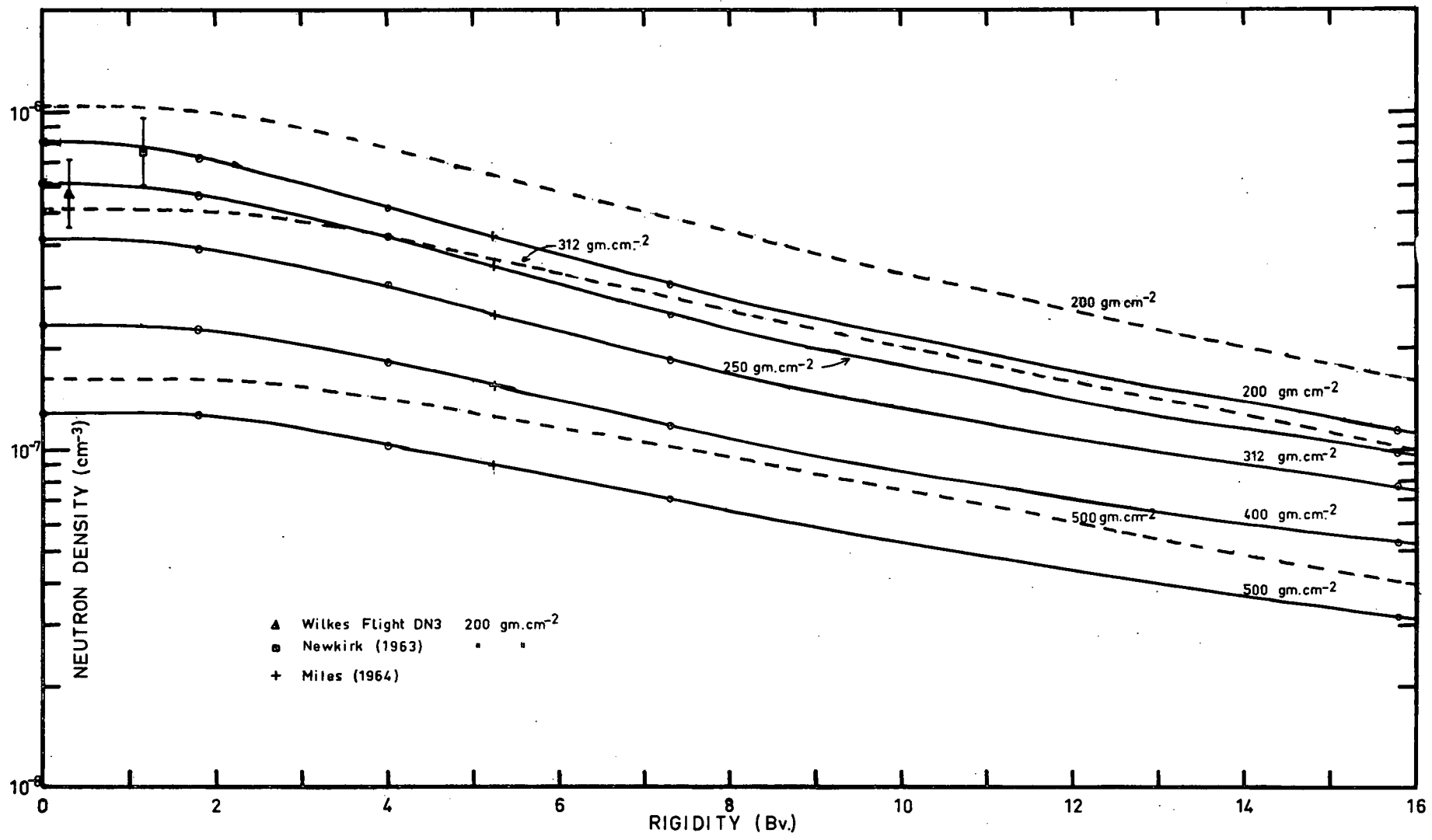

Fig 8.6 Slow neutron density distributions in the equilibrium region of the atmosphere.

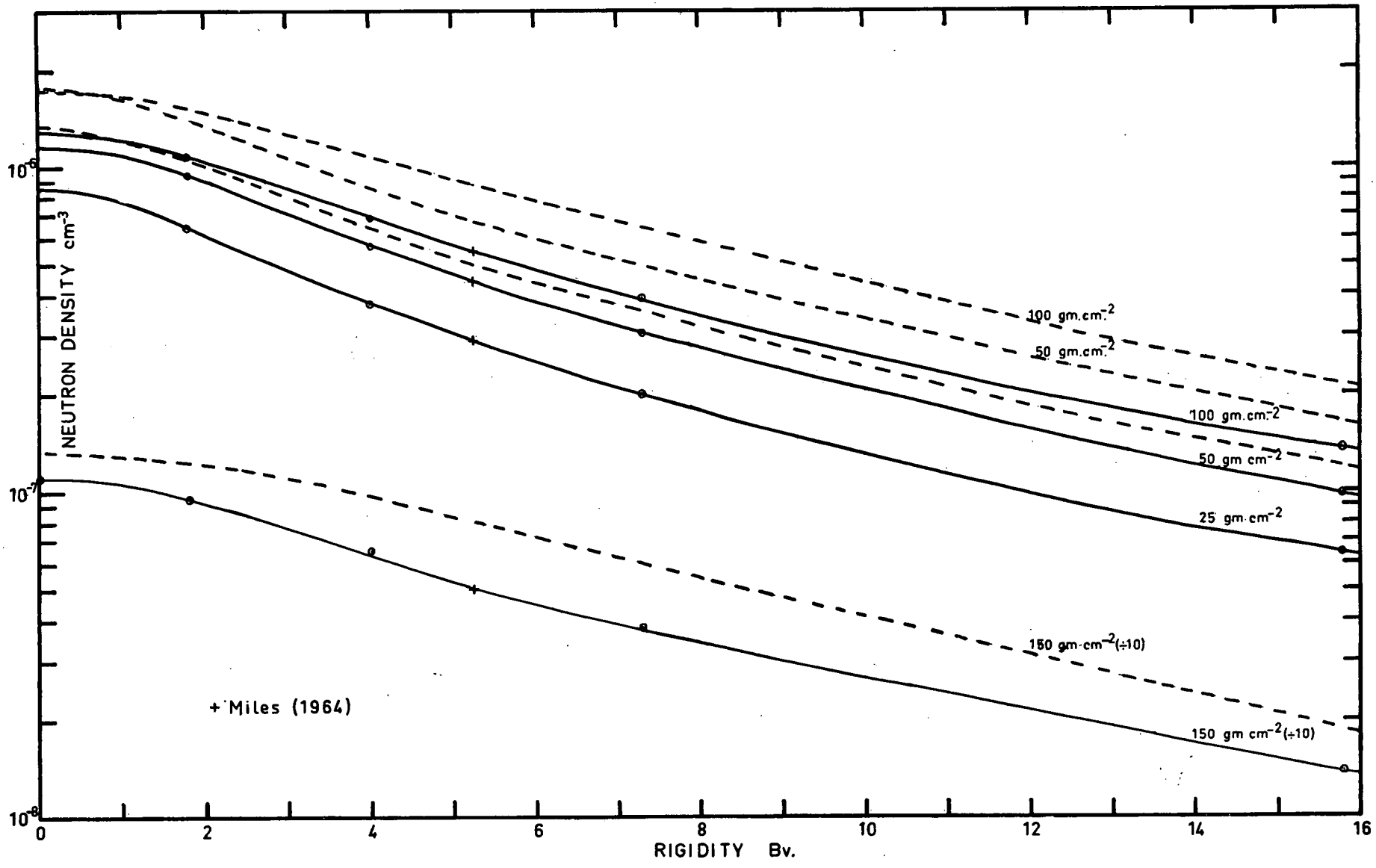

Fig. 8.7 Slow neutron density distributions in the upper atmosphere.

the $N^{14}(n,p)$ reaction at thermal energies.

v_o is the average thermal neutron velocity

Equation 8.15 is not the general relationship between neutron density and thecarbon 14 production rate since it is based on the assumption that all the carbon 14 is produced in the $1/v$ capture process. As noted previously, a significant fraction (Anderson 1953) is produced by the resonance capture of neutrons in the hundreds of Kev energy range. Equation (8.15) is valid here, however, since Lingenfelter has ignored the resonance capture contribution in the normalisation of his results.

The nuclear cross-section of nitrogen 14 for the (n,p) reaction at thermal energies is given by the Hughes and Schwartz (1958) as 1.75 ± 0.05 barns. This value was obtained by Coon and Nobles (1949) and is based on the assumption that the thermal neutron cross-section for natural boron is 703 barns. This cross-section was obtained by Fermi in 1947 and has since been increased to 755 ± 2 barns (Hughes and Schwartz 1958). The effect of this on the nitrogen cross-section appears to have been overlooked and the published value of 1.75 barns should be increased to 1.88 barns. In the present calculations however, we use the smaller cross-section since this has been used by Lingenfelter (1963). Assuming an atmosphere containing 78% nitrogen we obtain $\Sigma_{ao} = 0.0585 \text{ cm}^2 \text{ gm}^{-1}$.

The absolute slow neutron density distribution, evaluated from Lingenfelter's data using equation (8.15)

are compared with our results in figures 8.6 and 8.7. Lingenfelter's results lie consistently above ours at all altitudes and latitudes. The minimum difference is, as expected, (section 8.3) at low cut-off rigidities and atmospheric depths greater than about 150gm cm^{-2}. Even in this region Lingenfelter's results are 20-25% above ours. This difference is slightly greater than the uncertainties ($\pm$ 19%) in normalisation quoted by Lingenfelter and $\pm$ 20% by Miles (1964).

At higher altitudes, in the low cut-off rigidity region, the discrepancy increases to 35% at 100gm cm^{-2} and over 50% at 50 and 25gm cm^{-2}. This trend is in keeping with our observations in section 8.4 about the altitude dependence of Lingenfelter's slow neutron densities.

At mid and low latitudes Lingenfelter's results are 30-60% above our data with the discrepancy increasing with altitude.

The density at 200gm cm^{-2} and P_c = 1.2 Bv has been obtained from the results of Newkirk (1963) using the relation

$$\rho = \int_0^\infty \phi(E) . \frac{1}{v(E)} \, dE \qquad (8.16)$$

where $\phi(E)$ is the differential flux given by Newkirk (1963). Newkirk's data are normalised to measurements by Smith et al (1962) in 1961. We have therefore increased the value of obtained above, by 30% to allow for the increase in the cosmic ray intensity between 1961 and the time of our measurement.

This gives a neutron density of $7.7 \pm 2 \times 10^{-7}$ cm^{-3} which is in good agreement with the value of 7.8×10^{-7} cm^{-3} obtained from our measurements.

(vi) Comparison with experimental data.

The results of flight DN3 must be reduced by about 6% to correct them to the time of the latitude survey measurements. Even after this correction the flight DN3 densities are in better agreement with the results of Lingenfelter than with our data in figures 8.6 and 8.7. This is apparent in table 8.2 where a number of experimental and theoretical results are given for atmospheric depths of 200 and 50gm cm^{-2} at P_c = 0 and 14.4 Bv. Thus, at 200gm cm^{-2} and P_c = 0 the flight DN3 flux of 9.7×10^{-7} cm^{-3} is much nearer the value of 10.3×10^{-7} cm^{-3} given by Lingenfelter than the value of 8.0×10^{-7} obtained from our latitude survey measurements. Table 8.2 contains two sets of density values ρ_1 and ρ_2 for the measurements of Soberman (1956) and for our flight DN3. These were obtained from the counting rates using the theoretical counter cross-section (equation 8.9) and the cross-section estimated from Yuan's calibration. The latter (ρ_2) density values give the best agreement with the results of Lingenfelter. This is to be expected since Lingenfelter's normalisation procedure was based largely on Yuan's counter calibration. Newkirk's value for the density at 200gm cm^{-2} (estimated above) has been translated

from P_c = 1.2 Bv to P_c = 0 using the rigidity dependence curve for 200gm cm^{-2} in figure 8.6.

Atmospheric depth (gm cm^{-2})	$P_c = 0$		$P_c = 14.4$ Bv	
	200	50	200	50
This experiment (September 1964)	8.0	11.5	1.33	1.16
Lingenfelter (1963)	10.3	17.6	1.91	1.94
Newkirk (1963)	7.9	-	-	-
Soberman 1956 ρ_1	5.2	7.1	1.0	-
ρ_2	11.6	16.0	2.3	-
Flight DN3 ρ_1	4.3	-	-	-
ρ_2	9.7	-	-	-

Table 8.2: Neutron density ($x10^7 cm^{-3}$). The results of Newkirk (1963) and of flight DN3 have been adjusted to September 1964. Newkirk's data have been translated to P_c = 0.

The difference between our results and Lingenfelter's at 200gm cm^{-2} and P_c = 0 is, in part, due to the higher level of solar activity at the time of our measurements. It is, in any case, within the experimental uncertainties of the data. At higher altitudes at P_c = 0 a further discrepancy arises from the difference in altitude dependence discussed in section 8.4.

The differences between our results and those of

Lingenfelter at mid and low latitudes follow largely from the normalisation of our data to those of Miles (1964). Although these differences could be regarded as being a consequence of the very substantial errors (Boella et al 1963, Mendell and Korff 1963, Newkirk 1963, Haymes 1964, Miles 1964) in the results of Hess et al (1959) which were used in the normalisation of Lingenfelter's data it is difficult to explain the differences between our results and Sobermans. These differences depend ultimately on the calibrations of the detectors used by Soberman (1956) and Miles (1964).

It seems likely that the present very substantial uncertainties will remain until further absolute measurements have been made. This will require the solution of the present anomaly (section 8.5 iii) concerning the counter efficiency. Further information is also required on time variations during the solar cycle.

8.6 Carbon 14 Production

(i) Calculations: Atmospheric carbon 14 is produced principally in the $^{1}/_{v}$ capture by nitrogen of slow neutrons. Having evaluated the slow neutron density in the atmosphere it is a simple matter to calculate the rate of carbon 14 production due to this reaction. Carbon 14 is also produced by resonance capture by nitrogen of neutrons in the energy interval 0.5-2.0 Mev (Kouts and Yuan 1953, Anderson 1953) and by N^{14} (n,p) reactions at higher energies

(Lal and Peters, Progress in Elementary Particle and Cosmic Ray Physics Vol. VI, North-Holland Publishing Co. Amsterdam 1962). These authors estimate a global average carbon 14 production rate of 0.7 $cm^{-2}sec^{-1}$ due to resonance and high energy neutrons. This value will undoubtedly have to be modified in the light of new evidence on reaction cross-sections and on the equilibrium and leakage flux distributions. We are not, however, in a position to make these calculations and we shall confine our discussion to the contribution of the $\frac{1}{v}$ process to the carbon 14 production rate.

In order to facilitate the calculation of the carbon 14 production rate we have drawn a series of altitude distribution curves for the neutron density at representative cut-off rigidities between 0 and 18 Bv. Twelve curves have been drawn and a selection of these is shown in figure 8.8. The curves are based on the data in figures 8.6 and 8.7 and, for $Z<25 gm\ cm^{-2}$, the altitude dependence given by Newkirk (1963). At atmospheric depths between 500 and 750gm cm^{-2} we have used the absorption lengths given by Lingenfelter (1963) and at depths greater than 750gm cm^{-2} a constant absorption length of 140gm cm^{-2} has been assumed.

The carbon 14 production rate (due to slow neutrons) can be evaluated from these curves by means of equation (8.15). The production rate per square centimeter of the earth's surface has been calculated for the selected cut-off rigidities by integrating over altitude. To determind the global average production rate we have divided the rigidity range

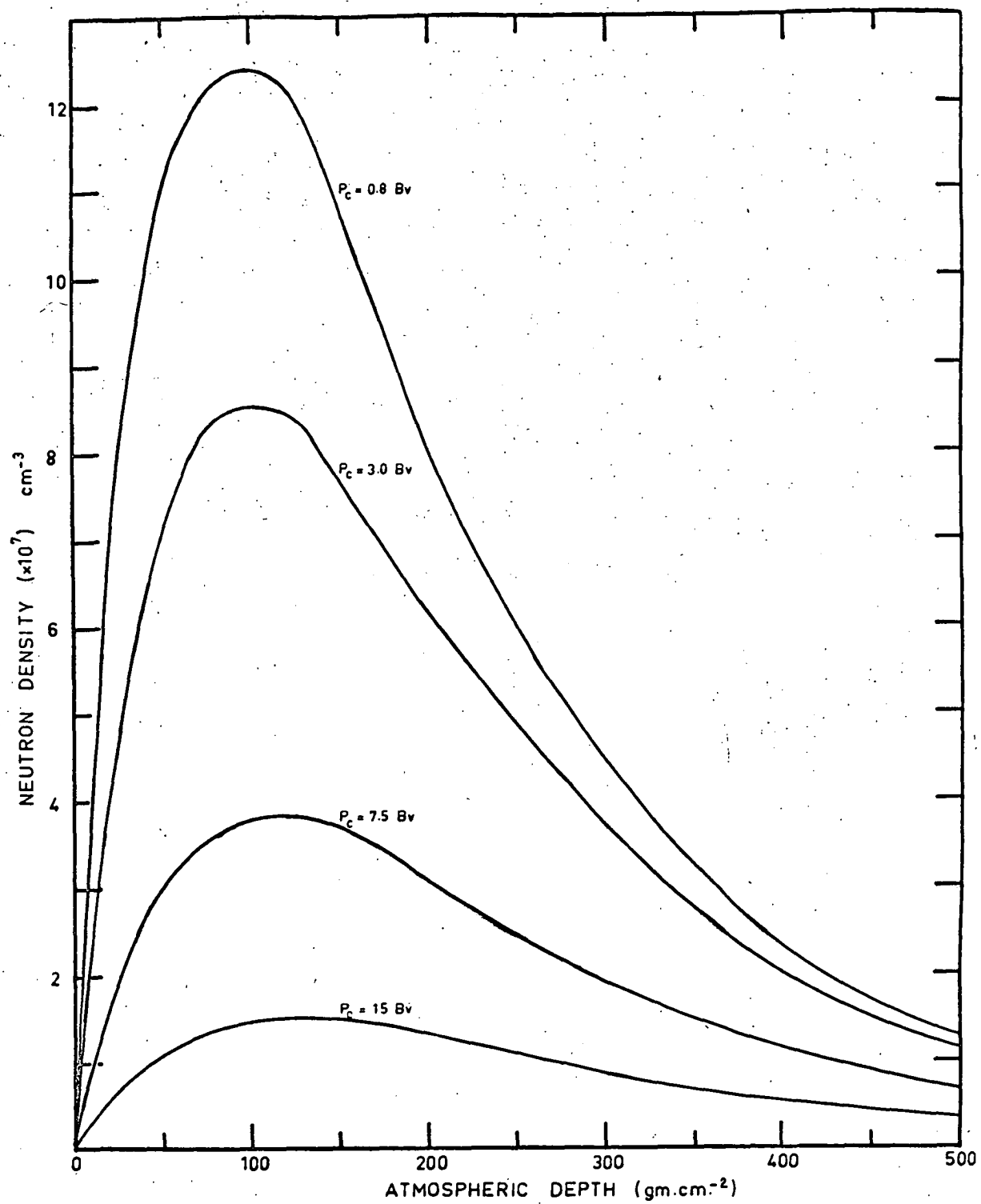

Fig. 8.8. Absolute neutron density distributions estimated from figures 8.6 and 8.7

from 0 to 18 Bv into 12 intervals, centred on the 12 rigidity values used above, and estimated the fraction of the earth's surface corresponding to each of these intervals. The fractions were evaluated graphically by drawing, on a cylindrical (equal areas) projection of the earth, a series of isometric lines of vertical cut-off rigidity given by Quenby and Wenk (1962) and measuring the area between the lines with a planimeter. Finally, the global average production rate was determined by summing the products of these fractions with the production rate for the corresponding rigidity interval. The results are given in table 8.3. The global average carbon 14 production rate is 1.85 ± 0.5 atoms $cm^{-2}sec^{-1}$. The uncertainty arises principally from the uncertainty in the measurements by Miles (1964) to which our data have been normalised. Statistical errors are quite small. It is difficult to estimate the uncertainty arising from use of the Quenby Wenk values for the geomagnetic cut-off but this should be relatively small.

Rigidity interval (Bv)	Corresponding fraction of earth's surface	Average carbon 14 production rate Q ($cm^{-2}sec^{-1}$)
0-1	0.149	4.10
1-2	0.060	3.82
2-4	0.095	3.07
4-6	0.082	2.21
6-9	0.096	1.51
9-11	0.073	1.10
11-13	0.099	0.88
13-14	0.090	0.75
14-15	0.097	0.69
15-16	0.083	0.62
16-17	0.052	0.57
17-18	0.024	0.53

Global average production rate $\bar{Q} = 1.85$ $cm^{-2}sec^{-1}$

Table 8.3: Fractions of the earth's surface having cut-off rigidities in the specified intervals and the carbon 14 production rate per square centimeter of the earth's surface in September 1964.

(ii) Discussion: The estimated carbon 14 production rate Q, of 1.85 ± 0.5 $cm^{-2}sec^{-1}$ is considerably lower than the values of 2.08 ± 0.4 $cm^{-2}sec^{-1}$ for solar maximum and 2.61 ± 0.5 $cm^{-2}sec^{-1}$ for solar minimum, calculated by Lingenfelter (1963). In order to estimate the long term

average value of $\bar{Q}$ Lingenfelter assumed that the deviation of $\bar{Q}$ from its solar minimum value to be directly proportional to the average sunspot number. Then the carbon 14 production rate $\bar{Q}t$ at time t is given by

$$\bar{Q}_t = \bar{Q}\text{min} - (\bar{Q}\text{min} - \bar{Q}\text{max}) \frac{(S_{t-1} - S\text{min})}{S\text{max} - S\text{min}} \qquad (8.17)$$

where S is the sunspot number, the subscripts "min" and "max" refer to the values of S and $\bar{Q}$ at solar minimum and solar maximum respectivelly and S_{t-1} is the sunspot number one year previous to the time t. We use a phase difference of one year following Martin (1965) since, according to Neher and Anderson (1962), cosmic ray modulation lags about one year behind the sunspot number.

Using equation (8.17) we can estimate the value of $\bar{Q}$ for Lingenfelter's data at the period during last solar cycle corresponding to the time of our measurements. This gives a value of $\bar{Q} = 2.56\ \text{cm}^{-2}\text{sec}^{-1}$ which is almost 40% greater than our estimate. This is not surprising in view of the discrepancy between our neutron density results and those of Lingenfelter. It does, however, underline the need for a comprehensive series of measurements of the slow neutron density. These measurements might resolve the present uncertainty about the carbon 14 production decay balance. Lingenfelter used the average value of the sunspot numbers for the last ten solar cycles to estimate the average carbon 14 production rate during this period. His value of

2.50 ± 0.5 atoms $cm^{-2}sec^{-1}$ is 30-40% greater than the average decay rate of 1.8 ± 0.2 $cm^{-2}sec^{-1}$ estimated by Craig (1957) and 1.9 ± 0.2 $cm^{-2}sec^{-1}$ estimated by Fergusson (1963). This imbalance would be further increased by inclusion of production by resonance and high energy neutrons. Our results are more in keeping with the data on decay rates although a production excess seems likely when allowance is made for the resonance and high energy reactions.

8.7 Conclusions

1. The latitude variations in the counting rate of a neutron flux detector are very similar to the neutron density variations if the latitude dependence of the albedo neutron energy spectrum given by Lingenfelter (1963a) is correct. The corrections required are so small at atmospheric depths greater than about 10gm cm^{-2} that even substantial errors in these spectra can have little effect on this conclusion.

2. Our measurements indicate a significantly greater latitude variation of the slow neutron density at most altitudes than that estimated by Lingenfelter (1963). When the latitude curves are normalised at P_c=0 Lingenfelter's data are 20-30% high at mid and low latitudes.

3. The relationship between the altitude dependence of our fast neutron rate at P_c = 5.2 Bv and the

$1/v$ detector rate of Miles (1964) at the same rigidity, is in good agreement with the predictions of Newkirk (1963) although the actual altitude dependences are substantially different because of the lower cut-off rigidity for Newkirk's results. Using the theoretical relationship between the two detector rates we find that Lingenfelter's altitude dependence for the slow neutron density is too steep above the equilibrium region of the atmosphere. This is especially so in polar regions where, relative to their values at 250gm cm^{-2} Lingenfelter's neutron densities are 30% and 60% too high at 50 and 10 gm cm^{-2} respectively.

4. Normalisation of our latitude distribution curves (~~corrected to give the slow neutron variation~~) to the measurements of Miles (1964) gives a density distribution which is 15 - 40% below the results of Lingenfelter (1963). The minimum difference occurs at high latitudes and atmospheric depths between 150 and 500gm cm^{-2}. The difference in this region is within the normalisation errors quoted by Lingenfelter and the uncertainty in the results of Miles.

5. The global average carbon 14 production rate (excluding the contribution due to resonance and higher energy neutrons) was 1.85 ± 0.5 atoms $cm^{-2}sec^{-1}$ at the time of our measurements. This is less than 75% of the value given by Lingenfelter (1963) for the equivalent period of the last solar cycle.

6. Two methods of obtaining the efficiency of slow neutron detectors have been described in the literature. One method depends on calibration in a known neutron flux and the other on calculations using the $B^{10}(n, \alpha)$ cross-section and the number of boron 10 nuclei in the sensitive region of the detector. The two methods give efficiency values for the same detector which differ by a factor of about 2. This anomaly has lead to a dichotomy in the experimental results. Its origin is not obvious and requires further investigation.

APPENDIX I

Derivation of the age equation.

The stationary state form of the Boltzmann transport equation (section 1.6) in the absence of neutron capture ($l_s(u) = l(u)$) may be written

$$l(u)\,\mu\,\frac{\partial \psi}{\partial z} + \psi(z,\Omega,u)$$

$$= \int du' \int \psi(z,\Omega',u')\,F(\mu_o,u-u')\,d\Omega' + S(z,u) \quad . \quad . \quad (1)$$

where $\psi(z,\Omega,u) = \frac{vN}{l(u)}(z,\Omega,u)$

The other symbols are defined in section 1.6.

If scattering is spherically symmetrical in the centre of mass system, the scattering function $F(\mu_o,u-u')$ may be determined directly by application of the principles of conservation of energy and momentum (Sneddon 1951, p.210). This gives

$$F(\mu_o,u) = \left(\frac{M+1}{8\pi M}\right)^2 e^{-u}\,\delta\left\{\mu_o - \left[\left(\frac{M+1}{2}\right) e^{-\frac{u}{2}} - \left(\frac{M-1}{2}\right) e^{\frac{u}{2}}\right]\right\}. \quad . \quad . \quad (2)$$

for $0 \le u \le \varepsilon$

and

$F(\mu_o,u) = 0$ for $u > \varepsilon$

where we take the mass ofthe neutron as unity, and

M is the mass of the atoms of the moderator

δ is the Dirac delta function

$\varepsilon = \log \left(\frac{M+1}{M-1}\right)^2$ is the logarithm of the maximum possible energy loss per collision.

We may also show that the average logarithmic energy loss per collision

$$\xi = \int_0^{\varepsilon} u\,du \int F(\mu_0,u)\,d\Omega \qquad (3)$$

$$= 1 - \left(\frac{M+1}{4M}\right)^2 \varepsilon\, e^{-\varepsilon}$$

$$\simeq \frac{2}{M} \quad \text{for large M.}$$

The effective value of M in air is 14.6 and

$\xi \simeq 0.141$

Similarly we may show that average value of the cosine of the scattering angle in the laboratory co-ordinate system is given by

$$\langle \cos\theta \rangle_{AV} = \int_0^{\varepsilon} du \int \mu_0 F(\mu_0,u)\,d\Omega \qquad (4)$$

$$= \frac{2}{3M}$$

$$\simeq 0.046 \text{ in air.}$$

The assumption of spherically symmetric scattering is valid in air for neutrons with energies up to about 10 Mev.

The first condition upon which the age approximation is based is that the distribution function $\psi(z,\Omega,u)$ is almost isotropic, so that we may neglect all but the first two terms of an expansion in Legendre polynomials. That is,we put

$$\psi(z,\Omega,u) = \frac{1}{4\pi}\left[\psi_0(z,u) + 3\mu\,\psi_1(z,u)\right] \qquad (5)$$

where $\psi_0(z,u) = \int \psi(z,\Omega,u)\,d\Omega$

and $\psi_1(z,u) = \int \mu\,\psi(z,\Omega,u)\,d\Omega$

This approximation is equivalent to the one velocity diffusion theory approximation, and is valid provided:

(i) we are far (compared with the diffusion mean free path) from a neutron source,

(ii) we are far from any boundary regions or regions in which the properties of the medium change appreciably within a distance comparable with the diffusion mean free path,

(iii) the probability of capture is small compared with the probability of scattering.

Although these conditions appear, intuitively, to be necessary for near isotropy of the distribution function, it is necessary to compare a solution employing these approximations with a solution of the rigorous transport equation to show that they are sufficient conditions (Marshak et al 1949a). Because of the over-riding nature of one of the other restrictions of age theory (section 1.9), condition (i) does not apply (Appendix II) to the age equation.

We now expand the scattering function $F(\mu_o, u-u')$ in Legendre polynomials and take the first two terms as in equation (5). Substituting in equation (1) and integrating over μ we obtain

$$1(u)\frac{\partial \psi_1}{\partial z} + \psi_o(z,u) = \int_o^u \psi_o(z,u')F_o(u-u')du' + 4\pi S \quad . . \quad (6)$$

If we had multiplied both sides of the equation by μ and then integrated, we would have obtained

$$\frac{1}{3}\,1(u)\frac{\partial \psi_o}{\partial z} + \psi_1(z,u) = \int_o^u \psi_1(z,u')F_1(u-u')du' \quad . . \quad (7)$$

In equations (6) and (7) we integrate only over the interval ε since F, and therefore F_o and F_1, vanish for $u-u' > \varepsilon$. This follows from equation (2).

In the age theory approximation we make the further assumption that the functions ψ_o and ψ_1, under the integral signs in equations (6) and (7) vary slowly with u' so that we

may use a Taylor expansion. Assuming $\psi_0 \gg \psi_1$ we may write

$$\psi_0(z,u') = \psi_0(z,u) + (u-u') \frac{\partial \psi_0}{\partial u} (z,u) \tag{8}$$

$$\psi_1(z,u') = \psi_1(z,u) \tag{9}$$

The limitations on age theory, following from these approximations, are discussed in section 1.9 and in Appendix II.

Using the approximations of (8) and (9) in (6) and (7), and making use of equations (3) and (4) and the fact (section 1.6) that

$$\int d\Omega \int F(\mu_0, u-u')\, du' = 1$$

we may show that

$$1(u) \frac{\partial \psi_1}{\partial z} = -\xi \frac{\partial \psi_0}{\partial u} + 4\pi S(z,u) \tag{10}$$

and

$$\psi_1 = \frac{1(u)}{3\left[1-\langle\cos\theta\rangle_{AV}\right]} \frac{\partial \psi_0}{\partial z} \tag{11}$$

Substituting (11) into (10) and introducing the symbolic age τ defined by

$$\tau = \frac{1}{3} \int_0^u \frac{1^2(u')}{\xi\left[1-\langle\cos\theta\rangle_{AV}\right]}\, du' \tag{12}$$

leads to the age equation

$$\frac{\partial \chi}{\partial \tau}(z,\tau) = \frac{\partial^2 \chi}{\partial z^2} (z,\tau) + T(z,\tau) \tag{13}$$

where $T(z,\tau) = 4\pi S(z,u) \frac{\partial u}{\partial \tau}$ and

$$\chi(z,\tau) = \xi \psi_0(z,u) \tag{14}$$

is called the "slowing down density" and represents the

number of neutrons per unit volume per unit time which reach the age τ..

The solution of the age equation for a plane monochromatic source

$$T(z,\tau) = \delta(z)\,\delta(\tau)$$

at $z = 0$ in an infinite slowing down medium is

$$\chi(z,\tau) = \frac{1}{(4\pi\tau)^{3/2}} \exp\left(\frac{-z^2}{4\tau}\right) \tag{15}$$

The mean square distance to neutrons of age τ is

$$\bar{z}^2(u) = \frac{\int_0^\infty z^2(u) \exp\left(\frac{-z^2}{4\tau}\right) dz}{\int_0^\infty \exp\left(\frac{-z^2}{4\tau}\right) dz}$$

$$= 2\tau$$

The "slowing down length" (Marshak 1947) is defined by the equation

$$L_s(u) = \left[\frac{\bar{z}^2}{2}(u)\right]^{\frac{1}{2}} \tag{16}$$

so that $L_s^2 = \tau$

Thus, the age τ of neutrons with energy given by u is equal to the square of the slowing down length to that energy. τ has the dimensions of length squared.

The transport mean free path $l_t(u)$ is defined by the equation

$$l_t(u) = \frac{l(u)}{1-\langle\cos\theta\rangle_{AV}} \tag{17}$$

APPENDIX II

Restrictions on age theory.

In section 1.9 we noted the restrictions on age theory introduced by expanding the density distribution functions $\psi_o(z,u)$ and $\psi_1(z,u)$ in a Taylor series (Appendix I). We now make use of the solution (Appendix I) of the age equation, for a plane source in an infinite medium, to determine these limitations more explicitly.

The validity of the Taylor expansions (Appendix I, equations (8) and (9)) requires that $\psi_1 \ll \psi_o$. Now, from the solution of the age equation mentioned above

$$\frac{\partial \psi_o}{\partial z} = -\frac{z}{2\tau}\,\psi_o(z,\tau) \tag{1}$$

We also have (Appendix I, equation (11))

$$\psi_1 = \frac{l(u)}{3(1-\langle\cos\theta\rangle_{AV})}\,\frac{\partial \psi}{\partial z}o \tag{2}$$

Thus

$$\psi_1 = \frac{z l_t(u)}{6\tau}\,\psi_o \tag{3}$$

Hence we require that

$$z \ll \frac{6\tau}{l_t} = \frac{6L_s^2}{l_t} \tag{4}$$

Equation (4) is the mathematical formulation of condition (iii) in section 1.9. Another condition was that

$$\varepsilon \frac{\partial \psi_o}{\partial u} \ll \psi_o \tag{5}$$

Now, for large M (as in air),

$$\varepsilon \approx 2\xi$$

Making use of the solution of the age equation with plane source as mentioned previously, and writing $\frac{\partial \psi}{\partial u}o = \frac{\partial \psi}{\partial \tau}o \cdot \frac{d\tau}{du}$ we obtain the inequality

$$\frac{l(u)\, l_t(u)}{3}\left\{\frac{z^2}{2\tau^2} + \frac{1}{\tau}\right\}\psi_0 \ll \psi_0 \qquad (6)$$

We therefore require at least that

$$\tau \gg \frac{l(u)\, l_t(u)}{3} \qquad (7)$$

Equation (7) gives rise to condition (ii), section 1.9, that age theory can only be applied where the neutrons have made a large number of collisions.

Finally, if the expansion of $\psi_1(z,u')$ is valid

$$\varepsilon \frac{\partial \psi}{\partial u}_1 \ll \psi_1 \qquad (8)$$

From equation (3)

$$\frac{\partial \psi}{\partial u}_1 = \frac{zl}{6\tau}t \left\{\left(\frac{1}{l_t}\frac{dl}{du}t + \frac{1}{\tau}\frac{d\tau}{du}\right)\right\}\psi_0 + \frac{\partial \psi}{\partial u}_0$$

Substituting for ψ_0 from (3) and using

$$\frac{d\tau}{du} = \frac{l(u)\, l_t(u)}{3\xi} \qquad (9)$$

we obtain

$$\frac{\partial \psi}{\partial u}_1 \approx \left(\frac{1}{l_t}\frac{dl}{du}t - \frac{1^2}{3\xi\,\tau}t + \frac{\partial \psi}{\partial u}_0 \cdot \frac{1}{\psi_0}\right)\psi_1 \quad . \quad (10)$$

Thus, equation (8) is equivalent to the condition that

$$\frac{\varepsilon}{l_t}\frac{dl}{du}t - \frac{\varepsilon\, l l_t}{3\xi\,\tau}t + \frac{\varepsilon}{\partial u}\frac{\partial \psi}{\partial u}_0 \cdot \frac{1}{\psi_0} \ll 1 \quad . \quad . \quad . \quad (11)$$

Now the second term on the LHS of (11) is approximately $\frac{2l(u)\, l_t(u)}{3\tau}$ which, assuming (7) to be well satisfied, is very much less than unity. The third term is also very much less than unity if (7) is satisfied, since this implies (5).

Hence, condition (8) is satisfied provided (7) is, and

$$\frac{\varepsilon}{l_t}\frac{dl}{du}t \ll 1 \qquad (12)$$

Condition (12) is well satisfied for neutrons in air,

but the other two conditions (4) and (7) limit the range of application of age theory in the atmosphere. Thus equation (4) limits the distance from the source so that

$$z \ll \frac{\tau}{3} \quad \text{for } E \sim 1 \text{ Mev}$$

and $$z \ll 2\tau \quad \text{for } E \sim 10 \text{ Kev.}$$

If, for example, we have a 4 Mev neutron source, the age of 500 Kev neutrons is about 1600 $gm^2 cm^{-4}$ in air and age theory is satisfactory for $z \ll 500$ $gm.cm^{-2}$. The age of a thermal neutron diffusing down from a 500 Kev source is about 280 $gm.cm^{-2}$, and condition (4) requires that $z \ll 560$ $gm.cm^{-2}$. Marshak (1947) has shown that age theory is satisfactory for $z < \frac{\tau}{1(u)}$ (about 90 $gm.cm^{-2}$ in air), and that the Gaussian solution of equation (15) (Appendix I) goes over into an exponential solution for larger z. Consequently, age theory will under-estimate the neutron flux at large atmospheric depths for solar flare events where neutron production is confined to a thin layer near the top of the atmosphere. It will, however, be more reliable for neutrons from galactic cosmic rays because of the distributed nature of the neutron source.

The breakdown of diffusion theory close to neutron sources, implied in condition (i), Appendix I, arises from neutrons which have not made any collisions after leaving the source. These neutrons are excluded by the requirement of equation (7), so this condition does not apply to age theory.

Equation (7) requires that in air $\tau \gg 110$ $gm.cm^{-2}$ for $E > 500$ Kev, and the age equation may be used in the vicinity of neutron sources provided this condition is satisfied.

APPENDIX III

Boundary conditions for neutron diffusion in the atmosphere.

The atmosphere may be assumed to be a semi-infinite slowing down medium bounded by a vacuum at $z = 0$. The boundary conditions are:

(i) $\chi(z, \tau)$ tends to zero as $z \to \infty$

(ii) the total incoming current of neutrons, across the $z = 0$ plane, is zero.

Condition (ii) may be written

$$\int_0^1 \psi(z,\mu,u)\, \mu d\mu = 0. \qquad (1)$$

(all symbols are defined in sections 1.6 and 1.7).
Now, from equations (5) and (11) in Appendix I

$$\psi(z,\mu,u) = \frac{1}{4\pi} \left\{ \psi_0(z,u) - \mu\, l_t(u) \frac{\partial \psi}{\partial z}_0 \right\} \qquad (2)$$

Substituting in equation (1) we find

$$\frac{1}{8\pi} \left\{ \psi_0(z,u) - \frac{2}{3} l_t(u) \frac{\partial \psi}{\partial z}_0 \right\} = 0 \qquad (3)$$

or

$$\chi(z, \tau) - \frac{2}{3} l_t(u) \frac{\partial \chi}{\partial z} = 0 \qquad (4)$$

at $z = 0$ for all τ.

APPENDIX IV

The counting rate of a vertical, cylindrical detector.

Consider a cylindrical detector with its axis vertical in a flux of ionising particles J $cm^{-2}sec^{-1}ster^{-1}$, isotropic over the upper hemisphere and zero over the lower. Suppose that any particle which strikes the surface of this detector is counted, and that the area of the flat, circular, top surface is A_1 and that of the sides is A_2.

Consider a small element of area ΔA on the top surface of the detector. The number of particles dN_1 having zenith angles between θ and $\theta + d\theta$ and azimuth between ϕ and $\phi + d\phi$ which pass through the area ΔA is

$$dN_1 = J\, dA\, d\Omega \qquad (1)$$

where

$$dA = \Delta A \cos\theta \qquad (2)$$

is the projected area of ΔA normal to the beam and

$$d\Omega = \sin\theta\, d\theta\, d\phi \qquad (3)$$

is the solid angle containing the beam. Thus, the total number of particles passing through ΔA is

$$\Delta N_1 = J\, \Delta A \int_0^{\frac{\pi}{2}} \int_0^{2\pi} \sin\theta \cos\theta\, d\theta\, d\phi \qquad (4)$$

$$= \pi J\, \Delta A$$

and the total number incident on the top surface

$$N_1 = \pi J A_1 \qquad (5)$$

Similarly, for an element of area on the vertical side surface

$$dA = \Delta A \sin\theta \cos\phi \qquad (6)$$

where the zenith angle ϕ is measured from the normal to ΔA.

Hence the total number of particles incident on ΔA

$$\Delta N_2 = J\,\Delta A \int_0^{\frac{\pi}{2}} \int_{-\frac{\pi}{2}}^{\frac{\pi}{2}} \sin^2\theta \cos\phi \, d\theta \, d\phi \qquad (7)$$

$$= 2\,J\,\Delta A \int_0^{\frac{\pi}{2}} \sin^2\theta \, d\theta$$

$$= \frac{\pi J \Delta A}{2}$$

Thus the total number of particles incident on the sides of the cylinder

$$N_2 = \frac{\pi J A}{2} 2 \qquad (8)$$

If the cylinder has radius r and length l, the total number of particles incident on it

$$N = N_1 + N_2 = \pi^2 r J (r + l) \qquad (9)$$

Equation (9) may also be written

$$N = 2\pi J A \qquad (10)$$

where $A = \frac{\pi r}{2} (r + l)$ (11)

is the "projected area" of the detector.

APPENDIX V

Attenuation of the γ-ray flux from a plane isotropic source.

Consider a plane γ-ray source at the top of the atmosphere ($z = 0$). The flux I_o $cm^{-2}sec^{-1}ster^{-1}$ at $z = 0$ is assumed isotropic over the lower hemisphere and zero over the upper. We wish to estimate the flux $I(z)$ at depth z assuming rectilinear propagation of the γ-rays (i.e. no scattering). To do this we consider a spherical detector of radius r at z and determine the counting rate $\Delta R(z,\theta)$ due to the flux between θ and $\theta + d\theta$ in an annular cone about the vertical. In the absence of attenuation

$$\Delta R = 2\pi r \sin\theta . rd\theta . I_o \qquad (1)$$

Now the attenuation factor is $f(x)$ where x is the path length of the rays. At zenith angle θ

$$x = \frac{z}{\cos\theta}$$

and
$$f(x) = e^{-\frac{\mu z}{\cos\theta}} \qquad (2)$$

where μ is the mass absorption coefficient for the γ-rays. With attenuation (1) becomes

$$\Delta R = 2\pi r^2 I_o e^{-\frac{\mu z}{\cos\theta}} \sin\theta \, d\theta \qquad (3)$$

The total counting rate $R(z)$ is given by

$$R(z) = 2\pi r^2 I_o \int_o^{\frac{\pi}{2}} \sin\theta \, e^{-\frac{\mu z}{\cos\theta}} d\theta \qquad (4)$$

If we write

$$\frac{\mu z}{\cos\theta} = S \qquad (5)$$

$$d\theta = \frac{\cos^2\theta}{\sin\theta} \cdot \frac{1}{\mu z} dS \qquad (6)$$

and equation (4) becomes

$$R(z) = 2\pi r^2 I_o \mu z \int_{\mu z}^{\infty} \frac{e^{-S}}{S^2} dS \qquad (7)$$

At the top of the atmosphere the counting rate

$$R_o = 2\pi r^2 \int_0^{\frac{\pi}{2}} I_o \sin\theta \, d\theta$$

$$= 2\pi r^2 I_o \qquad (8)$$

Hence the ratio of the flux at z to the flux at the top of the atmosphere

$$\frac{I(z)}{I_o} = \frac{R(z)}{R_o}$$

$$= \mu z \int_{\mu z}^{\infty} \frac{e^{-S}}{S^2} dS \qquad (9)$$

This is the Gold integral $\varepsilon_1(\mu z)$. It may be solved using the curves given (for example) by Rossi (1952). Equation (9) may be written in the alternative forms

$$\frac{I(z)}{I_o} = e^{-\mu z} - \mu z \int_{\mu z}^{\infty} \frac{e^{-S}}{S} dS \qquad (10)$$

$$= \int_1^{\infty} \frac{e^{-\mu z S}}{S^2} dS \qquad (11)$$

APPENDIX VI

The efficiency of the BF_3 filled ionisation chambers used by Miles 1964.

Consider an ionisation chamber of volume V filled with BF_3 at pressure p (atmospheres). Assume that one "count" of the electrometer corresponds to the collection of q coulombs. Suppose the electrometer "count rate" due to the ionising component of the cosmic rays is C_i. Then the number of ion pairs produced in the chamber per second (assuming saturation and no recombination) is

$$n = \frac{C_i q}{e} \qquad (1)$$

where e is the electronic charge.

The ionisation per unit volume per atmosphere of BF_3 is

$$n_1 = \frac{C_i q}{Vpe} \text{ ion pairs } cm^{-3}sec^{-1} \text{ per atmosphere of } BF_3 \quad . \quad . \quad . \quad .(2)$$

If k is the ratio of the probable specific ionisation in air to that in BF_3 we obtain

$$n_2 = \frac{C_i qk}{Vpe} \text{ ion pairs } cm^{-3}sec^{-1} \text{ per atmosphere of air} \quad . \quad . \quad . \quad .(3)$$

i.e. n_2 is the "current" in "equivalent ion pairs" as defined by Miles (1964). Thus

$$n_2 = \alpha C_i \qquad (4)$$

where α is a constant, characteristic of the chamber.
In the presence of neutrons, as well as ionising radiation, the electrometer rate increases to

$$C_t = C_i + C_n \qquad (5)$$

where C_n is the rate due to neutrons. Thus the current becomes

$$n_3 = \alpha(C_i + C_n) \qquad (6)$$

Now $C_n = \frac{\text{no of } B^{10}(n,\alpha) \text{ events x charge released/event}}{\text{charge per electrometer count}}$

$$= \frac{R_n E e G}{q \Delta E} \qquad (7)$$

where E is the mean energy released in the $B^{10}(n,\alpha)$ reaction.

ΔE is the average energy required to produce an ion pair in BF_3

R_n is the number of $B^{10}(n,\alpha)$ events

G is a wall effect correction factor to allow for the loss of energy when the products of the $B^{10}(n,\alpha)$ events lose part of their energy in the walls of the chamber. G is slightly less than unity for Miles' chamber.

We have already shown in section 8.5 that

$$R_n = p L V v_o \sigma_o \varepsilon . \rho \qquad (8)$$

In this case ρ stands for the average neutron density in the chamber. Self shading effects cause this value to be lower than the density in the absence of the chamber. Miles obtained a value for the chamber efficiency in the absence of self shading effects and applied a correction to results obtained in measurements with the chamber. Consequently, we can ignore self shading effects for the present purposes. Thus, from (7) and (8)

$$C_n = \frac{p L V v_o \sigma_o \varepsilon E e G . \rho}{q \Delta E} \qquad (9)$$

Now, during calibration, equation (6) becomes

$$n_3 = \alpha C_n \quad \text{equivalent ion pairs} \qquad (10)$$

(this is also true in the analysis of flight data since the ionising background is eliminated by the two chamber technique). Combining (9) and (10) we find

$$\rho = \frac{\Delta E \, n_3}{k L v_o \sigma_o \varepsilon E G} \qquad (11)$$

Inserting numerical values and assuming G = 0.95 (an approximate value estimated using the method described by Coon and Nobles 1949) we find

$$\rho = 1.3 \times 10^{-9} n_3 \qquad (12)$$

This value is directly comparable with the value obtained by calibration by Miles (1964). He found

$$\rho = 2.6 \pm 0.5 \times 10^{-9} n_3 \qquad (13)$$

The difference between these results is discussed in section 8.5.

The densities obtained using equations (12) or (13) must be increased by a self shading correction factor. Miles estimates this factor to be 1.17 for his chamber in the atmospheric neutron flux.

REFERENCES

(Arranged Alphabetically)

Addario, M., and S. Tamburino, Phys. Rev., 76, 983 - 984 (1949)

Alaoglu, L., and N.M. Smith, Phys. Rev., 53, 832 - 836 (1938)

Albert, R.D., C. Gilbert and W.N. Hess, J. Geophys. Res., 67, 3537 (1962)

Anderson, E.C., Annual Review of Nuclear Science 2, 63 - 78 (1953)

Axford, W.I., and G.C. Reid, J.Geophys. Res., 67, 1692 - 1696 (1962)

Bachelet, F., P. Balata, E. Dyring and N. Iucci, unpublished 1964 (as reported by Forman 1965)

Bame, S.J., J.P. Conner, F.B. Brumley, R.L. Hostetler and A.C. Green, J. Geophys. Res., 68,1221 - 1228 (1963)

Bethe, H.A., S.A. Korff and G. Placzek, Phys. Rev., 57, 573 (1940)

Bhavsar, P.D., J. Geophys. Res., 67, 2627 - 2637 (1962)

Biswas, S. and C.E. Fitchel, Composition of Solar Cosmic Rays, Goddard Space Flight Center Report X-611-65-219, Greenbelt, Maryland (May 1965)

Boella, G., G. Degli Antoni, C. Dilworth, G. Gianelli, E. Rocca, L. Scarsi and D. Shapiro, Nuovo Cimento, 29, 103 - 117 (1963)

Boella, G., G. Degli Antoni, C. Dilworth, M. Panetti and L. Scarsi and D.S. Intriligator, J. Geophys. Res., 70, 1019 - 1030 (1965)

Bryant, D.A., T.L. Cline, U.D. Desai and F.B. McDonald, J. Geophys. Res., 67, 4983 - 5000 (1962)

Bryant, D.A., T.L. Cline, U.D. Desai and F.B. McDonald, Phys. Rev. Letters, 11, 144 (1963)

Camerini, U., P.H. Fowler, W.O. Lock, and H. Muirhead, Phil. Mag., 41, 413 (1950)

Colgate, S.A., Phys. Rev., 99, 665 (1955)

Coon, J.H. and R.A. Nobles, Phys. Rev., 75, 1358 - 1361 (1949)

Craig, H., Tellus 9, 1 - 17 (1957)

Davison, B., Neutron Transport Theory, Oxford University Press, London, 450 pp., (1957)

Davisson, C.M. and R.D. Evans, Rev. Mod. Phys., 24, 79 - 107 (1952)

Davis, L.R., O.E. Berg and L.H. Meredith, Space Research, North-Holland Publishing Co., Amsterdam (1960)

Duthie, J.G., E.M.Hafner, M.F. Kaplon and G.G. Fazio, Phys. Rev. Letters, 10, 364 - 368, (1963)

Edwards, P.J.,Proc. I. R. E. (Aust.), 24, 639 (1963)

Edwards, P.J., High Altitude Studies of Ionising Radiation, Ph.D. Thesis, University of Tasmania,Hobart (1964)

Elsasser, W., E.P. Ney and J.R. Winckler, Nature 178, 1226 - 1227 (1956)

Erlich, R., and H. Hurwitz, Nucleonics, 12 (2), 23 - 30 (1954)

Fan, C.Y., G. Gloeckler and J.A. Simpson, Phys. Rev. Letters, 13, 149 - 153 (1964)

Fenton, A.G., and K.B. Fenton, Nucl. Instr. and Methods, in press 1965

Fergusson, G.J., Geofis. Pura Appl., in press 1963, (as reported by Lingenfelter 1963)

Fermi, E., Nuclear Physics, The University of Chicago Press, Chicago (1950)

Flügge, S., Cosmic Radiation, p 144 - 158, Edited by W. Heisenberg, Springer - Verlag, Berlin (1943), (English translation by T.H.Johnson,Dover,New York 1946)

Forman, M.A., J. Geophys. Res., 70, 2469 - 2474 (1965)

Fraki, R., M. Leimdoerfer, and S. Malmskog, Nucl. Instr. and Methods, 23, 341 (1963)

Frank, L.A. and J.A. Van Allen, J. Geophys. Res., 69, 4923 (1964)

Freier, P.S. and W.R. Webber, J. Geophys. Res., 68, 1605 - 1629 (1963)

Fujimoto, Y. and T. Tamura, Prog. Theoret. Phys. Kyoto, 8, 221 - 230 (1952)

Galli, M., Nuovo Cimento, [9] 10, 1187 - 1195 (1953)

Galperin, Y.I., Planet. Space Sci., 10, 187 - 193 (1963)

Gauger, J., J. Geophys. Res., 69, 2209 - 2222 (1964)

Gauger, J., J. Geophys. Res., 70, 3571 - 3574 (1965)

Glasstone, S. and M.C. Edlund, The Elements of Nuclear Reactor Theory, MacMillan and Co. Ltd., London (1952)

Goulding, F.S., Nucleonics, 17, 69 (1959)

Greenhill, J.G., Measurements of Cosmic Ray Activity with Balloon Borne Equipment, B.Sc. (Hons.) Thesis, University of Tasmania, Hobart (1960)

Gregory, J.B. and R.E. Newdick, J. Geophys. Res., 69, 2383 - 2385 (1964)

Haymes, R.C., Phys. Rev., 116, 1231 - 1237 (1959)

Haymes, R.C., J. Geophys. Res., 69, 841 - 852 (1964)

Haymes, R.C., J. Geophys. Res., 69, 853 - 860 (1964 a)

Haymes, R.C., and S.A. Korff, Phys. Rev., 120, 1460 (1960)

Haymes, R.C., and Van Paassen, New York University (Cosmic Ray Group) Report, (June 1958)

Hess, W.N., E.H. Canfield and R.E. Lingenfelter, J. Geophys. Res., 66, 665 - 677 (1961)

Hess, W.N., H.W. Patterson, R. Wallace and E.L. Chupp, Phys. Rev., 116, 445 - 457 (1959)

Hess, W.N., and A.K. Starnes, Phys. Rev. Letters, 5, 48-50 (1960)

Hoffman, D.J. and J.R. Winckler, J. Geophys. Res., 68, 2067 - 2098 (1963)

Hughes, D.J. and R.B. Schwartz, Neutron Cross Sections (2nd ed.), Brookhaven Natl. Lab Rept. BNL-325 (July 1958)

Jokipii, J.R. and Leverett Davis Jr., Phys. Rev. Letters, 13, 739 - 741 (1964)

Kamphouse, J.L., J. Geophys. Res., 68, 5608 (1963)

Kaufmann, R., J. Geophys. Res., 68, 371 - 386 (1963)

Korff, S.A. and R.C. Haymes, J. Geophys. Res., 65, 3163 - 3167 (1960)

Kouts, H.J. and L.C.L. Yuan, Phys. Rev. 86, 128 - 129 (1952)

Laby, J.E., Y.K. Lim and V.D. Hopper, Nuovo Cimento 5, 249-259 (1957)

La Pointe, S.M. and D.C. Rose, Can. J. Phys., 40, 687 (1962)

Larsson, K.E., Ark. f. Fys., 7/25, 323 (1953)

Lawson, J.L. and G.E. Uhlenbeck, Threshold Signals, M.I.T. Radiation Lab. Series, No.24, McGraw - Hill, New York (1950)

Lingenfelter, R.E., Rev. Geophys., 1, 35 - 55 (1963)

Lingenfelter, R.E., J. Geophys. Res., 68, 5633 - 5640 (1963a)

Lingenfelter, R.E. and E.J. Flamm, J. of the Atm. Sciences, 21, 134 - 140 (1964)

Lingenfelter, R.E. and E.J. Flamm, Science 144, 292 - 294 (April 17, 1964a)

Lingenfelter, R.E. and E.J. Flamm, J. Geophys. Res., 69, 2199 (1964b)

Lockwood, J.A., L. Friling and T. Wilson, University of New Hampshire Report, Durham, New Hampshire (September 1965)

Lord, J.J., Phys. Rev., 81, 901 - 909 (1951)

Maeda, K., Nuovo Cimento 20, 587 - 590 (1961)

Marshak, R.E., Rev. Mod. Phys., 19, 185 - 238 (1947)

Marshak, R.E., H. Brooks and H. Hurwitz Jr., Nucleonics 4, 10 - 22; 4, 43 - 49; 5, 53 - 60; 5, 59 - 68 (1949)

Martin, J.P., J. Geophys. Res., 70, 2057 - 2064 (1965)

Martin, J.P., L. Witten and L. Katz, J. Geophys. Res., 68, 2613 - 2618 (1963)

McCracken, K.G., U.R. Rao, B.C. Fowler, M.A. Shea and D.F. Smart, IQSY Instruction Manual No. 10, Cosmic Ray Tables, IQSY Committee, London (1965)

McDiarmid, I.B., D.C. Rose and E. Budzinski, Can. J. Phys., 39, 1888 - 1900 (1961)

McDonald, F.B. and G.H. Ludwig, Measurement of Low Energy Primary Cosmic Ray Protons on Imp - 1 Satellite, Goddard Space Flight Center Report X-611-64-363, Greenbelt, Maryland, November 1964

McIlwain, C.E., J. Geophys. Res., 65, 2727 (1960)

Mendell, R.B. and S.A. Korff, J. Geophys. Res., 68, 5487 - 5495 (1963)

Meyer, P. and J.A. Simpson, Phys. Rev., 99, 1517 - 1523 (1955)

Miles, R.F., J. Geophys. Res., 69, 1277 - 1284 (1964)

Miyake, S., K. Hinotani and K. Nunogaki, J. Phys. Soc. Japan, 12, 113 - 121 (1957)

Montgomery, C.G. and A.R. Tobey, Phys. Rev. 76, 1478 - 1481 (1949)

Muirhead, H. and W.G.V. Rosser, Phil. Mag., 46 - 1, 652 - 662 (1955)

Neher, H.V., Phys. Rev., 103, 228 - 236 (1956)

Neher, H.V. and H.R. Anderson, Proc. Moscow. Cosmic Ray Conf., IV (1960)

Neher, H.V. and H.R. Anderson, J. Geophys. Res., 67, 1309 - 1316 (1962)

Newkirk, L.L., J. Geophys. Res., 68, 1825 - 1833 (1963)

Nichols, M.H. and L.L. Rauch, Radio Telemetry, Wiley, New York (1956)

Parker, E.N., Phys. Rev. Letters, 14, 55 - 57 (1965)

Patterson, H.W. and R. Wallace, Lawrence Radiation Lab Report, UCRL - 8359, Berkeley (1958) (as reported in Miles 1964)

Phillips, J., Some Investigations of the Secondary Nucleonic Radiation, B.Sc.(Hons.) Thesis, University of Tasmania, Hobart (September 1961)

Price, W.J., Nuclear Radiation Detection, McGraw - Hill, New York (1958)

Quenby, J.J. and G.J. Wenk, Phil. Mag., 7, 1457 (1962)

Reidy, W.P., R.C. Haymes and S.A. Korff, J. Geophys. Res., 67, 459 - 465 (1962)

Roederer, J.G. and H.S. Ghielmetti, Sparmo Bulletin, No. 2, 15 (June 1964)

Rose, D.C., K.B. Fenton, J. Katzman, and J.A. Simpson, Can. J. Phys., 34, 968 - 977 (1956)

Rossi, B., High Energy Physics, Prentice - Hall, Englewood Cliffs, N.J. (1952)

Simpson, J.A., Phys. Rev., 83, 1175 - 1188 (1951)

Simpson, J.A., Recent Investigations of the Low Energy Cosmic and Solar Particle Radiations, University of Chicago Report EFINS - 63 - 8, Chicago (1963)

Simpson, J.A. and W.C. Fagot, Phys. Rev., 90, 1068 - 1072 (1953)

Singer, S.F., Phys. Rev. Letters, 1, 181 - 183 (1958)

Smith, R.V., L.F. Chase, W.L. Imhof, J.B. Reagan and M. Walt, Radiation Measurements with Balloons, ARL - TDR - 62- 2, 6571 st, Aeromedical Research Lab., Holloman AFB, New Mexico, 57 pp, (1962)

Sneddon, I.N., Fourier Transforms, Mc Graw - Hill, New York (1951)

Soberman, R.K., Phys. Rev., 102, 1399 - 1409 (1956)

Staker, W.P., Phys. Rev., 80, 52 (1950)

Staker, W.P., M. Pavalov, and S.A. Korff, Phys. Rev., 81, 889 (1951)

Storey, J.R., Phys. Rev., 117, 573 - 577 (1960)

Stuiver, M., J. Geophys. Res., 66, 273 - 276 (1961)

Swetnick, M.J., H.A.C. Neuburg and S.A. Korff, Phys. Rev., 86, 589 (1952)

Tibbs, C.E., Frequency Modulation Engineering, Chapman and Hall, London (1947)

Trainor, J.H. and J.A. Lockwood, J. Geophys. Res., 69, 3115 - 3123 (1964)

Van Allen, J.A., W.C. Lin, and H. Leinbach, J. Geophys. Res., 69, 4481 - 4492 (1964)

Waugh, J.B., Atomic Energy Commission of Canada Report CREL - 828 (1958)

Webber, W.R., J. Geophys. Res., 67, 5091 - 5106 (1962)

Williams, D.J. and C.O. Bostrom, J. Geophys. Res., 69, 377 - 391 (1964)

Winckler, J.R., P.D. Bhavsar and K.A. Anderson, J. Geophys. Res., 67, 3717 - 3736 (1962)

Yuan, L.C.L., Phys. Rev., 81, 175 (1951)

Zaglio, E., Nuovo Cimento, 6, 512 (1957)

Zmuda, A.J., G.F. Pieper and C.O. Bostrom, J. Geophys. Res., 68, 1160 - 1165 (1963)